Statistical mechanics of non equilibrium matter: from minimal models to morphogen gradients

a thesis presented for the degree of

Doctor of Philosophy of Imperial College London

and the

Diploma of Imperial College

by

Luca Cocconi

Department of Mathematics

Imperial College

180 Queen's Gate, London SW7 2AZ

November 2022

Declaration of Originality

I declare that this thesis is an original report of the research I carried out during the course of my doctoral degree, that it has been composed by myself and that the present document has not been submitted for any other degree or professional qualification. I confirm that the work submitted is my own, except where work which has formed part of jointly-authored publications has been included, always in accordance with the standard referencing practices. My contribution and those of the other authors have been clearly indicated in such a way that appropriate credit has been given wherever reference has been made to instances of collaborative work. All permissions to reproduce are included in the appendix of this thesis.

Luca Cocconi

Copyright Declaration

Thesis advisor: Dr. Guillaume Salbreux, Dr. Gunnar Pruessner

Statistical mechanics of non equilibrium matter: from minimal models to morphogen gradients

Luca Cocconi

Abstract

Living systems are by definition far from thermodynamic equilibrium, a condition that can be maintained only at the cost of a continuous injection of energy at the microscale, e.g. via cellular metabolic processes, and dissipation into the surrounding environment. The absence of thermodynamic equilibrium, formalised in the breaking of the global detailed balance condition, allows for a wealth of exotic and often counterintuitive phenomena. Our understanding of the capabilities and limitations of living matter has been greatly informed by thermodynamic approaches, which have to be generalised with respect to their traditional counterparts in order to deal with systems subject to strong random fluctuations. The resulting toolkit of stochastic thermodynamics, in particular the concept of entropy production, gives us a quantitative handle on the degree of "non-equilibriumness" of such stochastic processes. Recently, stochastic thermodynamics has benefitted from cross-contamination with the field-theoretic literature and the techniques developed in the latter for the study of collective behaviour have opened the doors to the thermodynamic characterisation of increasingly complex systems. Starting from minimal mathematical models of single active particles and moving up across scales to the level of morphogenetic processes in real organisms (in particular, the formation of morphogen gradients), this thesis contributes to laying the foundations for a bridge between physical understanding and biological insight. While the focus is here on generic mechanisms and on the development of theoretical tools, the applicability to specific experimental scenarios will be pointed out where relevant.

To Aldo and Paola

Acknowledgments

I am endlessly grateful to the many colleagues and friends who have accompanied and guided me throughout my doctorate, whether by sharing their academic expertise and insight, or simply by offering a empathetic ear in times of need.

To my supervisors, Gunnar and Guillaume, for the invaluable scientific and human advice, and for being excellent examples of how rigour and intellectual integrity can coexist with cheerful curiosity. Much of my current appreciation for what it means to do *good science* I have acquired through my discussions with them, be our meetings held at the Tate Modern café or elsewhere.

To all the members of the Non-equilibrium Systems group at Imperial College and the Theoretical Physics of Biology lab, first at the Francis Crick Institute and later at Unige, in their various iterations over the years, for sharing this journey with me and always making me feel part of a passionate and welcoming community. Special thanks go to Benjamin, Rosalba, Marc and Silvia for the friendship and advice.

To my collaborators at the Epithelial Cell Interactions Laboratory at the Francis Crick Institute: Kristina, Anqi, Gantas and JP, for teaching me so much, for their patience and for their willingness and enthusiasm to engage in the difficult exercise of cross-disciplinary research. To the rest of the group for adopting this stray physicist into their midst and to Maria for giving me my first ever lab tour.

I would also like to thank my present and past scientific collaborators which do not fall into the categories mentioned above: Kim, Ana, Alexander, Malte, Nicholas, Henry and Thibault, as well as the regular attendees of the Imperial Biophysics Journal Club for the many exciting discussions.

None of the research presented in this thesis would have been possible without the financial support of the Francis Crick Insitute, which receives its core funding from Cancer

Research UK, the UK Medical Research Council, and the Wellcome Trust (FC001317).

An especially heartfelt thanks goes to the friends, old and new, that, albeit scattered across the globe, were a close presence through the joys and frustrations of my doctoral studies: Edoardo, Arkin, Kwok Ho, Alexander, Valentina, Malte, Karla and many others.

Last but not least are of course my parents, Paola and Aldo, to whom I owe so much and whose unconditional support I could count on at every step of the way.

Contents

List of figures

7.2 (A) A threshold level of surface density of bound receptors n_B^* determines the boundary of the activation domain (x^*) of a hypothetical downstream target (orange). (B) On/off target boundary (x^*) as a function of the total receptor surface density, in the absence of receptor saturation and ligands in the hemolymph. The activation threshold ($n_B^* = 10$nM. μm) was used to determine x^* for different receptor surface density (dots). A maximal target domain size can be found for intermediate values of the total receptor surface density. (C) Phase diagram of target activation domain size, as a function of total receptor surface density and effective ligand degradation rate in the hemolymph. Receptor saturation is not taken into account. At low receptor density level, no activation occurs; at intermediate receptor density and for low enough degradation in the hemolymph, a region of full activation appears; the third domain of parameter space is that of biologically relevant spatially restricted activation. (D) Phase diagram as described for panel F, but with receptor saturation included. Color code corresponds to the size of the activated domain. 270

7.3 (A) Normalized fluorescent GFP intensity in the Nb^{high} condition (hh-$Nb1^{high}$CD8, green bar) and Nb^{high} overexpression condition (hh-Gal4, UAS-$Nb1^{high}$CD8, orange bar) after ex vivo incubation in a GFP bath. The difference in GFP intensity suggests that (Gal4-mediated) overexpression leads to a $\sim$ 20 fold increase in surface receptor levels. (B) Nb^{high}-expressing discs ($Nb1^{high}$CD8 condition) were saturated with GFP on ice, washed, incubated for different durations and imaged. Normalized GFP intensity in hh- $Nb1^{high}$CD8 wing discs decreased by $\sim$25% over the time course of 6 h. Since GFP is quenched in late endosomes due to a low pH (58), this observation suggests that Nb^{high} is degraded only slowly (on the scale of several hours as predicted by modelling). (C) To estimate the concentration of $Nb1^{high}$CD8 at the cell surface, a GFP invasion assay was used. hh-$Nb1^{high}$CD8 discs were incubated in 2 nM, 20 nM and 200 nM GFP baths for 5 min at 25°C. The resulting basal-to-apical GFP gradient in the posterior compartment was imaged and quantified. (D) A simple model of apico-basal gradient formation. . 274

List of tables

Preface

I can see no other escape from this dilemma (lest our true aim be lost forever) than that some of us should venture to embark on a synthesis of facts and theories, albeit with second-hand and incomplete knowledge of some of them – and at the risk of making fools of ourselves.

E. Schroedinger [251]

This thesis is structured around a selection of the papers that I have published in peer-reviewed journals over the course of my doctoral studies. It also contains material appearing in a paper that is currently under review, as well as other work that is either in progress, in preparation for publication or which was at some point excised from submitted manuscripts for the sake of brevity, see Table 1. Chapters are for the most part self-contained. However, some of the key mathematical machinery used across the thesis is only introduced thoroughly in occasion of its first appearance, while familiarity with these methods is assumed in subsequent chapters.

A glance at the Table of Contents appearing a few pages above will have been sufficient for the reader to realise that the material covered in this thesis spans a fairly vast thematic territory. Although this is to an extent the result of my personal academic trajectory and fortunate position as a member of research groups with very diverse interests, it is also the case that such variety is not uncommon in the work of other researchers who, coming from a mathematical background, have grown interested in the interface between biology and theoretical physics. While "theoretical biophysics" has at this point a long history and a large number of established sub-fields, I have been wondering if this tendency might be a sign that this discipline is yet to reach its maturity and to identify some of its key *principles*. Speculations aside and on a much more modest scale, I have attempted here to contextualise the various pieces of research that make up this thesis within the statistical mechanics (and thermodynamics) of non-equilibrium matter, organising them so as to present a logical progression from toy models up to biologically-relevant models which are heavily inspired by experimental insight.

I have received permission from all rights holders to reproduce third-party copyrighted material. The rights holders are: the journals, if the paper has been published, and the co-authors, if the paper has not yet been published. I have also received permission

from all co-authors by email. See App. A for evidence of the above.

Table 1: Summary of chapters in this thesis, specifying its publication status (published, submitted, accepted or in preparation), reference, whether I wrote the main body of the paper (first author), and the type of reproduction (verbatim, minor modifications, and new sections). Co-first authorship is indicated with a dagger (†) symbol in the relevant column.

Chap.	Ref.	Status	I am first author	Repr.
1	[64]	P: Entropy **22** (11), 1252 (2020)	Yes†	Verb.
2	[6]	P: J. Phys. A Math. Theor. **55** (27) (2022)	Yes†	Verb.
3	[66]	P: Phys. Rev. E **105** (2022)	Yes	New App.
4	[42]	S: arXiv:2205.10409 (2022)	No	New App.
5	[196]	P: Phys. Rev. Res. **2** (2), 023421 (2020)	No	Verb.
6		In preparation	Yes	New
7	[273]	P: Science **370** (6514), 321-327 (2020)	No	Minor mod.
8		In progress	Yes	New

Introduction

Unlike the inert matter that surrounds us, which is to a good approximation either at thermodynamic equilibrium or relaxing thereto when not systematically perturbed by an external force, the type of matter than constitutes the building blocks of biological organisms is intrinsically active in nature, meaning that it is maintained out of equilibrium at all times by a continuous injection of energy at the cellular and subcellular scale [251]. While this energy might be invested into generating biomass and into translating a genetic blueprint into structure during the course of developmental processes, energy conservation requires that, on average, fully formed individuals dissipate a corresponding amount of energy into their environment, albeit in a "degraded" form, typically as heat. In this sense, the popular view that living organisms sustain themselves by "consuming" the energy (or matter) contained in their food is somewhat misleading. Rather, the dynamical steady-state that we call Life evades thermodynamic equilibrium by feeding on the negative entropy [251] of the energy and matter that continuously flows *through* (rather than *into*) it. In fact, the same argument applies to the planet Earth as a whole [158], with the energy coming from the Sun and contributing to sustaining our global ecosystem eventually being released back into space in the form of higher-entropy infrared radiation. It is thus not much of a stretch to picture our planet as a gigantic, composite biological system, as posited e.g. in Lovelock's Gaia hypothesis [183].

These so called *non-equilibrium steady-states* [295] are one subject of study of thermodynamics, which is the branch of physics that investigates the conversion of energy from one form to another, historically with the aim of channelling it into a useful form (e.g. the work output of a steam engine) in some optimal way and to identify any related constraints [74]. Over the last few decades, technological advances in experimental biology have stirred a growing interest in understanding the capabilities and limitations of microscopic living matter from an energetic perspective [306, 17]. In fact, it is only through energetically-costly, genuinely out-of-equilibrium mechanism that fundamen-

tal biological processes can be performed with the required level of precision (think of biochemical clocks [19] or kinetic proofreading in DNA transcription [245]). On the other hand, non-specific subcellular machinery such as molecular motors can operate remarkably close to the maximum efficiency allowed by the laws of physics [14, 222].

The theoretical interest in how such microscopic biological process are evolved in, controlled and "budgeted" by living organisms must soon be faced with the difficulty that the tool-kit of traditional thermodynamics is unsuitable to be applied in situations where environmental fluctuations play a prominent role. This becomes increasingly the case as the characteristic energy scale of the process approaches the thermal scale k_BT (corresponding approximately to 4.11×10^{-21} J or 25.7 meV at room temperature), the typical example being the Brownian motion induced by the coupling of microscopic particles with a fluid [89]. For comparison, dephosphorylation of ATP, one of the key currencies of intracellular energy transfer, into ADP releases about 500 meV. The subfield of stochastic thermodynamics addresses precisely this difficulty by generalising the notions of traditional thermodynamics to stochastic processes [256, 220]. The resulting physical laws are often probabilistic in nature, e.g. the second law of thermodynamics turns into a statement about the non-negativity of the *average* entropy production, while transients of negative entropy production are in principle allowed. Furthermore, the inclusion of stochastic fluctuations "around" the deterministic average system trajectory led to the discovery of fascinating principles, such as the thermodynamic uncertainty relation [18] (TUR), relating the precision and energetic cost of non-equilibrium processes.

Entropy production, generalised to a single stochastic trajectory [254], plays a key role in stochastic thermodynamics by connecting thermal dissipation, and thus the energetic cost of maintaining a system out of equilibrium, with time-reversal symmetry breaking and the arrow of time . In particular, it was shown for Markov (memory-less) processes that the "distinguishability" of forward- and reverse-time trajectories increases in time proportionally to the rate of entropy production [113]. A direct computation of the entropy production for a given process relies on our ability to resolve its dynamics in full microscopic detail. While this is achievable for simple toy models (see Chapter 1 for various examples), more complex models, e.g. those involving multiple interacting active units (active matter [23]), quickly become intractable with increasing system size. For this reason, continuum models, in particular field theories, have been invoked

in the past to describe the effective dynamics of these systems at a mesoscopic scale and path-integral methods have been designed to estimate the entropy production of the resulting theory [202, 53]. This has been a somewhat controversial approach, in part because the effect of coarse-graining on the connection between dissipation and time-reversal symmetry is an open problem [91, 59, 280], and more specifically because the loss of 'single particle entity' is suspected to have important consequences on the final result [111]. Both of these problems are addressed in this thesis, the first by developing a theory for the scaling of the mesoscopic entropy production under phase-space coarse graining (Chapter 3), and the second by presenting the first, to the best of our knowledge, formalisation and systematic study of the concept of point-particle entity in the context of statistical field theory (Chapter 4).

While technically challenging, the application of thermodynamic approaches to increasingly complex models paves the way to a deeper understanding of many fascinating biological processes that emerge at the mesoscopic scale from many-agent interactions. One such generic mechanism of Life is morphogenesis , namely the specification of an organism's body plan through conformational changes and local differentiation, typically driven by a combination of spontaneous self-organisation and external cues. Many morphogenetic processes are orchestrated through inter-cellular signalling, often mediated by specialised secreted molecules known as morphogens [288] . After being released by a localised patch of 'source' cells, morphogens typically spread over tissue-scale distances to form non-homogeneous concentration profiles (gradients), which are eventually decoded by individual cells to extract positional information [274, 85]. Both the generation of such gradients and their interpretation are out of equilibrium processes and can in principle be studied through the lens of active matter physics. A prerequisite to do so, however, is to develop a reliable microscopic theory of how these process occur *in vivo*, e.g. how morphogens actually spread and are internalised by receiving cells (which turns out to be a fairly controversial topic, see Chapter 7). We will also see in Chapter 8 that information processing at the single agent level has non-trivial thermodynamic implications and argue how expanding the toolkit of stochastic thermodynamics in this direction might offer a point of contact between minimal models and biologically relevant mechanisms.

Outline of the thesis

The chapters making up this thesis all deal with the statistical mechanics and dynamics of non-equilibrium matter, albeit from different perspectives (stochastic thermodynamics, path-integral techniques in stochastic processes, continuum models of developmental processes). Chapter 1 opens with a pedagogical review of entropy production in analytically tractable models and introduces many of the techniques and concepts invoked in subsequent Chapters. Chapter 2 then focuses on the thermodynamics of passive Brownian dynamics driven away from equilibrium by a fluctuating external potential, with non-trivial implications e.g. for realistic stochastic resetting and optical manipulation of colloids. As anticipated in the introduction, Chapter 3 and 4 address two difficulties arising when applying the toolkit of stochastic thermodynamics to coarse-grained models, namely the determination of the scaling of the mesoscopic entropy production as a function of the coarse-graining block size, and the importance for continuum approaches to preserve point-particle entity. Interestingly, we find in Chapter 3 that the exponent controlling the algebraic scaling of the mesoscopic entropy production per mesostate can take either sign depending on the microscopic features of the underlying process, thus suggesting a criterion to distinguish between equilibrium-like and genuinely non-equilibrium processes. In Chapter 5 and 6, after having introduced the Coupon Collector Problem and its generalisation to the case of dynamically accelerated protocols, we demonstrate that the Doi-Peliti formalism (one of the two field-theoretic formalisms possessing particle entity introduced in Chapter 4) can be utilised to address probabilistic problems involving aging and extreme value statistics. In doing so, we contribute to a growing body of literature aiming at applying this formalism to increasingly complex setups, often in the context of active matter. Finally, in Chapter 7, we take the long step into the realm of mesoscopic models of morphogenetic signalling in developing tissues and present a theory of morphogen gradient formation with leakage and multiple co-receptor interactions. This theory constitutes the mathematical backbone for the analysis of the experimental results appearing in [273], most of which are however excluded from the Chapter for the sake of brevity as well as thematic coherence with the rest of the thesis. In Chapter 8, we discussion of how the gap between analytically tractable and biologically relevant models could be bridged, at least in some regards, through the systematic study of information processing in "adaptive" active matter. A brief summary of the work presented in this thesis and outlook for future research

concludes the thesis.

Each chapter starts with its title, the list of authors who contributed to the work (as well as their contributions) and the full citation reference of the corresponding article, where applicable. A brief overview to contextualise the chapter within the whole of this thesis and to provide further background when required (e.g. a brief introduction to *Drosophila* wing disc development in Chapter 7) follows. This overview also works a summary of the key ideas discussed in the chapter aimed at the non-technical reader.

The meaning of *I* and *we* should be clear by the context throughout.

1

Entropy Production in Exactly Solvable Systems

L. Cocconi†, R. Garcia-Millan†, Z. Zhen, B. Buturca, G. Pruessner

Entropy **22**, 1252 (2020) [64]
Published 3 November 2020
DOI 10.3390/e22111252

Overview All genuinely non-equilibrium processes, i.e. processes that exhibit motion and flows at steady-state even in the presence of dissipative forces such as friction, need to be sustained by a continuous input of energy [74]. Assuming that energy cannot accumulate indefinitely in the internal degrees of freedom of the system, the former will eventually be released back into the surrounding environment, typically in a "less useful" form, such as heat or waste material. This degradation of energy (and, as it turns out, information) is captured quantitatively by the *entropy production* of the system, which constitutes a key concept in non-equilibrium thermodynamics. It is a fundamental principle in thermodynamics that the entropy of an isolated system should *on average* not decrease over time; this is known as the second law of thermodynamics. However, the connection between entropy production and the arrow of time runs even

deeper, as it can be proven under fairly general assumptions that the former measures the typical 'distinguishability' between recordings of a given process played in forward vs reverse time [113]. In this Chapter, we review the mathematical tool-kit of entropy production in the context of stochastic thermodynamics and calculate it in closed form for a number of paradigmatic, minimal models. While these models are often an extreme simplification compared to their real-life counterparts, they nevertheless allow us to isolate important aspects of this theory for closer inspection without having to resort to approximations or numerical techniques.

Author contributions: LC wrote the first original draft of the review section. All authors contributed to the formal analysis: BB calculated the entropy production (EP) for the two- and three- state Markov process; LC calculate the EP for N independent processes (distinguishable, indistinguishable two-state, indistinguishable d-state) and the switching diffusion process on a ring; RGM calculated the EP for a random walk on a (ring) lattice and for run-and-tumble motion with diffusion on a ring; ZZ calculated the EP for driven Brownian particles. GP supervised the project and edited the original draft of the manuscript.

Abstract

The rate of entropy production by a stochastic process quantifies how far it is from thermodynamic equilibrium. Equivalently, entropy production captures the degree to which detailed balance and time-reversal symmetry are broken. Despite abundant references to entropy production in the literature and its many applications in the study of non-equilibrium stochastic particle systems, a comprehensive list of typical examples illustrating the fundamentals of entropy production is lacking. Here, we present a brief, self-contained review of entropy production and calculate it from first principles in a catalogue of exactly solvable setups, encompassing both discrete- and continuous-state Markov processes, as well as single- and multiple-particle systems. The examples covered in this work provide a stepping stone for further studies on entropy production of more complex systems, such as many-particle active matter, as well as a benchmark for the development of alternative mathematical formalisms.

1.1 Introduction

Stochastic thermodynamics has progressively evolved into an essential tool in the study of non-equilibrium systems as it connects the quantities of interest in traditional thermodynamics, such as work, heat and entropy, to the properties of microscopically-resolved fluctuating trajectories [256, 149, 257]. The possibility of equipping stochastic processes with a consistent thermodynamic and information-theoretic interpretation has resulted in a number of fascinating works, with the interface between mathematical physics and the biological sciences proving to be a particularly fertile ground for new insights (e.g. [17, 167, 54, 246, 223]). The fact that most of the applications live on the small scale is not surprising, since it is precisely at the microscopic scale that fluctuations start to play a non-negligible rôle.

The concept of entropy and, more specifically, entropy production has attracted particular interest, as a consequence of the quantitative handle it provides on the distinction between equilibrium systems, passive systems relaxing to equilibrium and genuinely non-equilibrium, 'active' systems. While there exist multiple routes to the mathematical formulation of entropy production [248, 185, 113, 254, 202, 169], the underlying physical picture is consistent: the entropy production associated with an ensemble of stochastic trajectories quantifies the degree of certainty with which we can assert that a particular event originates from a given stochastic process or from its suitably defined conjugate (usually, its time-reverse). When averaged over long times (or over an ensemble), a non-vanishing entropy production signals time-reversal symmetry breaking at the microscopic scale. This implies, at least for Markovian systems, the existence of steady-state probability currents in the state space, which change sign under time-reversal. When a thermodynamically consistent description is available, the average rate of entropy production can be related to the rate of energy or information exchange between the system, the heat bath(s) it is connected to, and any other thermodynamic entity involved in the dynamics, such as a measuring device [201, 182, 213]. Whilst the rate of energy dissipation is of immediate interest since it captures how 'costly' it is to sustain specific dynamics (e.g. the metabolism sustaining the development of an organism [237, 270]), entropy production has also been found to relate non-trivially to the efficiency and precision of the corresponding process via uncertainty relations [141, 258]. Entropy production along fluctuating trajectories also plays a fundamental

rôle in the formulation of various fluctuation theorems [254].

Given the recent interest in stochastic thermodynamics and entropy production in particular, as well as the increasing number of mathematical techniques implemented for the quantification of the latter, it is essential to have available a few, well-understood reference systems, for which exact results are known. These can play the rôle of benchmarks for new techniques, while helping neophytes to develop intuition. In this work, we will present results exclusively in the framework proposed by Gaspard [113], specifically in the form of Eqs. (1.4), (1.14) and (1.15), which we review and contextualise by deriving them via different routes in Section 1.2. In Section 1.3 we begin the analysis with processes in discrete state space (Sections 1.3.1-1.3.8), and subsequently extend it to the continuous case (Sections 1.3.9-1.3.11). Finally, in sections 1.3.12 and 1.3.13 we consider processes that involve both discrete and continuous degrees of freedom. Time is taken as a continuous variable throughout.

1.2 Brief review of entropy production

Entropy production of jump processes. The concept of time-dependent informational entropy associated with a given ensemble of stochastic processes was first introduced by Shannon [261]. For an arbitrary probability mass function $P_n(t)$ of time t over a discrete set of states $n \in \Omega$, the Shannon entropy is defined as

$$S(t) = -\sum_n P_n(t) \ln P_n(t) \tag{1.1}$$

with the convention henceforth of $x \ln x = 0$ for $x = 0$. It quantifies the inherent degree of uncertainty about the state of a process. In the microcanonical ensemble P_n is constant in t and n and upon providing an entropy scale in the form of the Boltzmann constant k_B, Shannon's entropy reduces to that of traditional thermodynamics given by Boltzmann's $S = k_B \ln |\Omega|$, where $|\Omega| = 1/P_n$ is the cardinality of Ω. In Markovian systems, the probability $P_n(t)$ depends on n and evolves in time t according to the master equation

$$\dot{P}_n(t) = \sum_m P_m(t) w_{mn} - P_n(t) w_{nm} \tag{1.2}$$

with non-negative transition rates w_{mn} from state m to state $n \neq m$. Eq. (1.2) reduces to $\dot{P}_n(t) = \sum_m P_m(t) w_{mn}$ by imposing the Markov condition $\sum_m w_{nm} = 0$, which we will use in the following. For simplicity we will restrict ourselves to time-independent rates w_{nm} but as far as the following discussion is concerned, generalising to time-dependent rates is a matter of replacing w_{nm} by $w_{nm}(t)$. The rate of change of entropy for a continuous time jump process can be derived by differentiating $S(t)$ in Eq. (1.1) with respect to time and substituting (1.2) into the resulting expression [113, 92], thus obtaining

$$\dot{S}(t) = -\sum_{m,n} P_m(t) w_{mn} \ln\left(P_n(t)\right) = \sum_{m,n} P_n(t) w_{nm} \ln\left(\frac{P_n(t)}{P_m(t)}\right) = \dot{S}_e(t) + \dot{S}_i(t) \tag{1.3}$$

where we define

$$\begin{aligned}
\dot{S}_e(t) &= -\frac{1}{2}\sum_{m,n} \left(P_n(t) w_{nm} - P_m(t) w_{mn}\right) \ln\left(\frac{w_{nm}}{w_{mn}}\right) && \text{(1.4a)} \\
&= -\sum_{m,n} P_n(t) w_{nm} \ln\left(\frac{w_{nm}}{w_{mn}}\right) = -\sum_{m,n} \left(P_n(t) w_{nm} - P_m(t) w_{mn}\right) \ln\left(\frac{w_{nm}}{w_0}\right) \\
\dot{S}_i(t) &= \frac{1}{2}\sum_{m,n} \left(P_n(t) w_{nm} - P_m(t) w_{mn}\right) \ln\left(\frac{P_n(t) w_{nm}}{P_m(t) w_{mn}}\right) && \text{(1.4b)} \\
&= \sum_{m,n} P_n(t) w_{nm} \ln\left(\frac{P_n(t) w_{nm}}{P_m(t) w_{mn}}\right) = \sum_{m,n} \left(P_n(t) w_{nm} - P_m(t) w_{mn}\right) \ln\left(\frac{P_n(t) w_{nm}}{w_0}\right)
\end{aligned}$$

with arbitrary positive rate w_0 to restore dimensional consistency, that cancel trivially. Here we follow the convention [256] to split the rate of entropy change into two contributions: the first, Eq. (1.4a), commonly referred to as “external" entropy production or entropy flow, is denoted by $\dot{S}_e$. It contains a factor $\ln(w_{nm}/w_{mn})$ corresponding, for systems satisfying local detailed balance , to the net change in entropy of the reservoir(s) associated with the system's transition from state n to state m. For such thermal systems, $\dot{S}_e$ can thus be identified as the rate of entropy production in the environment [173, 248]. The second contribution, Eq. (1.4b), termed “internal" entropy production and denoted by $\dot{S}_i$ is non-negative because $(x-y)\ln(x/y) \geq 0$ for any two real, positive x, y and using the convention $z \ln z = 0$ for $z = 0$. The internal entropy production vanishes when the detailed balance condition $P_n(t) w_{nm} = P_m(t) w_{mn}$ is satisfied for all pairs of states. In this sense, a non-vanishing $\dot{S}_i$ is the fingerprint of non-equilibrium

phenomena. At steady-state, namely when $\dot{P}_n(t) = 0$ for all n, $\dot{S}(t)$ in Eq. (1.3) vanishes by construction, so that the internal and external contributions to the entropy production cancel each other exactly, $\dot{S}(t) = \dot{S}_e(t) + \dot{S}_i(t) = 0$, while they vanish individually only for systems at equilibrium. Equations (1.4) will be used throughout the present work to compute the entropy productions of discrete-state processes.

Entropy production as a measure of time-reversal-symmetry breaking. As it turns out, a deeper connection between internal entropy production and time-reversal symmetry breaking can be established [113]. The result, which we re-derive below, identifies $\dot{S}_i$ as the relative dynamical entropy (*i.e.* the Kullback-Leibler divergence [163]) per unit time of the ensemble of forward paths and their time-reversed counterparts. To see this, we first need to define a path $\mathbf{n} = (n_0, n_1, \ldots, n_M)$ as a set of trajectories starting at time t_0 and visiting states n_j at successive discrete times $t_j = t_0 + j\tau$ with $j = 0, 1, \ldots, M$, equally spaced by a time interval τ. For a time-homogeneous Markovian jump process in continuous time, the joint probability of observing a particular path is

$$\mathcal{P}(\mathbf{n}; t_0, M\tau) = P_{n_0}(t_0) W(n_0 \to n_1; \tau) W(n_1 \to n_2; \tau) \ldots W(n_{M-1} \to n_M; \tau) \tag{1.5}$$

where $P_{n_0}(t_0)$ is the probability of observing the system in state n_0 at time t_0, while $W(n_j \to n_{j+1}; \tau)$ is the probability that the system is in state n_{j+1} time τ after being in state n_j. This probability can be expressed in terms of the transition rate matrix w with elements w_{mn}. It is $W(n \to m; \tau) = [\exp(w\tau)]_{nm}$, the matrix elements of the exponential of the matrix $w\tau$ with the Markov condition imposed. It can be expanded in small τ as

$$W(n \to m; \tau) = \delta_{n,m} + w_{nm}\tau + O(\tau^2) \ , \tag{1.6}$$

where $\delta_{n,m}$ is the Kronecker-δ function. We can now define a dynamical entropy per unit time [261] as

$$h(t_0, \Delta t) = \lim_{M \to \infty} -\frac{1}{\Delta t} \sum_{n_0, \ldots, n_M} \mathcal{P}(\mathbf{n}; t_0, \Delta t) \ln \mathcal{P}(\mathbf{n}; t_0, \Delta t) \ . \tag{1.7}$$

where the limit is to be considered a continuous time limit taken at fixed $\Delta t = t_M - t_0 = M\tau$ [78], thus determining the sampling interval τ, and the sum runs over all possible paths $\mathbf{n}$. Other than τ, the paths are the only quantity on the right-hand side of

Eq. (1.7) that depend on M. The dynamical entropy $h(t_0, \Delta t)$ may be considered the expectation of $\ln(\mathcal{P}(\mathbf{n}; t_0, \Delta t))$ across all paths. Similarly to the static Shannon entropy, the dynamical entropy $h(t_0, \Delta t)$ quantifies the inherent degree of uncertainty about the evolution over a time Δt of a process starting at a given time t_0. To compare with the dynamics as observed under time-reversal, one introduces the time-reversed path $\mathbf{n}^R = (n_M, n_{M-1}, \ldots, n_0)$ and thus the time-reversed dynamical entropy per unit time as

$$h^R(t_0, \Delta t) = \lim_{M\to\infty} -\frac{1}{\Delta t} \sum_{n_0,\ldots,n_M} \mathcal{P}(\mathbf{n}; t_0, \Delta t) \ln \mathcal{P}(\mathbf{n}^R; t_0, \Delta t) \ . \tag{1.8}$$

While similar in spirit to $h(t_0, \Delta t)$, the physical interpretation of $h^R(t_0, \Delta t)$ as the expectation of $\ln\big(\mathcal{P}(\mathbf{n}^R; \Delta t)\big)$ under the forward probability $\mathcal{P}(\mathbf{n}; t_0, \Delta t)$ is more convoluted since it involves the forward and the backward paths simultaneously, which have potentially different statistics. However, time-reversal symmetry implies precisely identical statistics of the two ensembles, whence $h(t_0, \Delta t) = h^R(t_0, \Delta t)$. The motivation for introducing $h^R(t_0, \Delta t)$ is that the difference of the two dynamical entropies defined above is a non-negative Kullback-Leibler divergence given by

$$h^R(t_0, \Delta t) - h(t_0, \Delta t) = \lim_{M\to\infty} \frac{1}{\Delta t} \sum_{\mathbf{n}} \mathcal{P}(\mathbf{n}; t_0, \Delta t) \ln \left(\frac{\mathcal{P}(\mathbf{n}; t_0, \Delta t)}{\mathcal{P}(\mathbf{n}^R; t_0, \Delta t)} \right) \ . \tag{1.9}$$

Using Eq. (1.5) in (1.9) with Eq. (1.6) provides the expansion

$$h^R(t_0, \Delta t) - h(t_0, \Delta t) = \sum_{nm} P_n(t_0) w_{nm} \ln \left(\frac{P_n(t_0) w_{nm}}{P_m(t_0) w_{mn}} \right) + \mathcal{O}(\Delta t) \ , \tag{1.10}$$

which is an instantaneous measure of the Kullback-Leibler divergence. The limit of $h^R(t_0, \Delta t) - h(t_0, \Delta t)$ in small Δt is finite and identical to the internal entropy production (1.4b) derived above. This result establishes the profound connection between broken detailed balance, Eq. (1.4), and Kullback-Leibler divergence, Eq. (1.10), both of which can thus be recognised as fingerprints of non-equilibrium systems. In light of this connection, it might not come as a surprise that the steady-state rate of entropy production is inversely proportional to the minimal time needed to decide on the direction of the arrow of time [238].

Entropy production for continuous degrees of freedom. The results above were obtained

for Markov jump processes within a discrete state space. However, the decomposition of the rate of change of entropy in Eq. (1.3) into internal and external contributions can be readily generalised to Markovian processes with continuous degrees of freedom, for example a spatial coordinate. For simplicity we will restrict ourselves to processes in one dimension but as far as the following discussion is concerned, generalising to higher dimensions is a matter of replacing spatial derivatives and integrals over the spatial coordinate with their higher dimensional counterparts. The dynamics of such a process with probability density $P(x,t)$ to find it at x at time t are captured by a Fokker-Planck equation of the form $\dot{P}(x,t) = -\partial_x j(x,t)$, with j the probability current, augmented by an initial condition $P(x,0)$. Starting from the Gibbs-Shannon's entropy for a continuous random variable $S(t) = -\int \mathrm{d}x\, P(x,t) \ln(P(x,t)/P_0)$ with some arbitrary density scale P_0 for dimensional consistency, we differentiate with respect to time and substitute $-\partial_x j(x,t)$ for $\dot{P}(x,t)$ to obtain

$$\dot{S}(t) = -\int \mathrm{d}x\, \dot{P}(x,t) \ln\left(\frac{P(x,t)}{P_0}\right) = -\int \mathrm{d}x\, \frac{(\partial_x P(x,t)) j(x,t)}{P(x,t)} \;, \tag{1.11}$$

where the second equality follows upon integration by parts using $\int \mathrm{d}x\, \dot{P}(x,t) = 0$ by normalisation. For the paradigmatic case of an overdamped colloidal particle, which will be discussed in more detail below (Secs. 1.3.9 – 1.3.11), the probability current is given by $j(x,t) = -D\partial_x P(x,t) + \mu F(x,t) P(x,t)$ with local, time-dependent force $F(x,t)$. We can then decompose the entropy production $\dot{S}(t) = \dot{S}_i(t) + \dot{S}_e(t)$ into internal and external contributions as

$$\dot{S}_i(t) = \int \mathrm{d}x\, \frac{j(x,t)^2}{DP(x,t)} \geq 0 \tag{1.12}$$

and

$$\dot{S}_e(t) = -\int \mathrm{d}x\, \frac{\mu}{D} F(x,t) j(x,t) \;, \tag{1.13}$$

respectively. The Kullback-Leibler divergence between the densities of forward and time-reversed paths can be calculated as outlined above for discrete state systems, thus

producing an alternative expression for the internal entropy production in the form

$$\begin{aligned}
&\dot{S}_i(t) \\
&= \lim_{\Delta t \to 0} h^R(t, \Delta t) - h(t, \Delta t) \\
&= \lim_{\tau \to 0} \frac{1}{2\tau} \int \mathrm{d}x \mathrm{d}x' \left(P(x,t) W(x \to x', \tau) - P(x',t) W(x' \to x, \tau) \right) \ln \frac{P(x,t) W(x \to x', \tau)}{P(x',t) W(x' \to x, \tau)} \, .
\end{aligned} \tag{1.14}$$

Here we have introduced the propagator $W(x' \to x, \tau)$, the probability density that a system observed in state x' will be found at x time τ later. In general, here and above, the density $W(x \to x', \tau)$ depends on the absolute time t, which we have omitted here for better readability. The corresponding expression for the entropy flow is obtained by substituting (1.14) into the balance equation $\dot{S}_e(t) = \dot{S}(t) - \dot{S}_i(t)$, whence

$$\dot{S}_e(t) = - \lim_{\tau \to 0} \frac{1}{2\tau} \int \mathrm{d}x \mathrm{d}x' \left(P(x,t) W(x \to x', \tau) - P(x',t) W(x' \to x, \tau) \right) \ln \frac{W(x' \to x, \tau)}{W(x \to x', \tau)} \, . \tag{1.15}$$

Since $\lim_{\tau \to 0} W(x \to x', \tau) = \delta(x - x')$ [300] and $P(x,t)\delta(x - x') = P(x',t)\delta(x' - x)$ the factor in front of the logarithm in (1.14) and (1.15) vanishes in the limit of small τ, $\lim_{\tau \to 0} P(x,t) W(x \to x'; \tau) - P(x',t) W(x' \to x; \tau) = 0$. Together with the prefactor $1/\tau$ this necessitates the use of L'Hôpital's rule

$$\begin{aligned}
&\lim_{\tau \to 0} \frac{1}{\tau} \left(P(x,t) W(x \to x'; \tau) - P(x',t) W(x' \to x; \tau) \right) \\
&= P(x,t) \dot{W}(x \to x') - P(x',t) \dot{W}(x' \to x)
\end{aligned} \tag{1.16}$$

where we used the shorthand

$$\dot{W}(x \to x') := \lim_{\tau \to 0} \frac{\mathrm{d}}{\mathrm{d}\tau} W(x \to x'; \tau) \, , \tag{1.17}$$

which is generally given by the Fokker-Planck equation of the process, so that

$$\dot{P}(x,t) = \int \mathrm{d}x' \, P(x',t) \dot{W}(x' \to x) \, . \tag{1.18}$$

In the continuum processes considered below, in particular Sec. 1.3.11, 1.3.12 and 1.3.13, $\dot{W}(x \to x')$ is a kernel in the form of Dirac δ-functions and derivatives thereof, acting

under the integral as the adjoint Fokker-Planck operator on $P(x,t)$. With Eq. (1.16) the internal entropy production of a continuous process (1.14) may conveniently be written as

$$\begin{aligned}
&\dot{S}_i(t) \\
&= \frac{1}{2}\int \mathrm{d}x\mathrm{d}x' \left(P(x,t)\dot{W}(x\to x') - P(x',t)\dot{W}(x'\to x)\right) \times \lim_{\tau\to 0} \ln\left(\frac{P(x,t)W(x\to x';\tau)}{P(x',t)W(x'\to x;\tau)}\right) && \text{(1.19a)} \\
&= \int \mathrm{d}x\mathrm{d}x'\, P(x,t)\dot{W}(x\to x') \times \lim_{\tau\to 0} \ln\left(\frac{P(x,t)W(x\to x';\tau)}{P(x',t)W(x'\to x;\tau)}\right) && \text{(1.19b)} \\
&= \int \mathrm{d}x\mathrm{d}x' \left(P(x,t)\dot{W}(x\to x') - P(x',t)\dot{W}(x'\to x)\right) \times \lim_{\tau\to 0} \ln\left(\frac{P(x,t)W(x\to x';\tau)}{W_0 P_0}\right) && \text{(1.19c)}
\end{aligned}$$

with suitable constants W_0 and P_0. Correspondingly, the (external) entropy flow (1.15) is

$$\begin{aligned}
&\dot{S}_e(t) \\
&= -\frac{1}{2}\int \mathrm{d}x\mathrm{d}x' \left(P(x,t)\dot{W}(x\to x') - P(x',t)\dot{W}(x'\to x)\right) \times \lim_{\tau\to 0} \ln\left(\frac{W(x\to x';\tau)}{W(x'\to x;\tau)}\right) && \text{(1.20a)} \\
&= -\int \mathrm{d}x\mathrm{d}x'\, P(x,t)\dot{W}(x\to x') \times \lim_{\tau\to 0} \ln\left(\frac{W(x\to x';\tau)}{W(x'\to x;\tau)}\right) && \text{(1.20b)} \\
&= -\int \mathrm{d}x\mathrm{d}x' \left(P(x,t)\dot{W}(x\to x') - P(x',t)\dot{W}(x'\to x)\right) \times \lim_{\tau\to 0} \ln\left(\frac{W(x\to x';\tau)}{W_0}\right). && \text{(1.20c)}
\end{aligned}$$

All of these expressions assume that the limits of the logarithms exist. Naively replacing them by $\ln(\delta(x-x')/\delta(x'-x))$ produces a meaningless expression with a Dirac δ-function in the denominator. Eqs. (1.19) and (1.20) are identically obtained in the same manner as Eqs. (1.4) with the master Eq. (1.2) replaced by the Fokker-Planck Eq. (1.18). All of these expressions, Eq. (1.4), (1.19) and (1.20), may thus be seen as Gaspard's [113] framework.

Langevin description and stochastic entropy. We have seen in Eqs. (1.12) and (1.13)

how the notion of entropy production can be extended to continuous degrees of freedom by means of a Fokker-Planck description of the stochastic dynamics. The Fokker-Planck equation is a deterministic equation for the probability density and thus provides a description at the level of ensembles, rather than single fluctuating trajectories. A complementary description can be provided by means of a Langevin equation of motion, which is instead a stochastic differential equation for the continuous degree of freedom [218]. The presence of an explicit noise term, which usually represents faster degrees of freedom or fluctuations induced by the contact with a heat reservoir, allows for a clearer thermodynamic interpretation. A paradigmatic example is that of the overdamped colloidal particle mentioned above, whose dynamics are described by

$$\dot{x}(t) = \mu F(x,t) + \zeta(t) \tag{1.21}$$

with μ a mobility, $F(x,t)$ a generic force and $\zeta(t)$ a white noise term with covariance $\langle \zeta(t)\zeta(t')\rangle = 2D\delta(t-t')$. For one-dimensional motion on the real line, the force $F(x,t)$ can always be written as the gradient of a potential $V(x,t)$, namely $F(x,t) = -\partial_x V(x,t)$, so that it is conservative. For time-independent, stable potentials, $V(x,t) = V(x)$, this leads at long times to an equilibrium steady-state. This property does not hold in higher dimensions and for different boundary conditions (e.g. periodic), in which case the force $\mathbf{F}(\mathbf{x},t)$ need not have a corresponding potential $V(\mathbf{x},t)$ for which $\mathbf{F}(\mathbf{x},t) = -\nabla V(\mathbf{x},t)$ [295].

The concept of entropy is traditionally introduced at the level of ensembles. However, due to its rôle in fluctuation theorems [256, 173], a consistent definition at the level of single trajectories is required. This can be constructed along the lines of [254] by positing the trajectory-dependent entropy $S(x^*(t),t)$ where $x^*(t)$ is a random trajectory as given by Eq. (1.21) and

$$S(x,t) = -\ln(P(x,t)/P_0)\ . \tag{1.22}$$

Here $P(x,t)$ denotes the probability density of finding a particle at position x at time t as introduced above and P_0 is a scale as used above to maintain dimensional consistency. Given that $x^*(t)$ is a random variable, so is $S(x^*(t),t)$, which may be regarded as an

instantaneous entropy. Taking the total derivative with respect to t produces

$$\begin{aligned}\frac{\mathrm{d}}{\mathrm{d}t}S(x^*(t),t) &= -\left.\frac{\partial_t P(x,t)}{P(x,t)}\right|_{x=x^*(t)} - \left.\frac{\partial_x P(x,t)}{P(x,t)}\right|_{x=x^*(t)} \circ \dot{x}^*(t) \\ &= -\left.\frac{\partial_t P(x,t)}{P(x,t)}\right|_{x=x^*(t)} + \frac{j(x^*(t),t)}{DP(x^*(t),t)} \circ \dot{x}^*(t) - \frac{\mu}{D}F(x^*(t),t) \circ \dot{x}^*(t)\end{aligned} \tag{1.23}$$

where we have used the processes' Fokker-Planck equation $\partial_t P(x,t) = -\partial_x j(x,t)$ with $j(x,t) = \mu F(x,t)P(x,t) - D\partial_x P(x,t)$. The total time derivative has been taken as a conventional derivative implying the Stratonovich convention indicated by $\circ$, which will become relevant below. The term in (1.23) containing $\partial_t P(x,t)$ accounts for changes in the probability density due to its temporal evolution, such as relaxation to a steady state, and any time-dependent driving protocol. The product $F(x^*(t),t) \circ \dot{x}^*(t)$ can be interpreted as a power expended by the force and in the absence of an internal energy of the particle, dissipated in the medium. With Einstein's relation defining the temperature of $T = D/\mu$ of the medium, the last term may be written as

$$\dot{S}_m(t) = \frac{F(x^*(t),t) \circ \dot{x}^*(t)}{T} \tag{1.24}$$

and thus interpreted as the entropy change in the medium. Together with the entropy change of the particle, this gives the total entropy change of particle and medium,

$$\dot{S}_{\mathrm{tot}}(t) = \frac{\mathrm{d}}{\mathrm{d}t}S(x^*(t),t) + \dot{S}_m(t) = -\left.\frac{\partial_t P(x,t)}{P(x,t)}\right|_{x=x^*(t)} + \frac{j(x^*(t),t)}{DP(x^*(t),t)} \circ \dot{x}^*(t)\,, \tag{1.25}$$

which is a random variable, as it depends on the position $x^*(t)$. It also draws on $P(x,t)$ and $j(x,t)$ which are properties of the ensemble. To make the connection to the entropies constructed above we need to take an ensemble average of the instantaneous $\dot{S}_{\mathrm{tot}}(t)$. To do so, we need an interpretation of the last term of (1.25), where the noise $\zeta(t)$ of $\dot{x}^*(t)$, Eq. (1.21), multiplies $j(x^*(t),t)/P(x^*(t),t)$. Equivalently, we need the joint density $P(x,\dot{x};t)$ of position x and velocity $\dot{x}$ at time t. In the spirit of Ito this density trivially factorises into a normally distributed $\dot{x} - \mu F(x,t)$ and $P(x,t)$ as the increment $\dot{x}dt$ on the basis of (1.21) depends only on the particle's current position $x(t)$. However, this is not so in the Stratonovich interpretation of $P(x,\dot{x};t)$, as here the

increment depends equally on $x(t)$ and $x(t+dt)$ [256, 255, 224]. Taking the ensemble average of $\dot{S}_{\mathrm{tot}}$ thus produces

$$\begin{aligned}\langle \dot{S}_{\mathrm{tot}}(t)\rangle &= \int \mathrm{d}x^* \mathrm{d}\dot{x}^*\, \dot{S}_{\mathrm{tot}}(t) P(x^*,\dot{x}^*;t) \\ &= -\int \mathrm{d}x^*\, \frac{\partial_t P(x^*,t)}{P(x^*,t)} \int \mathrm{d}\dot{x}^*\, P(x^*,\dot{x}^*;t) + \int \mathrm{d}x^* \mathrm{d}\dot{x}^*\, \frac{j(x^*,t)}{DP(x^*,t)} \dot{x}^* P(x^*,\dot{x}^*;t)\,,\end{aligned} \tag{1.26}$$

where x^* and $\dot{x}^*$ are now dummy variables. The first term on the right hand side vanishes, because $P(x^*,t) = \int \mathrm{d}\dot{x}^*\, P(x^*,\dot{x}^*;t)$ is the marginal of $P(x^*,\dot{x}^*;t)$ and $\int \mathrm{d}x^*\, \partial_t P(x^*,t) = 0$ by normalisation. The integral over $\dot{x}^*$ in the second term produces the expected particle velocity conditional to its position,

$$\langle \dot{x}^* | x^*, t\rangle = \int \mathrm{d}\dot{x}^*\, \dot{x}^* \frac{P(x^*,\dot{x}^*;t)}{P(x^*,t)} \tag{1.27}$$

in the Stratonovich sense, where it gives rise to the current [254], $\langle \dot{x}^* | x^*, t\rangle = j(x^*,t)/P(x^*,t)$, so that

$$\langle \dot{S}_{\mathrm{tot}}(t)\rangle = \int \mathrm{d}x^*\, \frac{j^2(x^*,t)}{DP(x^*,t)} \geq 0\,, \tag{1.28}$$

which vanishes only in the absence of any probability current, *i.e.* in thermodynamic equilibrium. In the Ito sense, the conditional expectation (1.27) would have instead given rise to the ensemble-independent drift, $\langle \dot{x}^* | x^*, t\rangle = \mu F(x^*,t)$. Comparing to Eq. (1.12), the expectation $\langle \dot{S}_{\mathrm{tot}}(t)\rangle$ turns out to be the internal entropy production $\dot{S}_i(t)$, so that $\dot{S}_{\mathrm{tot}}(t)$ of Eq. (1.25) may be regarded as its instantaneous counterpart.

Path integral methods. An interesting aspect of working with the Langevin description is the possibility of casting probability densities $p([x];t)$ for paths $x(t')$ with $t' \in [0,t]$ into path integrals, for example in the Onsager-Machlup formalism [211, 289]. For the colloidal particle introduced in (1.21), it gives $p([x];t) = \mathcal{N} \exp\{-\mathcal{A}([x];t)\}$ with the action functional

$$\mathcal{A}([x];t) = \int_0^t \mathrm{d}t'\, \frac{(\dot{x}(t') - \mu F(x(t'),t'))^{\circ 2}}{4D} - \frac{\mu}{2} \int_0^t \mathrm{d}t'\, \partial_x F(x(t'),t') \tag{1.29}$$

in the Stratonovich discretisation, which differs from the Ito form only by the second

term [289, Sec. 4.5], which is the Jacobian of the transform of the noise $\zeta(t)$ to $x(t)$, Eq. (1.21). The Stratonovich form is needed so that the action does not give preference to a particular time direction [72]. This choice plays a rôle in every product of white noise, as is implicit to $\dot{x}$, and a random variable. We therefore indicate the choice by a $\circ$ also in powers, reminding us that $F(x(t'),t')$ should be read as $F((x(t')+x(t'+\Delta t))/2, t'+\Delta t)$ and $\dot{x}(t')$ as $(x(t'+\Delta t)-x(t'))/2$ with discretisation time step Δt. Evaluating the action for the reversed path $x^R(t') = x(t-t')$ then gives

$$\mathcal{A}([x^R];t) = \int_0^t \mathrm{d}t' \, \frac{(\dot{x}^R(t') - \mu F(x^R(t'),t'))^{\circ 2}}{4D} - \frac{\mu}{2}\int_0^t \mathrm{d}t' \, \partial_x F(x^R(t'),t') \tag{1.30}$$

$$= \int_0^t \mathrm{d}t' \, \frac{(\dot{x}(t') + \mu F(x(t'),t-t'))^{\circ 2}}{4D} - \frac{\mu}{2}\int_0^t \mathrm{d}t' \, \partial_x F(x(t'),t-t') \; . \tag{1.31}$$

If the force is even under time reversal, $F(x,t') = F(x,t-t')$, in particular when it is independent of time, the path probability density obeys

$$\ln \frac{p([x];t)}{p([x^R];t)} = \int_0^t \mathrm{d}t' \, \frac{F(x(t'),t') \circ \dot{x}(t')}{T} = S_m(t) \; , \tag{1.32}$$

with random variables multiplied with Stratonovich convention. With Eq. (1.24), the integral in Eq. (1.32) can be identified as the entropy of the medium. When the driving is time-independent and the system's probability distribution eventually becomes stationary, such that $\lim_{t\to\infty}\langle \dot{S}(x^*,t)\rangle = 0$, Eq. (1.22), the only contribution to the total entropy change is due to change of entropy in the medium, Eq. (1.25). Assuming that the system is ergodic, we have the equivalence $\lim_{t\to\infty} S_m(t)/t = \lim_{t\to\infty}\langle \dot{S}_{\mathrm{tot}}(t)\rangle$, where $\langle\bullet\rangle$ denotes an ensemble average. Using Eqs. (1.12) and (1.28) gives $\lim_{t\to\infty} S_m(t)/t = \lim_{t\to\infty} \dot{S}_i(t)$. Equation (1.32) can therefore be used directly to compute the steady-state internal entropy production rate. The equivalence between the long-time limit $t\to\infty$ and the ensemble average holds only for ergodic systems, whose unique steady-state does not depend on the specific initialisation $x(0)$. This connection between stochastic thermodynamics and field theory has stimulated a number of works aimed at characterising the non-equilibrium features of continuum models of active matter [202, 99].

1.3 Systems

In this section we calculate the entropy production rate on the basis of Gaspard's framework [113], Eqs. (1.4), (1.14) and (1.15), for different particle systems. We cover the systems listed in Tab. 1.1, with both discrete and continuous states and with one or multiple particles.

Table 1.1: List of particle systems for which we have calculated their entropy production $\dot{S}_i(t)$.

	System	$\dot{S}_i(t)$
1.3.1	Two-state Markov process	(1.36)
1.3.2	Three-state Markov process	(1.40)
1.3.3	Random walk on a complete graph	(1.43), (1.44)
1.3.4	N independent, distinguishable Markov processes	(1.51)
1.3.5	N independent, indistinguishable two-state Markov processes	(1.54b)
1.3.6	N independent, indistinguishable d-state processes	(1.67)
1.3.7	Random Walk on a lattice	(1.81)
1.3.8	Random Walk on a ring lattice	(1.87), (1.89)
1.3.9	Driven Brownian particle	(1.95)
1.3.10	Driven Brownian particle in a harmonic potential	(1.101)
1.3.11	Driven Brownian particle on a ring with potential	(1.115d)
1.3.12	Run-and-tumble motion with diffusion on a ring	(1.124)
1.3.13	Switching diffusion process on a ring	(1.130)

1.3.1 Two-state Markov process

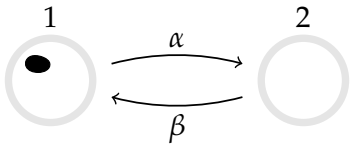

Figure 1.1: Two-state Markov chain in continuous time. The black blob indicates the current state of the system. Independently of the choice of α and β, this processes settles into an equilibrium steady-state at long times (in the absence of an external time-dependent diving).

Consider a particle that hops between two states, 1 and 2, with transition rates $\dot{W}(1 \to 2) = \alpha$ and $\dot{W}(2 \to 1) = \beta$, see Fig. 1.1 [92, 177], and using the notation in Eq. (1.17)

for discrete states. The rate-matrix (see Eq. (1.6)) may thus be

$$w = \begin{pmatrix} -\alpha & \alpha \\ \beta & -\beta \end{pmatrix} , \tag{1.33}$$

with $\mathbf{P}(t) = (P_1(t), P_2(t))$ the probability of the particle to be in state 1 or 2 respectively as a function of time. By normalisation, $P_1(t) + P_2(t) = 1$, with probabilistic initial condition $\mathbf{P}(0) = (p, 1-p)$. Solving the master equation in Eq. (1.2) yields

$$\mathbf{P}(t) = (P_1(t), P_2(t)) = \frac{1}{\alpha+\beta}\left(\beta + r\, e^{-(\alpha+\beta)t}, \alpha - r\, e^{-(\alpha+\beta)t}\right) , \tag{1.34}$$

with $r = \alpha p - \beta(1-p)$, corresponding to an exponentially decaying probability current

$$P_1(t)\alpha - P_2(t)\beta = r\, e^{-(\alpha+\beta)t} . \tag{1.35}$$

The internal entropy production (1.4b) is then

$$\dot{S}_i(t) = [P_1(t)\alpha - P_2(t)\beta] \ln\left[\frac{P_1(t)\alpha}{P_2(t)\beta}\right] = r \exp\{-(\alpha+\beta)t\} \ln\left[\frac{1 + \frac{r}{\beta}\, e^{-(\alpha+\beta)t}}{1 - \frac{r}{\alpha}\, e^{-(\alpha+\beta)t}}\right] , \tag{1.36}$$

and the entropy flow (1.4a),

$$\dot{S}_e(t) = -r\, \exp\{-(\alpha+\beta)t\}\, \ln\left(\frac{\alpha}{\beta}\right) . \tag{1.37}$$

At stationarity, $\dot{S}_i = \dot{S}_e = 0$ and therefore the two-state Markov process reaches equilibrium. In this example, the topology of the transition network does not allow a sustained current between states, which inevitably leads to equilibrium in the steady state and, therefore, there is production of entropy only due to the relaxation of the system from the initial state.

1.3.2 Three-state Markov process

We extend the system in Sec. 1.3.1 to three states, 1, 2 and 3, with transition rates $\dot{W}(1 \to 2) = \alpha$, $\dot{W}(2 \to 3) = \alpha$, $\dot{W}(3 \to 1) = \alpha$, $\dot{W}(2 \to 1) = \beta$, $\dot{W}(3 \to 2) = \beta$, and $\dot{W}(1 \to 3) = \beta$, see Fig. 1.2, and using the notation Eq. (1.17) for discrete states. The

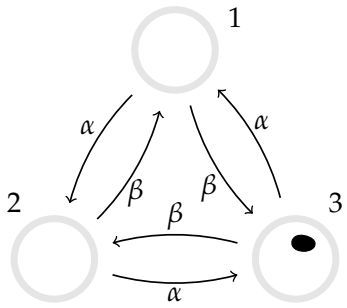

Figure 1.2: Three-state Markov chain in continuous time. The black blob indicates the current state of the system. Symmetry under cyclic permutation is introduced by imposing identical transition rates α and β for counter-clockwise and clockwise transition, respectively.

rate matrix (see Eq. (1.6)) is then

$$w = \begin{pmatrix} -(\alpha+\beta) & \alpha & \beta \\ \beta & -(\alpha+\beta) & \alpha \\ \alpha & \beta & -(\alpha+\beta) \end{pmatrix} . \tag{1.38}$$

Assuming the initial condition $\mathbf{P}(0) = (1, 0, 0)$, the probabilities of states 1, 2 and 3 respectively, evolve according to Eq. (1.2), which has solution

$$P_1(t) = \frac{1}{3}\left(1 + 2\exp\{-3\phi t\}\cos\left(\sqrt{3}\psi t\right)\right) , \tag{1.39a}$$

$$P_2(t) = \frac{1}{3}\left(1 - 2\exp\{-3\phi t\}\cos\left(\sqrt{3}\psi t - \pi/3\right)\right) , \tag{1.39b}$$

$$P_3(t) = \frac{1}{3}\left(1 - 2\exp\{-3\phi t\}\cos\left(\sqrt{3}\psi t + \pi/3\right)\right) , \tag{1.39c}$$

with $\phi = (\alpha+\beta)/2$ and $\psi = (\alpha-\beta)/2$.

The entropy production (1.4b) is then, using (1.39),

$$\begin{aligned} \dot{S}_i(t) = &\left(P_1(t)\alpha - P_2(t)\beta\right)\ln\left(\frac{P_1(t)\alpha}{P_2(t)\beta}\right) \\ &+ \left(P_2(t)\alpha - P_3(t)\beta\right)\ln\left(\frac{P_2(t)\alpha}{P_3(t)\beta}\right) + \left(P_3(t)\alpha - P_1(t)\beta\right)\ln\left(\frac{P_3(t)\alpha}{P_1(t)\beta}\right), \end{aligned} \tag{1.40}$$

and the entropy flow (1.4a),

$$\dot{S}_e(t) = -(\alpha - \beta) \ln \left(\frac{\alpha}{\beta} \right), \tag{1.41}$$

which is constant throughout. At stationarity, the system is uniformly distributed and, if $\alpha \neq \beta$, the entropy production and flow satisfy $\dot{S}_i = -\dot{S}_e \neq 0$. If $\alpha \neq \beta$, the particle has a net drift that sustains a probability current $(\alpha - \beta)/3$ in the system, which prevents the system from reaching equilibrium.

1.3.3 Random walk on a complete graph

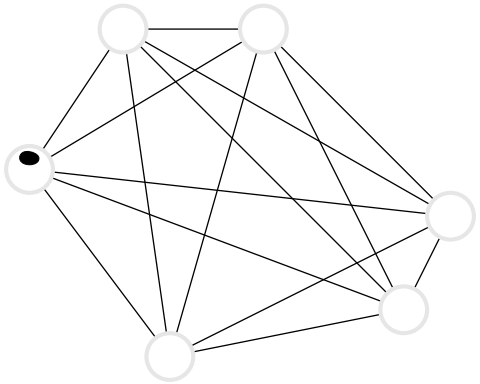

Figure 1.3: Random walk on a complete graph of d nodes (here shown for $d = 6$). The black blob indicates the current state of the system. For uniform transition rates, the symmetry under node relabelling leads to an equilibrium, homogeneous steady-state with $P_j = 1/d$ for all j.

Consider a random walker on a complete graph with d nodes, where each node is connected to all other nodes, and the walker jumps from node $j \in \{1, 2, \ldots, d\}$ to node $k \in \{1, 2, \ldots, d\}$, $k \neq j$, with rate w_{jk}, see Fig. 1.3. These are the off-diagonal elements of the corresponding Markov matrix whose diagonal elements are $w_{jj} = -\sum_{i=1, i\neq j}^{d} w_{ji}$. The probability vector $\mathbf{P}(t) = (P_1(t), P_2(t), \ldots, P_d(t))$ has components $P_j(t)$ that are the probability that the system is in state j at time t. The general case of arbitrary transition rates is impossible to discuss exhaustively. In the uniform case, $w_{jk} = \alpha$, the Markov matrix has only two distinct eigenvalues, namely eigenvalue αd with degeneracy $d-1$ and eigenvalue 0 with degeneracy 1. Assuming an arbitrary initial condition $\mathbf{P}(0)$,

the probability distribution at a later time t is

$$P_j(t) = \frac{1}{d} + e^{-d\alpha t}\left(P_j(0) - \frac{1}{d}\right) . \tag{1.42}$$

The steady state, which is associated with the vanishing eigenvalue, is the uniform distribution $\lim_{t\to\infty} P_j(t) = 1/d$ for all $j \in \{1, 2, \ldots, d\}$. The entropy production (1.4b) of the initial state relaxing to the uniform state is

$$\dot{S}_i(t) = \frac{1}{2}\alpha e^{-d\alpha t} \sum_{j,k} (P_j(0) - P_k(0)) \ln\left(\frac{1 + e^{-d\alpha t}\,(P_j(0)d - 1)}{1 + e^{-d\alpha t}\,(P_k(0)d - 1)}\right) , \tag{1.43}$$

and the entropy flow (1.4a) is $\dot{S}_e = 0$ throughout. If the walker is initially located on node k, so that $P_j(0) = \delta_{j,k}$, the entropy production simplifies to

$$\dot{S}_i(t) = (d-1)\alpha e^{-d\alpha t} \ln\left(1 + \frac{d e^{-d\alpha t}}{1 - e^{-d\alpha t}}\right) . \tag{1.44}$$

We can see that the system reaches equilibrium at stationarity, since $\lim_{t\to\infty} \dot{S}_i(t) = \dot{S}_e(t) = 0$. At long times ($de^{-d\alpha t} \ll 1$), the asymptotic behaviour of $\dot{S}_i$ is

$$\dot{S}_i(t) = d(d-1)\alpha e^{-2d\alpha t} + \mathcal{O}(e^{-3d\alpha t}) , \tag{1.45}$$

by expanding the logarithm in the small exponential.

1.3.4 N independent, distinguishable Markov processes

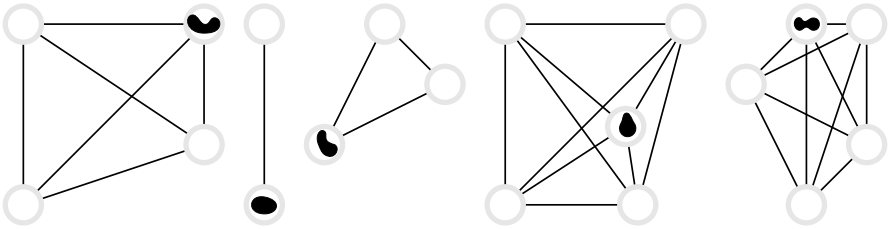

Figure 1.4: Example of $N = 5$ non-interacting, distinguishable processes with $d_1 = 4$, $d_2 = 2$, $d_3 = 3$, $d_4 = 5$ and $d_5 = 5$. The black blobs indicate the current state of each sub-system.

In the following we consider N non-interacting, distinguishable particles undergoing Markovian dynamics on a discrete state space. Each of the N particles carries an index

$\ell \in \{1, 2, \ldots, N\}$ and is in state $n_\ell \in \{1, 2, \ldots, d_\ell\}$, so that the state of the entire system is given by an N-particle state $\mathbf{n} = (n_1, n_2, \ldots, n_N)$. Particle distinguishability implies the factorisation of state and transition probabilities into their single-particle contributions, whence the joint probability $P_{\mathbf{n}}(t)$ of an N-particle state $\mathbf{n}$ factorises into a product of single particle probabilities $P^{(\ell)}_{n_\ell}(t)$ of particle ℓ to be in state n_ℓ,

$$P_{\mathbf{n}}(t) = \prod_{\ell=1}^{N} P^{(\ell)}_{n_\ell}(t) \ . \tag{1.46}$$

Further, the Poissonian rate $w_{\mathbf{nm}}$ from N-particle state $\mathbf{n}$ to N-particle state $\mathbf{m} \neq \mathbf{n}$ vanishes for all transitions $\mathbf{n} \to \mathbf{m}$ that differ in more than one component ℓ, *i.e.* $w_{\mathbf{nm}} = 0$ unless there exists a single $\ell \in \{1, 2, \ldots, N\}$ such that $m_k = n_k$ for all $k \neq \ell$, in which case $w_{\mathbf{nm}} = w^{(\ell)}_{n_\ell m_\ell}$, the transition rates of the single particle transition of particle ℓ.

The entropy production of this N-particle system according to Eq. (1.4b),

$$\dot{S}_i(t) = \frac{1}{2} \sum_{\mathbf{nm}} (P_{\mathbf{n}}(t) w_{\mathbf{nm}} - P_{\mathbf{m}}(t) w_{\mathbf{mn}}) \ln \left(\frac{P_{\mathbf{n}}(t) w_{\mathbf{nm}}}{P_{\mathbf{m}}(t) w_{\mathbf{mn}}} \right) \tag{1.47}$$

simplifies considerably due to $w_{\mathbf{nm}}$, as the sum may be re-written as

$$\sum_{\mathbf{nm}} \ldots w_{\mathbf{nm}} \ldots = \sum_{\mathbf{n}} \sum_{\ell} \sum_{m_\ell} \ldots w_{\mathbf{nm}_\ell} \ldots \tag{1.48}$$

with $\mathbf{m}_\ell = (n_1, n_2, \ldots, n_{\ell-1}, m_\ell, n_{\ell+1}, \ldots, n_N)$ so that $w_{\mathbf{nm}_\ell} = w^{(\ell)}_{n_\ell m_\ell}$ and

$$\begin{aligned} &\dot{S}_i(t) \\ &= \frac{1}{2} \sum_{\mathbf{n}} \sum_{\ell=1}^{N} \sum_{m_\ell} \left\{ \left(\prod_{k=1}^{N} P^{(k)}_{n_k}(t) \right) w^{(\ell)}_{n_\ell m_\ell} - \left(\prod_{k=1}^{N} P^{(k)}_{m_k}(t) \right) w^{(\ell)}_{m_\ell n_\ell} \right\} \ln \left(\frac{\prod_{k=1}^{N} P^{(k)}_{n_k}(t) w^{(\ell)}_{n_\ell m_\ell}}{\prod_{k=1}^{N} P^{(k)}_{m_k}(t) w^{(\ell)}_{m_\ell n_\ell}} \right) \ . \end{aligned} \tag{1.49}$$

Since $m_k = n_k$ for any $k \neq \ell$ inside the curly bracket, we may write

$$\prod_{k=1}^{N} P^{(k)}_{n_k}(t) = P^{(\ell)}_{n_\ell}(t) \prod_{\substack{k=1 \\ k \neq \ell}}^{N} P^{(k)}_{n_k}(t) \qquad \text{and} \qquad \prod_{k=1}^{N} P^{(k)}_{m_k}(t) = P^{(\ell)}_{m_\ell}(t) \prod_{\substack{k=1 \\ k \neq \ell}}^{N} P^{(k)}_{n_k}(t) \ . \tag{1.50}$$

The product $\prod_{k\neq\ell}^{N} P_{n_k}^{(k)}(t)$ can thus be taken outside the curly bracket in Eq. (1.49) and be summed over, as well as cancelled in the logarithm. After changing the dummy variables in the remaining summation from n_ℓ and m_ℓ to n and m respectively, the entropy production is

$$\dot{S}_i(t) = \frac{1}{2}\sum_{\ell=1}^{N}\sum_{nm}\left(P_n^{(\ell)}(t)w_{nm}^{(\ell)} - P_m^{(\ell)}(t)w_{mn}^{(\ell)}\right)\ln\left(\frac{P_n^{(\ell)}(t)w_{nm}^{(\ell)}}{P_m^{(\ell)}(t)w_{mn}^{(\ell)}}\right), \tag{1.51}$$

which is the sum of the entropy productions of the single particle $\ell \in \{1, 2, \ldots, N\}$, Eq. (1.4b), irrespective of how each particle is initialised. The same argument applies to $\dot{S}_e$, the entropy flow Eq. (1.4a). The entropy production and flow obviously simplify to an N-fold product of the single particle expressions if $w_{nm}^{(\ell)}$ do not depend on ℓ and all particles are initialised by the same $P_n^{\ell}(0)$ independent of ℓ. This result may equally be found from the dynamical entropy per unit time, Eq. (1.7).

1.3.5 N independent, indistinguishable two-state Markov processes

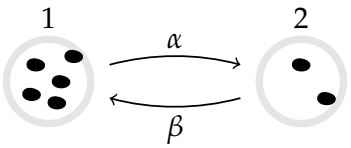

Figure 1.5: N independent, indistinguishable two-state Markov processes in continuous time. The black blobs indicate the current state of the single-particle sub-system. Since processes are indistinguishable, states are fully characterised by the occupation number of either state, if the total number of particles is known.

Suppose that N identical, indistinguishable, non-interacting particles follow the two-state Markov process described in Sec. 1.3.1, Fig. 1.5 [92]. There are $\Omega = N+1$ distinct states given by the occupation number $n \in \{0, 1, \ldots, N\}$ of one of the two states, say state 1, as the occupation number of the other state follows as $N - n$ given the particle number N is fixed under the dynamics. In the following, $P(n, t)$ denotes the probability of finding n particles in state 1 at time t. The master equation is then

$$\dot{P}(n,t) = -\alpha n P(n,t) + \alpha(n+1)P(n+1,t) - \beta(N-n)P(n,t) + \beta(N-n+1)P(n-1,t)\,. \tag{1.52}$$

The state space and the evolution in it can be thought of as a hopping process on a one-

dimensional chain of states with non-uniform rates. Provided $P(n,0)$ initially follows a binomial distribution, $P(n,0) = \binom{N}{n} p^n (1-p)^{N-n}$ with probability p for a particle to be placed in state 1 initially, the solution of Eq. (1.52) is easily constructed from the solution $P_1(t)$ in Eq. (1.34) of Sec. 1.3.1 via

$$P(n,t) = \binom{N}{n} P_1^n(t)(1-P_1(t))^{N-n} \quad \text{for} \;\; 0 \leq n \leq N \tag{1.53}$$

with $P_1(0) = p$, as $\dot{P}_1(t) = -\alpha P_1(t) + \beta(1-P_1(t))$, which can be verified by substituting Eq. (1.53) into Eq. (1.52). Using Eqs. (1.33) and (1.53) in (1.4b) the entropy production reads

$$\dot{S}_i(t) = \sum_{n=1}^{N} [P(n,t)\alpha n - P(n-1,t)\beta(N-n+1)] \ln \left[\frac{P(n,t)\alpha n}{P(n-1,t)\beta(N-n+1)} \right] \tag{1.54a}$$

$$= N[P_1(t)\alpha - (1-P_1(t))\beta] \ln \left[\frac{P_1(t)\alpha}{(1-P_1(t))\beta} \right] \;, \tag{1.54b}$$

which is the N-fold multiple of the result of the corresponding single particle system, Eq. (1.36). This result, Eq. (1.54b), depends on the initialisation being commensurable with Eq. (1.53) which otherwise is recovered only asymptotically and only if the stationary distribution is unique. Further, the entropy production of N indistinguishable particles being the N-fold entropy production of a single particle does not extend to the external entropy flow, which lacks the simplification of the logarithm and gives

$$\begin{aligned} \dot{S}_e(t) = &- N[\alpha P_1(t) - \beta(1-P_1(t))] \\ &\times \left\{ \ln\left(\frac{\alpha}{\beta}\right) + \sum_{n=0}^{N-1} P_1^n(t)(1-P_1(t))^{N-1-n} \binom{N-1}{n} \ln\left(\frac{n+1}{N-n}\right) \right\} \end{aligned} \tag{1.55}$$

thus picking up a correction in the form of the additional sum in the curly bracket that vanishes only at $N = 1$ or $P_1(t) = 1/2$, but does not contribute at stationarity because of the overall prefactor $\alpha P_1 - \beta(1-P_1)$ that converges to 0. To make sense of this correction in relation to particle indistinguishability, with the help of Eq. (1.53) we can rewrite the difference between the right hand side of Eq. (1.55) and the N-fold entropy

flow of a single two-state system (1.37) as

$$
\begin{aligned}
&-N[\alpha P_1(t) - \beta(1 - P_1(t))] \sum_{n=0}^{N-1} P_1^n(t)(1 - P_1(t))^{N-1-n} \binom{N-1}{n} \ln\left(\frac{n+1}{N-n}\right) \\
&= -\sum_{n=0}^{N-1} [\alpha(n+1)P(n+1,t) - \beta(N-n)P(n,t)] \ln\left(\frac{n+1}{N-n}\right)
\end{aligned} \tag{1.56}
$$

which now explicitly involves the net probability current from the occupation number state with $n+1$ particles in state A to that with n particles in state A, as well as a the logarithm

$$
\ln\left(\frac{n+1}{N-n}\right) = \ln\left[\binom{N}{n}\right] - \ln\left[\binom{N}{n+1}\right] \ . \tag{1.57}
$$

Written in terms of the same combinatorial factors appearing in Eq. (1.53), the logarithm (1.57) can be interpreted as a difference of microcanonical (Boltzmann) entropies, defined as the logarithm of the degeneracy of the occupation number state if we were to assume that the N particles are distinguishable. With the help of the master Eq. (1.52) as well as Eqs. (1.53) and (1.57), the term Eq. (1.56) may be rewritten to give

$$
\dot{S}_e(t) = -N[\alpha P_1(t) - \beta(1 - P_1(t))] \ln\left(\frac{\alpha}{\beta}\right) - \sum_{n=0}^{N-1} \dot{P}(n,t) \ln\left[\binom{N}{n}\right] \tag{1.58}
$$

This result is further generalised in Eq. (1.69).

1.3.6 N INDEPENDENT, INDISTINGUISHABLE d-STATE PROCESSES

We generalise now the results in Sec. 1.3.3 and Sec. 1.3.5 to N independent d-state Markov processes, see Fig. 1.6. These results represent a special case of those obtained in [132] when the N processes are non-interacting. In this section we consider non-interacting, indistinguishable particles hopping on a graph of d nodes with edge-dependent hopping rates w_{jk}. As in the two-state system in Sec. 1.3.5, we find that the internal (but not the external) entropy production of the d-state system $\dot{S}_i$ is N times the entropy production of the individual processes assuming the initial condition is probabilistically identical for all single-particle sub-systems. The entropy productions

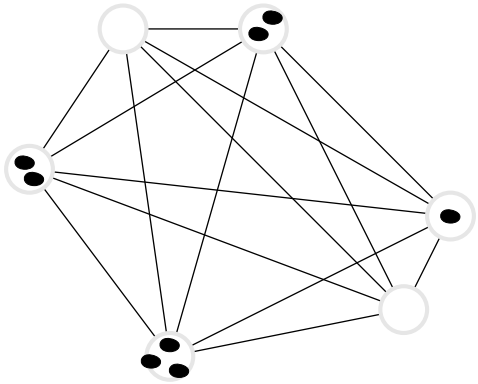

Figure 1.6: N independent, indistinguishable d-state Markov processes (here shown for $d = 6$ and $N = 8$) in continuous time. Black blobs indicate the current state of the single-particle sub-systems. Due to indistinguishably, multi-particle states are fully characterised by the occupation number of an arbitrary subset of $d - 1$ states, if the total number of particles is known.

of a single such process according to Eq. (1.4) read

$$\dot{S}_i^{(1)}(t) = \frac{1}{2}\sum_{jk}[P_j(t)w_{jk} - P_k(t)w_{kj}]\ln\left(\frac{P_j(t)w_{jk}}{P_k(t)w_{kj}}\right) , \tag{1.59a}$$

$$\dot{S}_e^{(1)}(t) = -\frac{1}{2}\sum_{jk}[P_j(t)w_{jk} - P_k(t)w_{kj}]\ln\left(\frac{w_{jk}}{w_{kj}}\right) , \tag{1.59b}$$

where $P_j(t)$ is the time-dependent probability of a single-particle process to be in state j, Sec. 1.3.3. To calculate the entropy production of the N concurrent indistinguishable processes using the occupation number representation, we first derive the probability of an occupation number configuration $\mathbf{n} = (n_1, n_2, \ldots, n_d)$, with $\sum_{j=1}^{d} n_j = N$, which similar to Eq. (1.53) is given by the multinomial distribution

$$P_{\mathbf{n}}(t) = N!\prod_{j=1}^{d}\frac{P_j^{n_j}(t)}{n_j!} \tag{1.60}$$

for the probability $P_{\mathbf{n}}(t)$ of the system to be in state $\mathbf{n}$ at time t assuming that each particle is subject to the same single-particle distribution $P_j(t)$, $j \in \{1, 2, \ldots, d\}$ for all t, *i.e.* in particular assuming that all particles are initialised identically, by placing them all at the same site or, more generally, by placing them initially according to the

same distribution $P_j(0)$. Given this initialisation, Eq. (1.60) solves Eq. (1.2)

$$\dot{P}_{\mathbf{n}}(t) = \sum_{\mathbf{m}} P_{\mathbf{m}}(t) w_{\mathbf{mn}} - P_{\mathbf{n}}(t) w_{\mathbf{nm}} \tag{1.61}$$

with the transition rates $w_{\mathbf{mn}}$ discussed below.

For non-interacting processes with a unique stationary distribution, Eq. (1.60) is always obeyed in the limit of long times after initialisation, since the single-particle distributions $P_j(t)$ are identical at steady state. The entropy production Eq. (1.4b) of the entire system has the same form as Eq. (1.47) of Sec. 1.3.4 (N independent, *distinguishable* particles) with $w_{\mathbf{nm}}$ however now the transition rate between the occupation number state $\mathbf{n} = (n_1, n_2, \ldots, n_d)$ with $0 \leq n_k \leq N$ to occupation number state $\mathbf{m} = (m_1, m_2, \ldots, m_d)$. The rate $w_{\mathbf{nm}}$ vanishes except when $\mathbf{m}$ differs from $\mathbf{n}$ in exactly two distinct components, say $m_j = n_j - 1 \geq 0$ and $m_k = n_k + 1 \geq 1$ in which case $w_{\mathbf{nm}} = n_j w_{jk}$ with w_{jk} the transition rates of a single particle from j to k as introduced above. For such $\mathbf{m}$, the rate obeys $w_{\mathbf{mn}} = m_k w_{kj}$ and the probability $P_{\mathbf{m}}(t)$ fulfills

$$P_{\mathbf{m}}(t) = P_{\mathbf{n}}(t) \frac{P_k(t) n_j}{P_j(t) m_k} = P_{\mathbf{n}}(t) \frac{P_k(t) w_{\mathbf{nm}} w_{kj}}{P_j(t) w_{\mathbf{mn}} w_{jk}} \ , \tag{1.62}$$

which simplifies the entropy production Eq. (1.47) to

$$\begin{aligned} \dot{S}_i(t) &= \frac{1}{2} \sum_{\mathbf{nm}} (P_{\mathbf{n}}(t) w_{\mathbf{nm}} - P_{\mathbf{m}}(t) w_{\mathbf{mn}}) \ln \left(\frac{P_{\mathbf{n}}(t) w_{\mathbf{nm}}}{P_{\mathbf{m}}(t) w_{\mathbf{mn}}} \right) \\ &= \frac{1}{2} \sum_{\mathbf{n}} \sum_{jk} (P_{\mathbf{n}}(t) n_j w_{jk} - P_{\mathbf{m}}(t) m_k w_{kj}) \ln \left(\frac{P_j(t) w_{jk}}{P_k(t) w_{kj}} \right) \end{aligned} \tag{1.63}$$

where the sum $\sum_{\mathbf{n}}$ runs over all allowed configurations, namely $0 \leq n_j \leq N$ for $j = 1, 2, \ldots, d$ with $\sum_j n_j = N$ and $\mathbf{m} = (n_1, n_2, \ldots, n_j - 1, \ldots, n_k + 1, \ldots, n_d)$ is derived from $\mathbf{n}$ as outlined above. Strictly, $P_{\mathbf{n}}(t)$ has to be defined to vanish for invalid states $\mathbf{n}$, so that the first bracket in the summand of Eq. (1.63) vanishes in particular when $n_j = 0$, in which case $m_j = -1$. To proceed, we introduce the probability

$$\bar{P}_{\bar{\mathbf{n}}_j}(t) = (N-1)! \frac{P_j^{n_j - 1}}{(n_j - 1)!} \prod_{i=1, i \neq j}^{d} \frac{P_i^{n_i}}{n_i!} \ , \tag{1.64}$$

defined to vanish for $n_j = 0$, so that $P_{\mathbf{n}}(t)n_j = NP_j(t)\bar{P}_{\bar{\mathbf{n}}_j}(t)$. The probability $\bar{P}_{\bar{\mathbf{n}}_j}(t)$ is that of finding n_i particles at states $i \neq j$ and $n_j - 1$ particles at state j. It is Eq. (1.60) evaluated in a system with only $N-1$ particles and configuration $\bar{\mathbf{n}}_j = (n_1, n_2, \ldots, n_{j-1}, n_j - 1, n_{j+1}, \ldots, n_d) = \bar{\mathbf{m}}_k$ a function of $\mathbf{n}$. Eq. (1.63) may now be rewritten as

$$\dot{S}_i(t) = \frac{N}{2}\sum_{jk}\left\{\left(\sum_{\mathbf{n}}\bar{P}_{\bar{\mathbf{n}}_j}(t)\right)P_j(t)w_{jk} - \left(\sum_{\mathbf{n}}\bar{P}_{\bar{\mathbf{m}}_k}(t)\right)P_k(t)w_{kj}\right\}\ln\left(\frac{P_j(t)w_{jk}}{P_k(t)w_{kj}}\right) \tag{1.65}$$

where we have used that the arguments of the logarithm are independent of $\mathbf{n}$ and $\mathbf{m}$. The summation over $\mathbf{n}$ gives

$$\sum_{\mathbf{n}}\bar{P}_{\bar{\mathbf{n}}_j}(t) = \sum_{\mathbf{n}}\bar{P}_{\bar{\mathbf{m}}_k}(t) = 1 \tag{1.66}$$

so that

$$\dot{S}_i(t) = \frac{N}{2}\sum_{jk}(P_j(t)w_{jk} - P_k(t)w_{kj})\ln\left(\frac{P_j(t)w_{jk}}{P_k(t)w_{kj}}\right) = N\dot{S}_i^{(1)}(t) \tag{1.67}$$

which is the N-fold entropy production of the single particle system $\dot{S}_i(t)$, Eq. (1.59a), or equivalently that of N distinguishable particles, Eq. (1.51), Sec. 1.3.4. As in Sec. 1.3.5, this dramatic simplification does not carry over to the external entropy flow Eq. (1.4a)

$$\begin{aligned}\dot{S}_e(t) &= -\frac{N}{2}\sum_{jk}\sum_{\mathbf{n}}\bar{P}_{\bar{\mathbf{n}}_j}(t)(P_j(t)w_{jk} - P_k(t)w_{kj})\ln\left(\frac{n_j w_{jk}}{(n_k+1)w_{kj}}\right)\\ &= -\frac{N}{2}\sum_{jk}(P_j(t)w_{jk} - P_k(t)w_{kj})\ln\left(\frac{w_{jk}}{w_{kj}}\right)\\ &\quad -\frac{N}{2}\sum_{jk}\sum_{\mathbf{n}}\bar{P}_{\bar{\mathbf{n}}_j}(t)(P_j(t)w_{jk} - P_k(t)w_{kj})\ln\left(\frac{n_j}{n_k+1}\right),\end{aligned} \tag{1.68}$$

where of the last two terms only the first is the N-fold entropy flow of the single particle system $\dot{S}_e(t)$, Eq. (1.59b). The reason for the second term is the lack of a cancellation mechanism to absorb the n_j and $n_k + 1$ from the logarithm. Rewriting the second term

as

$$
\begin{aligned}
&-\frac{N}{2}\sum_{jk}\sum_{\mathbf{n}}\bar{P}_{\bar{\mathbf{n}}_j}(t)(P_j(t)w_{jk}-P_k(t)w_{kj})\ln\left(\frac{n_j}{n_k+1}\right)\\
&=-\frac{1}{2}\sum_{\mathbf{n}}\sum_{jk}\left(P_{\mathbf{n}}(t)n_j w_{jk}-P_{\mathbf{n}}\left(\frac{P_k(t)n_j}{P_j(t)(n_k+1)}\right)(n_k+1)w_{kj}\right)\ln\left(\frac{n_j}{n_k+1}\right) \qquad (1.69)\\
&=-\sum_{\mathbf{n}}\dot{P}_{\mathbf{n}}(t)\ln\left[\binom{N}{n_1,...,n_d}\right]\ , \qquad (1.70)
\end{aligned}
$$

using Eq. (1.61) where we re-expressed the logarithm as

$$
\ln\left(\frac{n_j}{n_k+1}\right)=\ln\left[\binom{N}{n_1,\ldots,n_j-1,\ldots,n_k+1,\ldots,n_d}\right]-\ln\left[\binom{N}{n_1,\ldots,n_d}\right]\ , \qquad (1.71)
$$

shows that the correction term has the same form as the corresponding term in the two-state system, Eq. (1.56), namely that of a difference of microcanonical (Boltzmann) entropies of the multi-particle states. It vanishes when all n_j are either 0 or 1, as expected for $d \gg N$ and also at stationarity when $\dot{P}_{\mathbf{n}}(t)=0$. In that limit $\dot{S}_e=-\dot{S}_i$ when indeed Eq. (1.59a) gives

$$
\lim_{t\to\infty}\dot{S}_i^{(1)}(t)=\frac{1}{2}\sum_k(P_j w_{jk}-P_k w_{kj})\ln\left(\frac{w_{jk}}{w_{kj}}\right)\ , \qquad (1.72)
$$

with $P_j=\lim_{t\to\infty}P_j(t)$. As far as the entropy production $\dot{S}_i(t)$ is concerned, we thus recover and generalise the result in Sec. 1.3.5 on indistinguishable particles in a two-state system, which produce N times the entropy of a single particle. In Sec. 1.3.4 it was shown that N *distinguishable* particles have the same entropy production and flow as the sum of the entropy productions of individual particles. In Sec. 1.3.5 and 1.3.6 it was shown that the entropy production of *indistinguishable* particles, which require the states to be represented by occupation numbers, show the N-fold entropy production of the single particle system, provided suitable initialisation, but asymptotically independent of initialisation, provided the stationary state has a unique distribution. The same does not apply to the entropy flow, which generally acquires additional logarithmic terms accounting for the degeneracy of the occupation number states. The extra terms, however, are bound to vanish at stationarity, when $\dot{S}_e(t)=-\dot{S}_i(t)$.

1.3.7 Random Walk on a lattice

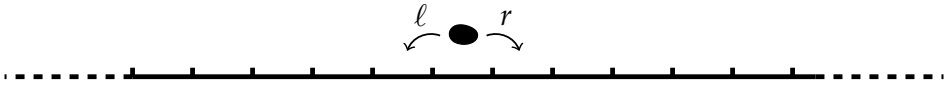

Figure 1.7: Simple random walk on an infinite, one-dimensional lattice in continuous time. The black blob indicates the current position of the random walker. The left and right hopping rates, labelled ℓ and r respectively, are assumed to be homogeneous but not equal in general, this leading to a net drift of the average position.

In this section we study a particle on a one-dimensional lattice that hops to the right nearest neighbouring site with rate r and to the left with rate ℓ, see Fig. 1.7. The position x of the particle at time t, after $N(t)$ jumps, is

$$x = x_0 + \sum_{i=1}^{N(t)} \Delta x_i, \tag{1.73}$$

where the random hops Δx_i are independent and identically distributed, and x_0 is the initial position at time $t = 0$. If a is the lattice spacing, the distance increments are $\Delta x_i = +a$ with probability $r/(\ell + r)$ and $\Delta x_i = -a$ with probability $\ell/(\ell + r)$. The probability distribution of the particle position is

$$P(x, t; x_0) = \sum_{n=0}^{\infty} H(n, t) P_n(x; x_0)\,, \tag{1.74}$$

where $H(n, t)$ is the probability that by time t, the particle has hopped $N(t) = n$ times, and $P_n(x; x_0)$ is the probability that the particle is at position x after n hops starting from x_0. Since jumping is a Poisson process with rate $r + \ell$, the random variable $N(t)$ has a Poisson distribution,

$$H(n, t) = \frac{((\ell + r)t)^n}{n!} \exp\{-(\ell + r)t\}\,. \tag{1.75}$$

On the other hand, the distribution of the position x after n jumps is the binomial distribution

$$P_n(x; x_0) = \binom{n}{k_x} \frac{r^{k_x} \ell^{n-k_x}}{(\ell + r)^n}\,, \tag{1.76}$$

where $k_x = (n + (x - x_0)/a)/2$ is the number of jumps to the right, $0 \le k_x \le n$ with

(1.76) implied to vanish if k_x is not integer. From Eq. (1.73) the parity of $(x-x_0)/a$ and $N(t)$ are identical. Using (1.75) and (1.76), the probability distribution in (1.74) reads

$$P(x,t;x_0) = \exp\{-(\ell+r)t\}\left(\frac{r}{\ell}\right)^{\frac{x-x_0}{2a}} \mathcal{I}\left(\frac{|x-x_0|}{a}, 2t\sqrt{r\ell}\right) , \tag{1.77}$$

where $\mathcal{I}(n,z)$ is the modified Bessel function of the first kind. * The transition probability is then,

$$W(x\to y;\tau) = \exp\{-(\ell+r)\tau\}\left(\frac{r}{\ell}\right)^{\frac{y-x}{2a}} \mathcal{I}\left(\frac{|y-x|}{a}, 2\tau\sqrt{r\ell}\right) . \tag{1.79}$$

Using (1.77) and (1.79) to calculate the entropy production (1.4b), we need the following identity for $|y-x|/a = |m| \geq 1$,

$$\lim_{\tau\to 0}\frac{1}{\tau}\mathcal{I}\left(|m|, 2\tau\sqrt{r\ell}\right) = \sqrt{r\ell}\delta_{|m|,1} , \tag{1.80}$$

which follows immediately from Eq. (1.78). It indicates that the only transitions that contribute to the entropy production are those where the particle travels a distance equal to the lattice spacing a. Then, the entropy production reads,

$$\begin{aligned}\dot{S}_i(t) =& \frac{1}{2}(r-\ell)\ln\left(\frac{r}{\ell}\right) + \exp\{-(\ell+r)t\}\sum_{m=-\infty}^{\infty}\left(\frac{r}{\ell}\right)^{\frac{m}{2}}\mathcal{I}\left(|m|, 2t\sqrt{r\ell}\right) \\ &\times\left[r\ln\left(\frac{\mathcal{I}\left(|m|,2t\sqrt{r\ell}\right)}{\mathcal{I}\left(|m+1|,2t\sqrt{r\ell}\right)}\right) + \ell\ln\left(\frac{\mathcal{I}\left(|m|,2t\sqrt{r\ell}\right)}{\mathcal{I}\left(|m-1|,2t\sqrt{r\ell}\right)}\right)\right] .\end{aligned} \tag{1.81}$$

and the entropy flow $\dot{S}_e(t) = -(r-\ell)\ln(r/\ell)$ independent of t, which owes its simplicity to the transition rates being independent of the particle's position. We are not aware of a method to perform the sum in (1.81) in closed form and, given that this expression involves terms competing at large times t, we cannot calculate the stationary entropy

*The modified Bessel function of the first kind of $m, z \in \mathbb{C}$ is defined as [187]

$$\mathcal{I}(m,z) = \sum_{j=0}^{\infty}\frac{1}{j!\Gamma(j+m+1)}\left(\frac{z}{2}\right)^{2j+m} . \tag{1.78}$$

production $\lim_{t\to\infty}\dot{S}_i(t)$. If we assume that the sum in Eq. (1.81) converges such that the exponential $\exp\{-(r+\ell)t\}$ eventually suppresses it, then the entropy production $\dot{S}_i$ appears to converge to $\frac{1}{2}(r-\ell)\ln(r/\ell)$. If that were the case, $\dot{S}=\dot{S}_i+\dot{S}_e$ would converge to a negative constant, while $S(t)$, Eq. (1.1), which vanishes at $t=0$ given the initialisation of $P(x,t;x_0)=\delta_{(x-x_0)/a,0}$, is bound to be strictly positive at all finite t. Given that $P(x,t;x_0)$ does not converge, not much else can be said about $S(t)$ or $\dot{S}$. Using the master equation

$$\dot{P}(x,t;x_0)=-(r+\ell)P(x,t;x_0)+\ell P(x+a,t;x_0)-rP(x-a,t;x_0) \tag{1.82}$$

in

$$\begin{aligned}
&\dot{S}(t)\\
&=-\sum_m \dot{P}(ma,t;x_0)\ln(P(ma,t;x_0)) &\text{(1.83a)}\\
&=\sum_m\{(r+\ell)P(ma,t;x_0)-\ell P((m+1)a,t;x_0)-rP((m-1)a,t;x_0)\}\ln(P(ma,t;x_0)) &\text{(1.83b)}\\
&=\sum_m rP(ma,t;x_0)\ln\left(\frac{P(ma,t;x_0)}{P((m+1)a,t;x_0)}\right)+\ell P(ma,t;x_0)\ln\left(\frac{P(ma,t;x_0)}{P((m-1)a),t;x_0}\right) &\text{(1.83c)}
\end{aligned}$$

still requires an approximation such as the continuum limit in Eq. (1.85) either in the logarithm of the ratios in Eq. (1.83c) or in the logarithm of $P(ma,t;x_0)$ in Eq. (1.83b). The resulting sum can be performed elegantly using, for example, $\sum_m P(ma,t;x_0)m-P((m+1)a,t;x_0)(m+1)=0$. Remarkably, either approach produces $-\frac{1}{2}(r-\ell)\ln(r/\ell)$ for $\dot{S}$. Using $a/\sqrt{t}$ as the integration mesh, the sum can be re-interpreted as a Riemann sum and the difference in the summand Taylor expanded to give $\dot{S}=0$ in large t. Even when this result is more reasonable than negative $\lim_{t\to\infty}\dot{S}(t)$, we are not aware of a rigorous proof that $\lim_{t\to\infty}\dot{S}(t)=0$, and thus not of a proof of the corresponding limit $\lim_{t\to\infty}\dot{S}(t)=(r-\ell)\ln(r/\ell)$. The closely related Brownian particle, discussed in Sec. 1.3.9 does not suffer from this difficulty.

To take the continuum limit $a\to 0$ of the probability distribution (1.77), we define v

and D such that $r + \ell = 2D/a^2$ and $r - \ell = v/a$. Using the asymptotic expansion[†] of $\mathcal{I}(m, z)$ in m, we obtain in fact the Gaussian distribution,

$$\lim_{a\to 0} \frac{1}{a} P\left(\frac{x}{a}, t; \frac{x_0}{a}; r(v, D, a), \ell(v, D, a)\right) = \frac{1}{\sqrt{4\pi D t}} \exp\left\{-\frac{(x - x_0 - vt)^2}{4Dt}\right\}, \quad (1.85)$$

which corresponds to the distribution of a drift-diffusive particle, which is studied in Sec. 1.3.9. Therefore, all results derived in Sec. 1.3.9, apply to the present system in the continuum limit.

1.3.8 Random Walk on a ring lattice

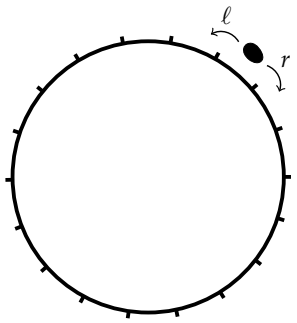

Figure 1.8: Simple random walk on an periodic, one-dimensional 'ring' lattice in continuous time. This model generalises the three-state Markov chain discussed in Section 1.3.2 to L states. The black blob indicates the current position of the random walker. Due to the finiteness of the state space, this process is characterised by a well defined steady-state, which is an equilibrium one for symmetric rates $\ell = r$.

In this section we extend the system in Sec. 1.3.7 to a random walk on a ring lattice of length $L > 2$, so that $1 \leq x \leq L$, see Fig. 1.8. The probability distribution $P_L(x, t)$ of the particle on the ring follows from the distribution on the one-dimensional lattice $P(x, t)$ in (1.77), by mapping all positions $x + jL$ on the one-dimensional lattice to position $x \in \{1, 2, \ldots, L\}$ on the ring with j being the winding number irrelevant to

[†]We use the asymptotic expansion in m of the modified Bessel function [187]

$$\mathcal{I}(m, z) \sim \frac{\exp\{z\}}{\sqrt{2\pi z}} \left(1 - \frac{4m^2 - 1}{8z} + \frac{(4m^2 - 1)(4m^2 - 9)}{2!(8z)^2} - \frac{(4m^2 - 1)(4m^2 - 9)(4m^2 - 25)}{3!(8z)^3} + \ldots\right), \quad (1.84)$$

which is valid for $|\arg z| < \pi/2$.

the evolution of the walker. Then, the distribution on the ring lattice reads,

$$P_L(x,t;x_0) = \sum_{j=-\infty}^{\infty} P(x+jL,t;x_0) \tag{1.86}$$

and similarly for the transition probability $W(x \to y,\tau) = P_L(y,\tau;x)$. To calculate the entropy production (1.4b), each pair of points x, y on the lattice is mapped to a pair of points on the ring. For $L > 2$, as $\tau \to 0$ only transitions to distinct, nearest neighbours contribute and the expression for the entropy production simplifies dramatically,

$$\begin{aligned}\dot{S}_i(t) =& (r-\ell)\ln\left(\frac{r}{\ell}\right) \\ &+ \sum_{m=1}^{L/a} P_L(ma,t;x_0)\left\{r\ln\left(\frac{P_L(ma,t;x_0)}{P_L((m+1)a,t;x_0)}\right) + \ell\ln\left(\frac{P_L(ma,t;x_0)}{P_L((m-1)a,t;x_0)}\right)\right\}\end{aligned} \tag{1.87}$$

and similar for

$$\dot{S}_e(t) = -(r-\ell)\ln\left(\frac{r}{\ell}\right). \tag{1.88}$$

While the entropy flow $\dot{S}_e$ on a ring is thus identical to that of a particle on a one-dimensional lattice, the entropy production $\dot{S}_i$ on a ring is in principle more complicated, but with a lack of cancellations of $\sqrt{r/\ell}$ in the logarithm as found in Sec. 1.3.7 and P_L reaching stationarity comes the asymptote

$$\lim_{t\to\infty} \dot{S}_i(t) = (r-\ell)\ln\left(\frac{r}{\ell}\right). \tag{1.89}$$

This is easily derived from $\lim_{t\to\infty} P_L(x,t;x_0) = 1/L$ taken into the finite sum of Eq. (1.87). It follows that $\dot{S}(t) = \dot{S}_i(t) + \dot{S}_e(t)$ converges to 0 at large t, as expected for a convergent stationary distribution.

The case $L = 2$ and the less interesting case $L = 1$ are not covered above, because of the different topology of the phase space of $L > 2$ compared to $L = 2$. The difference can be observed in the different structure of the transition matrices (1.33) and (1.38). The framework above is based on each site having two outgoing and two incoming rates, $2L$ in total. However, for $L = 2$ there are only two transitions, which cannot be separated into four to fit the framework above, because even when rates of concurrent transitions

between two given states are additive, their entropy production generally is not. The case of $L = 2$ is recovered in the two-state system of Sec. 1.3.1 with $\alpha = \beta = r + \ell$, which is at equilibrium in the stationary state.

1.3.9 Driven Brownian particle

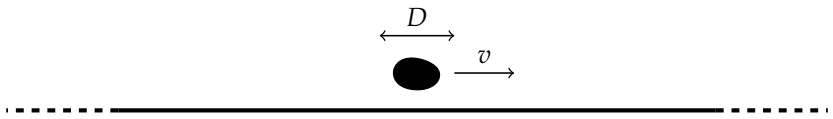

Figure 1.9: Driven Brownian particle on the real line. The black blob indicates the particle's current position.

In continuum space, the motion of a freely diffusive particle with diffusion constant D and drift v is governed by the Langevin equation $\dot{x} = v + \sqrt{2D}\xi(t)$, where $\xi(t)$ is a Gaussian white noise with zero mean, $\langle \xi(t) \rangle = 0$, and covariance $\langle \xi(t)\xi(t') \rangle = \delta(t-t')$, see Fig. 1.9 [290]. The corresponding Fokker-Planck equation for the probability distribution $P(x,t)$ is [234]

$$\partial_t P(x,t) = -v\partial_x P(x,t) + D\partial_x^2 P(x,t)\,. \tag{1.90}$$

Assuming the initial condition $P(x,0) = \delta(x - x_0)$, the solution to the Fokker-Planck equation is the Gaussian distribution

$$P(x,t) = \frac{1}{\sqrt{4D\pi t}} \exp\left\{ -\frac{(x - x_0 - vt)^2}{4Dt} \right\}, \tag{1.91}$$

which is also the Green function of the Fokker-Planck equation (1.90). We therefore also have the transition probability density from state x to state y over an interval τ,

$$W(x \to y, \tau) = \frac{1}{\sqrt{4D\pi\tau}} \exp\left\{ -\frac{(y - x - v\tau)^2}{4D\tau} \right\}. \tag{1.92}$$

Substituting (1.91) and (1.92) into Eq. (1.14) for the internal entropy production of a

continuous system gives,

$$\dot{S}_i = \lim_{\tau\to 0}\frac{1}{\tau}\int \mathrm{d}x\mathrm{d}y\,\frac{1}{\sqrt{4D\pi t}}\exp\left\{-\frac{(x-x_0-vt)^2}{4Dt}\right\} \times \frac{1}{\sqrt{4D\pi\tau}}\exp\left\{-\frac{(y-x-v\tau)^2}{4D\tau}\right\}\left(\frac{(y-x_0)^2-(x-x_0)^2}{4Dt}+\frac{(y-x)v}{2D}\right), \tag{1.93}$$

where the Gaussian integrals can be evaluated in closed form,

$$\dot{S}_i(t) = \lim_{\tau\to 0}\left[1/(2t)+v^2/D+v^2\tau/(2Dt)\right] . \tag{1.94}$$

Taking the limit $\tau \to 0$ then gives the entropy production rate [290, 186, 272],

$$\dot{S}_i(t) = \frac{1}{2t}+\frac{v^2}{D}\,. \tag{1.95}$$

Similarly, following (1.15), the entropy flow reads $\dot{S}_e(t) = -v^2/D$ independent of time t. As $\dot{S}_i(t) \neq 0$, we see that for finite t or $v \neq 0$, the system is out of equilibrium with a sustained probability current, so that there is in fact no steady-state distribution. We can verify Eq. (1.95) for the time-dependent internal entropy production by computing the probability current

$$j(x,t) = (v - D\partial_x)P(x,t) = \left(\frac{v}{2}+\frac{(x-x_0-vt)}{4t}\right)\frac{e^{-\frac{(x-x_0-vt)^2}{4Dt}}}{\sqrt{\pi Dt}} \tag{1.96}$$

and substituting it together with (1.91), into (1.28). As expected, the two procedures return identical results. The independence of the transient contribution $1/(2t)$ to the internal entropy production on the diffusion constant is remarkable although necessary on dimensional grounds, as a consequence of $\dot{S}_i$ having dimensions of inverse time. The diffusion constant characterising the spatial behaviour of diffusion suggests that it is the temporal, rather than spatial features of the process that determine its initial entropy production.

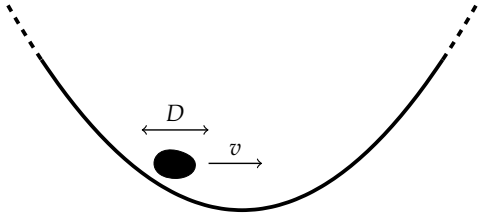

Figure 1.10: Driven Brownian particle in a harmonic potential. This process reduces to the standard Ornstein-Uhlenbeck process upon rescaling $x \to x' + v/k$. The black blob indicates the particle's current position. The presence of a binding potential implies that the system relaxes to an equilibrium steady-state at long times.

1.3.10 Driven Brownian particle in a harmonic potential

Consider a drift-diffusive particle such as in Section 1.3.9 that is confined in a harmonic potential $V(x) = \frac{1}{2}kx^2$, where k is the potential stiffness, see Fig. 1.10 [9]. The Langevin equation is $\dot{x} = v - kx + \sqrt{2D}\xi(t)$, where $\langle \xi(t) \rangle = 0$ and $\langle \xi(t)\xi(t') \rangle = \delta(t - t')$ and the Fokker-Planck equation for $P(x,t)$ is [234]

$$\partial_t P(x,t) = -\partial_x((v - kx)P(x,t)) + D\partial_x^2 P(x,t)\,. \tag{1.97}$$

Assuming the initial condition $P(x,0) = \delta(x - x_0)$, the solution to the Fokker-Plank equation is the Gaussian distribution

$$P(x,t) = \sqrt{\frac{k}{2\pi D(1 - \exp\{-2kt\})}} \exp\left\{ -\frac{(kx - v - (kx_0 - v)\exp\{-kt\})^2}{2Dk(1 - \exp\{-2kt\})} \right\}, \tag{1.98}$$

corresponding to a probability current $j(x,t) = (v - kx - D\partial_x)P(x,t)$ of the form

$$\begin{aligned} j(x) =& \frac{\sqrt{\frac{k}{2\pi D(1-e^{-2kt})}} e^{-kt} \left(v\left(1 - e^{-kt}\right) - k\left(x_0 - xe^{-kt}\right)\right)}{1 - e^{-2kt}} \\ & \times \exp\left\{ -\frac{(v(1 - e^{-kt}) - k(x - x_0 e^{-kt})^2}{2Dk(1 - e^{-2kt})} \right\}. \end{aligned} \tag{1.99}$$

The transition probability density within τ is then also of Gaussian form, namely

$$W(x \to y, \tau) = \sqrt{\frac{k}{2\pi D(1 - \exp\{-2k\tau\})}} \exp\left\{ -\frac{(ky - v - (kx - v)\exp\{-k\tau\})^2}{2Dk(1 - \exp\{-2k\tau\})} \right\}. \tag{1.100}$$

Using (1.98) and (1.100) in (1.14) gives the entropy production rate

$$\dot{S}_i = \left(\frac{(v - kx_0)^2}{D} - k \right) \exp\{-2kt\} + \frac{k \exp\{-2kt\}}{1 - \exp\{-2kt\}} \tag{1.101}$$

and in (1.15) the external entropy flow

$$\dot{S}_e = - \left(\frac{(v - kx_0)^2}{D} - k \right) \exp\{-2kt\} \, . \tag{1.102}$$

In the limit $t \to \infty$, the system will reach equilibrium as $P(x,t)$ in Eq. (1.98) converges to the Boltzmann distribution $\sqrt{\frac{k}{2\pi D}} \exp\left\{ -\frac{(kx-v)^2}{2Dk} \right\}$ of the effective potential $\frac{1}{2}kx^2 - vx$ at temperature D. This is consistent with (1.101) and (1.102) since $\lim_{t\to\infty} \dot{S}_i(t) = \lim_{t\to\infty} \dot{S}_e(t) = 0$. Similarly to drift diffusion on the real line, Eq. (1.95), there is a transient contribution to the entropy production that is independent of the diffusion constant D but does now depend on the stiffness k, which has dimensions of inverse time, through the rescaled time kt.

1.3.11 Driven Brownian particle on a ring with potential

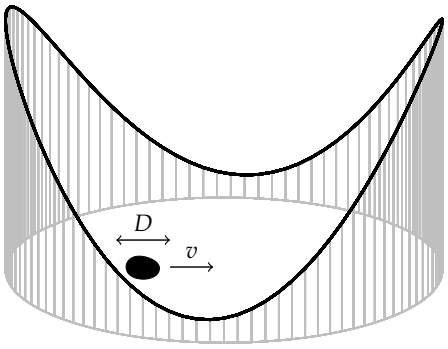

Figure 1.11: Driven Brownian particle on a ring $x \in [0, L)$ with a periodic potential satisfying $V(x) = V(x + L)$. Any finite diffusion constant $D > 0$ results in a stationary state at long times that is non-equilibrium for $v \neq 0$. The black blob indicates the particle's current position.

Consider a drift-diffusive particle on a ring $x \in [0, L)$ in a smooth potential $V(x)$, Fig. 1.11, initialised at position x_0. The Langevin equation of the particle is [230, 225, 205] $\dot{x} = v - \partial_x V(x) + \sqrt{2D}\xi(t)$, where $\xi(t)$ is Gaussian white noise. The Fokker-Planck

equation is then

$$\partial_t P(x,t;x_0) = -\partial_x((v - V'(x))P(x,t;x_0)) + D\partial_x^2 P(x,t;x_0) \tag{1.103}$$

with $V'(x) = \frac{d}{dx}V(x)$ and boundary condition $P^{(n)}(0,t;x_0) = P^{(n)}(L,t;x_0)$ for all $n \geq 0$ derivatives and $t \geq 0$. At stationarity, in the limit $t \to \infty$, where $\partial_t P(x,t;x_0) = 0$, the solution to the Fokker-Planck equation (1.103) is [142, 218, 205]

$$P_s(x) = \lim_{t\to\infty} P(x,t) = \mathcal{Z} \exp\left\{-\frac{V(x) - vx}{D}\right\} \int_x^{x+L} \mathrm{d}y \, \exp\left\{\frac{V(y) - vy}{D}\right\}, \tag{1.104}$$

where $\mathcal{Z}$ is the normalisation constant. The corresponding steady-state probability current $j = (v - \partial_x V)P_s - D\partial_x P_s$ is independent of x by continuity, $0 = \partial_t P = -\partial_x j$, and reads [234]

$$j = \mathcal{Z}\left(\exp\left\{-\frac{vL}{D}\right\} - 1\right) . \tag{1.105}$$

In order to calculate the entropy production according to (1.14) and (1.15) using (1.16), we need $W(x \to y;\tau)$ for small τ. As discussed after Eq. (1.16), $W(x \to y;\tau)$ obeys the Fokker-Planck Eq. (1.103) in the form

$$\partial_\tau W(x \to y;\tau) = -\partial_y \left[(v - V'(y))\, W(x \to y;\tau)\right] + D\partial_y^2 W(x \to y;\tau) \tag{1.106}$$

with $\lim_{\tau\to 0} W(x \to y;\tau) = \delta(y - x)$, so that

$$\dot{W}(x \to y) = \lim_{\tau\to 0} \partial_\tau W(x \to y;\tau) = V''(y)\delta(y-x) - (v - V'(y))\delta'(y-x) + D\delta''(y-x) \tag{1.107}$$

to be evaluated under an integral, where $\delta'(y-x) = \frac{d}{dy}\delta(y-x)$ will require an integration by parts. As for the logarithmic term, we use [300, 234]

$$W(x \to y;\tau) = \frac{1}{\sqrt{4\pi D\tau}} e^{-\frac{(y-x-\tau(v-V'(x)))^2}{4D\tau}} (1 + \mathcal{O}(\tau)) \tag{1.108}$$

so that

$$\ln\left(\frac{W(x \to y;\tau)}{W(y \to x;\tau)}\right) = \frac{y-x}{2D}(2v - V'(x) - V'(y)) + \mathcal{O}(\tau). \tag{1.109}$$

The entropy flow Eq. (1.15) in the more convenient version Eq. (1.20a) can be obtained easily using Eqs. (1.107) and (1.109),

$$\dot{S}_e(t) = -\int_0^L \mathrm{d}x\mathrm{d}y\, P(x,t)\Big(V''(y)\delta(y-x) - (v-V'(y))\delta'(y-x) + D\delta''(y-x)\Big) \tag{1.110}$$

$$\times \frac{y-x}{2D}\left(2v - V'(x) - V'(y)\right) \tag{1.111}$$

$$= -\int_0^L \mathrm{d}x\, P(x,t)\left(\frac{1}{D}\left(v - V'(x)\right)^2 - V''(x)\right) \tag{1.112}$$

after suitable integration by parts, whereby derivatives of the δ-function are conveniently interpreted as derivatives with respect to y to avoid subsequent differentiation of $P(x,t)$. Since $\delta(y-x)(y-x) = 0$, the factor $(y-x)/(2D)$ needs to be differentiated for a term to contribute. In the absence of a potential, $P(x,t) = 1/L$ at stationarity, so that Eq. (1.112) simplifies to $\dot{S}_e(t) = -v^2/D$ and $\lim_{t\to\infty} \dot{S}_i(t) = v^2/D$, Eq. (1.95). Using the probability current $j(x,t) = -D\partial_x P(x,t) + (v - V'(x))\, P(x,t)$, the entropy flow simplifies further to

$$\dot{S}_e(t) = -\int_0^L \mathrm{d}x\, j(x,t)\frac{v - V'(x)}{D} \tag{1.113}$$

so that at stationarity, when the current is spatially uniform,

$$\lim_{t\to\infty} \dot{S}_e(t) = -\lim_{t\to\infty} j(x,t) vL/D \tag{1.114}$$

as the potential is periodic, entering only via the current.

An equivalent calculation of $\dot{S}_i$ on the basis of (1.19a) gives

$$\dot{S}_i(t) + \dot{S}_e$$
$$= \int_0^L \mathrm{d}x\mathrm{d}y\, P(x,t)\Big(V''(y)\delta(y-x) - (v - V'(y))\delta'(y-x) + D\delta''(y-x)\Big) \ln\left(\frac{P(x,t)}{P(y,t)}\right) \tag{1.115a}$$
$$= \int_0^L \mathrm{d}x\, \left\{ D\frac{(P'(x,t))^2}{P(x,t)} - P(x,t)V''(x) \right\} \tag{1.115b}$$
$$= -\int_0^L \mathrm{d}x\, j(x,t)\partial_x \ln P(x,t)\ , \tag{1.115c}$$

whence

$$\dot{S}_i(t) = \int_0^L \mathrm{d}x \frac{j^2(x,t)}{DP(x,t)}\,, \tag{1.115d}$$

with the last equation identical to Eq. (1.12).

By considering the functional derivative $\delta Z/\delta V(z)$ in $\int_0^L \mathrm{d}x P(x) = 1$ of Eq. (1.104), one can show that the stationary current $j(x,t)$ Eq. (1.105) is extremal for constant $V(x)$, indicating that the magnitude of the stationary entropy flow Eq. (1.115d) is maximised in a constant potential.

1.3.12 Run-and-tumble motion with diffusion on a ring

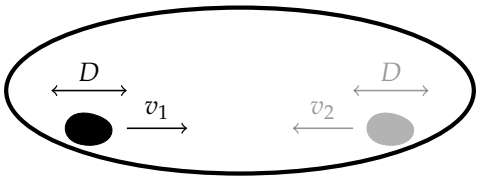

Figure 1.12: Run-and-tumble motion with diffusion on a ring $x \in [0, L)$. A run-and-tumble particle switches stochastically, in a Poisson process with rate α, between two modes 1 and 2 characterised by an identical diffusion constant D but distinct drift velocities v_1 and v_2. The two modes are here represented in black and grey, respectively. For arbitrary positive diffusion constant D or tumbling rate α with $v_1 \neq v_2$ the steady state is uniform but generally non-equilibrium.

Consider the dynamics of a run-and-tumble particle on a ring $x \in [0, L)$ [250] with Langevin equation $\dot{x} = v(t) + \sqrt{2D}\xi(t)$, where the drift $v(t)$ is a Poisson process with

rate α that alternates the speed of the particle between the constants v_1 and v_2, and $\xi(t)$ is Gaussian white noise, Fig. 1.12. The drift being $v(t) = v_1$ or $v(t) = v_2$ will be referred to as the mode of the particle being 1 or 2 respectively. Defining $P_1(x,t)$ and $P_2(x,t)$ as the joint probabilities that the particle is at position x at time t and in mode 1 or 2 respectively, the coupled Fokker-Planck equations for P_1 and P_2 are

$$\partial_t P_1(x,t) = -v_1 \partial_x P_1(x,t) + D\partial_x^2 P_1(x,t) - \alpha(P_1(x,t) - P_2(x,t)) \tag{1.116a}$$

$$\partial_t P_2(x,t) = -v_2 \partial_x P_2(x,t) + D\partial_x^2 P_2(x,t) - \alpha(P_2(x,t) - P_1(x,t)) \tag{1.116b}$$

whose stationary solution is the uniform distribution $\lim_{t\to\infty} P_1(x,t) = \lim_{t\to\infty} P_2(x) = 1/(2L)$ as is easily verified by direct substitution. The corresponding steady-state probability currents thus read $j_1 = v_1/(2L)$ and $j_2 = v_2/(2L)$.

In the following, we denote by the propagator $W(x \to y, Q \to R; \tau)$ the probability density that a particle at position x in mode Q is found time τ later at position y in mode R. For $Q = R$, this propagation is a sum over all even numbers m of Poissonian switches, that occur with probability $(\alpha\tau)^m \exp\{-\alpha\tau\}/m!$, which includes the probability $\exp\{-\alpha\tau\}$ of not switching at all over a total of time τ. For $Q \neq R$, the propagation is due to an odd number of switches.

For $m = 0$, the contribution to $W(x \to y, Q \to R; \tau)$ is thus $\exp\{-\alpha\tau\}W(x \to y; \tau)$, with $W(x \to y; \tau)$ of a drift diffusion particle on a ring, Section 1.3.11, but without potential, approximated at short times τ by the process on the real line, Eq. (1.92) with drift $v = v_1$ or $v = v_2$ according to the particle's mode. For $m = 1$ the contribution is a single convolution over the time $t' \in [0, \tau)$ at which the particle changes mode, most easily done after Fourier transforming. Before presenting this calculation in real space, we argue that any such convolution will result in some approximate Gaussian with an amplitude proportional to $1/\sqrt{\tau}$ multiplied by a term of order $(\alpha\tau)^m$. In small τ, therefore only the lowest orders need to be kept, $m = 0$ for $Q = R$ and $m = 1$ for $Q \neq R$.

More concretely,

$$
\begin{aligned}
&W(x \to y, 1 \to 2; \tau) \\
=&\int_{-\infty}^{\infty} \mathrm{d}z \int_0^{\tau} \mathrm{d}\tau' \frac{1}{\sqrt{4\pi D\tau'}} \exp\left\{-\frac{(z-x-v_1\tau')^2}{4D\tau'}\right\} \\
&\quad \times \exp\{-\alpha\tau'\} \frac{1}{\sqrt{4\pi D(\tau-\tau')}} \exp\left\{-\frac{(y-z-v_2(\tau-\tau'))^2}{4D(\tau-\tau')}\right\} \exp\{-\alpha(\tau-\tau')\} + \ldots
\end{aligned} \tag{1.117}
$$

$$
= \frac{\alpha \exp\{-\alpha\tau\}}{2(v_1-v_2)} \left[\mathrm{erf}\left(\frac{x-y+v_1\tau}{\sqrt{4D\tau}}\right) - \mathrm{erf}\left(\frac{x-y+v_2\tau}{\sqrt{4D\tau}}\right)\right] + \ldots \tag{1.118}
$$

which in small τ, when $v_{1,2}\tau/\sqrt{4D\tau} \ll 1$, so that $\mathrm{erf}(r+\varepsilon) = \mathrm{erf}(r) + 2\varepsilon\, e^{-r^2}/\sqrt{\pi} + \ldots$, expands to

$$
\begin{aligned}
W(x \to y, 1 \to 2; \tau) &= \frac{\alpha\tau}{\sqrt{4\pi D\tau}} e^{-\frac{(y-x)^2}{4D\tau}} \left(1 + \mathcal{O}(\tau^2)\right) \\
&= W(x \to y, 2 \to 1; \tau) \ ,
\end{aligned} \tag{1.119}
$$

whereas $W(x \to y, Q \to Q; \tau)$, the propagator with an even number of mode switches, is given by Eq. (1.92) to leading order in τ,

$$
W(x \to y, Q \to Q; \tau) = \frac{1}{\sqrt{4\pi D\tau}} e^{-\frac{(y-x-v_Q\tau)^2}{4D\tau} - \alpha\tau} \left(1 + \mathcal{O}(\tau^2)\right) \ . \tag{1.120}
$$

Much of the calculation of the entropy production follows the procedure in Secs. 1.3.9 and 1.3.11 to be detailed further below. To this end, we also need

$$
\begin{aligned}
\lim_{\tau\to 0} \frac{\mathrm{d}}{\mathrm{d}\tau} W(x \to y, 1 \to 2; \tau) &= \dot{W}(x \to y, 1 \to 2) = \alpha\delta(x-y) \\
&= \dot{W}(x \to y, 2 \to 1) \, .
\end{aligned} \tag{1.121}
$$

As far as processes are concerned that involve a change of particle mode, therefore only the transition rates enter, not diffusion or drift. Given a uniform stationary spatial distribution of particles of any mode, mode changes between two modes cannot result

in a sustained probability current, even when the switching rates differ,

$$\Big(P_1\dot{W}(1\to 2) - P_2\dot{W}(2\to 1)\Big)\ln\left(\frac{P_1\dot{W}(1\to 2)}{P_2\dot{W}(2\to 1)}\right) = 0 \tag{1.122}$$

for $P_1\dot{W}(1\to 2) = P_2\dot{W}(2\to 1)$ at stationarity as in the process discussed in Section 1.3.1. A probability current and thus entropy production can occur when different particle modes result in a different distribution, Section 1.3.10, or when mode switching between more than two modes results in a current in its own rights, Secs. 1.3.2 and 1.3.13.

Since the full time-dependent density is beyond the scope of the present work, we calculate entropy flow and production at stationary on the basis of a natural extension of Eqs. (1.4), (1.15) and (1.20a) to a mixture of discrete and continuous states

$$-\lim_{t\to\infty}\dot{S}_e(t) = \lim_{t\to\infty}\dot{S}_i(t) \tag{1.123}$$

$$= \sum_{Q,R\in\{1,2\}}\int_0^L \mathrm{d}x\mathrm{d}y P_Q(x,t)\dot{W}(x\to y, Q\to R)\lim_{\tau\to 0}\ln\left(\frac{W(x\to y, Q\to R;\tau)}{W(y\to x, R\to Q;\tau)}\right)$$

$$= \frac{v_1^2+v_2^2}{2D} \tag{1.124}$$

which immediately follows from Secs. 1.3.9 and 1.3.11, as the stationary density is constant, $P_Q = P_R = 1/(2L)$, and only $Q = R$ contribute, with

$$\lim_{\tau\to 0}\ln\left(\frac{W(x\to y, 1\to 2;\tau)}{W(y\to x, 2\to 1;\tau)}\right) = 0\ . \tag{1.125}$$

If the drifts are equal in absolute value $|v_1| = |v_2| = v$, then we recover the entropy production of a simple drift-diffusive particle, $\dot{S}_i = v^2/D$. This is because we can think of run-and-tumble as a drift-diffusion particle that changes direction instantly. Since changing the direction produces no entropy, the total entropy production rate should be the same as a drift-diffusion particle. The entropy production can alternatively be derived via (1.28) by computing $\dot{S}_i = \int \mathrm{d}x\,(j_1^2/(DP_1) + j_2^2/(DP_2))$ with the steady-state currents stated above.

1.3.13 Switching diffusion process on a ring

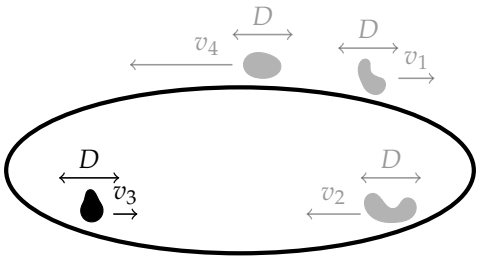

Figure 1.13: Switching diffusion process on a ring $x \in [0, L]$ in continuous time. A switching diffusion process involves a stochastic switching between M modes characterised by an identical diffusion constant D but distinct drifts v_i ($i = 1, 2, \ldots, M$). The marginal switching dynamics are characterised as an M-state Markov process with transition rates α_{ij} from mode i to mode j.

The dynamics of a one-dimensional run-and-tumble particle discussed above can be readily generalised to the so called switching diffusion process [305] by allowing for an extended set $\{v_i\}$ of drift modes $i = 1, \ldots, M$, Fig. 1.13. The corresponding Langevin equation for the particle position on a ring $x \in [0, L]$ is almost identical to that of run-and-tumble, namely $\dot{x} = v(t) + \sqrt{2D}\xi(t)$, with the exception that the process $v(t)$ is now an M-state Markov process. In the general case, a single switching rate α is thus not sufficient and the full transition rate matrix α_{ij} needs to be provided. In this formulation, the run-and-tumble dynamics Sec. 1.3.12 correspond to the choice $M = 2$ with symmetric rates $\alpha_{12} = \alpha_{21} = \alpha$. Defining $P_i(x, t)$ as the joint probability that at time t the particle is at position x and in mode i, thereby moving with velocity v_i, the system (1.116) of Fokker-Planck equations generalises to

$$\partial_t P_i(x,t) = -\partial_x[(v_i - D\partial_x)P_i(x,t)] + \sum_j P_j(x,t)\alpha_{ji} \tag{1.126}$$

where the transmutation rates α_{ij} from mode i to mode j are assumed to be independent of position. To ease notation we use the convention $\alpha_{jj} = -\sum_{i\neq j}\alpha_{ji}$. For non-vanishing diffusion constant, the stationary solution is uniform for all modes and given by $\lim_{t\to\infty} P_i(x,t) = z_i/L$, where z_i is the ith element of the eigenvector $\mathbf{z}$ satisfying $\sum_j z_j = 1$ and the eigenvalue relation $\sum_j z_j\alpha_{ji} = 0$, which we assume to be unique for simplicity.

The calculation of the steady-state entropy production follows very closely that of run-and-tumble presented above. The conditional transition probabilities including up to

one transmutation event read to leading order

$$W(x \to y, i \to j; \tau) = \begin{cases} \frac{e^{\alpha_{ii}\tau}}{\sqrt{4\pi D\tau}} \exp\left\{-\frac{(y-x-v_i\tau)^2}{4D\tau}\right\} (1 + \mathcal{O}(\tau^2)) & \text{for } i = j \\ \frac{\alpha_{ij}}{2(v_i - v_j)} \left[\operatorname{erf}\left(\frac{x-y+v_i\tau}{\sqrt{4D\tau}}\right) - \operatorname{erf}\left(\frac{x-y+v_j\tau}{\sqrt{4D\tau}}\right)\right] (1 + \mathcal{O}(\tau^2)) & \text{for } i \neq j \end{cases} , \tag{1.127}$$

so that

$$\lim_{\tau \to 0} \frac{\mathrm{d}}{\mathrm{d}\tau} W(x \to y, i \to j; \tau) = \begin{cases} D\partial_y^2 \delta(y-x) - v_i \partial_y \delta(y-x) + \alpha_{ii}\delta(y-x) & \text{for } i = j \\ \alpha_{ij}\delta(y-x) & \text{for } i \neq j \end{cases} . \tag{1.128}$$

We could perform the calculation of the entropy production using the procedure of Sec. 1.3.9 rather than drawing on the operator for $i = j$, which, however, is used in the following for convenience, see Sec. 1.3.11. Substituting (1.127) and (1.128) into (1.19a) and assuming steady-state densities, we arrive at

$$\begin{aligned} \lim_{t\to\infty} \dot{S}_i(t) &= -\lim_{t\to\infty} \dot{S}_e(t) \\ &= \int_0^L \mathrm{d}x\mathrm{d}y \sum_i \frac{z_i}{L} \left(D\partial_y^2 \delta(y-x) - v_i \partial_y \delta(y-x) + \alpha_{ii}\delta(y-x)\right)(y-x)\frac{v_i}{D} \\ &\quad + \int_0^L \mathrm{d}x\mathrm{d}y \sum_{i,j\neq i} \frac{z_i}{L} \alpha_{ij}\delta(y-x) \ln\left(\frac{\alpha_{ij}}{\alpha_{ji}}\right) , \end{aligned} \tag{1.129}$$

where we have used Eq. (1.128) in the operators containing the δ-functions and Eq. (1.127) in the logarithms. The term $\ln(\alpha_{ij}/\alpha_{ji})$ is obtained by the same expansion as used in Eq. (1.119), Sec. 1.3.12. Both terms contributing to the entropy production above are familiar from previous sections: the first is a sum over the entropy production of M drift-diffusion processes with characteristic drift v_i, Sec. 1.3.11 without potential, weighted by the steady-state marginal probability z_i for the particle to be in state i; the second is the steady-state entropy production of an M-state Markov process with transition rate matrix α_{ij}, which reduces to Eq. (1.4) after integration. Carrying out all integrals, we finally have

$$\lim_{t\to\infty} \dot{S}_i(t) = \lim_{t\to\infty} -\dot{S}_e(t) = \sum_i z_i \frac{v_i^2}{D} + \frac{1}{2}\sum_{i,j} (z_i\alpha_{ij} - z_j\alpha_{ji}) \ln\left(\frac{\alpha_{ij}}{\alpha_{ji}}\right) . \tag{1.130}$$

Unlike run-and-tumble, Sec. 1.3.12, the transmutation process in switching diffusion does in general contribute to the entropy production for $M > 2$, since the stationary state generally does not satisfy detailed balance. However, contributions to the total entropy production originating from the switching and those from the diffusion parts of the process are effectively independent at steady state, as only the stationary marginal probabilities z_i of the switching process feature as weights in the entropy production of the drift-diffusion. Otherwise the parameters characterising the two processes stay separate in Eq. (1.130). Further, the drift-diffusion contributions of the form v_i^2/D are invariant under the time-rescaling $\alpha_{ij} \to T\alpha_{ij}$. This property originates from the steady-state distributions $P_i(x)$ being uniform and would generally disappear in a potential, Sec. 1.3.10.

1.4 Discussion and concluding remarks

In this work we calculate the rate of entropy production within Gaspard's framework [113] from first principles in a collection of paradigmatic processes, encompassing both discrete and continuous degrees of freedom. Based on the Markovian dynamics of each system, where we can, we derive the probability distribution of the particle (or particles) as a function of time $P(x,t)$ from Dirac or Kronecker-δ initial conditions $P(x,0) = \delta(x - x_0)$, from which the transition probability $W(x \to y;\tau)$ follows straightforwardly. In some cases, we determine only the stationary density and the (short-time) propagator $W(x \to y;\tau)$ to leading order in τ. We then use Eq. (1.4) for discrete systems or Eqs. (1.19) and (1.20) for continuous systems to calculate the time-dependent entropy production. We set out to give concrete, exact results in closed form, rather than general expressions that are difficult to evaluate, even when we allowed for general potentials in Sec. 1.3.11. In summary, the ingredients that are needed to calculate the entropy production in closed form in the present framework are: a) the probability (density) $P(x,t)$ to find the system in state x ideally as a function of time t and b) the propagator $W(x \to y;\tau)$, the probability (density) that the system is found at a certain state y after some short time τ given an initial state x. If the propagator is known for any time τ, it can be used to calculate the probability $P(x,t;x_0) = W(x_0 \to x;t)$ for some initial state x_0. However, this full time dependence is often difficult to obtain. The propagator is further needed in two forms, firstly $\lim_{\tau\to 0} \partial_\tau W(x \to y;\tau)$

when it is most elegantly written as an operator in continuous space, and secondly $\lim_{\tau\to 0}\ln(W(x\to y;\tau)/W(y\to x;\tau))$.

For completeness, where feasible, we have calculated the probability current $j(x,t)$ in continuous systems at position x. The mere presence of such a flow indicates broken time-reversal symmetry and thus non-equilibrium. Our results on the discrete systems (Sec. 1.3.1 to 1.3.8) illustrate two important aspects of entropy production. First, the need of a probability flow $P_A\dot{W}(A\to B)-P_B\dot{W}(B\to A)$ between states: in the two-state system Sec. 1.3.1 there are no transition rates α and β such that there is a sustained probability flow and therefore, the system inevitably relaxes to equilibrium. However, in the three-state system Sec. 1.3.2 the transition rates can be chosen so that there is a perpetual flow $(\alpha-\beta)/3$ between any two states and therefore there is entropy production not only during relaxation but also at stationarity. Hence, we can ascertain these as non-equilibrium steady states in the long time limit due to the non-vanishing rate of internal entropy production. Uniformly distributed steady states can be far from equilibrium as a rigorous analysis on the basis of the microscopic dynamics reveals, although an effective dynamics may suggest otherwise.

Second, we see how the extensivity of entropy production arises in the N-particle systems (Secs. 1.3.4, 1.3.5 and 1.3.6), independently of whether the particles are distinguishable or not. We therefore conclude that the number of particles in the system must be accounted for when calculating the entropy production, and doing otherwise will not lead to a correct result. This is sometimes overlooked, especially when using effective theories. In the continuous systems (Sec. 1.3.9 to 1.3.11), which involve a drift v and a diffusion constant D, we always find the contribution v^2/D to the entropy production emerging one way or another. Moreover, in the case of drift-diffusion on the real line (Sec. 1.3.9) we find that the contribution due to the relaxation of the system $1/(2t)$ is independent of any of the system parameters.

Finally, we have studied two systems (Sec. 1.3.12 and 1.3.13) where the state space has a discrete and a continuous component. The discrete component corresponds to the transmutation between particle species, *i.e.* their mode of drifting, whereas the continuous component corresponds to the particle motion. We find that both processes, motion and transmutation, contribute to the entropy production rate essentially independently since any term that combines both processes is a higher-order term contribution in τ, and therefore vanishes in the limit $\tau\to 0$.

This work has applications to the field of active particle systems, where particles are subject to local non-thermal forces. In fact, the systems studied in sections 1.3.2 and 1.3.8 – 1.3.13 are prominent examples of active systems. We have shown that their entropy production crucially relies on the microscopic dynamics of the system, which are captured by the Fokker-Planck equation (or the master equation for discrete systems) and its solution. However, in interacting many-particle systems, such a description is not available in general. Instead, we may choose to use the Doi-Peliti formalism [80, 219, 279, 267, 39, 170, 216, 107, 109] to describe the system, since it provides a systematic approach based on the microscopic dynamics and which retains the particle entity.

ACKNOWLEDGMENTS

The authors would like to thank Letian Chen, Greg Pavliotis and Ziluo Zhang for discussions and kind advice. The authors gratefully acknowledge Kin Tat (Kenneth) Yiu's much earlier, related work [307].

2

Non-equilibrium thermodynamics of diffusion in fluctuating potentials

H. Alston†, L. Cocconi†, T. Bertrand

JPA **55**, 27 (2022) [6]
Published 14 June 2022
DOI 10.1088/1751-8121/ac726b

Overview After having reviewed the mathematical machinery of entropy production in Chapter 1, we focus here on a particular family of non-equilibrium processes, namely those involving a single passive particle suspended in a viscous fluid and subject to an external potential force that evolves stochastically over time. We assume that the passive particle is 'small enough' such that its coupling to the surrounding environment leads to non-negligible thermal fluctuations, resulting in so-called Brownian or diffusive motion [89]. While fluctuations in the external force directly affect the dynamics of the particle position, the reverse does not apply and the resulting asymmetry drives the system away from thermodynamic equilibrium. An exact calculation of the entropy production for various simple setups demonstrates that a constant expenditure of energy is required to sustain this type of dynamics even when force fluctuations are fast and

thus supposedly 'negligible' in some sense to be made precise in the following. We will refer to this as an *entropic anomaly* [59]. Interestingly, stochastic forces originating from fluctuating potentials are bound to occur in many real-world problems involving microscopic particles. For example, the manipulation of microbeads and other colloids by means of optical tweezers relies on realistic lasers, whose power output exhibits small fluctuations during the course of a single experiment [125].

Author contributions: HA performed preliminary calculations on the entropy production with intermittent harmonic potentials. LC explained the methodology and suggested various generalisations, in particular to continuous Markov processes. HA and LC collaborated on all of the analytical calculations. HA performed the numerical simulations. TB supervised the project and edited the final manuscript.

Abstract

A positive rate of entropy production at steady state is a distinctive feature of truly non-equilibrium processes. Exact results, while being often limited to simple models, offer a unique opportunity to explore the thermodynamic features of these processes in full detail. Here we derive analytical results for the steady-state rate of entropy production in single particle systems driven away from equilibrium by the fluctuations of an external potential of arbitrary shapes. Subsequently, we provide exact results for a diffusive particle in a harmonic trap whose potential stiffness varies in time according to both discrete and continuous Markov processes. In particular, studying the case of a fully intermittent potential allows us to introduce an effective model of stochastic resetting for which it is possible to obtain finite non-negative entropy production. Altogether, this work lays the foundation for a non-equilibrium thermodynamic theory of fluctuating potentials, with immediate applications to stochastic resetting processes, fluctuations in optical traps and fluctuating interactions in living systems.

2.1 Introduction

Stochastic thermodynamics represents one of the most powerful tools at our disposal in the effort to characterize generic properties of non-equilibrium processes. It provides a framework to extend the ideas of traditional thermodynamics to regimes and scales

where some of the assumptions underlying the latter theory break down [220, 256, 64]. In particular, the possibility of developing a thermodynamically-consistent description of mesoscopic systems subject to non-negligible noise (a paradigmatic example being overdamped colloidal particles) has unveiled a wealth of fascinating relations among the fluctuating counterparts of traditional thermodynamic observables, such as work, heat and entropy [254, 147, 260]. For instance, in the presence of fluctuations, the second law of thermodynamics is only satisfied upon taking suitable averages over an ensemble of stochastic trajectories or over long observation times.

Over the last decades, the average rate of entropy production, denoted $\dot{S}_i$, has attracted considerable attention as a way of quantifying the degree of departure from equilibrium. For instance, genuinely non-equilibrium processes (as opposed to those relaxing to equilibrium), such as overdamped active particles driven by injection and dissipation of energy at the single-agent level [23, 192], are characterized by a positive average entropy production at steady-state which equals the rate at which heat is dissipated into the environment.

Interestingly, entropy production has also been formalized as a measure of the breaking of the global detailed balance condition [64, 248, 173]. In particular, it has long been established for Markovian processes [113] that the thermodynamic entropy production has an equivalent information-theoretic interpretation as the relative dynamical entropy (i.e., the Kullback–Leibler divergence [163]) per unit time of the ensemble of forward paths and their time-reversed counterparts, thus signaling the breaking of time-reversal symmetry whenever $\dot{S}_i > 0$. Based on this perspective, it was further shown that the rate of entropy production is inversely proportional to the minimal time needed to decide on the direction of the arrow of time [238, 253]. Entropy production has additionally been found to relate non-trivially to the precision and efficiency of the underlying stochastic process via uncertainty relations [257, 141].

In this work, we consider the average entropy production associated with a Brownian particle subject to diffusion in a fluctuating trapping potential $V(x;\alpha(t))$ whose shape is governed by a parameter $\alpha(t)$. In most of what follows, we will assume the potential to be harmonic and centered at the origin, with fluctuations acting solely on the potential stiffness. In the absence of fluctuations, this model reduces to the well-known Ornstein-Uhlenbeck (OU) process [112], a prototypical equilibrium stochastic process characterized by a Gaussian steady-state probability density function for the particle

position x, and zero entropy production. As we will demonstrate, letting $\alpha(t)$ evolve stochastically results generically in a departure from thermodynamic equilibrium, signaled by non-vanishing probability currents at steady-state and thus a positive rate of entropy production.

Introducing fluctuations into what would otherwise be time-independent model parameters is a recurrent theme in non-equilibrium physics. Indeed, think for example of Run-and-Tumble (RnT) and Active Ornstein-Uhlenbeck (AOUPs) particles , whose self-propulsion velocity is described by a telegraph process and an OU process, respectively [43, 109]. Fluctuating interactions are a generic feature of living systems and can have striking consequences including clustering in populations of bacteria interacting via type IV pili [7, 37, 315], arrested coalescence in cellular aggregates [212] and fluidization of embryonic tissues [156]. Moreover, a clear thermodynamic understanding of trapping by fluctuating harmonic potentials could have important implications in a number of mesoscopic systems. For instance, experimental manipulation of colloidal beads [13] and molecular motor cargoes [14, 129, 206, 52] by optical tweezers are likely to be subject to non-negligible fluctuations (e.g. from the laser intensity).

Furthermore, Brownian motion in an intermittent harmonic confining potential represents a realistic implementation of stochastic resetting [244, 148, 128, 127, 97]. Originally introduced to allow Brownian dynamics to reach a non-equilibrium stationary state (NESS) at long times [94, 97], stochastic resetting has been under intense scrutiny over the last decade partly due to its non-trivial impact on first-passage statistics [94, 93] and has imposed itself as a pillar of non-equilibrium statistical mechanics. As a consequence, the effects of resetting have been studied in a swath of physical systems: from classical diffusive processes such as Brownian motion, random walks, Lévy walks and Lévy flights [189, 126, 264, 199, 317, 165], to the random acceleration process [265] and the asymmetric exclusion processes [21, 153]. More recently, resetting has also found applications in stochastic living systems including in models of active particles [96, 243, 164], active transport in living cells [46], enzymatic reactions [233, 232], population genetics [73] and in models of cell division [115].

Of interest here is the fact that the vast majority of these studies generically consider fully irreversible and instantaneous resetting. While various works have addressed the non-equilibrium thermodynamics of resetting, the typically assumed irreversibility of resetting events requires a special treatment [105, 50, 214]. In particular, these studies

made use of alternative definitions for the entropy production whose connection with time-reversal symmetry breaking remains unclear. Here, we argue that a realistic implementation of an effective resetting protocol can offer a relevant perspective on these controversies.

The paper is structured as follows: in Section 2.2, we derive equations for the steady-state entropy production for a general single-particle drift-diffusion system with fluctuating potentials, considering both discrete and continuous state spaces for the potential states. The rest of the paper is dedicated to specific examples of these single-particle systems. In Section 2.3, we consider the simple example of an intermittent harmonic potential to illustrate a practical application of the theory, calculating the steady-state entropy production exactly in Eq. (2.29). We then consider a generalized two-state OU model in Section 2.4 and derive its entropy production in Eq. (2.40), before extending this result to an arbitrary number of states in Section 2.5, deriving Eq. (2.47). In Section 2.6, we study an OU process with a stiffness that varies continuously in time, writing the entropy production in terms of the variance of the particle position in Eq. (2.63). Finally, our results are summarized in Section 2.7.

2.2 Steady-state entropy production in drift-diffusion processes with fluctuating potentials

In this first section, we derive the general expression for the steady-state entropy production of a Brownian particle diffusing on the real line, $x \in \mathbb{R}$, in a confining potential $V(x;\alpha(t))$, whose shape is set by $\alpha(t)$, a random variable that evolves in continuous time according to Markovian dynamics (see Fig. 2.1). While in the rest of this study we focus on the case of a harmonic confining potential $V(x;\alpha(t)) = \alpha(t)x^2/2$, the functional form of the potential will remain generic in this section. First, we derive the steady-state entropy production in the case where the potential follows a discrete Markov process; in this case, we assume that the potential jumps in between different 'states' corresponding to particular values of $\alpha(t)$. We then derive the corresponding results in the case where $\alpha(t)$ follows a generic continuous Markov process. Note that for the sake of simplicity, we will only consider in what follows one-dimensional systems; however, our results can be straightforwardly generalized to higher dimensions, assuming independent Brownian fluctuations in each dimension, by treating each coordinate

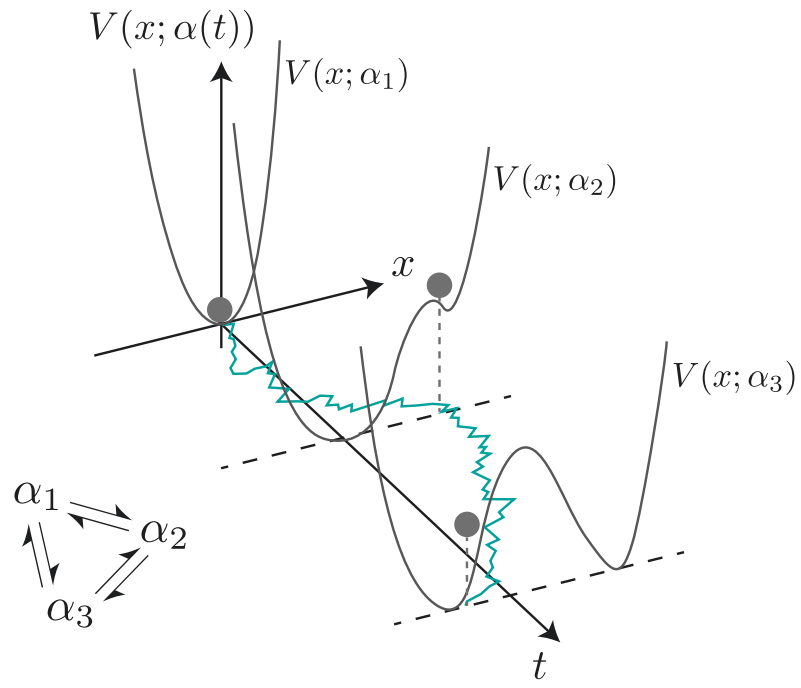

Figure 2.1: *Diffusion in fluctuating potentials* — In many realistic settings, trapping potentials can be subject to stochastic fluctuations. This phenomenon generically breaks global detailed balance and can thus drive a passive Brownian particle trapped in the potential away from thermodynamic equilibrium, such that the corresponding entropy production is non-zero even at steady-state. In the simplest case, a stochastic potential switches between a pre-defined set of functional forms $V_i(x) = V(x;\alpha_i)$, with $i \in \{1,2,3\}$, according to a Markov jump process with given, time-independent transition rates.

as a separate degree of freedom.

2.2.1 Fluctuating potentials as a discrete Markov process

First, we model the fluctuations in the confining potential as arising from jumps among a finite set of N distinct states. Namely, we let $\alpha(t) \in \{\alpha_1, \alpha_2, ..., \alpha_N\}$ evolve according to a continuous-time, N-state Markov jump process with transition rate matrix K, where the matrix element K_{ij} with $i \neq j$ denotes the rate at which the parameter switches from value α_j to α_i. The diagonal elements are generically fixed by enforcing conservation of total probability, $\sum_i K_{ij} = 0$, so that $K_{jj} = -\sum_{i \neq j} K_{ij}$.

The resulting stochastic dynamics for the parameter $\alpha(t)$ is thus given by

$$\mathbb{P}\big(\alpha(t+\Delta t)=\alpha_i|\alpha(t)=\alpha_j\big)=\delta_{ij}+\Delta t K_{ij}+\mathcal{O}\big(\Delta t^2\big) \tag{2.1}$$

while the particle position is governed by the overdamped Langevin equation

$$\dot{x}(t)=-\frac{1}{\gamma}\,\partial_x V(x;\alpha(t))+\sqrt{2D}\eta(t)\ , \tag{2.2}$$

where γ is a friction coefficient and $\eta(t)$ denotes a Gaussian white noise with zero mean, $\langle\eta(t)\rangle=0$, and unit variance, $\langle\eta(t)\eta(t')\rangle=\delta(t-t')$. We set $\gamma=1$ without loss of generality. The corresponding Fokker-Planck equation takes the form [112, 234]

$$\partial_t P_i(x,t)=-\partial_x J_i(x,t)+\sum_j K_{ij}P_j(x,t) \tag{2.3}$$

for $i=1,2,...,N$, with $P_i(x,t)$ the joint probability density that the particle is found at position x with the potential in state i and $J_i(x,t)$ the state-dependent probability current density, given by

$$J_i(x,t)=-\big(\partial_x V(x;\alpha_i)\big)P_i(x,t)-D\partial_x P_i(x,t)\ . \tag{2.4}$$

The total probability is defined as $P(x,t)=\sum_{i=1}^N P_i(x,t)$.

The Gibbs-Shannon entropy [261] of the joint probability density $P_i(x,t)$ is defined as

$$S(t)=-\sum_i\int dx\ P_i(x,t)\log\left(\frac{P_i(x,t)}{\bar{P}}\right) \tag{2.5}$$

where $\bar{P}$ is an arbitrary density introduced for dimensional consistency and we work in units such that $k_B=1$. While an entropy $\tilde{S}(t)$ could in principle be defined for any marginal of the full probability density, as in e.g.

$$\tilde{S}(t)=-\int dx\left[\sum_i P_i(x,t)\right]\log\left[\frac{\sum_i P_i(x,t)}{\bar{P}}\right] \tag{2.6}$$

it is only for the couple (x,α) that the dynamics are Markovian and the standard toolkit of stochastic thermodynamics can be applied straightforwardly. Further, our choice to

consider the full dynamics for the variables (x, α) allows us to define as we will see drift and switching contributions to the entropy production which we relate to the heat dissipated in the various heat baths coupled to the process. Differentiating $S(t)$ with respect to time, we see

$$\dot{S}(t) = -\sum_i \int dx\ \partial_t P_i(x,t) \log\left(\frac{P_i(x,t)}{\bar{P}}\right) \tag{2.7}$$

and using Eq. (2.3), we obtain after integration by parts

$$\dot{S}(t) = -\sum_i \int dx \left[\frac{J_i(x,t)\partial_x P_i(x,t)}{P_i(x,t)} + \sum_j K_{ij} P_j(x,t) \log\left(\frac{P_i(x,t)}{\bar{P}}\right)\right] \tag{2.8}$$

which using Eq. (2.4), we rewrite as

$$\dot{S}(t) = \sum_i \int dx \left[\frac{J_i^2(x,t)}{D P_i(x,t)} + \frac{J_i(x,t)\partial_x V(x;\alpha_i)}{D} - \sum_j K_{ij} P_j(x,t) \log\left(\frac{P_i(x,t)}{\bar{P}}\right)\right]. \tag{2.9}$$

By conservation of probability, we have

$$K_{ii} P_i(x,t) = -\sum_{j\neq i} K_{ji} P_i(x,t)\ , \tag{2.10}$$

which allows us to rewrite the third term on the right-hand side of Eq. (2.9) as

$$\begin{aligned}\int dx \sum_{i,j} K_{ij} P_j(x,t) \log\left(\frac{P_i(x,t)}{\bar{P}}\right) = \\ -\frac{1}{2}\int dx \sum_{i,j\neq i} (K_{ij}P_j(x,t) - K_{ji}P_i(x,t)) \log\left(\frac{K_{ij}P_j(x,t)}{K_{ji}P_i(x,t)}\right) \\ +\frac{1}{2}\int dx \sum_{i,j\neq i} (K_{ij}P_j(x,t) - K_{ji}P_i(x,t)) \log\left(\frac{K_{ij}}{K_{ji}}\right)\ ,\end{aligned} \tag{2.11}$$

where we first re-write the sum on the LHS using Eq. (2.10), then consider the corresponding sum with the indices i and j swapped. Since i and j are dummy indices, we write the original sum as half times itself plus half times its counterpart with indices being swapped. We finally multiply the fraction in the $\log(\cdot)$ term by a factor $\frac{K_{ij}K_{ji}}{K_{ij}K_{ji}} = 1$

which changes only the appearance of the terms on the RHS, then expanding to obtain the desired form in Eq. (2.11).

Following the standard procedure [256, 64], the contributions to the rate of change of the Gibbs-Shannon entropy are split into two terms

$$\dot{S}(t) = \dot{S}_i(t) + \dot{S}_e(t) \ , \tag{2.12}$$

with the internal (or total) entropy production defined as

$$\dot{S}_i(t) = \sum_i \left[\int dx \ \frac{J_i^2(x,t)}{D P_i(x,t)} \right] + \frac{1}{2} \int dx \sum_{i,j \neq i} \left(K_{ij} P_j(x,t) - K_{ji} P_i(x,t) \right) \log \left(\frac{K_{ij} P_j(x,t)}{K_{ji} P_i(x,t)} \right) \tag{2.13}$$

and the external entropy production (or entropy flow) as

$$\dot{S}_e(t) = \sum_i \left[\int dx \ \frac{J_i(x,t) \partial_x V(x;\alpha_i)}{D} \right] - \frac{1}{2} \sum_{i,j \neq i} \left(K_{ij} P_j^{\mathrm{tot}}(t) - K_{ji} P_i^{\mathrm{tot}}(t) \right) \log \left(\frac{K_{ij}}{K_{ji}} \right) , \tag{2.14}$$

where $P_i^{\mathrm{tot}}(t) = \int dx \ P_i(x,t)$ denotes the marginal probability for the potential to be in state α_i at time t, irrespective of the particle position. We note that the entropy flow is written as the sum of two terms: the first term, which we call the *drift* contribution, accounts for steady-state currents in position space and is proportional to the heat dissipated into the bath driving the fluctuations of the particle position; the second term, which we call the *switching* contribution, originates purely from the switching dynamics. Physically, this contribution captures the rate of heat dissipation into the bath driving the fluctuations of the potential.

This marginal probability satisfies the master equation

$$\partial_t P_i^{\mathrm{tot}}(t) = \sum_j K_{ij} P_j^{\mathrm{tot}}(t) \tag{2.15}$$

and its steady-state value $P_{i,\infty}^{\mathrm{tot}} = \lim_{t \to \infty} P_i^{\mathrm{tot}}(t)$ can thus be obtained straightforwardly by identifying the unique eigenvector with eigenvalue zero of the matrix K. Note that while the entropy flow is commonly associated with the rate of heat dissipation into the environment [248, 173], the internal entropy production is usually the quantity of interest in the thermodynamic characterization of non-equilibrium stochastic processes due

to its connection with time-reversal symmetry breaking [113], its link to the Kullback-Leibler divergence [163] and its role in fluctuation theorems [254, 260]. For the sake of brevity, the denomination of *entropy production* will henceforth be reserved for the internal contribution, $\dot{S}_i(t)$, only.

Assuming that the joint probability density $P_i(x,t)$ relaxes to a steady-state at long times, we have the equality

$$\lim_{t\to\infty} \dot{S}(t) = \lim_{t\to\infty} [\dot{S}_i(t) + \dot{S}_e(t)] = 0 \ . \tag{2.16}$$

While both $\dot{S}_i$ and $\dot{S}_e$ vanish individually only for systems at equilibrium, the internal and external contributions to the entropy production cancel each other exactly even in systems out of thermal equilibrium. As a consequence, the steady-state internal entropy production can equivalently be computed via the entropy flow and it is thus directly related to heat dissipation. This is often a convenient route, since the logarithmic term in Eq. (2.14) does not contain information about the steady-state distribution itself.

Note that for Eqs. (2.13) and (2.14) to be well-defined, transitions between potential states α_i must be individually reversible, i.e. $K_{ij} > 0$ if $K_{ji} > 0$, while in general $K_{ij} \neq K_{ji}$. If the marginal dynamics for the potential state α satisfy the detailed balance condition [248, 173], i.e. if a global potential function $F_i = F(\alpha_i)$ can be defined such that $K_{ij}/K_{ji} \propto \exp(-(F_i - F_j))$ for all pairs $\{i,j\}$, the second term in Eq. (2.14) vanishes at steady-state, although the first term remains generally positive. This global potential construction is always possible for $N = 2$ and, more generally, when the state-space is tree-like, i.e. when it features no closed circuits [249].

2.2.2 Fluctuating potentials as a continuous Markov process

The formulation above can be straightforwardly extended to continuous α dynamics by taking $N \to \infty$ together with a suitable continuum limit in α-space, whereby $P_i(x,t) \to P(x,\alpha,t)d\alpha$ and $P_i^{\mathrm{tot}}(t) \to P^{\mathrm{tot}}(\alpha,t)d\alpha$. In this case, Eq. (2.1) thus generalizes to

$$\mathbb{P}(\alpha(t+\Delta t) = \alpha' | \alpha(t) = \alpha) = G(\alpha \to \alpha'; \Delta t) \tag{2.17}$$

where G denotes the propagator (Green's function) for the chosen dynamics. The associated marginal Fokker-Planck equation, which corresponds to the continuum limit of Eq. (2.15), reads

$$\partial_t P^{\mathrm{tot}}(\alpha, t) = \mathcal{L} P^{\mathrm{tot}}(\alpha, t) \tag{2.18}$$

with $\mathcal{L}$ the linear Fokker-Planck operator [234]. For the case of a fluctuating potential with control parameter $\alpha(t)$ described by Brownian motion with diffusion coefficient D_α (which is independent of α) in a potential $\mathcal{V}(\alpha)$, we have for instance

$$\mathcal{L} P^{\mathrm{tot}}(\alpha, t) = D_\alpha \partial_\alpha^2 P^{\mathrm{tot}}(\alpha, t) + \partial_\alpha (P^{\mathrm{tot}}(\alpha, t) \partial_\alpha \mathcal{V}(\alpha)) \ . \tag{2.19}$$

Further, in line with Eq. (2.4), the probability current for the particle position satisfies

$$J(x, \alpha, t) = -(\partial_x V(x; \alpha)) P(x, \alpha, t) - D \partial_x P(x, \alpha, t) \ , \tag{2.20}$$

while the probability current in α-space, denoted $\mathcal{J}(x, \alpha, t)$, reads

$$\mathcal{J}(x, \alpha, t) = -(\partial_\alpha \mathcal{V}(\alpha)) P(x, \alpha, t) - D_\alpha \partial_\alpha P(x, \alpha, t) \ . \tag{2.21}$$

The full Fokker-Planck equation can thus be written as

$$\partial_t P(x, \alpha, t) = -\partial_x J(x, \alpha, t) - \partial_\alpha \mathcal{J}(x, \alpha, t) \ . \tag{2.22}$$

The calculation of the entropy flow starts once again from the expression for the Gibbs-Shannon entropy,

$$S(t) = -\iint dx \ d\alpha \ P(x, \alpha, t) \log \left(\frac{P(x, \alpha, t)}{\bar{P}} \right) \ , \tag{2.23}$$

which combines with the now two-dimensional Fokker-Planck equation to give, for the particular case of Eq. (2.19),

$$\dot{S}_i(t) = \int d\alpha \ dx \ \frac{1}{P(x, \alpha, t)} \left[\frac{J^2(x, \alpha, t)}{D} + \frac{\mathcal{J}^2(x, \alpha, t)}{D_\alpha} \right] \tag{2.24a}$$

$$\dot{S}_e(t) = \int d\alpha \ \left[\int dx \ \frac{J(x, \alpha, t) \partial_x V(x; \alpha)}{D} \right] + \frac{1}{D_\alpha} \int d\alpha \ \mathcal{J}^{\mathrm{tot}}(\alpha, t) \partial_\alpha \mathcal{V}(\alpha) \ , \tag{2.24b}$$

where we have introduced the marginal current $\mathcal{J}^{\mathrm{tot}}(\alpha, t) = \int dx \ \mathcal{J}(x, \alpha, t)$.

Armed with the general expressions for the entropy production in drift-diffusion processes with fluctuating potentials, we now study a number of specific examples. For the rest of this study, we focus on the case of a harmonic potential $V(x;\alpha(t)) = \alpha(t)x^2/2$, where the fluctuating parameter $\alpha(t)$ controls the potential stiffness. The simplest discrete process that the stiffness of the harmonic potential can follow is a two-state Markov process, also known as dichotomous noise or telegraph process [291].

As a preliminary example, we study the case of a fully intermittent harmonic potential [244]. We suppose that $\alpha(t) \in \{0, \alpha_0\}$ switches between its two states with symmetric rate k. The two states are characterized as follows: (i) when $\alpha(t) = 0$, the particle diffuses on the real line and we say that the system is in an *off* state, (ii) when $\alpha(t) = \alpha_0 > 0$, the harmonic confining potential is present and the system is said to be in its *on* state. Clearly, in its *off* state the particle will be freely diffusing, while in the *on* state the confining potential leads to a forcing of the motion of the particle towards the center of the potential. Effectively, this system corresponds to the simplest single-particle system with a non-instantaneous resetting mechanism.

We denote by $P_{\text{off}}(x,t)$ and $P_{\text{on}}(x,t)$ the joint probability density of finding a particle at position x in the *off* and *on* state, respectively, at time t. The kinetic equations for this process read

$$\partial_t P_{\text{off}}(x,t) = -\partial_x \big[J_{\text{off}}(x,t)\big] + kP_{\text{on}}(x,t) - kP_{\text{off}}(x,t) \tag{2.25a}$$

$$\partial_t P_{\text{on}}(x,t) = -\partial_x \big[J_{\text{on}}(x,t)\big] + kP_{\text{off}}(x,t) - kP_{\text{on}}(x,t) \tag{2.25b}$$

with

$$J_{\text{off}}(x,t) = -D\partial_x P_{\text{off}}(x,t), \tag{2.26a}$$

$$J_{\text{on}}(x,t) = -D\partial_x P_{\text{on}}(x,t) - \alpha_0 x P_{\text{on}}(x,t) \tag{2.26b}$$

The stationary probabilities exist provided that $\alpha_0 > 0$ [310]. While it is relatively easy to obtain these stationary probabilities in Fourier space, deriving a closed-form analytic expression for the probability distribution in real space is highly non-trivial [84, 313, 244] (see also 2.A). In what follows, we interestingly show that such an analytic form is not

required for the calculation of the steady-state entropy production.

Indeed, to calculate the entropy production for this system, we will evaluate the entropy flow. Starting from Eq. (2.14), it is clear that the second term is zero as by construction $K_{\text{on,off}} = K_{\text{off,on}} = k$. For our choice of potentials, the first term reduces to

$$\dot{S}_e(t) = \frac{\alpha_0}{D} \int dx \big[x J_{\text{on}}(x,t) \big]. \tag{2.27}$$

At steady-state, the probability currents satisfy the flux balance equation $\partial_x J_{\text{on}}(x) = -\partial_x J_{\text{off}}(x)$. Integrating the right-hand side of Eq. (2.27) by parts and substituting one current for the other, we obtain

$$\lim_{t\to\infty} \dot{S}_i(t) = \lim_{t\to\infty} \alpha_0 \int dx \left[\frac{x^2}{2} \partial_x^2 P_{\text{off}}(x,t) \right]. \tag{2.28}$$

Finally, integrating by parts twice and solving Eq. (2.15) at steady-state to obtain $P^{\text{tot}}_{\text{on},\infty} = P^{\text{tot}}_{\text{off},\infty} = 1/2$, leaves us with the simple expression

$$\lim_{t\to\infty} \dot{S}_i(t) = \frac{\alpha_0}{2} \ , \tag{2.29}$$

indicating that the steady-state entropy production in this setup is independent of both the switching rate k and the diffusion coefficient D. Here and in the following, we drop boundary terms whenever integration by parts is performed. This procedure relies on a sufficiently fast decay of the relevant probability densities as $x \to \pm\infty$ and, more precisely, on the finiteness of the second moment of $P_i(x)$, which is a reasonable assumption for all processes considered herein.

As shown in Fig. 2.2, we confirm numerically this result through: (1) the numerical integration of Eq. (2.27) using the stationary current derived from Eq. (2.25) (see 2.A and [244, 313]) and (2) the analysis of single particle trajectories from the simulated underlying microscopic process governed by Eq. (2.2) (see 2.B for further numerical details). Strikingly, while the process is *dynamically* equivalent in the limit $k \to \infty$ to an equilibrium OU process with reduced potential stiffness $\alpha_0/2$ [217], we observe here a finite and strictly positive steady-state rate of entropy production. Similarly, entropy production remains finite and positive for free run-and-tumble particles, whose motion is effectively diffusive in the limit of infinite tumbling rate or large times [64, 109]. This

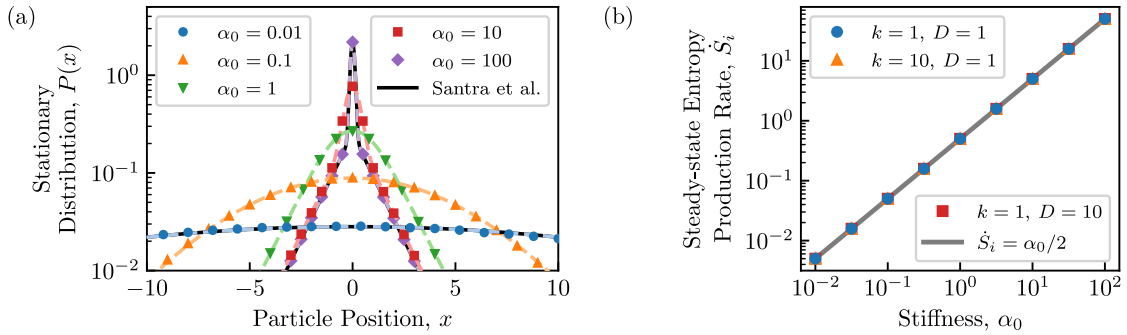

Figure 2.2: *Steady-state entropy production of a Brownian particle in an intermittent quadratic potential* — (a) Stationary distribution $P(x)$ at different values of $\alpha_0 \in [10^{-2}, 10^2]$ with $k = D = 1$ fixed. We show agreement between the distributions measured numerically from single particle trajectories (marked by symbols) and the result (2.86) which we have integrated numerically (dashed lines). We plot in black the analytic solutions for the limit $\alpha_0 \gg k$ as in Eq.(2.88) and $\alpha_0 \ll k$ as in Eq.(2.89). (b) We confirm our analytic result (2.29) by evaluating (2.27) numerically from our stationary distributions for three sets of values for k, D.

is sometimes referred to as an *entropic anomaly* [59, 32].

Note that the independence of the steady-state entropy production vis-à-vis the switching rate k and the diffusion coefficient D is specific to our choice of potential and can be derived from physical arguments. Namely, the first law of thermodynamics at steady-state,

$$0 = \int dx \, [V(x;\alpha_0)\partial_t P_{\rm on}(x) + V(x;0)\partial_t P_{\rm off}(x)] = \dot{W} - \dot{Q} \ , \tag{2.30}$$

imposes the rate of heat dissipation, $\dot{Q}$, to be equal to the work done per unit time by the potential on the particle, $\dot{W}$. Clearly, work is only being done in the *on* state as the potential disappears in the *off* state. In turn, the average work done equals the change in average potential energy $U = \langle \alpha_0 x^2/2 \rangle$ before the next transition to the *off* state. In the *off* state, the particle motion is purely diffusive and the variance of the position probability density grows linearly, i.e. $\partial_t \langle x^2 \rangle = 2D$. Thus, the average work done by the potential during a *on* phase of typical duration k^{-1} is given by

$$\langle W \rangle = \frac{D\alpha_0}{k} \ . \tag{2.31}$$

Given that the average duration of an *on-off* cycle is by construction $2/k$, the average rate of heat dissipation is $\langle \dot{Q} \rangle = k\langle W \rangle/2 = D\alpha_0/2$. Finally, the particle self-diffusion

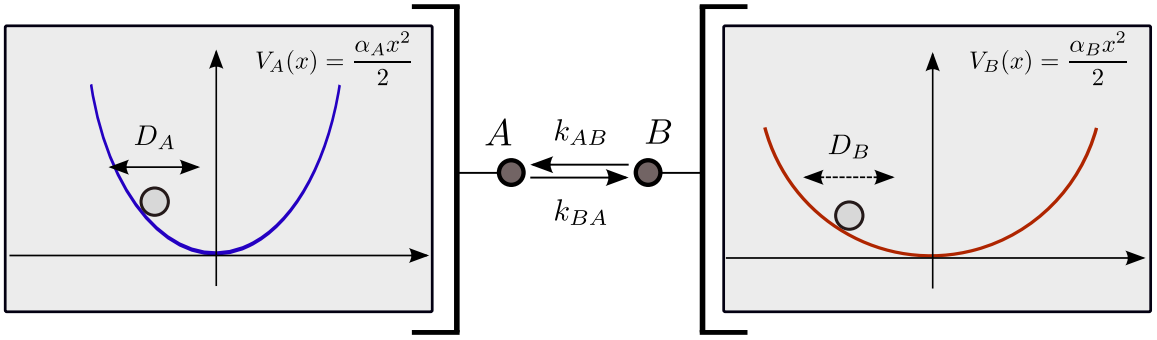

Figure 2.3: *Fluctuating potentials as a general two-state Ornstein-Uhlenbeck Markov process* — The inequality (2.32) is the condition for the existence of a stationary solution to the Fokker-Planck equation, and thus for the steady-state entropy production to be well-defined.

coefficient being proportional to the temperature by Einstein's relation, we write in our units that $\dot{S}_i = \langle \dot{Q} \rangle / D$ and finally recover $\dot{S}_i = \alpha_0/2$, which we confirm to be independent of k and D.

Importantly, this argument relies on the variance $\langle x^2 \rangle$ growing linearly with time (without bounds) in the *off* state, an assumption that breaks down as soon as the *off* state of the potential has a finite stiffness α_1, in which case the variance of the particle position in the *off* state instead satisfies $\partial_t \langle x^2 \rangle = 2D(1 - \alpha_1 \langle x^2 \rangle / D)$. We show how this leads to an explicit k dependence of the entropy production in Section 2.4.2. Finally, to highlight the importance of the functional form of the potential, we repeat this procedure for an intermittent *quartic* potential and argue that the steady-state entropy production can not be independent of k or D in Appendix 2.C.

2.4 General two-state Ornstein-Uhlenbeck Markov process

We now broaden our focus and study the case of a generalized two-state Ornstein-Uhlenbeck Markov process, of which the preliminary model introduced in the previous section is a limiting case. Here, we consider a system with two states denoted A and B. In state A, the particle diffuses in a harmonic potential, $V_A(x) = \alpha_A x^2/2$, with diffusion coefficient D_A. In state B, the restoring force comes from a second potential, $V_B(x) = \alpha_B x^2/2$, and the particle self-diffusion is set by D_B. As shown in Fig. 2.3, the particle switches from state A to B with rate k_{BA} and returns with rate k_{AB}.

2.4.1 Analytic expression for the entropy production

In this general case, one needs to carefully chose the potential strengths and switching rates. Indeed, the steady-state probabilities only exist for this system when the following inequality is satisfied [310]:

$$\frac{\alpha_A k_{AB} + \alpha_B k_{BA}}{k_{AB} + k_{BA}} = \langle \alpha \rangle > 0 \tag{2.32}$$

where we have defined $\langle \alpha \rangle = \sum_i \alpha_i P^{\text{tot}}_{i,\infty}$, where $P^{\text{tot}}_{i,\infty}$ are the solutions to Eq. (2.15) in steady-state. It is easily interpreted as the sum of the two values for the stiffness α weighted by the fraction of time spent in each state. Namely, while the independent confining potential strengths do not need to be strictly positive, we require the effective potential strength (as time-averaged over a full $A \to B \to A$ cycle) to be positive.

Granted that condition (2.32) is met, we start from Eq. (2.14) and follow the same procedure as above. We thus argue that the steady-state entropy flow reads

$$\lim_{t\to\infty} \dot{S}_e(t) = \frac{\alpha_A}{D_A} \int dx \big[x J_A(x)\big] + \frac{\alpha_B}{D_B} \int dx \big[x J_B(x)\big]. \tag{2.33}$$

Importantly, we note that the switching contribution to the entropy production vanishes in the case of a two-state process as detailed balance holds. Indeed, the switching contribution is non-zero when detailed balance is broken which requires at least three states.

We then substitute in the form of the currents from the Fokker-Planck equations for the process, given in Eq. (2.4), and write the internal entropy production as

$$\lim_{t\to\infty} \dot{S}_i(t) = -\langle \alpha \rangle + \frac{\alpha_A^2}{D_A} \int dx \big[x^2 P_A(x)\big] + \frac{\alpha_B^2}{D_B} \int dx \big[x^2 P_B(x)\big], \tag{2.34}$$

where we recognize that the two integrals are proportional to the variances of the steady-state probability distributions conditioned on the potential being in either of the two states A and B.

We introduce the conditional variance

$$\sigma_i^2(t) = \frac{\int dx\ x^2 P_i(x,t)}{\int dx\ P_i(x,t)} \tag{2.35}$$

and define

$$\Xi_i(t) = \int dx\ x^2 P_i(x,t) = \sigma_i^2(t) P_i^{\mathrm{tot}}(t) \tag{2.36}$$

for $i \in \{A, B\}$, where $P_i^{\mathrm{tot}}(t) = \int dx\ P_i(x,t)$ is the marginal probability of the potential having stiffness α_i independent of the position x of the trapped particle.

First, note that

$$\partial_t \Xi_i(t) = \int dx \big[x^2 \partial_t P_i(x,t)\big] \tag{2.37}$$

and so after taking the second moment of the Fokker-Planck equation (2.3), we obtain

$$\partial_t \Xi_A(t) = 2D_A P_A(t) - (2\alpha_A + k_{BA})\Xi_A(t) + k_{AB}\Xi_B(t) \tag{2.38a}$$

$$\partial_t \Xi_B(t) = 2D_B P_B(t) - (2\alpha_B + k_{AB})\Xi_B(t) + k_{BA}\Xi_A(t). \tag{2.38b}$$

We can now solve Eqs. (2.38a) and (2.38b) at steady-state to derive explicit expressions for $\Xi_A(t)$ and $\Xi_B(t)$ as $t \to \infty$:

$$\lim_{t\to\infty} \Xi_A(t) = \frac{k_{AB}}{k_{AB}+k_{BA}} \left[\frac{(2\alpha_B + k_{AB})D_A + k_{BA}D_B}{2\alpha_A\alpha_B + \alpha_A k_{AB} + \alpha_B k_{BA}}\right], \tag{2.39a}$$

$$\lim_{t\to\infty} \Xi_B(t) = \frac{k_{BA}}{k_{AB}+k_{BA}} \left[\frac{k_{AB}D_A + (2\alpha_A + k_{BA})D_B}{2\alpha_A\alpha_B + \alpha_A k_{AB} + \alpha_B k_{BA}}\right]. \tag{2.39b}$$

Substituting (2.39a) and (2.39b) into (2.34), we obtain a closed-form exact expression for the entropy production in a general two-state Ornstein-Uhlenbeck Markov process, which reads

$$\begin{aligned}\lim_{t\to\infty} \dot{S}_i(t) = &- \frac{\alpha_A k_{AB} + \alpha_B k_{BA}}{k_{AB}+k_{BA}} \\ &+ \frac{\alpha_A^2}{D_A}\left[\frac{k_{AB}}{k_{AB}+k_{BA}}\right]\left[\frac{(2\alpha_B + k_{AB})D_A + k_{BA}D_B}{2\alpha_A\alpha_B + \alpha_A k_{AB} + \alpha_B k_{BA}}\right] \\ &+ \frac{\alpha_B^2}{D_B}\left[\frac{k_{BA}}{k_{AB}+k_{BA}}\right]\left[\frac{k_{AB}D_A + (2\alpha_A + k_{BA})D_B}{2\alpha_A\alpha_B + \alpha_A k_{AB} + \alpha_B k_{BA}}\right]\end{aligned} \tag{2.40}$$

where the first term is equal to the opposite of the mean stiffness $\langle\alpha\rangle$, as defined in Eq. 2.32.

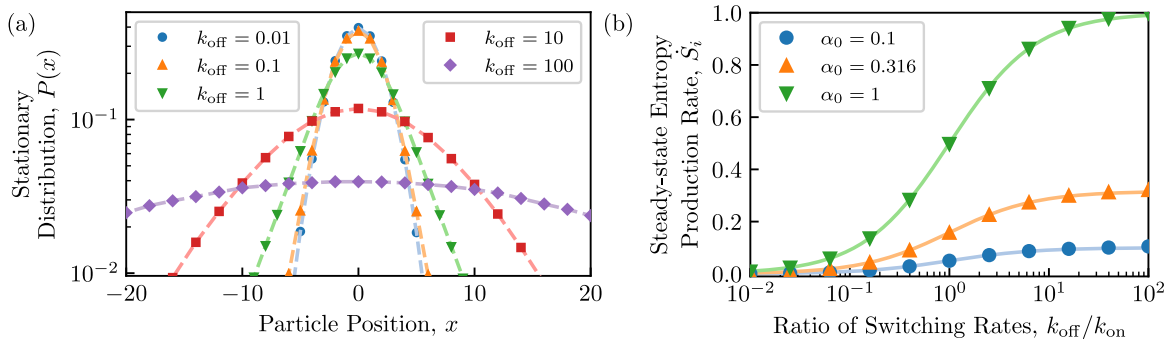

Figure 2.4: *Steady-state entropy production rate for a Brownian particle in an intermittent quadratic potential with asymmetric switching rates* — (a) Stationary distribution $P(x)$ for the particle position measured numerically from single particle trajectories for varying switching rates $k_{\text{off}} \in \{10^{-2}, 10^{2}\}$ with $k_{\text{on}} = D = \alpha_0 = 1$ fixed. (b) Entropy production rate measured by integrating (2.34) numerically (symbols) showing good agreement with our analytic result, (2.41), for fixed $k_{\text{on}} = D = 1$.

2.4.2 Some models of interest

We now apply this result to a number of important limiting cases of the generalized two-state Ornstein-Uhlenbeck model.

Intermittent Harmonic Potential with Asymmetric Switching Rates —

First we return to the preliminary example, in which we stipulated that the diffusion was independent of the state, $D_A = D_B = D$, and we let $\alpha_A = 0$ and $\alpha_B = \alpha_0$. Here, we consider more generally the case of distinct switching rates: k_{on} to switch from state A to state B and k_{off} from state B to A. For these parameters, Eq. (2.40) reduces to

$$\lim_{t\to\infty} \dot{S}_i(t) = \alpha_0 \frac{k_{\text{off}}}{k_{\text{on}} + k_{\text{off}}} = \alpha_0 - \langle \alpha \rangle. \tag{2.41}$$

We conclude that in this case, the entropy production explicitly depends on the switching rates k_{on} and k_{off}. Note that we naturally recover the result from Eq. (2.29) when symmetrizing the switching rates and setting $k_{\text{on}} = k_{\text{off}}$. We study the system numerically and plot the stationary probabilities and entropy production rate in Fig. 2.4. We note in particular that the entropy production rate can be written in terms of the potential strength α_0 and ratio of switching rates $k_{\text{off}}/k_{\text{on}}$, justifying our choice of parameters.

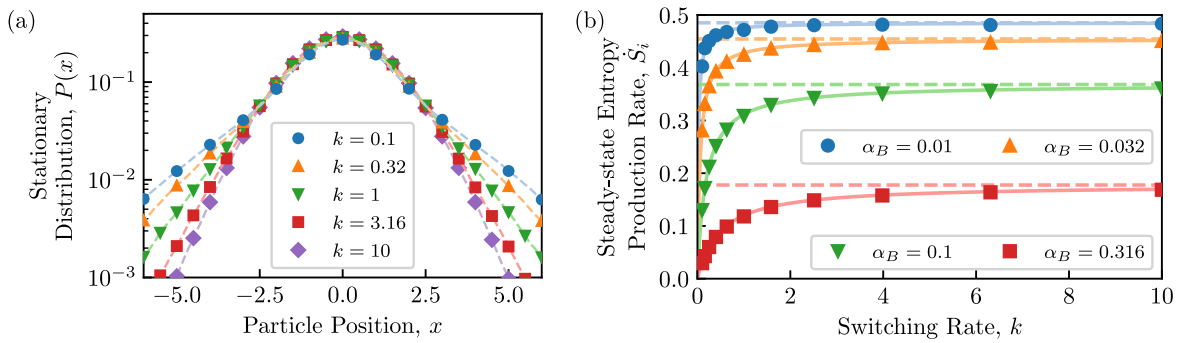

Figure 2.5: *Steady-state entropy production rate for a Brownian particle in a harmonic potential switching between two non-zero stiffnesses with rate k* — (a) Stationary distributions for the process with $\alpha_B = 0.1$ and $\alpha_A = D = 1$ for switching rates $k \in \{0.1, 10\}$. (b) Entropy production rate evaluated from the numerical integration of (2.34) using the stationary distributions obtained from single particle trajectories (symbols). We show a perfect quantitative agreement with our exact analytical result (2.42) (solid line) for a wide range of switching rates. We also show the entropy production rate in the limit $k \to \infty$ in each case from (2.44) (dashed line).

Next, we consider the case of a non-disappearing harmonic potential. Namely, we consider that $k_{AB} = k_{BA} = k$ and $D_A = D_B = D$, while letting $\alpha_A > \alpha_B > 0$. Here, we obtain

$$\lim_{t\to\infty} \dot{S}_i(t) = -\frac{\alpha_A + \alpha_B}{2} + \frac{(\alpha_B + k)\alpha_A^2 + (\alpha_A + k)\alpha_B^2}{2\alpha_A\alpha_B + k(\alpha_A + \alpha_B)} = \frac{k(\alpha_A - \alpha_B)^2}{4\alpha_A\alpha_B + 2k(\alpha_A + \alpha_B)} , \tag{2.42}$$

which displays an explicit dependence on the switching rate k.

We also conclude on the scaling of the entropy production when the switching rate is either much smaller or much larger than the two values for the stiffness. In particular, we observe a crossover from a small k regime characterized by a linear k dependence

$$\lim_{t\to\infty} \dot{S}_i(t) \simeq \frac{(\alpha_A - \alpha_B)^2}{4\alpha_A\alpha_B} k \quad \text{for} \quad k \ll \alpha_{A,B} \tag{2.43}$$

that extends from $k = 0$ up to a cross-over rate $k^* = 2\alpha_A\alpha_B/(\alpha_A + \alpha_B)$, to a large k regime that is asymptotically independent of k,

$$\lim_{k\to\infty}\lim_{t\to\infty} \dot{S}_i(t) = \frac{(\alpha_A - \alpha_B)^2}{2(\alpha_A + \alpha_B)} . \tag{2.44}$$

We conclude that the k-dependent regime vanishes to a single point in the limit where $\alpha_B \to 0$ for fixed α_A as shown in Fig. 2.5. This limit is consistent with a vanishing intermittent harmonic potential and we confirm here that we recover the result of Eq. (2.29).

Switching diffusion in harmonic potential —

Suppose now that the switching is symmetric with rate $k_{AB} = k_{BA} = k$ and the harmonic potential stiffness $\alpha_A = \alpha_B = \alpha$ is the same in each state, but the diffusion coefficient switches between two values, D_A and D_B. We then vary D_A and D_B to see how the entropy production depends on the ratio of the diffusion coefficients. Starting from (2.40), we eventually obtain

$$\lim_{t\to\infty} \dot{S}_i(t) = \frac{\alpha k}{4(\alpha+k)}\left[\left(\frac{D_B}{D_A}+\frac{D_A}{D_B}\right)-2\right] = \frac{\alpha k (D_A-D_B)^2}{4D_AD_B(\alpha+k)}\,. \tag{2.45}$$

The entropy production is clearly non-negative and vanishes at $D_A = D_B$, which corresponds to the recovery of a standard (equilibrium) Ornstein-Uhlenbeck process with stiffness α and diffusion coefficient D (see Fig. 2.6 for a comparison with numerical results).

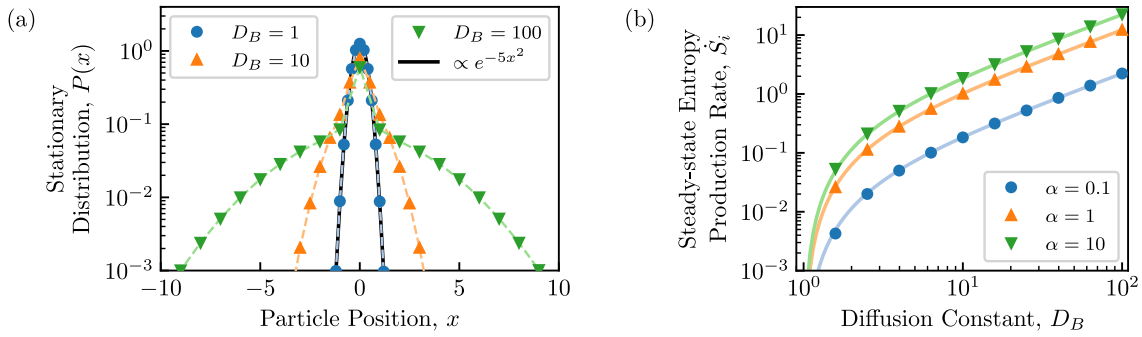

Figure 2.6: *Steady-state entropy production for a Brownian particle switching between two diffusion coefficients in a constant harmonic potential* — (a) Stationary distributions for the process with $D_A = k = 1$, $\alpha = 10$ and varying $D_B \in [1, 100]$. We show in black the Gaussian distribution expected in the case where $D_A = D_B$. (b) Entropy production rate as a function of the diffusion coefficient D_B obtained by integrating numerically (2.34) using the single particle trajectories (symbols), in perfect agreement with our analytic result (2.45) (solid line).

Effective resetting with harmonic potential —

Evaluating the entropy production for systems with (instantaneous) resetting is a problem that has seen much attention [105, 50]. The irreversible nature of the stochastic resetting process is a good indication that the entropy production is infinite: it completely breaks time-reversal symmetry. For this reason, previous work addressing the thermodynamics of resetting has made use of alternative definitions for the entropy production [105, 50], whose connection with time-reversal symmetry breaking in the spirit of [113] is unclear.

The framework we introduce here allows us to study models of *effective* resetting, where a particle diffuses in a fluctuating harmonic potential. Namely, near-instantaneous resetting with a refractory period [95] of typical duration $1/k_{\text{off}}$ can be modeled with an intermittent potential of infinite stiffness $\alpha_0 \to \infty$. Note that in the limit where $k_{\text{off}} \to \infty$ while keeping $k_{\text{off}} \ll \alpha_0$, this refractory period vanishes. From the results of Section 2.4.2, it is clear that an infinitely stiff confining potential implies infinite steady-state entropy production, but more generally, we are here able to quantify entropy production in systems approaching instantaneous resetting but with finite confining potentials and show that the entropy production diverges linearly with the potential stiffness.

2.5 General N-state Ornstein-Uhlenbeck Markov process

2.5.1 General framework

We generalize the results above to the case where the stiffness α of the confining harmonic potential and the diffusion coefficient D can switch stochastically between N distinct pairs of values (α_i, D_i) with $i = 1, 2, ..., N$ following a general Markov jump process with transition rate matrix K. As noted earlier, the matrix elements K_{ij} represent the probability per unit time that a harmonic potential with stiffness α_j switches to stiffness α_i; note that in general, while $K_{ij} > 0$ whenever $K_{ji} > 0$ to enforce local reversibility, these transition rates need not satisfy global detailed balance. The diagonal elements of K are fixed by imposing $\sum_i K_{ij} = 0$ for all j, corresponding to the requirement that the total probability be conserved.

Similarly to Eq. (2.36), we define

$$\Xi_i(t) = \int dx\ x^2 P_i(x,t) = \sigma_i^2(t) P_i^{\rm tot}(t) \tag{2.46}$$

for $i = 1, 2, ..., N$, with $P_i^{\rm tot}(t) = \int dx\ P_i(x,t)$ the marginal probability of the potential having stiffness α_i independently of the particle position. For our choice of potential, the entropy flow is given by Eq. (2.14):

$$\dot{S}_e(t) = \sum_i \alpha_i P_i^{\rm tot}(t) - \sum_i \frac{\alpha_i^2}{D_i}\Xi_i(t) - \frac{1}{2}\sum_{i\neq j}\left(K_{ij}P_j^{\rm tot}(t) - K_{ji}P_i^{\rm tot}(t)\right)\log\left(\frac{K_{ij}}{K_{ji}}\right). \tag{2.47}$$

Note that in the present case, the contribution from the pure switching component of the process does not generally vanish for $N \geq 3$, since the switching rates K_{ij} do not generically need to satisfy the detailed balance condition. Based on the Fokker-Planck equation (2.3), we obtain the following system of kinetic equations

$$\partial_t \Xi_i(t) = 2D_i P_i^{\rm tot}(t) - 2\alpha_i \Xi_i(t) + \sum_j K_{ij}\Xi_j(t)\ . \tag{2.48}$$

At steady-state, computing the entropy production $\lim_{t\to\infty}\dot{S}_i(t) = -\lim_{t\to\infty}\dot{S}_e(t)$ for this system only depends on our ability to compute the quantities Ξ_i at steady-state. From Eq. (2.48), these steady-state quantities can be obtained by solving the linear system

$$2D_i P_{i,\infty}^{\rm tot} + \sum_j (K_{ij} - 2\alpha_i\delta_{ij})\Xi_j = 0 \tag{2.49}$$

which involves the steady-state marginal probabilities $P_{i,\infty}^{\rm tot}$ of the Markov switch process; these correspond to the unique eigenvector with eigenvalue 0 of the transition rate matrix K (assuming that the corresponding graph has a single connected component), rather than the full space-dependent probabilities $P_i(x,t)$, which are typically hard to compute [313, 244].

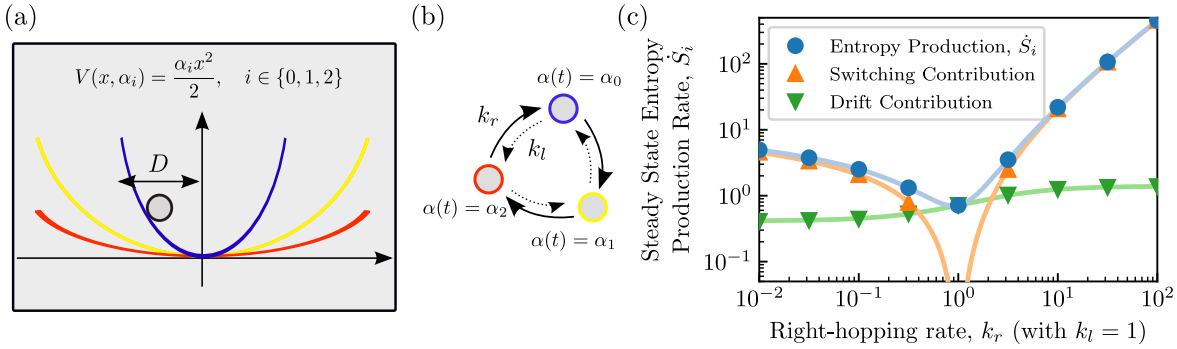

Figure 2.7: *Steady-state entropy production for a Brownian particle in $N = 3$ harmonic potentials of varying stiffness* — Schematic for (a) the different potentials in a typical three state system and (b) the discrete Markov jump process that controls the stiffness of the harmonic potential. (c) Entropy production rates for the process, consisting of two contributions: the *switching* contribution, stemming purely from the switching dynamics, vanishes when the jump process satisfies detailed balance (here, $k_r = k_l$); the *drift* contribution, accounting for steady-state currents in position space, is generically positive in the presence of stiffness fluctuations. For the simulations, we set $\alpha_0 = 0.5$, $\alpha_1 = 2$, $\alpha_2 = 5$ and $D = k_l = 1$.

2.5.2 Simple example: N-state ring with homogeneous right- and left-hopping rates

The case of a ring with N states (see Fig. 2.7 for $N = 3$) is the simplest setup for which the switching contribution to the entropy flow is non-trivial. Let $K_{i,i+1} = k_l$ and $K_{i,i-1} = k_r$ with periodic boundary conditions and assume that in state i, the particle has a diffusion constant, D_i. By rotational symmetry of this cyclic configuration, we have that the steady-state marginal probabilities satisfy $P^{\mathrm{tot}}_{i,\infty} = 1/N$ for all i. We thus also have that the mean stiffness is defined as $\langle\alpha\rangle = (\alpha_1 + \alpha_2 + \cdots + \alpha_N)/N$. The contribution to the entropy flow from the switching part of the process can easily be calculated and reads

$$\frac{1}{2}\sum_{i,j\neq i}\left(K_{ij}P^{\mathrm{tot}}_{j,\infty} - K_{ji}P^{\mathrm{tot}}_{i,\infty}\right)\log\left(\frac{K_{ij}}{K_{ji}}\right) = (k_l - k_r)\log\left(\frac{k_l}{k_r}\right) \tag{2.50}$$

which vanishes for $k_l = k_r$, as expected. We can now plug this result into Eq. (2.47) to obtain an expression for the entropy production as a function of the stiffnesses α_i and the switching rates,

$$\lim_{t\to\infty}\dot{S}_i(t) = \lim_{t\to\infty} -\dot{S}_e(t) = (k_r - k_l)\log\frac{k_r}{k_l} + \sum_{i=1}^{N}\alpha_i\left(\frac{\alpha_i\Xi_i}{D_i} - \frac{1}{N}\right). \tag{2.51}$$

where the steady-state quantities Ξ_i are solutions to the following linear equation

$$\mathbf{\Xi} = -\frac{2}{N}\mathbf{\Sigma}^{-1} \cdot \mathbf{D} \tag{2.52}$$

with $\mathbf{D}$ the vector of diffusivities and where the matrix $\mathbf{\Sigma}$ is a tri-diagonal matrix defined in the case $N = 3$ as

$$\mathbf{\Sigma} = \begin{pmatrix} -k_r - k_l - 2\alpha_1 & k_l & k_r \\ k_r & -k_r - k_l - 2\alpha_2 & k_l \\ k_l & k_r & -k_r - k_l - 2\alpha_3 \end{pmatrix} \tag{2.53}$$

From Eq. (2.51), we note again that the entropy production in this general N-state Markov jump process is formed of two contributions: (i) the first term, which we call the *switching* contribution, which vanishes when the jump process satisfies detailed balance (here, $k_r = k_l$). Physically, this contribution captures the rate of heat dissipation into the bath driving the fluctuations of the potential; (ii) the second term, which we call the *drift* contribution, is proportional to the heat dissipated into the bath driving the fluctuations of the particle position. Since the potential fluctuations are independent of the particle position, both the total entropy production and the switching contribution are individually non-negative, while the drift contribution can a priori take on positive or negative values.

We explore the case $N = 3$ in Fig. 2.7 finding the dependence on the switching rates k_r and k_l of the two contributions to the entropy production. In the special case of equal stiffnesses and diffusivities $(\alpha_i, D_i) = (\alpha, D)$ for $i = \{1, 2, 3\}$, we obtain $\Xi_i = D/(3\alpha)$ and the *drift* contribution in Eq. (2.51) vanishes. Despite this, we may still observe a non-zero rate of entropy production accounting for the heat being dissipated into the bath driving the fluctuations in the potential, i.e. due to the control of the switching process. Indeed, a non-zero rate of entropy production is expected when detailed balance is not satisfied in the switching mechanism which we recover in Eq. (2.51) when $k_r \neq k_l$ as required. In contrast, Fig. 2.7 shows the evolution of the entropy production as a function of k_r/k_l for a more general case where the stiffnesses α_i are not equal.

2.6 Continuous state Markov process for the potential stiffness

The final generalization consists in allowing the potential stiffness α to vary continuously according to a continuous stochastic process. While we derived general results about the internal entropy production and the entropy flow for continuous processes in Section 2.2.2, here we focus on the particular example of a particle diffusing in a confining harmonic potential whose stiffness obeys an Ornstein-Uhlenbeck process.

2.6.1 Ornstein-Uhlenbeck process governing the potential stiffness

In this model, the position of the particle x obeys the following overdamped Langevin equation

$$\dot{x}(t) = -\partial_x V(x;\alpha(t)) + \sqrt{2D}\,\eta(t) \tag{2.54}$$

with a confining potential $V(x;\alpha) = \alpha x^2/2$ whose stiffness $\alpha(t)$ is governed by the following mean-reverting process

$$\dot{\alpha}(t) = -\partial_\alpha \mathcal{V}(\alpha) + \sqrt{2D_\alpha}\,\xi(t) \tag{2.55}$$

where D_α is the diffusion constant for the stiffness which is independent of α and $\eta(t)$ and $\xi(t)$ are two zero mean, unit variance Gaussian white noises. Here, we thus consider the special case where the *stiffness* confining potential is defined as

$$\mathcal{V}(\alpha) = \frac{1}{2}\mu(\alpha - \alpha_0)^2 \tag{2.56}$$

where $\alpha_0 > 0$ is required for the steady-state to be well-defined.

As before, $P^{\mathrm{tot}}(\alpha,t) = \int dx\, P(x,\alpha,t)$ denotes the marginal probability density for the potential having a particular stiffness α independently of the position x of the trapped particle. Starting from Eq. (2.24), the entropy flow for this model can be written as

$$\dot{S}_e(t) = \int d\alpha \left[\alpha P^{\mathrm{tot}}(\alpha,t) - \frac{\alpha^2}{D}\Xi(\alpha,t)\right] + \frac{1}{D_\alpha}\int d\alpha\; \mathcal{J}^{\mathrm{tot}}(\alpha,t)\mathcal{V}'(\alpha) \tag{2.57}$$

where $\mathcal{J}^{\mathrm{tot}}$ is the probability current in *stiffness space* and the marginal variances are defined as $\Xi(\alpha,t) = \int dx\; x^2 P(x,\alpha,t)$.

In this continuum limit, the marginal probability density is determined by the Fokker-Planck operator (2.19). Therefore, the steady-state marginal probability density $P^{\mathrm{tot}}(\alpha)$ is Gaussian and is given by

$$P^{\mathrm{tot}}(\alpha) = \sqrt{\frac{\mu}{2\pi D_\alpha}} \exp\left(-\frac{\mu(\alpha-\alpha_0)^2}{2D_\alpha}\right) \tag{2.58}$$

with $\mathcal{J}^{\mathrm{tot}}(\alpha) = 0$ since this is an equilibrium process and the average stiffness reduces to $\langle\alpha\rangle = \alpha_0$. We are left to calculate the second term in Eq. (2.57) to finally obtain the entropy production.

The Fokker-Planck equation for $P(x,\alpha,t)$ is written as

$$\partial_t P = D\partial_x^2 P + \alpha\partial_x\big[xP\big] + D_\alpha\partial_\alpha^2 P + \mu\partial_\alpha\big[(\alpha-\alpha_0)P\big] \tag{2.59}$$

where we have dropped the functional dependencies for the sake of simplicity. From here, we can follow a similar procedure to that used to obtain Eq. (2.38) and find that the marginal variance $\Xi(\alpha,t)$ is governed by the following kinetic equation

$$\partial_t\Xi(\alpha,t) = 2DP^{\mathrm{tot}}(\alpha,t) - 2\alpha\Xi(\alpha,t) + \partial_\alpha\big[D_\alpha\partial_\alpha\Xi(\alpha,t) + \mu(\alpha-\alpha_0)\Xi(\alpha,t)\big]. \tag{2.60}$$

The marginal variances satisfy at steady-state the following linear equation

$$(\mathcal{L} - 2\alpha)\Xi(\alpha) + 2DP^{\mathrm{tot}}(\alpha) = 0\ . \tag{2.61}$$

Integrating this last equation with respect to α leads to $\langle\alpha x^2\rangle = D$ where $\langle\cdot\rangle$ represents the average with respect to the steady-state probability distribution, $\lim_{t\to\infty} P(x,\alpha,t)$. This itself is a remarkable result, indicating that the effect on positional fluctuations, as captured by the variance $\langle x^2\rangle$, associated with changes in α_0, D_α or μ is exactly canceled when the displacement is rescaled by the fluctuating stiffness $\alpha(t)$, such that the scaled variance $\langle\alpha x^2\rangle$ is independent of the stiffness dynamics.

We then multiply (2.60) by α before again integrating over α to obtain

$$\int d\alpha\left[\frac{\alpha^2}{D}\Xi(\alpha)\right] = \langle\alpha\rangle - \frac{1}{2D}\int d\alpha\left[D_\alpha\partial_\alpha\Xi(\alpha) + \mu(\alpha-\alpha_0)\Xi(\alpha)\right] \tag{2.62}$$

with $\langle\alpha\rangle = \alpha_0$. Combining Eq. (2.62) with (2.57), integrating by parts once assuming

a sufficiently fast decay of $P(x,\alpha)$ as $x,\alpha \to \pm\infty$ and using $\langle \alpha x^2 \rangle = D$, we conclude that the entropy production rate at steady-state can be expressed as

$$\lim_{t\to\infty} \dot{S}_i = -\frac{\mu}{2D}\langle(\alpha-\alpha_0)x^2\rangle = \frac{\mu\alpha_0}{2D}\left(\langle x^2\rangle - \frac{D}{\alpha_0}\right), \tag{2.63}$$

which is the simplest exact form for the entropy production that we can obtain here and the main result of this section. Note that the limit $D_\alpha \to 0$ represents an equilibrium limit for the system. We argue that in this case the variance of the particle position is given by $\langle x^2 \rangle = D/\alpha_0$ and thus one would observe no entropy production, as expected for an equilibrium process. We have thus expressed the entropy production in this system through the difference between the particle positional variances in the fully non-equilibrium process and its equilibrium limit. A closed-form solution for the entropy production in this system relies on our ability to calculate the variance of the particle position; while this can easily be achieved numerically (see Fig. 2.8), to the best of our knowledge, it is not possible to write an analytical expression for it in general and writing down a solution to Eq. (2.59) remains an interesting open problem.

As shown in Fig. 2.8, we observe that the steady-state entropy production rate decays with increasing diffusion coefficient D. For low values of D, while Brownian motion becomes progressively weaker, fluctuations in the particle position (as captured by $\langle x^2 \rangle$) remain significant due to the existence of periods of transiently negative potential stiffnesses. As a consequence, we expect the bracketed terms in Eq. (2.63) to remain finite as D approaches 0, leading to the observed increase of the entropy production in this limit. On the other hand, the steady-state entropy production rate converges to a finite value and becomes independent of D at large enough diffusivities. When $\alpha_0, D \gg \mu, D_\alpha$, we effectively obtain a separation of timescales between the dynamics in x-space and α-space. Assuming $\alpha_0^2 \gg D_\alpha/\mu$, the variance of the particle position is then well-approximated by the average over positive α of the variance of particle in a fixed potential with stiffness α, $\langle x^2 \rangle_\alpha = D/\alpha$, weighted by the probability to observe such a potential stiffness $P(\alpha, t)$. Altogether, we thus expect the term in the brackets in Eq. (2.63) to scale like D and the D dependence to finally scale out of the steady-state entropy production rate. Finally, we confirm our intuition that the entropy production rate should increase with increasing values of diffusivity in α-space and show that $\dot{S}_i \sim D_\alpha^\beta$, with $\beta \approx 1$.

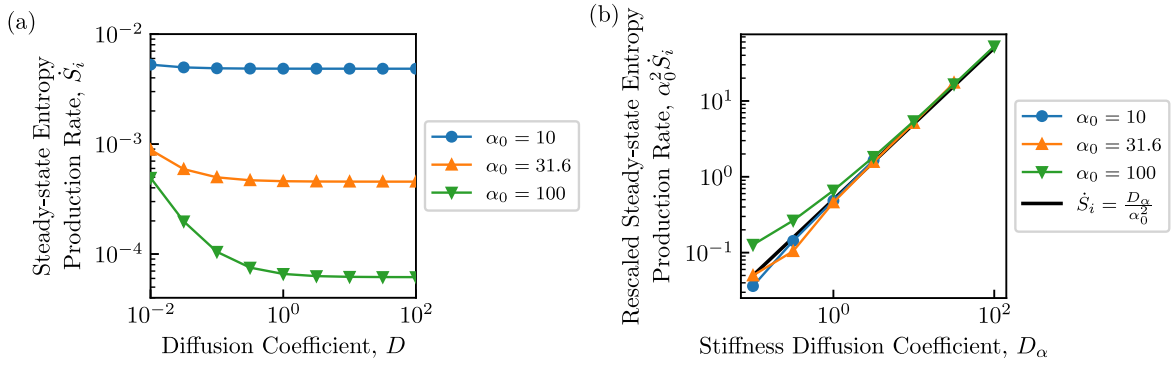

Figure 2.8: *Steady-state entropy production for a Brownian particle in a harmonic potential with continuously varying stiffness* — (a) Steady-state entropy production rate as a function of the particle self-diffusivity D, for $\mu = D_\alpha = 1$ and different values of α_0. The entropy production rate becomes independent of the positional diffusion coefficient for large enough values of D and remains finite and non-negative at low values of D. (b) Steady-state entropy production rate increases with D_α. We find that $\dot{S}_i \sim D_\alpha/\alpha_0^2$. Here, we set $D = \mu = 1$ and vary D_α and α_0.

Furthermore, we can verify that entropy production (2.63) is non-negative by considering

$$\langle(\alpha - \alpha_0)^2 x^2\rangle = \langle\alpha^2 x^2\rangle - 2\alpha_0\langle\alpha x^2\rangle + \alpha_0^2\langle x^2\rangle \geq 0 \ , \tag{2.64}$$

where the equality is only saturated in the deterministic limit, i.e. for $D = D_\alpha = 0$. Substituting once again $\langle\alpha x^2\rangle = D$ in the above equation, and using

$$\langle\alpha^2 x^2\rangle = D\alpha_0 - \frac{D\mu}{2} + \frac{\mu\alpha_0}{2}\langle x^2\rangle, \tag{2.65}$$

which is obtained by multiplying the Fokker-Planck equation (2.59) by αx^2 and integrating over both x and α, we eventually find

$$\langle(\alpha - \alpha_0)^2 x^2\rangle = \left(\alpha_0 + \frac{\mu}{2}\right)\left(\alpha_0\langle x^2\rangle - D\right) \tag{2.66}$$

and hence $\alpha_0\langle x^2\rangle \geq D$, as required.

2.6.2 Fast stiffness dynamics

Finding an analytical expression for the entropy production rate of a diffusive particle in a harmonic potential whose stiffness is governed by an Ornstein-Uhlenbeck process

relies on our capacity to write down the variance of the particle position. To make some headway along this line, we consider the regime where the stiffness dynamics are much faster than the positional dynamics of the particle. Here, we work perturbatively and introduce a small parameter, $\varepsilon \ll 1$, characterizing the separation in timescales between the two processes, as is common practice in the literature for fast-slow dynamical systems [217].

At the level of the coupled Langevin equations, this re-scaling is written as

$$\dot{x}(t) = -\alpha x(t) + \sqrt{2D}\,\eta_x(t) \tag{2.67a}$$

$$\varepsilon\dot{\alpha}(t) = -\tilde{\mu}(\alpha(t) - \alpha_0) + \sqrt{2\tilde{D}_\alpha \varepsilon}\,\eta_\alpha(t) \tag{2.67b}$$

where we have taken care to re-scale the noise appropriately under the separation of timescales. The Fokker-Planck equation for the joint probability density now reads

$$\begin{aligned}\partial_t P(x,\alpha,t) = D\partial_x^2 P(x,\alpha,t) + \alpha\partial_x\big[xP(x,\alpha,t)\big] \\ + \frac{\tilde{D}_\alpha}{\varepsilon}\partial_\alpha^2 P(x,\alpha,t) + \frac{\tilde{\mu}}{\varepsilon}\partial_\alpha\big[(\alpha-\alpha_0)P(x,\alpha,t)\big]\ ,\end{aligned} \tag{2.68}$$

corresponding to the rescaling $D_\alpha \to \tilde{D}_\alpha/\varepsilon$, $\mu \to \tilde{\mu}/\varepsilon$, which preserves the variance of the stiffness.

In the limit $\varepsilon \to 0$, it is known that $P(x,\alpha) \to P(x;\alpha_0)P^{\mathrm{tot}}(\alpha)$ where $P(x;\alpha_0)$ is the stationary distribution in the case where $\alpha \equiv \alpha_0$ and $P^{\mathrm{tot}}(\alpha)$ is the stationary marginal distribution for α as given in Eq. (2.58) [217]. For small but finite ε, it is useful to write the stationary probability distribution perturbatively around this limit, namely

$$P(x,\alpha) = P_0(x;\alpha_0)P^{\mathrm{tot}}(\alpha) + \varepsilon P_1(x,\alpha), \tag{2.69}$$

where $P_1(x,\alpha)$ is some function of leading order $\mathcal{O}(\varepsilon^0)$ into which all higher order corrections have also been absorbed [217]. Note that $P_1(x,\alpha)$ should not be thought of as a probability distribution as it does not satisfy the normalization condition, rather

$$\int dx \int d\alpha\, P_1(x,\alpha) = 0. \tag{2.70}$$

We introduce the notation

$$\langle \cdot \rangle_1 = \int dx \int d\alpha \, (\cdot) \, P_1(x, \alpha) \tag{2.71}$$

whence

$$\langle x^2 \rangle - \frac{D}{\alpha_0} = \varepsilon \langle x^2 \rangle_1 \tag{2.72}$$

which allows us to express the variance of the position in terms of the variance in the uncoupled problem where $\alpha \equiv \alpha_0$ and a contribution from the first-order term in ε. From Eq. (2.63), it is clear that to compute the steady-state entropy production rate, we need to find an analytic expression for the quantity $\langle x^2 \rangle_1$. Multiplying the Fokker-Planck equation (2.68) by $x^2(\alpha - \alpha_0)^2$ and integrating with respect to both x and α at steady-state leads after some straightforward algebra to the following moments relation

$$D\langle (\alpha - \alpha_0)^2 \rangle - \langle \alpha(\alpha - \alpha_0)^2 x^2 \rangle + \frac{\tilde{D}_\alpha}{\varepsilon} \langle x^2 \rangle - \frac{\tilde{\mu}}{\varepsilon} \langle x^2 (\alpha - \alpha_0)^2 \rangle = 0 \tag{2.73}$$

While we have already expressed the variance of the particle position in terms of our perturbative expansion (2.69), similarly, we write the other moments as

$$\langle (\alpha - \alpha_0)^2 \rangle = \varepsilon \langle (\alpha - \alpha_0)^2 \rangle_1 + \frac{\tilde{D}_\alpha}{\tilde{\mu}} \tag{2.74a}$$

$$\langle (\alpha - \alpha_0)^2 x^2 \rangle = \varepsilon \langle (\alpha - \alpha_0)^2 x^2 \rangle_1 + \frac{D\tilde{D}_\alpha}{\alpha_0 \tilde{\mu}} \tag{2.74b}$$

$$\langle \alpha(\alpha - \alpha_0)^2 x^2 \rangle = \varepsilon \langle \alpha(\alpha - \alpha_0)^2 x^2 \rangle_1 + \frac{D\tilde{D}_\alpha}{\tilde{\mu}} \tag{2.74c}$$

Substituting (2.72) and (2.74) in (2.73), we obtain

$$\langle (\alpha - \alpha_0)^2 x^2 \rangle_1 = \frac{\tilde{D}_\alpha}{\tilde{\mu}} \langle x^2 \rangle_1 - \frac{\varepsilon}{\tilde{\mu}} \langle \alpha(\alpha - \alpha_0)^2 x^2 \rangle_1. \tag{2.75}$$

Furthermore, taking care to rescale $\mu \to \tilde{\mu}/\varepsilon$, Eq. (2.66) can be rewritten as follows

$$\langle (\alpha - \alpha_0)^2 x^2 \rangle = \left(\alpha_0 + \frac{\tilde{\mu}}{2\varepsilon} \right) \alpha_0 \varepsilon \langle x^2 \rangle_1 \tag{2.76}$$

Finally, we combine (2.74b), (2.75) and (2.76) to obtain a closed-form expression for

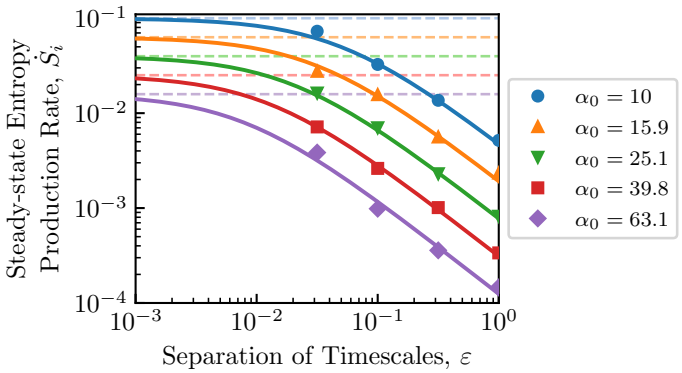

Figure 2.9: *Steady-state entropy production as a function of the separation of timescale, ε* — We fix $D = D_\alpha = \mu = 1$ and $\alpha_0 = 10$, then vary ε which represents the difference in the timescales of the two processes, introduced in Sec 2.6.2. We show good agreement between numerical simulations (symbols) and analytic result (2.78) (solid lines). We also show the analytic results for the entropy production rate as $\varepsilon \to 0$ (dotted lines) as given by (2.79).

$\langle x^2 \rangle_1$ valid up to order $\mathcal{O}(\varepsilon^2)$,

$$\langle x^2 \rangle_1 = \frac{D\tilde{D}_\alpha}{\alpha_0 \tilde{\mu}} \left[\frac{\tilde{\mu}\alpha_0}{2} + \varepsilon \left(\alpha_0^2 - \frac{\tilde{D}_\alpha}{\tilde{\mu}} \right) + \mathcal{O}(\varepsilon^2) \right]^{-1}. \tag{2.77}$$

We conclude that the entropy production as given in Eq. (2.63) is therefore

$$\lim_{t\to\infty} \dot{S}_i = \frac{\tilde{D}_\alpha}{\alpha_0 \tilde{\mu}} \left[1 + \frac{2\varepsilon}{\alpha_0 \tilde{\mu}} \left(\alpha_0^2 - \frac{\tilde{D}_\alpha}{\tilde{\mu}} \right) + \mathcal{O}(\varepsilon^2) \right]^{-1} \tag{2.78}$$

which we compare to the results of numerical simulations in Fig. 2.9. It follows that as we saw for the cases of discrete stiffness, the entropy production remains finite in the limit of fast stiffness dynamics, here $\varepsilon \to 0$. Namely, we obtain

$$\lim_{\varepsilon\to 0} \lim_{t\to\infty} \dot{S}_i(t) = \frac{\tilde{D}_\alpha}{\alpha_0 \tilde{\mu}}, \tag{2.79}$$

and conclude that it scales linearly with the variance of $P^{\text{tot}}(\alpha)$.

2.7 Conclusion and discussion

In this work, we have established a general framework for calculating the steady-state entropy production rate of diffusive single-particle systems in time-dependent, confining potentials subject to Markovian stochastic fluctuations, including both discrete and continuous "state spaces" for the fluctuating potential. Our exploration has been conducted within the formalism of [113], reviewed in [64]. After introducing our results for general Markovian processes, we obtain analytical results for a variety of important cases. In particular, we focus on harmonic confining potentials subject to fluctuations in the stiffness α.

As a first example, we study the diffusion of a particle in an intermittent harmonic potential switching *on* and *off* with a symmetric rate k. In this case, we conclude that the entropy production is independent of both the diffusivity D of the trapped passive particle and the switching rate k. This remarkably simple result emerges naturally from the quadratic form of the confining potential. Indeed, one expects the steady-state positional probability density, which determines the steady-state probability current, to generically depend on both of these parameters, as we show in the simple example of a quartic potential.

We then expanded this preliminary result to a general two-state Ornstein-Uhlenbeck process with Markovian switching. Using this model, we discussed the entropy production in a realistic model of stochastic resetting, a problem which has previously attracted the attention of several groups [105, 97, 50]. Within our framework, traditional stochastic resetting is associated with infinite entropy production on the basis of a complete breakdown of time reversal symmetry [97]. We reconcile this observation with the finite entropy production calculated in [105, 50] by recognizing that the measures of dissipation used in these latter works are not directly linked to time-reversal symmetry. Thereupon, we further generalized our results on entropy production to harmonic potentials with stiffnesses controlled by an N-state discrete Markov process. As a direct application, we studied a simple example of a 3-state process highlighting the emergence of a non-trivial contribution to the entropy production due to currents in the stiffness space.

Finally, we explored a model where the potential stiffness itself evolves in time according to an Ornstein-Uhlenbeck process with diffusivity D_α and coupling μ, modeling,

for instance, the diffusion of a particle confined in an optical trap whose strength is fluctuating continuously in time due to e.g. fluctuations in laser intensity. Strikingly, we give explicit analytical results for the entropy production in the regime where the stiffness fluctuations are fast compared to the positional dynamics of the particle.

Interestingly, we observed in some cases that the entropy production remains finite upon taking limits for which the *dynamics* of the trapped Brownian particle are indistinguishable from those of an equilibrium model, reminiscent of the diffusive limit for Run-and-Tumble particles with diverging tumbling rate [64, 109]. This phenomenon, which is sometimes referred to as an *entropic anomaly* [59, 32], is a common occurrence for systems with interacting fast and slow degrees of freedom, which points to the non-trivial correspondence between dynamic and thermodynamic features of non-equilibrium stochastic processes.

Altogether, this work forms a comprehensive study of the entropy production for single-particle systems with fluctuating potentials, which provides the foundations of a non-equilibrium thermodynamic theory of fluctuating potentials. While we have derived exact results for the case where the potential is of quadratic form, the framework developed here can be extended to more complex confining potentials and will generally result in a hierarchy of equations for the moments of the probability distribution. One is left to find an approximate closure to this hierarchy to conclude on the entropy production rate. Nevertheless, many trapping potentials are well-approximated by parabolic potentials, thus we believe that our results will prove very useful for calculating the entropy production due to potential fluctuations in practice. Further, we focus here on diffusive motion in confining fluctuating potentials but our framework itself can be generalized to a more general class of models like random acceleration processes [118, 49, 190, 265] or active particles including run-and-tumble particles [29, 28, 110, 269], active Brownian particles [269, 239, 23] and active Ornstein-Uhlenbeck particles [38, 55, 194, 259], which will be the subject of future work. Finally, we believe that our results provide a natural framework to study the stochastic thermodynamics of colloidal systems in optical traps [125, 86, 52].

2.A Steady-state densities for Brownian motion in an intermittent harmonic potential

In Section 2.3, we calculate the entropy production for a particle diffusing in an intermittent harmonic potential. Exact results are known for the stationary distributions for the specific process. Therefore, our analytical result for the entropy production can be directly compared to that obtained by directly integrating Eqs. (2.13) and (2.14). For completeness, we rederive here shortly the steady-state distributions following the derivations found in [313, 244].

To do so, we start from the Fokker-Planck equations (2.25) at steady-state which read

$$0 = D\partial_x^2 P_{\text{off}}(x) + kP_{\text{on}}(x) - kP_{\text{off}}(x) \tag{2.80a}$$

$$0 = D\partial_x^2 P_{\text{on}}(x) + \alpha_0 \partial_x \big[x P_{\text{on}}(x)\big] + kP_{\text{off}}(x) - kP_{\text{on}}(x) \tag{2.80b}$$

where we have dropped the time dependence in $P_{\text{on}}(x)$ and $P_{\text{off}}(x)$ to denote their stationary nature. To solve these coupled equations, it is easier to work in Fourier space. Using the following convention for Fourier transforms,

$$\widehat{P}_i(\nu, t) = \int_{-\infty}^{+\infty} P_i(x,t) e^{-i\nu x} dx \,, \tag{2.81}$$

these equations read in Fourier-transformed space

$$0 = -D\nu^2 \widehat{P}_{\text{off}}(\nu) + k\widehat{P}_{\text{on}}(\nu) - k\widehat{P}_{\text{off}}(\nu) \tag{2.82a}$$

$$0 = -D\nu^2 \widehat{P}_{\text{on}}(\nu) - \alpha_0 \nu \partial_\nu \widehat{P}_{\text{on}}(\nu) + k\widehat{P}_{\text{off}}(\nu) - k\widehat{P}_{\text{on}}(\nu) \tag{2.82b}$$

Using Eq. (2.82a), we can express $\widehat{P}_{\text{off}}(\nu)$ in terms of $\widehat{P}_{\text{on}}(\nu)$ which allows us to write the following single differential equation for $\widehat{P}_{\text{on}}(\nu)$

$$\alpha_0 \partial_\nu \widehat{P}_{\text{on}}(\nu) + D\nu \left[1 + \frac{k}{D\nu^2 + k}\right] \widehat{P}_{\text{on}}(\nu) = 0 \,. \tag{2.83}$$

The solution to Eq. (2.83) can easily be shown to read

$$\widehat{P}_{\text{on}}(\nu) = \left[\frac{k}{2(k + D\nu^2)}\right]^{\frac{k}{2\alpha_0}} \exp\left[-\frac{D\nu^2}{2\alpha_0}\right] \tag{2.84}$$

where we have used the fact that $\widehat{P}(0) = \widehat{P}_{on}(0) + \widehat{P}_{\text{off}}(0)$ by conservation of probability. Finally, using Eq. 2.82a, we obtain the full steady-state distribution in ν-space as

$$\widehat{P}(\nu) = \frac{1}{2}\left[\frac{e^{-D\nu^2/2\alpha_0}}{(1+D\nu^2/k)^{k/2\alpha_0}} + \frac{e^{-D\nu^2/2\alpha_0}}{(1+D\nu^2/k)^{1+k/2\alpha_0}}\right] \tag{2.85}$$

While it is not possible to obtain a closed-form expression for the total steady-state distribution in real space for general values of α_0, D and k, one can invert this relation and write $P(x)$ as the following sum of convolution integrals

$$P(x) = \frac{1}{2}\left\{\int_{-\infty}^{+\infty} dy\, f_2\left(y, \frac{k}{2\alpha_0}\right) f_1(x-y) + \int_{-\infty}^{+\infty} dy\, f_2\left(y, 1+\frac{k}{2\alpha_0}\right) f_1(x-y)\right\} \tag{2.86}$$

where

$$f_1(x) = \mathcal{F}^{-1}\left[e^{-D\nu^2/2\mu_0}\right] = \frac{1}{\sqrt{2\pi D/\alpha_0}} e^{-\alpha_0 x^2/2D} \tag{2.87a}$$

$$f_2(x,\beta) = \mathcal{F}^{-1}\left[(1+D\nu^2/k)^{\beta}\right] = \frac{\sqrt{\pi}}{\Gamma(\beta)}\left(\frac{k}{D}\frac{|x|}{2}\right)^{\beta-1/2} K_{\frac{1}{2}-\beta}\left(\sqrt{\frac{k}{D}}|x|\right) \tag{2.87b}$$

with $K_n(x)$ the modified Bessel function of the second kind.

The form of the steady-state distribution for the particle position emerges from a competition between two timescales: (i) k^{-1} the timescale set by the switching rate of the intermittent confining potential and (ii) α_0^{-1} which sets the particle position correlation time, or equivalently, the timescale at which the particle position converges back to the center of the confining potential. As shown in Ref. [244], it is possible to obtain exact expressions for the steady-state distribution in some asymptotic regimes. In particular, in the limit where the switching rate is very small compared to the confining potential strength, $k \ll \alpha_0$, the steady-state distribution is given by

$$P(x) \underset{k\ll\alpha_0}{=} \frac{1}{2}\left[\frac{e^{-\alpha_0 x^2/2D}}{\sqrt{2\pi D\alpha_0}} + \frac{\sqrt{k/D}e^{k/2\alpha_0}}{4} e^{-\sqrt{k/D}|x|}\,\text{Erfc}\left(\frac{\sqrt{k/D}}{2\alpha_0} - \sqrt{\frac{\alpha_0}{2D}}|x|\right)\right] \tag{2.88}$$

leading to a central Gaussian region followed by exponential tails. Conversely, in the

limit of a very fast switching rate $k \gg \alpha_0$, the steady-state distribution is given by

$$P(x) \underset{k \gg \alpha_0}{=} \frac{e^{-\alpha_0 x^2/4D}}{\sqrt{4\pi D/\alpha_0}} \tag{2.89}$$

which is the same as that of an equilibrium Ornstein-Uhlenbeck process with a reduced potential strength $\alpha_0/2$.

2.B Numerical analysis

As shown in Eq. (2.14), the entropy flow can easily be calculated if given the knowledge of the stationary distribution for the process. However, analytic forms for these stationary distributions are generically difficult to obtain. In order to confirm our analytical results, we can nonetheless resort to computing the entropy production numerically. To do so, we measure the stationary distribution (or histogram of the particle positions) for each of our models directly from simulated single particle trajectories over long times.

In all systems, the single particle trajectories are obtained by solving the associated Langevin equation using a second-order stochastic Runge-Kutta method with a fixed time step, $dt = 10^{-5}$, for $t \in [0, 10^4]$ [131, 145, 138, 45]. For any given data set for which we have used a fixed timestep, we made sure to take a timestep small enough to resolve the smallest timescale in the process (usually the switching dynamics), i.e. $dt \ll 1/k_{\max}$ where $k_{\max}$ is the largest switching rate considered in the process. When considering a discrete Markov process for the fluctuating potential, $\alpha(t)$ is updated by evaluating the transition probabilities based on the switching rates and timestep. For the continuous Markov process, the stiffness itself follows a Langevin equation, which we solve using a stochastic Runge-Kutta method as above [131, 145, 138, 45].

2.C Entropy production for intermittent quartic potential

We consider a simple modification of the preliminary example introduced in Section 2.3 in which we replace the intermittent quadratic potential by an intermittent *quartic* potential, $V(x; \alpha(t)) = \alpha(t)x^4/4$. The equation for the steady-state entropy production can be derived using the same procedure. The corresponding equation to (2.29) is in

this case

$$\lim_{t\to\infty} \dot{S}_i(t) = \lim_{t\to\infty} \alpha_0 \int dx\, \frac{x^4}{4} \partial_x^2 P_{\text{off}}(x,t) = \lim_{t\to\infty} 3\alpha_0 \int dx\, x^2 P_{\text{off}}(x,t) = 3\alpha_0 \Xi_{\text{off}}. \quad (2.90)$$

where $P_{\text{off}}(x)$ is the steady-state joint probability density of finding an agent at position x in the *off* state. It thus follows that the steady-state entropy production is independent of k and D if and only if Ξ_{off} is.

To show that this is not the case, suppose that Ξ_{off} is independent of k. At steady-state, we know that

$$0 = D\partial_x^2 P_{\text{off}}(x) + kP_{\text{on}}(x) - kP_{\text{off}}(x). \quad (2.91)$$

Multiplying (2.91) by x^2 and integrating over the spatial variable x, we find

$$\Xi_{\text{on}} = \Xi_{\text{off}} - \frac{2D}{k}. \quad (2.92)$$

If we fix D and α_0, then, by our earlier assumption, Ξ_{off} is a constant. However, this equation tells us that there exists a range for the switching rate k, namely $k < 2D/\Xi_{\text{off}}$, for which the variance of the steady-state probability of the *on* state is negative. This is a contradiction. We can use the same argument to show that Ξ_{off} can not be independent of D.

Finally, we conclude that, in the case of an intermittent quartic potential, the entropy production must depend on both k and D and the independence of Eq. (2.29) vis-à-vis these two parameters is solely due to the quadratic nature of the confining potential. We argue that there is thus no reason for the entropy production to be independent of k and D with a more general confining potential.

ACKNOWLEDGMENTS

The authors thank Gunnar Pruessner for fruitful discussions. HA was supported by a Roth PhD scholarship funded by the Department of Mathematics at Imperial College London. LC acknowledges support from the Francis Crick Institute, which receives its core funding from Cancer Research UK (FC001317), the UK Medical Research Council (FC001317), and the Wellcome Trust (FC001317).

3

Scaling of entropy production under coarse graining in disordered active media

L. Cocconi, G. Salbreux, G. Pruessner

PRE **105**, L042601 (2022) [66]
Published 25 April 2022
DOI 10.1103/PhysRevE.105.L042601

Overview Up to this point, the toolkit of entropy production has been applied mostly to models that, while being illustrative, were also sufficiently simple to be solved exactly. Unfortunately, models involving an increasing number of degrees of freedom quickly become analytically intractable, a difficulty that has stimulated the development of both numerical [82] and approximate approaches [202, 53]. Furthermore, a 'fully resolved' thermodynamic characterisation taking into account the microscopic features of dissipation might be of little interest when the relevant features of the model at hand emerge from the collective behaviour of many interacting components at a different, mesoscopic spatio-temporal scale (such as in non-equilibrium phase transitions). A natural way of addressing these difficulties is to resort to effective theories, which can be obtained from the original model of interest by one of the available coarse-graining procedures

[33] and are designed to capture the key properties of the former at a particular scale, while ignoring 'irrelevant' microscopic details. What remains ill-understood, however, is how such coarse-graining procedures affect our ability to infer energy dissipation and to quantify the degree of time-reversal symmetry breaking. In this Chapter, we investigate the scaling of the entropy production as a function of the coarse-graining scale for a Brownian particle placed in a disordered non-equilibrium environment. We thus demonstrate that the corresponding scaling exponent can differ depending on the specific properties of the environment, allowing for a natural distinction between models that look increasingly 'equilibrium-like' and others that remain genuinely out of equilibrium at all scales.

Author contributions: LC designed the project, developed the methods, performed the analysis and wrote original version of the manuscript. LC and GP wrote the code and performed the numerical experiments. GP and GS supervised the project throughout and suggested improvements to the original manuscript.

Abstract

Entropy production plays a fundamental role in the study of non-equilibrium systems by offering a quantitative handle on the degree of time-reversal symmetry breaking. It depends crucially on the degree of freedom considered as well as on the scale of description. How the entropy production at one resolution of the degrees of freedom is related to the entropy production at another resolution is a fundamental question which has recently attracted interest. This relationship is of particular relevance to coarse grained and continuum descriptions of a given phenomenon. In this work, we derive the scaling of the entropy production under iterative coarse graining on the basis of the correlations of the underlying microscopic transition rates for non-interacting particles in active disordered media. Our approach unveils a natural criterion to distinguish equilibrium-like and genuinely non-equilibrium macroscopic phenomena based on the sign of the scaling exponent of the entropy production per mesostate.

3.1 Introduction.

Under the umbrella term of “active matter", the study of systems driven by injection and dissipation of energy at the single-agent level has played a prominent role in the development of non-equilibrium physics and expanded its interface with biology. One of the key challenges that arise when developing models of biological matter is to quantify their degree of “non-equilibriumness", i.e. the extent to which their phenomenology differs from that of a collection of passive particles driven by a bath. The rate of entropy production [256, 64] allows for such differentiation by capturing time-reversal symmetry breaking at the microscopic scale [113]. While the injection of energy ensures a strong departure from equilibrium at the single-agent level, these systems do not necessarily exhibit nonequilibrium features at larger spatio-temporal scales [202, 263, 88, 58, 82]. The question of whether equilibrium is effectively restored at this mesoscopic level requires new methods to quantify how entropy production varies under spatial coarse-graining [91, 8, 120, 178, 53, 59, 308]. We offer a novel perspective on this issue by studying a single-particle driven-diffusion process obtained by perturbing homogeneous diffusion with a non-conservative quenched random forcing. A similar model was recently studied as an effective description for the collective motion of active matter in a random potential [235] and can be seen as a minimal description of a molecular motor self-propelling on a disordered network of cytoskeletal filaments [152]. These models are particular examples of active disordered media [210, 221, 62, 226], which we discuss for the first time from a thermodynamic perspective. On a more abstract level, our model may be seen as a many-particle system randomly exploring a complex phase space. From this perspective, our work determines the scaling behaviour of entropy production in a wider class of systems, including biochemical reaction networks [308].

We first analyse our model on a one-dimensional ring, where it is exactly solvable [76], and we identify a trivial scaling behaviour of the mesoscopic entropy production under block coarse-graining. We then move to higher dimensional lattices, where we show how the mesoscopic entropy production decays algebraically with block size under block coarse-graining. In order to characterise the non-trivial scaling exponents, we draw on a novel field theoretic formalism based on the Martin-Siggia-Rose construction [318, 133] and demonstrate that the scaling of the entropy production can be related to the small wavenumber behaviour of the probability current’s spectral density by

arguments reminiscent of those employed in the treatment of hyperuniform fluctuations [285]. Our main result, Eq. (3.18), provides a natural criterion to distinguish between equilibrium-like and genuinely non-equilibrium macroscopic phenomena based on the sign of the scaling exponent for the entropy production per mesostate.

3.2 Entropy production and coarse graining.

The starting point of our analysis is a Markovian jump process satisfying the master equation

$$\dot{P}_n(t) = \sum_m (P_m(t) w_{m,n} - P_n(t) w_{n,m}) \tag{3.1}$$

for the probability $P_n(t)$, with $w_{n,m}$ the non-negative transition rate from state n to state $m \neq n$. The average rate of internal entropy production at steady-state is defined as [64]

$$\dot{S}_i = \frac{1}{2} \sum_{n,m} J_{n,m} \ln \frac{\pi_n w_{n,m}}{\pi_m w_{m,n}} \tag{3.2}$$

where $\pi_n = \lim_{t\to\infty} P_n(t)$ is the steady-state probability mass function and $J_{n,m} = \pi_n w_{n,m} - \pi_m w_{m,n}$ is the net probability current from state n to state m. The entropy production $\dot{S}_i$ is non-negative and vanishes for systems that satisfy detailed balance. Computing $\dot{S}_i$ from Eq. (3.2) requires complete knowledge of the set of microscopic probability currents $j_{nm} = \pi_n w_{n,m}$, which renders this observable sensitive to time-reversal symmetry breaking induced by energy injection at the microscopic scale. However, this 'fully resolved' entropy production might be of little interest in the discussion of effective descriptions at the mesoscopic scale. In recent years, various works have addressed the issue of coarse-graining, which amounts to a partial loss of information about the microscopic currents j_{nm} [91, 8, 82, 228, 119, 208, 53]. The perennial difficulty is that the resulting mesoscopic description is in general non-Markovian [275, 33, 280]. Esposito [91] has identified a decomposition of the full entropy production under phase-space partitioning into three non-negative contributions. Assuming a separation of timescales between intra-mesostate and inter-mesostate transitions, it was also shown that the mathematical form of the entropy production, Eq. (3.2), is recovered at the mesoscopic level.

Previous work has focused on a single coarse-graining step, partly due to constraints

of Markovianity. However, if the state space is sufficiently large, it is natural to ask whether such coarse-graining procedure could be performed iteratively, in a spirit similar to Kadanoff's "block spin" renormalisation [151]. Characterising the scale dependence of suitable observables such as the entropy production per mesostate

$$\dot{s}_i^{(\mathrm{meso})} = \dot{S}_i^{(\mathrm{meso})} / N^{(\mathrm{meso})} \ , \tag{3.3}$$

with $N^{(\mathrm{meso})}$ the number of mesostates at a given coarse-graining level, will then convey important information regarding the degree of activity at different scales. To carry out this programme we first denote the steady-state probability current from mesostate α to mesostate β by

$$j_{\alpha\beta}(L) = \sum_{n\in\alpha} \sum_{m\in\beta} \pi_n w_{n,m} \tag{3.4}$$

with L the characteristic coarse-graining length scale, such that $j_{\alpha\beta}(1) = \pi_n w_{nm}$ for $\alpha = \{n\}$ and $\beta = \{m\}$. We then sidestep the issue of Markovianity by postulating an effective mesoscopic entropy production of the form

$$\dot{S}_i^{(\mathrm{meso})}(L) = \frac{1}{2} \sum_{\alpha,\beta} (j_{\alpha\beta}(L) - j_{\beta\alpha}(L)) \ln \frac{j_{\alpha\beta}(L)}{j_{\beta\alpha}(L)} \ , \tag{3.5}$$

as would be measured by any observer faithfully applying Eq. (3.2) to a process observed at a given resolution L. The observable $\dot{S}_i^{(\mathrm{meso})}(L)$ should be thought of as the entropy production of a different (Markovian) process constrained to displaying the coarse-grained currents of the original process. A similar approach has been recently discussed to characterise the scaling of energy dissipation in non-equilibrium reaction networks [308].

3.3 The model.

We will now introduce a minimal driven-diffusion model [247] on a regular lattice, such that the corresponding non-equilibrium steady-state is amenable to iterative block coarse-graining. Diffusion in a stable potential is the prototypical equilibrium phenomenon but there are many ways to modify the familiar diffusive dynamics into a non-equilibrium process, for example by allowing for an unstable potential [295]. An

alternative modification, which guarantees a steady-state, is to impose periodic boundary conditions in such a way that a global potential function cannot be defined. To see how this is done, we recall [248] that for a Markov jump process, Eq. (3.1), to have an equilibrium steady state, the affinity

$$A(\{w\}; n_1, \ldots, n_M) = \ln \frac{w_{n_1,n_2} w_{n_2,n_3} \ \ldots \ w_{n_M,n_1}}{w_{n_1,n_M} \ \ldots \ w_{n_3,n_2} w_{n_2,n_1}} \ . \tag{3.6}$$

of every cycle $\{n_1, n_2, ..., n_M, n_1\}$ has to be exactly zero. Henceforth, we will use the convention that $\ln(0/0) = 0$ as some of the $w_{n,m}$ may vanish. Whenever $A \neq 0$ for any cycle, the system is intrinsically out of equilibrium and we should expect steady-state probability currents [295]. A straightforward way of inducing non-equilibrium behaviour is therefore to allow for quenched disorder in the transition rates, which can be interpreted as a non-conservative random forcing [35, 44]. The resulting disordered steady-state is then non-equilibrium with exceedingly high probability. In the following we therefore consider a homogeneous diffusion process on a periodic lattice in d dimensions and allow for a quenched perturbation to the nearest-neighbour hopping rates such that

$$w_{n,m} = h + \zeta_{n,m} \ , \tag{3.7}$$

with $\zeta_{n,m} > -h$ a set of zero-mean random variables, Fig. 3.1. Henceforth, $\langle \cdot \rangle$ will denote averages over this random variable.

3.4 Ring topology ($d = 1$).

The one-dimensional version of this model has previously been considered in the context of random walks in random environments [44, 35]. Starting from an exact result by Derrida [76] for the net current, $J = J_{n,n+1}$, the entropy production, Eq. (3.2), can be calculated as $\dot{S}_i = JA(\{w\}; \{1, 2, \ldots, N\})$, on the basis of constant $J = \pi_n w_{n,n+1} - \pi_{n+1} w_{n+1,n}$ and the affinity A, Eq. (3.6), taken for the cycle passing through all sites of the ring once [249], Appendix 3.A. After substituting Eq. (3.7) into Eqs. (3.6) we eventually obtain

$$\dot{S}_i = \frac{1}{hN^2} \left(\sum_{n=1}^{N} (\zeta_{n,n+1} - \zeta_{n+1,n}) \right)^2 + \mathcal{O}(\zeta^3) \ , \tag{3.8}$$

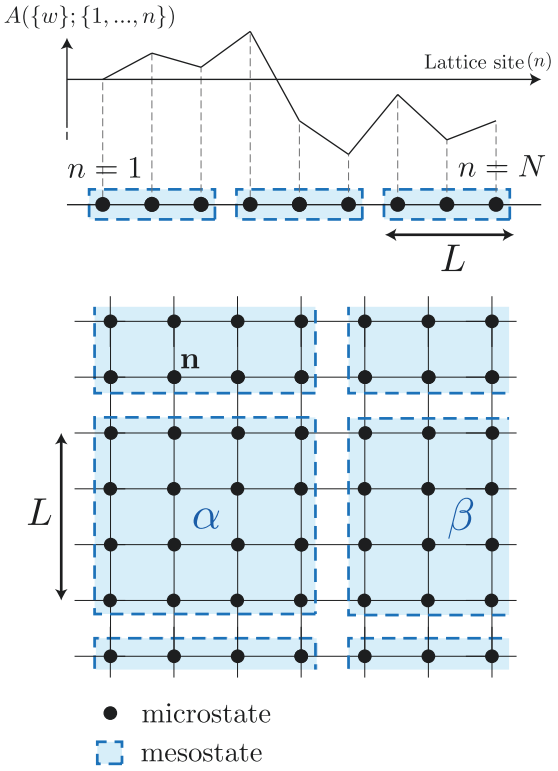

Figure 3.1: Coarse-graining procedure for a diffusion process on a periodic square lattice perturbed by a spatially quenched, non-conservative disorder. In one dimension (top), the transition rates locally define a random walk with increments $\nu_n = \zeta_{n,n+1} - \zeta_{n+1,n}$ and the affinity $A(\{w\};\{1,..,N\})$ of the closed cycle across all sites is to leading order proportional to the displacement of the random walk after N steps, Appendix 3.A. In higher dimensions (bottom), the random potential picture breaks down locally and the coarse-graining becomes non-trivial due to the current no longer being uniform.

where $\mathcal{O}(\zeta^k)$ stands for any term proportional to $\zeta_{i_1\pm1,i_1}...\zeta_{i_k\pm1,i_k}$ with any indices $i_1,...,i_k$. As can be seen by setting $\zeta_{i,j}=0$ for all i,j, the entropy production vanishes at zeroth order in the perturbation, as expected. Appendix 3.A explores the weak disorder limit of Eq. (3.8) in more detail.

We now apply the coarse-graining procedure based on Eqs. (3.4) and (3.5). In one dimension, the interface between distinct mesostates consists of a single edge (Fig. 3.1) and the net current $j_{\alpha\beta}(L)-j_{\beta\alpha}(L)=J$ is independent of the block size L. The mesoscopic entropy production $\dot{S}_i^{(\mathrm{meso})}$, Eq. (3.5), is thus given by a sum over a subset of the contributions to the microscopic entropy production $\dot{S}_i$, Eq. (3.2). By invoking translational invariance and linearity of expectation, the total entropy production rate in a system with originally N states coarse-grained into mesostate blocks of size L is

$$\left\langle \dot{S}_i^{(\mathrm{meso})} \right\rangle (L) = \left\langle J \sum_{k=1}^{N/L} \ln \frac{\pi_{kL} w_{kL,kL+1}}{\pi_{kL+1} w_{kL+1,kL}} \right\rangle \tag{3.9}$$

$$= \frac{N}{L} \left\langle J \ln \frac{\pi_n w_{n,n+1}}{\pi_{n+1} w_{n+1,n}} \right\rangle , \tag{3.10}$$

with arbitrary state index n. For uncorrelated noise in the weak disorder limit and using $\pi_n/\pi_m = r_n/r_m$ [76], $\left\langle \dot{S}_i^{(\mathrm{meso})} \right\rangle = 2\lambda/(NhL) + \mathcal{O}(\lambda^2)$, where λ denotes the variance of $\zeta_{n,m}$. Irrespective of the noise strength, the dependence of the total entropy production on the block size L is solely due to the absence of terms from currents within a microstate block. In one dimension, the entropy production per mesostate $\left\langle \dot{s}_i^{(\mathrm{meso})} \right\rangle = (L/N) \left\langle \dot{S}_i^{(\mathrm{meso})} \right\rangle$, Eq. (3.3), is thus independent of L. No current averaging at interfaces between blocks takes place. The situation is qualitatively different in $d>1$, as we will demonstrate now.

3.5 Periodic lattices with $d>1$.

In higher dimensions, the equilibrium condition $A(\{w\};\{n_1,...,n_M\})=0$ is generally broken at the local rather than global scale. No analytical expression for the steady-state currents is available and we resort to a perturbation theory in weak disorder, based on a Martin-Siggia-Rose field theory [318, 133], which allows us to extract various static correlation functions in arbitrary dimensions and for a wide class of disorders,

see Appendix 3.B. There, we introduce the net microscopic probability current $\boldsymbol{J}(\boldsymbol{x}) = (J^{(1)}(\boldsymbol{x}), ..., J^{(d)}(\boldsymbol{x}))$ as the continuum limit of $J_{\boldsymbol{n},\boldsymbol{m}}$ on a hypercubic lattice, together with its Fourier transform $\boldsymbol{\mathcal{J}}(\boldsymbol{k}) = (\mathcal{J}^{(1)}(\boldsymbol{k}), ..., \mathcal{J}^{(d)}(\boldsymbol{k}))$. We follow the convention

$$J^{(a)}(\boldsymbol{x}) = \frac{1}{V}\sum_{\boldsymbol{k}} \mathcal{J}^{(a)}(\boldsymbol{k}) e^{i\boldsymbol{k}\cdot\boldsymbol{x}} \tag{3.11}$$

with $\boldsymbol{k} = 2\pi\boldsymbol{n}/(N\ell)$ ($\boldsymbol{n} \in \mathbb{Z}^d$), assuming a hypercubic system, and $V = (N\ell)^d$ the phase space volume, with ℓ the dimensionful lattice spacing. We assume a disorder characterised by the covariance in Fourier space

$$\langle \zeta^{(a)}(\boldsymbol{k})\zeta^{(b)}(\boldsymbol{k}')\rangle = \tilde{\lambda}|\boldsymbol{k}|^{-\eta}\delta_{ab}V\delta_{\boldsymbol{k}+\boldsymbol{k}',0} \tag{3.12}$$

for $|\boldsymbol{k}| \to 0$, corresponding, for $\eta \neq 0$, to $\langle \zeta^{(a)}(\boldsymbol{r})\zeta^{(b)}(\boldsymbol{r}')\rangle \sim \delta_{ab}|\boldsymbol{r}-\boldsymbol{r}'|^{-d+\eta}$ at $|\boldsymbol{r}-\boldsymbol{r}'| \to \infty$, where $\zeta^{(a)}$ indicates the disorder affecting edges parallel to the a-th dimension of the lattice (see Appendix 3.B for details of the specification of backward rates). The spectral density tensor of the probability current evaluated at tree level then reads (Appendix 3.B), for $\boldsymbol{k} \neq 0$,

$$\langle \mathcal{J}^{(a)}(\boldsymbol{k})\mathcal{J}^{(b)}(\boldsymbol{k}')\rangle = \frac{4\tilde{\lambda}}{V}\left(\delta_{ab} - \frac{k_a k_b}{|\boldsymbol{k}|^2}\right)|\boldsymbol{k}|^{-\eta}\delta_{\boldsymbol{k}+\boldsymbol{k}',0}\ . \tag{3.13}$$

Eq. (3.13) matches the general form of the spectral density of a divergence-free, isotropic vector field, which is well known from the theory of turbulence of incompressible fluids [102, 198]. For $\eta < 0$, the vanishing of the spectral density as $\boldsymbol{k} \to 0$ indicates that the probability current is hyperuniform [285], i.e. exhibits an anomalous suppression of fluctuations at large wavelengths. The case $\eta = 0$ corresponds to uncorrelated (white) noise, $\langle \zeta^{(a)}(\boldsymbol{r})\zeta^{(b)}(\boldsymbol{r}')\rangle = \tilde{\lambda}\delta_{ab}\delta(\boldsymbol{r}-\boldsymbol{r}')$.

We can now carry out the coarse-graining procedure for the entropy production. First, we note that the mesoscopic entropy production, Eq. (3.5), is given by a sum over contributions from neighbouring mesostates, $\alpha \neq \beta$ in (3.5). By linearity of expectation, the disorder average $\left\langle \dot{S}_i^{(\mathrm{meso})} \right\rangle$ is therefore the expected contribution from a single interface multiplied by the number of interfaces. It follows that, for a hypercubic lattice

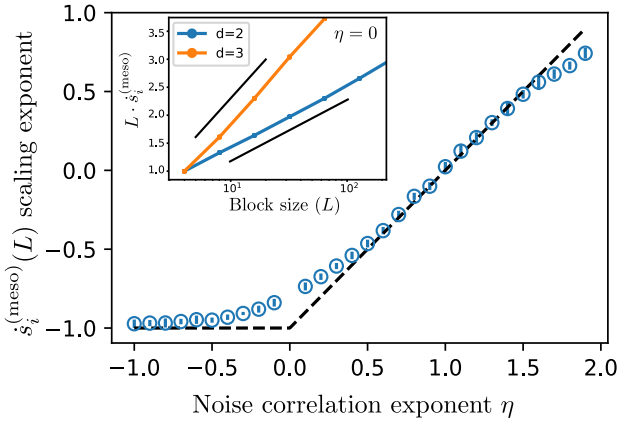

Figure 3.2: The dependence of the scaling exponent for the entropy production per mesostate, $\dot{s}_i^{(\mathrm{meso})}$, on η in the range $-1 \leq \eta \leq d$, shown here for $d = 2$ and $N = 2048^2$, is well captured by Eq. (3.18), shown in black dashed. For uncorrelated disorder, $\eta = 0$, the algebraic scaling of $\dot{s}_i^{(\mathrm{meso})}$ with block size L displays a logarithmic correction, shown in the inset for $d = 2, 3$, also in agreement with Eq. (3.18). Exact logarithmic scaling is shown in solid black for reference. The ordinate is here normalised to its value for the smallest block size considered.

with coordination number $2d$,

$$\left\langle \dot{s}_i^{(\mathrm{meso})} \right\rangle = d \left\langle (j_{\alpha\beta}(L) - j_{\beta\alpha}(L)) \ln \frac{j_{\alpha\beta}(L)}{j_{\beta\alpha}(L)} \right\rangle \tag{3.14}$$

where $\{\alpha, \beta\}$ is any pair of neighbouring mesostates. Asymptotically in large L, Eq. (3.14) can be approximated by

$$\left\langle \dot{s}_i^{(\mathrm{meso})} \right\rangle \simeq \frac{dN^d}{hL^{d-1}} \sigma_J^2(L) \tag{3.15}$$

where

$$\sigma_J^2(L) = \langle (j_{\alpha\beta}(L) - j_{\beta\alpha}(L))^2 \rangle \tag{3.16}$$

denotes the variance of the probability current integrated across an interface of linear dimension L. This relation is derived in Appendix 3.C. In the continuum limit, the asymptotic scaling of the entropy production per mesostate is therefore controlled by the asymptotic variance of the current integrated across the interface between states, which is in turn determined by the small wavenumber behaviour of the current spectral density tensor introduced in Eq. (3.13). In fact, the relationship between Eqs. (3.13) and (3.16) is exactly the type of problem addressed in the study of hyperuniform systems

[285]. Using results from these studies, one obtains

$$\sigma_J^2(L) \sim \begin{cases} L^{d-2}, & \text{for } \eta < 0 \\ L^{d-2}\ln(L), & \text{for } \eta = 0 \\ L^{d-2+\eta}, & \text{for } 0 < \eta < d \end{cases} . \tag{3.17}$$

A more thorough derivation of these scaling laws is provided in Appendix 3.D. We can think of $\sigma_J^2(L) \sim L^{d-2}$ as scaling with the perimeter of the interface. In this sense, it is instructive to draw a comparison with the case of a non-solenoidal random vector field with spectral density $\langle \mathcal{J}^{(a)}(\boldsymbol{k})\mathcal{J}^{(b)}(\boldsymbol{k'})\rangle = (\tilde{\lambda}/V)\delta_{ab}\delta_{\boldsymbol{k}+\boldsymbol{k}',0}$, in which case the variance of the integrated current instead scales with the area of the interface, $\sigma_J^2(L) \sim L^{d-1}$. The requirement that the steady-state is divergence-free thus plays an important role by imposing long-range correlations in the currents, even when these are not present in the substrate, i.e. for $\eta = 0$. Combining Eqs. (3.15) and (3.17) we eventually arrive at (Appendix 3.D)

$$\left\langle \dot{s}_i^{(\mathrm{meso})} \right\rangle (L) \propto \frac{\sigma_J^2(L)}{L^{d-1}} \sim \begin{cases} L^{-1}, & \text{for } \eta < 0 \\ L^{-1}\ln(L), & \text{for } \eta = 0 \\ L^{-1+\eta}, & \text{for } 0 < \eta < d \end{cases} , \tag{3.18}$$

which constitutes our key result. The scaling exponent changes sign at $\eta = 1$, corresponding to $\langle \zeta^{(a)}(\boldsymbol{r})\zeta^{(b)}(\boldsymbol{r'})\rangle \sim \delta_{ab}|\boldsymbol{r} - \boldsymbol{r'}|^{-(d-1)}$, suggesting a quantitative distinction between steady-states that are increasingly "equilibrium-like" at larger scales and genuinely non-equilibrium states where dissipation occurs at all scales. Numerical simulations for $\eta = 0$ in $d = 2, 3$, as well as the full range $-1 < \eta < d$ in $d = 2$ show excellent agreement with our analytical prediction (see Figure 3.2). Investigating entropy production numerically indicates that this scaling behaviour of the entropy production is unchanged in the strong disorder regime (Figure 3.3).

3.6 Concluding remarks and outlook.

Based on the effective entropy production introduced in Eq. (3.5), we have studied the mesoscopic scaling of the entropy production per mesostate under iterative block coarse graining for a family of non-equilibrium disordered steady-states with generic substrate correlations. We demonstrate that coarse-graining of degrees of freedom results in non-

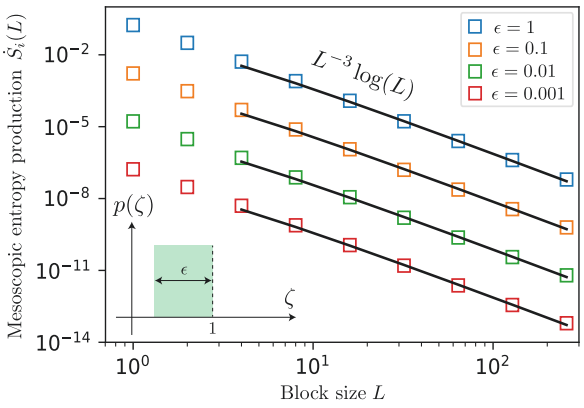

Figure 3.3: Mesoscopic entropy production as a function of block size and predicted scaling according to Eq. (3.18) (case $d = 2$, $\eta = 0$) for various noise strengths. The predicted scaling appears to hold numerically beyond the weak disorder approximation. The noise $\zeta_{n,m}$ is taken from a uniform distribution with support $\zeta \in \{[-1, -(1-\epsilon)) \cup (1-\epsilon, 1]\}$ and $h = 1$ to ensure positivity of the transition rates.

trivial *scaling* of the entropy production, Eqs. (3.18), so that its value on one scale is related to its value on another scale in a non-trivial fashion that ultimately draws on the correlations of the transition rates, Eq. (3.12). To characterise our model we have developed a static field-theoretic framework, which complements recent work [12] by considering problems involving multiplicative noise. Our main result, Eq. (3.18), offers conditions for which active disordered media appear equilibrium-like, $\eta \leq 1$, or genuinely non-equilibrium, $\eta > 1$, at the large scale and in a statistical sense, i.e. when the behaviour is averaged over many realisations.

3.7 Experiments.

A natural application of the theory above of active disordered media are active particles [23] on irregular surfaces, which phenomenologically behave as randomly driven passive particles [235]. This is due to ratchet effects, i.e. local asymmetries in the potential driving a net current [229]. In this case, correlations in the medium can be induced by controlling the ruggedness of the substrate [309]. Further, in vitro experiments involving active transport by molecular motors in a network of cytoskeletal filaments [242, 20] often involve cell extracts where these filaments are uniformly disordered ($\eta = 0$). Non-trivial, long-range correlations in this type of systems could be induced e.g. by coupling

tagged filaments to an external magnetic field, as done in [60] with actin.

3.A Weak disorder expansion of Derrida's exact result for $d = 1$

Using an exact result by Derrida [76] the net current $J = J_{n,n+1}$ is homogeneous,

$$J = \frac{1}{\sum_{n=1}^{N} r_n} \left[1 - \prod_{m=1}^{N} \left(\frac{w_{m+1,m}}{w_{m,m+1}} \right) \right] \tag{3.19}$$

for a lattice with N sites, where

$$r_n = \frac{1}{w_{n,n+1}} \left[1 + \sum_{\ell=1}^{N-1} \prod_{j=1}^{\ell} \frac{w_{n+j,n+j-1}}{w_{n+j,n+j+1}} \right] . \tag{3.20}$$

The entropy production, Eq. (3.2), can be calculated as $\dot{S}_i = JA(\{w\}; \{1, 2, \ldots, N\})$, on the basis of constant $J = \pi_n w_{n,n+1} - \pi_{n+1} w_{n+1,n}$ and the affinity A, Eq. (3.6), taken for the cycle passing through all sites of the ring once [248]. Eq. (3.7) can be substituted into Eqs. (3.6) and (3.19) to obtain

$$J = \frac{hA}{N^2} + \mathcal{O}(\zeta^2) = \frac{1}{N^2} \sum_{n=1}^{N} (\zeta_{n,n+1} - \zeta_{n+1,n}) + \mathcal{O}(\zeta^2) . \tag{3.21}$$

Correspondingly, using $\dot{S}_i = JA$,

$$\dot{S}_i = \frac{1}{hN^2} \left(\sum_{n=1}^{N} (\zeta_{n,n+1} - \zeta_{n+1,n}) \right)^2 + \mathcal{O}(\zeta^3) , \tag{3.22}$$

where $\mathcal{O}(\zeta^k)$ stands for any term proportional to $\zeta_{i_1 \pm 1, i_1} \ldots \zeta_{i_k \pm 1, i_k}$ with any indices $i_1, \ldots, i_k$. This is the expression we refer to in the main text, Eq. (3.8). In this regime, the current is dominated by the average of the approximate potential gradients, $(\zeta_{n,n+1} - \zeta_{n+1,n})/h$. The physical picture provided by Eq. (3.21) shows that the weak disorder expansion, $|\zeta_{n,m}| \ll h$, is equivalent to a linear response theory, $J \propto A$, with the cycle affinity playing the role of the thermodynamic force [74]. The behaviour away from the weak disorder limit is more subtle. In particular, the current J and therefore $\dot{S}_i$ are no longer a function only of the affinity but depend on the whole ran-

dom potential profile. This is due to the presence of traps, i.e. local minima of the random potential, at which probability tends to concentrate [67].

So far, we have not made any assumption about the autocorrelation of the noise ζ. However, by relating Eq. (3.22) to the square of the distance travelled by a random walker with zero-mean increments $\nu_n = \zeta_{n,n+1} - \zeta_{n+1,n}$, Fig. 3.1, we conclude that the system-size scaling of the disorder expectation $\langle \dot{S}_i \rangle$ in the large N limit is controlled by the Hurst exponent $H \in (0,1)$ [191] of the random walk. In particular,

$$\langle \dot{S}_i \rangle \sim N^{\delta} = N^{2H-2} \ , \tag{3.23}$$

where $H = 1/2$ corresponds to uncorrelated (or short-range correlated) disorder. By the central limit theorem for sufficiently uncorrelated ν_n, and more generally when $\sum_{n=1}^{N} \nu_n$ is a Gaussian random variable, the affinity is also Gaussian. As $\dot{S}_i$, Eq. (3.22), is essentially the square of the affinity, its distribution is of the chi-squared type. These results are indeed confirmed by simulations, Fig. 3.4.

3.B A Static Path Integral Approach to Diffusion with Quenched Noise

In the following we develop the field theoretic formalism used to study the correlation function of the steady-state probability currents for the model of diffusion on a lattice with spatially quenched, non-conservative noise in the hopping rates. This formalism is based on the well-known response-field construction by Martin-Siggia-Rose (MSR) and Janssen-De Dominicis [318, 133] but extends it in two ways: first, our approach deals with multiplicative noise in a static framework, complementing recent work by Antonov and co-workers [12], which focused on the case of additive noise . Second, we show how the MSR 'trick' of imposing physically relevant relations between the noise field and physical observables by means of suitable resolutions of identity can be exploited to directly probe observables that depend explicitly on the noise (in this case, the probability current). The formalism is first developed in one dimension, $d = 1$, for the case of white noise and it is subsequently generalised to higher integer dimensions and correlated noise. It turns out that we ultimately do not need the full field theory nor the renormalisation group, because the upper critical dimension $d_c = 2$ coincides

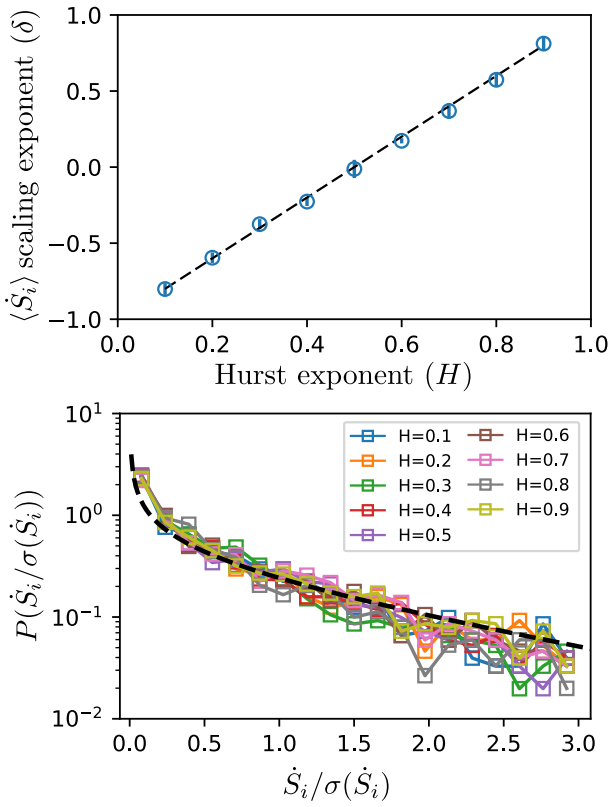

Figure 3.4: In one dimension and for weak disorder, the scaling of the entropy production with system size is controlled by the Hurst exponent according to Eq. (3.23). Top: the exponent δ obtained by fitting numerical estimates of $\langle \dot{S}_i \rangle$ against N^δ for different Hurst exponents $H \in (0, 1)$, shown with error bar in blue, is in perfect agreement with the analytical prediction, $\delta = 2H - 2$, Eq. (3.23), shown as a black dashed line. Bottom: the distribution of the entropy production $\dot{S}_i$ as a random variable is well described by the chi-squared distribution, shown as a black dashed line, as predicted by the theory.

with the lowest dimension we draw on the field theory. Nevertheless, the framework provides us with a firm basis to reliably determine the upper critical dimension and will form the well-tested foundation for the analysis of more advanced problems.

The analytical expressions derived in the following are in agreement with numerical results, as shown in Fig. 3.4 for the one-dimensional problem and in Figs. 3.2 and 3.5 for its generalisation to higher dimensional lattices. In one dimension, the steady state probability mass function π_n for a given noise realisation $\{\zeta_{m,m\pm1}\}$ is solved exactly by means of Kirchhoff's theorem [248] and the homogeneous current is obtained straightforwardly as $J = \pi_n w_{n,n+1} - \pi_{n+1} w_{n+1,n}$ for an arbitrary n. The entropy production is then calculated as $\dot{S}_i = JA$ on the basis of Eq. (3.6). In higher dimensions, a numerical approximation to the steady state probability is instead obtained by evolving a homogeneous initial condition, $P_n(t=0) = N^{-d}$, according to the master equation, Eq. (3.1).

3.B.1 One dimensional case, uncorrelated noise.

We consider a one-dimensional diffusion process on a ring of size N characterised by a homogeneous hopping rate h and a quenched perturbation $\zeta_{i,i\pm1}$ to the hopping rate from site i to site $i \pm 1$ satisfying $\zeta_{i,i\pm1} + h > 0$. We denote by ϕ_i the steady-state probability mass function at site i, with $i = 1, 2, \cdots, N$. By normalisation, $\sum_i \phi_i = 1$. In the following we apply periodic boundary conditions to all indices i, so that $i = 0$ is equivalent to $i = N$ and $i = N+1$ is equivalent to $i = 1$. The steady-state probability mass function is determined implicitly by the master equation

$$\begin{aligned} 0 = \partial_t \phi_i &= h(\phi_{i-1} + \phi_{i+1} - 2\phi_i) + \zeta_{i-1,i}\phi_{i-1} - \zeta_{i,i-1}\phi_i - \zeta_{i,i+1}\phi_i + \zeta_{i+1,i}\phi_{i+1} \\ &= h(\phi_{i-1} + \phi_{i+1} - 2\phi_i) + (\delta_{i-1}\phi_{i-1} + \delta_{i+1}\phi_{i+1} - 2\delta_i\phi_i) + (\zeta_{i-1}\phi_{i-1} - \zeta_{i+1}\phi_{i+1}) \end{aligned} \tag{3.24}$$

where for the second equality we have redefined the perturbation to the hopping rates according to

$$\zeta_{i,i+1} = \delta_i + \zeta_i \quad \text{and} \quad \zeta_{i,i-1} = \delta_i - \zeta_i \ . \tag{3.25}$$

The right hand side of Eq. (3.24) can be written more suggestively in continuum notation as a drift-diffusion equation,

$$0 = \partial_t \phi = \partial_x[(h + \delta)\partial_x \phi] + \partial_x[(\partial_x \delta - \zeta)\phi] \ , \tag{3.26}$$

where the symmetric part of the quenched noise, denoted by δ_i, appears both as an inhomogeneous perturbation of the diffusion constant h and, in the drift term, as a random forcing. The antisymmetric part of the noise, ζ_i, on the other hand, only affects the drift term. For simplicity, we will henceforth assume that the perturbation to the transition rate matrix satisfies

$$\zeta_{i,i+1} = -\zeta_{i,i-1} = \zeta_i \quad \text{i.e.} \quad \delta_i = 0 \ . \tag{3.27}$$

The lattice master equation (3.24) thus reduces to

$$0 = \partial_t \phi_i = h(\phi_{i-1} + \phi_{i+1} - 2\phi_i) + \zeta_{i-1}\phi_{i-1} - \zeta_{i+1}\phi_{i+1} \tag{3.28}$$

Numerical investigation indicates that this assumption does not modify the scaling behaviour of the mesoscopic entropy production, Figure 3.5. For weak disorder, this observation can be rationalised by arguing that the diffusive behaviour is dominated by its homogeneous component, while the drift term is dominated at large spatial scales by the term of lowest order in the spatial derivatives. Importantly, for i.i.d. rates, the steady-state remains generically non-equilibrium, which can be verified by computing the cycle affinity, Eq. (3.6), and exhibits non-zero steady-state currents. We further define the probability current field

$$J_{i,i+1} = (h + \zeta_{i,i+1})\phi_i - (h + \zeta_{i+1,i})\phi_{i+1} = h(\phi_i - \phi_{i+1}) + \zeta_i \phi_i + \zeta_{i+1}\phi_{i+1} \ . \tag{3.29}$$

as the *net* current from site i to site $i + 1$, such that

$$\partial_t \phi_i = -(J_{i,i+1} - J_{i-1,i}) \ , \tag{3.30}$$

and introduce a symmetrised, local, average current

$$J_i = \frac{1}{2}\left(J_{i,i+1} + J_{i-1,i}\right) = \frac{1}{2}[h(\phi_{i-1} - \phi_{i+1}) + \zeta_{i-1}\phi_{i-1} + \zeta_{i+1}\phi_{i+1} + 2\zeta_i \phi_i] \ . \tag{3.31}$$

In one dimension at stationarity, $J_{i,i+1} = J_{i-1,i} = J_i$ and there is therefore no difference between the local averaged currents and the more microscopic ones.

The non-negativity of the transition rates means that $\zeta_i + h \geq 0$. However, in order to be able to cast Eqs. (3.28) and (3.29) into a path integral form, we will assume that ζ_i is a weak Gaussian noise with variance λ and probability

$$P[\zeta_i] \propto \exp\left(\sum_{i=1}^{N} -\frac{\zeta_i^2}{2\lambda}\right) \ . \tag{3.32}$$

This assumption is justified *a posteriori* by comparing the analytical predictions in the weak disorder limit with numerical simulations where the positivity of the transition rates is confirmed at initialisation. Introducing the short-hand notation for the functional integral measure

$$\mathcal{D}\zeta = \prod_i d\zeta_i \ , \tag{3.33}$$

the expectation of a general noise-dependent observable $\mathcal{O}[\zeta]$ can be written as the path integral

$$\langle \mathcal{O} \rangle = \int \mathcal{D}\zeta \ \mathcal{O}[\zeta] P[\zeta] \ . \tag{3.34}$$

To impose the steady-state Eq. (3.28) at every site, we define

$$f_i(\phi_{i-1}, \phi_i, \phi_{i+1}) = h(\phi_{i-1} + \phi_{i+1} - 2\phi_i) + \zeta_{i-1}\phi_{i-1} - \zeta_{i+1}\phi_{i+1} \tag{3.35}$$

and introduce the following resolution of identity written in terms of Dirac delta functions fixing the functional relation between the probability mass function ϕ_i and the noise ζ_i

$$1 = \int \mathcal{D}f \prod_{i=1}^{n} \delta(f_i) \tag{3.36}$$

$$= \mathcal{M}[\zeta] \int \mathcal{D}\phi \ \prod_{i=1}^{N} \delta\Big(h(\phi_{i-1} + \phi_{i+1} - 2\phi_i) + \zeta_{i-1}\phi_{i-1} - \zeta_{i+1}\phi_{i+1}\Big) \tag{3.37}$$

$$= \mathcal{M}[\zeta] \int \mathcal{D}\phi \int \mathcal{D}\tilde{\phi} \ \exp\left[-\sum_{i=1}^{N} \tilde{\phi}_i \Big(- h(\phi_{i-1} + \phi_{i+1} - 2\phi_i) - \zeta_{i-1}\phi_{i-1} + \zeta_{i+1}\phi_{i+1}\Big)\right] \tag{3.38}$$

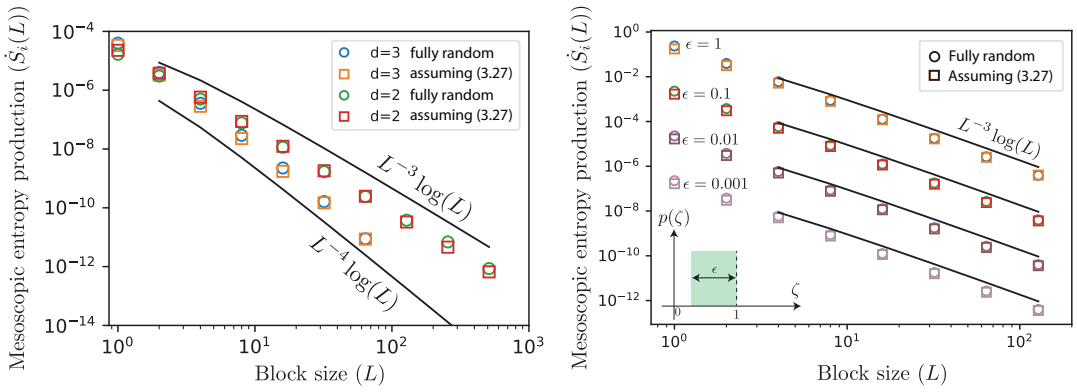

Figure 3.5: The scaling behaviour of the mesoscopic entropy production $\dot{S}_i(L)$, Eq. (3.5), as a function of block size L is not modified by imposing the antisymmetric condition (3.27) on the transition rates, as shown for $d = 2, 3$ in the case of uncorrelated disorder, $\eta = 0$ (left panel). Moreover, while out analytical approach relies on a weak disorder limit to allow for rate perturbation to be Gaussian without running into unphysical negative rates, numerical experiments suggest that the scaling laws we obtain remain valid in the strong disorder regime (independent of whether (3.27) is imposed), which is explored by considering a noise on the transition rates that is homogeneously distributed in the range $|\zeta| \in (1-\epsilon, 1]$ for various choices of the variance ϵ (right panel for $d = 2$ and $\eta = 0$). Theoretical predictions for the asymptotic scaling behaviour are plotted for reference (black curves in both panels).

with $\mathcal{D}f = df_1...df_N$, $\mathcal{D}\tilde{f} = d\tilde{f}_1...d\tilde{f}_N/(2\pi)^N$ and $\mathcal{M}[\zeta] = |df_i/d\phi_j|$ the Jacobian of the transformation $f \to \phi$. To go from Eq. (3.37) to Eq. (3.38) we have used the Fourier representation of the Dirac delta function,

$$\delta(f_i) = \int \frac{d\tilde{\phi}_i}{2\pi} \exp\left[-\tilde{\phi}_i f_i\right] \tag{3.39}$$

where $\tilde{\phi}_i$ is a purely imaginary auxiliary field, sometimes referred to as the response field. While $\mathcal{M}$ is independent of ϕ for a general master equation and can thus be taken outside of the ϕ integral, the Jacobian retains a dependence on the random variables $\zeta_1, ..., \zeta_N$ due to the multiplicative nature of the latter. While the sign of the auxiliary field determining that of the exponent in Eq. (3.38) is arbitrary, our choice gives the conventional sign for the response propagator [133]. The determinant $\mathcal{M}[\zeta]$ can be computed by means of Faddeev-Popov ghosts [318, 133], a standard procedure which requires the introducing two new Grassmann fields , denoted ξ_i and $\bar{\xi}_i$, satisfying the anti-commutation relations $\{\xi_i, \xi_j\} = \{\bar{\xi}_i, \bar{\xi}_j\} = \{\bar{\xi}_i, \xi_j\} = 0$. Using the Grassmann

path integral representation of the determinant [133],

$$\mathcal{M}[\zeta] = \int \mathcal{D}[\xi, \bar{\xi}] \, \exp\left[\sum_{ij} \bar{\xi}_i \left(\frac{df_i}{d\phi_j}\right) \xi_j\right] \tag{3.40}$$

$$= \int \mathcal{D}[\xi, \bar{\xi}] \, \exp\left[\sum_{i} \bar{\xi}_i \Big(h(\xi_{i-1} + \xi_{i+1} - 2\xi_i) + \zeta_{i-1}\xi_{i-1} - \zeta_{i+1}\xi_{i+1}\Big)\right] . \tag{3.41}$$

This path integral has the same structure as that in Eq. (3.38) because differentiating f_i with respect to ϕ_j effectively returns the Markov matrix of the process, now acting to the right on the Grassmann field ξ_j. The Jacobian (3.41) couples the Faddeev-Popov ghosts ξ_i and $\bar{\xi}_i$ to the noise field ζ_i, which is in turn coupled to the probability mass function ϕ_i and its response $\tilde{\phi}_i$ via Eq. (3.38). Integrating out the noise will thus result in a coupling between the ghosts and the MSR fields, as we will demonstrate after introducing the current field J_i and its response $\tilde{J}_i$.

In principle, the current J_i is fully defined in Eq. (3.31). However, this definition ceases to be useful once the noise field ζ_i has been integrated out, rendering J_i intractable. To avoid this, we introduce a resolution of the identity similar to Eq. (3.38) to enforce the definition Eq. (3.31) of the probability current J_i. It reads

$$1 = \int \mathcal{D}J \, \prod_{i=1}^{N} \delta\Big(J_i - \frac{1}{2}[h(\phi_{i-1} - \phi_{i+1}) + \zeta_{i-1}\phi_{i-1} + \zeta_{i+1}\phi_{i+1} + 2\zeta_i\phi_i]\Big) \tag{3.42}$$

$$= \int \mathcal{D}J \int \mathcal{D}\tilde{J} \, \exp\left[-\sum_{i=1}^{N} \tilde{J}_i \Big(J_i - \frac{1}{2}[h(\phi_{i-1} - \phi_{i+1}) + \zeta_{i-1}\phi_{i-1} + \zeta_{i+1}\phi_{i+1} + 2\zeta_i\phi_i]\Big)\right] . \tag{3.43}$$

where the trivial Jacobian $\mathcal{M} \equiv 1$ has been omitted.

Inserting Eqs. (3.38), (3.41) and (3.43) into the Gaussian path integral (3.34) we obtain

$$\begin{aligned}\langle \mathcal{O}[\phi, J]\rangle \propto & \int \mathcal{D}\phi \int \mathcal{D}\tilde{\phi} \int \mathcal{D}J \int \mathcal{D}\tilde{J} \int \mathcal{D}\xi \int \mathcal{D}\bar{\xi} \int \mathcal{D}\zeta \\ & \exp\left[-\sum_{i=1}^{N} \tilde{\phi}_i \Big(- h(\phi_{i-1} + \phi_{i+1} - 2\phi_i) - \zeta_{i-1}\phi_{i-1} + \zeta_{i+1}\phi_{i+1}\Big)\right] \\ & \times \exp\left[-\sum_{i=1}^{N} \tilde{J}_i \Big(J_i + \frac{h}{2}(\phi_{i+1} - \phi_{i-1}) - \frac{1}{2}(\zeta_{i-1}\phi_{i-1} + \zeta_{i+1}\phi_{i+1} + 2\zeta_i\phi_i)\Big)\right] \\ & \times \exp\left[\sum_i \bar{\xi}_i \Big(h(\xi_{i-1} + \xi_{i+1} - 2\xi_i) + \zeta_{i-1}\xi_{i-1} - \zeta_{i+1}\xi_{i+1}\Big)\right] \exp\left(\sum_{i=1}^{N} -\frac{\zeta_i^2}{2\lambda}\right) \mathcal{O}[\phi, J] \ .\end{aligned} \tag{3.44}$$

Since the noise ζ enters the exponent only linearly or quadratically, the functional integral over ζ is Gaussian and can be performed in closed form. In particular, isolating all terms on the right-hand side of Eq. (3.44) that depend on ζ,

$$\begin{aligned}& \int \mathcal{D}\zeta \, \exp\left(\sum_{i=1}^{N} -\frac{\zeta_i^2}{2\lambda} + \tilde{\phi}_i(\zeta_{i-1}\phi_{i-1} - \zeta_{i+1}\phi_{i+1}) + \frac{\tilde{J}_i}{2}(2\zeta_i\phi_i + \zeta_{i+1}\phi_{i+1} + \zeta_{i-1}\phi_{i-1})\right. \\ & \qquad \left. + \bar{\xi}_i(\zeta_{i-1}\xi_{i-1} - \zeta_{i+1}\xi_{i+1})\Big)\right. \qquad (3.45) \\ & = \int \mathcal{D}\zeta \, \exp\left(\sum_{i=1}^{N} -\frac{\zeta_i^2}{2\lambda} + \zeta_i\Big[(\tilde{\phi}_{i+1} - \tilde{\phi}_{i-1})\phi_i + \frac{1}{2}(2\tilde{J}_i + \tilde{J}_{i+1} + \tilde{J}_{i-1})\phi_i + (\bar{\xi}_{i+1} - \bar{\xi}_{i-1})\xi_i\Big]\right) \qquad (3.46) \\ & \propto \ \exp\left(\frac{\lambda}{2}\sum_{i=1}^{N}\Big[(\tilde{\phi}_{i+1} - \tilde{\phi}_{i-1})\phi_i + \frac{1}{2}(2\tilde{J}_i + \tilde{J}_{i+1} + \tilde{J}_{i-1})\phi_i + (\bar{\xi}_{i+1} - \bar{\xi}_{i-1})\xi_i\Big]^2\right) \ . \qquad (3.47)\end{aligned}$$

In the first equality we have re-indexed the summand, applying periodic boundary conditions, so that the noise field always appears with the same index and the completion of squares producing the last line can be carried out straightforwardly. We can now rewrite Eq. (3.44) as

$$\langle \mathcal{O}[\phi, J]\rangle = \int \mathcal{D}[\phi, \tilde{\phi}, J, \tilde{J}, \xi, \bar{\xi}] \, \exp\left[-(\mathcal{A}_0 + \mathcal{A}_{\text{int}})\right] \mathcal{O}[\phi, J] \tag{3.48}$$

where we have split the action into its bilinear part, denoted $\mathcal{A}_0$, and an interacting part, denoted $\mathcal{A}_{\rm int}$, which includes all higher order terms in products of fields. Denoting by

$$\partial_d \phi_i = \frac{1}{2}(\phi_{i+1} - \phi_{i-1}) \tag{3.49}$$

and

$$\partial_d^2 \phi_i = \phi_{i+1} - 2\phi_i + \phi_{i-1} \tag{3.50}$$

the discrete first and second spatial derivatives, respectively, these contributions are given explicitly by

$$\mathcal{A}_0 = \sum_{i=1}^{N} -h\tilde{\phi}_i \partial_d^2 \phi_i - h\bar{\xi}_i \partial_d^2 \xi_i + \tilde{J}_i J_i + h\tilde{J}_i \partial_d \phi_i \tag{3.51}$$

and

$$\begin{aligned} &\mathcal{A}_{\rm int} \\ &= -2\lambda \sum_{i=1}^{N} \left[(\partial_d \tilde{\phi}_i)^2 \phi_i^2 + \tilde{J}_i^2 \phi_i^2 + 2\tilde{J}_i (\partial_d \tilde{\phi}_i) \phi_i^2 + 2\tilde{J}_i (\partial_d \bar{\xi}_i) \phi_i \xi_i + 2(\partial_d \tilde{\phi}_i)(\partial_d \bar{\xi}_i) \phi_i \xi_i \right] + \text{h.o.t.} \end{aligned} \tag{3.52}$$

where h.o.t. denotes higher order terms in the spatial derivatives. In the following we are interested in the large scale (small wavenumber) features of the density and current correlation function, and we will thus ignore contributions from h.o.t. on relevance grounds. To arrive at Eq. (3.52) we have used the anticommutation relation $\{\xi_i, \xi_j\} = 0$, implying $\xi_i^2 = 0$, to eliminate the quartic term in the ghost fields.

Perturbative calculations by means of Feynman diagrams are more easily carried out in Fourier representation. For this reason we introduce the discrete Fourier transform of the fields $\{\phi, \tilde{\phi}, J, \tilde{J}, \xi, \bar{\xi}\}$, which we denote $\{\Phi, \tilde{\Phi}, \mathcal{J}, \tilde{\mathcal{J}}, \Xi, \bar{\Xi}\}$, respectively, according to the convention

$$\phi_j = \frac{1}{N} \sum_{n=0}^{N-1} e^{2\pi i j n/N} \Phi_n \quad \text{and} \quad N\delta_{n,m} = \sum_{j=0}^{N-1} e^{2\pi i j (n-m)/N} \ , \tag{3.53}$$

whence

$$\Phi_n = \sum_{j=0}^{N-1} e^{-2\pi i j n/N} \phi_j \ . \tag{3.54}$$

We proceed by introducing Fourier-summed fields in the non-linear action. A typical interaction term in the Fourier representation of the action reads

$$\lambda \sum_{i=1}^{N} (\partial_d \tilde{\phi}_i)^2 \phi_i^2 = -\frac{\lambda}{N^4} \sum_{k_1,k_2,k_3,k_4} \sin(k_1)\sin(k_2) \tilde{\Phi}_{k_1} \tilde{\Phi}_{k_2} \Phi_{k_3} \Phi_{k_4} N \delta_{k_1+k_2+k_3+k_4,0} \ . \ . \tag{3.55}$$

The field ϕ_i represents a probability mass function and it is therefore natural to study fluctuations around the normalised homogeneous steady-state $\langle \phi_i \rangle = N^{-1}$, so that $\Phi_{k=0} = 1$. Instead of implementing $\Phi_{k=0} = 1$ through the action along the lines of Eqs. (3.28) and (3.31), we perform a change of variable $\phi_i \to N^{-1} + \phi_i$ at the level of Eqs. (3.51) and (3.52), which leaves the bilinear action $\mathcal{A}_0$ unchanged but generates a number of new terms in $\mathcal{A}_{\rm int}$. For example,

$$\gamma (\partial_d \tilde{\phi}_i)^2 \phi_i^2 \to \gamma (\partial_d \tilde{\phi}_i)^2 \phi_i^2 + \gamma' (\partial_d \tilde{\phi}_i)^2 \phi_i + \gamma'' (\partial_d \tilde{\phi}_i)^2 \ , \tag{3.56}$$

with $\gamma = \lambda$, $\gamma' = 2N^{-1}\lambda$ and $\gamma'' = N^{-2}\lambda$ at bare level. The full shifted action reads, again at bare level,

$$\begin{aligned} \mathcal{A}_{\rm int} = -2\lambda \sum_{i=1}^{N} \Big[& (\partial_d \tilde{\phi}_i)^2 (\phi_i + N^{-1})^2 + \tilde{J}_i^2 (\phi_i + N^{-1})^2 + 2\tilde{J}_i (\partial_d \tilde{\phi}_i)(\phi_i + N^{-1})_i^2 \\ & + 2\tilde{J}_i (\partial_d \bar{\xi}_i)(\phi_i + N^{-1})\xi_i + 2(\partial_d \tilde{\phi}_i)(\partial_d \bar{\xi}_i)(\phi_i + N^{-1})\xi_i \Big] + \text{h.o.t.} \end{aligned} \tag{3.57}$$

The various coupling are more easily identifiable in the diagrammatic notation that we shall introduce shortly.

3.B.2 Propagators and diagrammatics

The bare propagators of the theory can then be extracted directly from the bilinear action, Eq. (3.51). They read

$$\langle \Phi_k \tilde{\Phi}_{k'} \rangle = \frac{1}{4h \sin^2(k/2) + r} N \delta_{k+k',0} \mathrel{\widehat{=}} \tag{3.58}$$

$$\langle \Xi_k \bar{\Xi}_{k'} \rangle = -\langle \bar{\Xi}_k \Xi_{k'} \rangle = \frac{1}{4h \sin^2(k/2) + r} N \delta_{k+k',0} \mathrel{\widehat{=}} \tag{3.59}$$

$$\langle \mathcal{J}_k \tilde{\mathcal{J}}_{k'} \rangle = N \delta_{k+k',0} \mathrel{\widehat{=}} \tag{3.60}$$

$$\langle \mathcal{J}_k \tilde{\Phi}_{k'} \rangle = \frac{h(-i \sin(k))}{4h \sin^2(k/2) + r} N \delta_{k+k',0} \mathrel{\widehat{=}} \tag{3.61}$$

where we have allowed for a mass r for the purpose of infrared regularisation, which would enter the bilinear action $\mathcal{A}_0$ of Eq. (3.51) via terms of the form $r\tilde{\phi}_i \phi_i$ and $r\bar{\xi}_i \xi_i$. All physical observables are evaluated in the limit of vanishing mass r since the theory is massless as a matter of conservation of probability. The diagrammatic notation for the amputated interaction vertices is

$\gamma(\partial\tilde{\phi})^2\phi^2 \mathrel{\widehat{=}}$  , $\kappa\tilde{J}^2\phi^2 \mathrel{\widehat{=}}$  , $\sigma\tilde{J}(\partial\tilde{\phi})\phi^2 \mathrel{\widehat{=}}$  ,

$\gamma'(\partial\tilde{\phi})^2\phi \mathrel{\widehat{=}}$  , $\kappa'\tilde{J}^2\phi \mathrel{\widehat{=}}$  , $\sigma'\tilde{J}(\partial\tilde{\phi})\phi \mathrel{\widehat{=}}$  ,

$\gamma''(\partial\tilde{\phi})^2 \mathrel{\widehat{=}}$  , $\kappa''\tilde{J}^2 \mathrel{\widehat{=}}$  , $\sigma''\tilde{J}(\partial\tilde{\phi}) \mathrel{\widehat{=}}$  , (3.62)

and

$\pi\tilde{J}(\partial\bar{\xi})\phi\xi \mathrel{\widehat{=}}$  , $\chi(\partial\tilde{\phi})(\partial\bar{\xi})\phi\xi \mathrel{\widehat{=}}$  ,

$\pi'\tilde{J}(\partial\bar{\xi})\xi \mathrel{\widehat{=}}$  , $\chi'(\partial\tilde{\phi})(\partial\bar{\xi})\xi \mathrel{\widehat{=}}$  . (3.63)

with dashed propagators denoting spatial derivatives. At bare level, $\gamma = \kappa = 2\lambda$ and $\sigma = \pi = \chi = 4\lambda$. Vertices appearing in the same column of the list (3.62) are generated from the same interaction term of Eq. (3.52) upon performing the shift $\phi_i \to \phi_i + N^{-1}$. Their coupling are thus related via $\gamma''/\gamma = \kappa''/\kappa = \sigma''/\sigma = N^{-2}$, $\gamma'/\gamma = \kappa'/\kappa = \sigma'/\sigma = 2N^{-1}$ and $\pi'/\pi = \chi'/\chi = N^{-1}$.

3.B.3 Correlation functions in one dimension

We are now ready to calculate the density and current correlation functions for the one-dimensional model. These are expressed as a power series in the small disorder strength λ, which we truncate to first order (tree level) to allow for direct comparison with the result obtained by expanding the analytical results by Derrida [76], Eq. (3.21). This approximation is controlled in $d = 1$ because we are interested in system of finite size N and will be justified on relevance grounds in higher dimensions, where we will work in the continuum limit. The correlation function for the probability mass function at tree level is given by

$$\langle \Phi_k \Phi_{k'} \rangle = \quad + \mathcal{O}(\lambda^2) = \frac{4\lambda}{(2Nh\sin(k/2))^2} N\delta_{k+k',0} + \mathcal{O}(\lambda^2) \tag{3.64}$$

for $k \neq 0$. For the current we have

$$\langle \mathcal{J}_k \mathcal{J}_{k'} \rangle = \quad + \quad + \quad + \mathcal{O}(\lambda^2) = \frac{4\lambda}{N^2} N\delta_{k+k',0}\delta_{k',0} + \mathcal{O}(\lambda^2)\ , \tag{3.65}$$

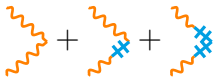

with Kronecker delta $\delta_{k',0}$ reflecting the constraint that $J_i = J_j = J$ is homogeneous. For $k \neq 0$, the three diagrams contributing to the right-hand side of Eq. (3.65) only differ in their symmetry factors and overall sign, which produces the desired cancellation. When $k = 0$, only the first diagram, which does not involve spatial derivatives, contributes and the cancellation does not occur. Since $\mathcal{J}_{k=0} = NJ$, we thus have that $\langle J^2 \rangle = N^{-2}\langle \mathcal{J}_0 \mathcal{J}_0 \rangle = 4\lambda N^{-3}$, recovering the leading order contribution obtained by expanding Derrida's [76] exact result, Eq. (3.21), with the antisymmetric condition $\zeta_{i,i+1} - \zeta_{i,i-1} = 2\zeta_i$,

$$\begin{aligned} \langle J^2 \rangle &= \frac{1}{N^4} \left\langle \left(\sum_{n=1}^{N} \zeta_{n,n+1} - \zeta_{n+1,n} \right) \left(\sum_{m=1}^{N} \zeta_{m,m+1} - \zeta_{m+1,m} \right) \right\rangle \\ &= \frac{4}{N^4} \sum_{n=1}^{N} \sum_{m=1}^{N} \langle \zeta_n \zeta_m \rangle = \frac{4\lambda}{N^3}\ . \end{aligned} \tag{3.66}$$

3.B.4 Higher dimensions

The derivation presented above can be straighforwardly generalised to periodic lattices of arbitrary dimension with sites $\boldsymbol{i} = (i_1, ..., i_d) \in \{1, ..., N\}^d$. We further need to modify the steady-state condition, Eq. (3.28), using higher dimensional extensions of Eqs. (3.49) and (3.50), $\boldsymbol{\nabla}_d = (\partial_{i_1}, ..., \partial_{i_d})$ and $\Delta_d = \partial_{i_1}^2 + ... + \partial_{i_d}^2$, so that

$$0 = \partial_t \phi_{\boldsymbol{i}} = h\Delta_d \phi_{\boldsymbol{i}} - 2\boldsymbol{\nabla}_d.(\boldsymbol{\zeta_i}\phi_{\boldsymbol{i}}) \tag{3.67}$$

where $\boldsymbol{\zeta_i} = (\zeta_{\boldsymbol{i}}^{(1)}, ..., \zeta_{\boldsymbol{i}}^{(d)}) \in \mathbb{R}^d$ is a d-dimensional noise with correlator

$$\langle \zeta_{\boldsymbol{k}}^{(a)} \zeta_{\boldsymbol{k}'}^{(b)} \rangle = \lambda \delta_{ab} N^d \delta_{\boldsymbol{k}+\boldsymbol{k}',0} \ . \tag{3.68}$$

Here, $\zeta_{\boldsymbol{i}}^{(a)}$ denotes the noise affecting the edges of node $\boldsymbol{i}$ along the ath dimension of the lattice and $\zeta_{\boldsymbol{k}}^{(a)}$ its Fourier transform, according to the convention

$$\zeta_{\boldsymbol{j}}^{(a)} = \frac{1}{N^d} \sum_{\boldsymbol{k}} e^{i\boldsymbol{k}\cdot\boldsymbol{j}} \zeta_{\boldsymbol{k}}^{(a)} \quad \text{and} \quad \zeta_{\boldsymbol{k}}^{(a)} = \sum_{\boldsymbol{j}} e^{-i\boldsymbol{k}\cdot\boldsymbol{j}} \zeta_{\boldsymbol{j}}^{(a)} \ , \tag{3.69}$$

with $\boldsymbol{k} = 2\pi\boldsymbol{n}/N$ and $\boldsymbol{n} \in \{1, ..., N\}^d$. Correspondingly Eq. (3.31) is modified to define a vector lattice field $\boldsymbol{J_i} \in \mathbb{R}^d$. Writing $\boldsymbol{J_i} = (J_{\boldsymbol{i}}^{(1)}, ..., J_{\boldsymbol{i}}^{(d)})$,

$$J_{\boldsymbol{i}}^{(a)} = -h\partial_{i_a}\phi_{\boldsymbol{i}} + \frac{1}{2}\partial_{i_a}^2(\zeta_{\boldsymbol{i}}^{(a)}\phi_{\boldsymbol{i}}) + 2\zeta_{\boldsymbol{i}}^{(a)}\phi_{\boldsymbol{i}} \ , \tag{3.70}$$

where $J_{\boldsymbol{i}}^{(a)}$ is once again the symmetric local average at site $\boldsymbol{i}$ of the probability current along the ath dimension of the lattice. The functional relationship between each component of the current vector field and the other fields, Eq. (3.70), is then imposed by means of d resolutions of the identity of the form (3.43). In the case of uncorrelated noise, the derivation of the action follows precisely the same lines as above and generates d copies of the type of terms we have already seen, each with spatial derivatives taken with respect to a different dimension. Explicitly,

$$\mathcal{A}_0 = \sum_{\boldsymbol{i}} -h\tilde{\phi}_{\boldsymbol{i}}\Delta_d\phi_{\boldsymbol{i}} - h\bar{\xi}_{\boldsymbol{i}}\Delta_d\xi_{\boldsymbol{i}} + \tilde{\boldsymbol{J}}_{\boldsymbol{i}} \cdot \boldsymbol{J_i} + h\tilde{\boldsymbol{J}}_{\boldsymbol{i}} \cdot \boldsymbol{\nabla}_d\phi_{\boldsymbol{i}} \tag{3.71}$$

cf. Eq. (3.51) and

$$\mathcal{A}_{\text{int}} = -2\lambda \sum_{\boldsymbol{i}} [(\boldsymbol{\nabla}_d \tilde{\phi}_{\boldsymbol{i}})^2 \phi_{\boldsymbol{i}}^2 + \tilde{\boldsymbol{J}}_{\boldsymbol{i}}^2 \phi_{\boldsymbol{i}}^2 + 2\tilde{\boldsymbol{J}}_{\boldsymbol{i}} \cdot (\boldsymbol{\nabla}_d \tilde{\phi}_{\boldsymbol{i}}) \phi_{\boldsymbol{i}}^2 + 2\tilde{\boldsymbol{J}}_{\boldsymbol{i}} \cdot (\boldsymbol{\nabla}_d \bar{\xi}_{\boldsymbol{i}}) \phi_{\boldsymbol{i}} \xi_{\boldsymbol{i}} + 2(\boldsymbol{\nabla}_d \tilde{\phi}_{\boldsymbol{i}}) \cdot (\boldsymbol{\nabla}_d \bar{\xi}_{\boldsymbol{i}}) \phi_{\boldsymbol{i}} \xi_{\boldsymbol{i}}] + \text{h.o.t.} \,, \tag{3.72}$$

cf. Eq. (3.52). Since vertices arising from Eq. (3.72) involve vector fields, the intepretation of diagrams needs to be modified slightly. For example, the mixed propagators in Fourier representation becomes

$$\langle \mathcal{J}_{\boldsymbol{k}}^{(a)} \tilde{\Phi}_{\boldsymbol{k}'} \rangle = \frac{N^d h(-i \sin(k_a))}{4h \sum_b \sin^2(k_b/2) + r} \delta_{\boldsymbol{k}+\boldsymbol{k}',0} \mathrel{\widehat{=}}$$  . (3.73)

Similarly,

$(\tilde{\boldsymbol{J}}_{\boldsymbol{i}})^2 \phi_{\boldsymbol{i}}^2 \mathrel{\widehat{=}}$  , $\tilde{\boldsymbol{J}}_{\boldsymbol{i}} \cdot (\boldsymbol{\nabla}_d \tilde{\phi}_{\boldsymbol{i}}) \phi_{\boldsymbol{i}}^2 \mathrel{\widehat{=}}$  , $(\boldsymbol{\nabla}_d \tilde{\phi}_{\boldsymbol{i}})^2 \phi_{\boldsymbol{i}}^2 \mathrel{\widehat{=}}$  ,

$\tilde{\boldsymbol{J}}_{\boldsymbol{i}} \cdot (\boldsymbol{\nabla}_d \bar{\xi}_{\boldsymbol{i}}) \phi_{\boldsymbol{i}} \xi_{\boldsymbol{i}} \mathrel{\widehat{=}}$, $(\boldsymbol{\nabla}_d \tilde{\phi}_{\boldsymbol{i}}) \cdot (\boldsymbol{\nabla}_d \bar{\xi}_{\boldsymbol{i}}) \phi_{\boldsymbol{i}} \xi_{\boldsymbol{i}} \mathrel{\widehat{=}}$. (3.74)

Using the field theory in $d > 1$ to characterise correlations is most covenient in the continuum limit. We thus take the limit $N \to \infty$ at fixed volume $V = (N\ell)^d$, with ℓ the dimensionful lattice spacing. Based on Eqs. (3.49) and (3.50) we define the differential operators in the continuum $\boldsymbol{\nabla}_d = \ell \boldsymbol{\nabla}$ and $\Delta_d = \ell^2 \Delta$, together with the fields ϕ and $\tilde{\phi}$ now being defined for all $\boldsymbol{x} \in (0, N\ell]^d$, such that

$$\phi(\boldsymbol{i}\ell) = \ell^{-d} \phi_{\boldsymbol{i}}, \quad \tilde{\phi}(\boldsymbol{i}\ell) = \ell^{\beta} \tilde{\phi}_{\boldsymbol{i}} \,, \tag{3.75}$$

where the dimension of $\phi(\boldsymbol{x})$ is pre-determined by the shift performed above, which in the continuum reads $\phi(\boldsymbol{x}) \to V^{-1} + \phi(\boldsymbol{x})$, while the exponent β is undetermined for the time being. Converting sums over lattice sites into integrals over space according to

$$\ell^d \sum_{\boldsymbol{i}} \equiv \int_V d^d x \tag{3.76}$$

and demanding that the action of Eqs. (3.71) and (3.72) is dimensionless term by term, defines the remaining fields

$$\boldsymbol{J}(\boldsymbol{i}\ell) = \ell^{-d+1-\beta}\boldsymbol{J}_{\boldsymbol{i}}, \quad \tilde{\boldsymbol{J}}(\boldsymbol{i}\ell) = \ell^{-1+\beta}\tilde{\boldsymbol{J}}_{\boldsymbol{i}}, \quad \bar{\xi}(\boldsymbol{i}\ell)\xi(\boldsymbol{i}\ell) = \ell^{\beta-d}\bar{\xi}_{\boldsymbol{i}}\xi_{\boldsymbol{i}} \tag{3.77}$$

and the dimensionful couplings of the continuum theory $D = h\ell^{2-\beta}$ and $\tilde{\lambda} = \ell^{d+2-2\beta}\lambda$. The exponent β is fixed by imposing that the diffusion constant D remains finite in the limit $\ell \to 0$, whence $\beta = 2$. Since now $\tilde{\lambda} = \lambda\ell^{d-2}$, we identify $d_c = 2$ as the upper critical dimension of the theory. For $d > 2$ all interactions become irrelevant and we expect the large scale behaviour of the theory to be well described by the tree-level diagrammatics, thus justifying the truncation of higher order terms. Precisely at $d = 2$, renormalisation group theory [318] predicts logarithmic corrections to tree-level scaling but these were not observed conclusively in our numerical investigation.

In the continuum we thus have the action $\mathcal{A}_0 + \mathcal{A}_{\text{int}}$ with

$$\mathcal{A}_0 = -\int_V d^dx\; D\tilde{\phi}(\boldsymbol{x})\Delta\phi(\boldsymbol{x}) + D\bar{\xi}(\boldsymbol{x})\Delta\xi(\boldsymbol{x}) - \tilde{\boldsymbol{J}}(\boldsymbol{x})\cdot\boldsymbol{J}(\boldsymbol{x}) - D\tilde{\boldsymbol{J}}(\boldsymbol{x})\cdot\boldsymbol{\nabla}\phi(\boldsymbol{x}) \tag{3.78}$$

$$\begin{aligned}\mathcal{A}_{\text{int}} = -2\tilde{\lambda}\int_V d^dx\; &[(\boldsymbol{\nabla}\tilde{\phi}(\boldsymbol{x}))^2(\phi(\boldsymbol{x}) + V^{-1})^2 + \tilde{\boldsymbol{J}}^2(\boldsymbol{x})(\phi(\boldsymbol{x}) + V^{-1})^2 \\ &+ 2\tilde{\boldsymbol{J}}(\boldsymbol{x})\cdot(\boldsymbol{\nabla}\tilde{\phi}(\boldsymbol{x}))(\phi(\boldsymbol{x}) + V^{-1})^2 + 2\tilde{\boldsymbol{J}}(\boldsymbol{x})\cdot(\boldsymbol{\nabla}\bar{\xi}(\boldsymbol{x}))(\phi(\boldsymbol{x}) + V^{-1})\xi(\boldsymbol{x}) \\ &+ 2(\boldsymbol{\nabla}\tilde{\phi}(\boldsymbol{x}))\cdot(\boldsymbol{\nabla}\bar{\xi}(\boldsymbol{x}))(\phi(\boldsymbol{x}) + V^{-1})\xi(\boldsymbol{x})] + \text{h.o.t.}\;.\end{aligned} \tag{3.79}$$

Absorbing the shift V^{-1} of ϕ into new couplings as done using dashed variables in Eq. (3.62) means that these differ now from each other in their engineering dimension, for example $[\gamma] = [V\gamma'] = [V^2\gamma'']$. Maintaining a finite volume V is important for the validity of the present theory, but it also means that Fourier transforming it by mean of Eq. (3.11) results in sums over suitable modes and δ-functions of the form

$$V\delta_{\boldsymbol{k},0} = \int_V d^dx\; e^{-i\boldsymbol{k}\cdot\boldsymbol{x}}, \quad \text{whence e.g.} \quad \Phi(\boldsymbol{k}) = \int_V d^dx\; e^{-i\boldsymbol{k}\cdot\boldsymbol{x}}\phi(\boldsymbol{x})\;. \tag{3.80}$$

We may occasionally approximate sums over momenta by integrals. To make the notation more suggestive of continuous $\boldsymbol{k} \in \mathbb{R}^d$ we write the Fourier transformed fields as $\Phi(\boldsymbol{k})$, $\boldsymbol{\mathcal{J}}(\boldsymbol{k})$, $\xi(\boldsymbol{k})$ etc.

The continuum propagators are structurally identical to their discrete counterpart and read

$$\langle \Phi(\boldsymbol{k})\tilde{\Phi}(\boldsymbol{k}')\rangle = \frac{V\delta_{\boldsymbol{k}+\boldsymbol{k}',0}}{D|\boldsymbol{k}|^2+r} \mathrel{\widehat{=}} \quad (3.81)$$

$$\langle \Xi(\boldsymbol{k})\bar{\Xi}(\boldsymbol{k}')\rangle = -\langle \bar{\Xi}(\boldsymbol{k})\Xi(\boldsymbol{k}')\rangle = \frac{V\delta_{\boldsymbol{k}+\boldsymbol{k}',0}}{D|\boldsymbol{k}|^2+r} \mathrel{\widehat{=}} \quad (3.82)$$

$$\langle \mathcal{J}^{(n)}(\boldsymbol{k})\tilde{\mathcal{J}}^{(m)}(\boldsymbol{k}')\rangle = \delta_{nm}V\delta_{\boldsymbol{k}+\boldsymbol{k}',0} \mathrel{\widehat{=}} \quad (3.83)$$

$$\langle \boldsymbol{\mathcal{J}}(\boldsymbol{k})\tilde{\Phi}(\boldsymbol{k}')\rangle = \frac{D(-i\boldsymbol{k})}{D|\boldsymbol{k}|^2+r}V\delta_{\boldsymbol{k}+\boldsymbol{k}',0} \mathrel{\widehat{=}} \quad . \quad (3.84)$$

3.B.5 Correlated noise

Generalising the formalism to allow for correlations in the transition rates is relatively straightforward. What changes is the form of the probability functional for the noise, originally Eq. (3.32), which should now include a non-trivial dependence on the power spectrum. The power spectrum $Q(\boldsymbol{k})$ characterises the noise correlation function for the different components of the disorder in Fourier space as

$$\langle \zeta^{(n)}(\boldsymbol{k})\zeta^{(m)}(\boldsymbol{p})\rangle = Q(\boldsymbol{k})V\delta_{\boldsymbol{k}+\boldsymbol{p},0}\delta_{n,m} \ . \quad (3.85)$$

The case of uncorrelated noise covered above corresponds to $Q(\boldsymbol{k}) = \tilde{\lambda}$, i.e. to the case where $Q(\boldsymbol{k})$ is independent of $\boldsymbol{k}$. The noise probability functional corresponding to Eq. (3.85) reads

$$P[\boldsymbol{\zeta}] \propto \exp\left[-\frac{1}{2V}\sum_{\boldsymbol{k}}\frac{\boldsymbol{\zeta}(\boldsymbol{k})\cdot\boldsymbol{\zeta}(-\boldsymbol{k})}{Q(\boldsymbol{k})}\right] \quad (3.86)$$

where the sample space of $\boldsymbol{\zeta}(\boldsymbol{k})$ is constrained to $\boldsymbol{\zeta}(\boldsymbol{k}) = \boldsymbol{\zeta}^*(-\boldsymbol{k})$ as to maintain $\boldsymbol{\zeta}(\boldsymbol{x})$, the inverse Fourier transform of $\boldsymbol{\zeta}(\boldsymbol{k})$, being real. The role of $Q(\boldsymbol{k})$ is to penalise spatial fluctuations of $\boldsymbol{\zeta}(\boldsymbol{k})$ depending on its wavenumber. Since our setup is rotationally symmetric we assume the general algebraic form of the correlator to be $Q(k) \sim \tilde{\lambda}k^{-\eta}$ for small k, where $k = |\boldsymbol{k}|$. For $\eta > 0$, the right hand side of Eq. (3.86) is regularised by excluding the homogeneous mode, $\boldsymbol{k} = 0$, from the summation. The derivation of the field theory with non-trivial correlator proceeds as outline above up until Eq. (3.45),

which has now a slightly different form,

$$\int \mathcal{D}\zeta \, \exp\left(\frac{1}{V}\sum_{\boldsymbol{k}} -\frac{k^\eta}{2\tilde{\lambda}}\boldsymbol{\zeta}(\boldsymbol{k})\cdot\boldsymbol{\zeta}(-\boldsymbol{k}) + \boldsymbol{\zeta}(\boldsymbol{k})\cdot\boldsymbol{F}(-\boldsymbol{k})\right) \tag{3.87}$$

$$\propto \exp\left(\frac{\tilde{\lambda}}{2V}\sum_{\boldsymbol{k}} k^{-\eta}\boldsymbol{F}(\boldsymbol{k})\cdot\boldsymbol{F}(-\boldsymbol{k})\right) \ , \tag{3.88}$$

where we have introduced the short-hand $\boldsymbol{F}(\boldsymbol{k})$ for the Fourier transform of the real expression

$$\boldsymbol{F}(\boldsymbol{x}) = 2(\boldsymbol{\nabla}\tilde{\phi}(\boldsymbol{x}))\phi(\boldsymbol{x}) + 2\tilde{\boldsymbol{J}}(\boldsymbol{x})\phi(\boldsymbol{x}) + 2(\boldsymbol{\nabla}\bar{\xi}(\boldsymbol{x}))\xi(\boldsymbol{x}) + \text{h.o.t} \ . \tag{3.89}$$

We thus find that the generalisation to correlated noise characterised by a power spectrum $Q(k) = \tilde{\lambda}k^{-\eta}$ amounts to augmenting the interaction terms (in Fourier space) of the original theory by a factor $k^{-\eta}$. The Fourier representation, originally Eq. (3.55), of the interaction vertices to be used in our subsequent calculation is upgraded to the its continuum form for general η according to


$$\widehat{=} (\gamma''/V)k^{-\eta}(-i\boldsymbol{k})\cdot(i\boldsymbol{k})\tilde{\Phi}(\boldsymbol{k})\tilde{\Phi}(-\boldsymbol{k}) \tag{3.90}$$


$$\widehat{=} (\kappa''/V)k^{-\eta}\tilde{\boldsymbol{\mathcal{J}}}(\boldsymbol{k})\cdot\tilde{\boldsymbol{\mathcal{J}}}(-\boldsymbol{k}) \tag{3.91}$$


$$\widehat{=} (\sigma''/V)k^{-\eta}(-i\boldsymbol{k})\cdot\tilde{\boldsymbol{\mathcal{J}}}(\boldsymbol{k})\tilde{\Phi}(-\boldsymbol{k}) \ , \tag{3.92}$$

with $\gamma'' = \kappa'' = 2\tilde{\lambda}/V^2$ and $\sigma'' = 4\tilde{\lambda}/V^2$. The effect of this modification on the spectral density of the currents becomes apparent already at tree level, where we now obtain, for $\boldsymbol{k} \neq 0$,

$$\langle \mathcal{J}^{(n)}(\boldsymbol{k})\mathcal{J}^{(m)}(\boldsymbol{k}')\rangle =$$ 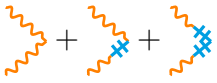 $$+ \mathcal{O}(\tilde{\lambda}^2/V^2) \tag{3.93}$$

$$= \left(\frac{4\tilde{\lambda}}{V}\delta_{n,m} - \frac{8\tilde{\lambda}}{V}\frac{k_n k_m}{|\boldsymbol{k}|^2} + \frac{4\tilde{\lambda}}{V}\sum_{\ell=1}^{d}\frac{k_n k_m k_\ell^2}{|\boldsymbol{k}|^4}\right)|\boldsymbol{k}|^{-\eta}\delta_{\boldsymbol{k}+\boldsymbol{k}',0} + \mathcal{O}(\tilde{\lambda}^2/V^2) \tag{3.94}$$

$$= \frac{4\tilde{\lambda}}{V}\left(\delta_{n,m} - \frac{k_n k_m}{|\boldsymbol{k}|^2}\right)|\boldsymbol{k}|^{-\eta}\delta_{\boldsymbol{k}+\boldsymbol{k}',0} + \mathcal{O}(\tilde{\lambda}^2/V^2) \ . \tag{3.95}$$

This is the result we invoke in the main text, Eq. (3.13). The special case of uncorrelated rates is recovered at $\eta = 0$. The momentum-dependent factor appearing in brackets in Eq. (3.95) is the fingerprint of a solenoidal vector field [102, 198]. For $\boldsymbol{k} = 0$ and $\eta \leq 0$, the second and third diagrams vanish and we instead find

$$\langle \mathcal{J}^{(n)}(0)\mathcal{J}^{(m)}(\boldsymbol{k}')\rangle = \frac{4\tilde{\lambda}}{V^2}|\boldsymbol{k}'|^{-\eta}\delta_{n,m}V\delta_{\boldsymbol{k}',0} \ , \tag{3.96}$$

consistently with Eq. (3.65).

3.B.6 Beyond tree level I: Ghosts and closed response circuits

Up to this point, calculating observables at tree level has allowed us to avoid discussing the role of the Faddeev-Popov ghosts. However, there are important differences between the way ghosts should be handled in this theory compared to both dynamic response field theories [133] and static response field theories with additive noise [12]. By construction, Eq. (3.41), the Grassman fields ξ and $\bar{\xi}$ only ever appear in the action as powers of the product $\bar{\xi}\xi$. Since physical observables do not involve ξ or $\bar{\xi}$ directly, ghost fields can only contribute diagrammatically via closed response circuits. In dynamical response field theories, causality ensures that closed response circuits of two or more propagators vanish, while the value of closed response loops of a single propagator is determined by the chosen convention for the time discretisation [139]. In static theories this causal mechanism is absent and ghost circuits play a non-trivial role, both by removing vacuum diagrams (thus ensuring that the normalisation condition, $\langle 1\rangle = 1$, is satisfied) and potentially by appearing as internal fields in connected diagrams. Recently in [12], it has been argued that, for problems involving additive noise, ghost contributions can simply be ignored by introducing additional restrictions on the diagrams contributing to physical observables, amounting to ignoring all diagrams containing closed response circuits. In other words, when noise is additive, the only relevant diagrams are directed acyclic graphs. This argument breaks down for problems involving multiplicative noise, where cyclic graphs produce non-vanishing contributions to physical observables. As an example of the non-trivial role played by the ghost fields, consider the one-loop contribution to the density correlation function, Eq. (3.64),

$$\langle \Phi(\boldsymbol{k})\Phi(-\boldsymbol{k})\rangle =$$  $$+ \cdots$$ (3.97)

which involves both directed acyclic as well as cycling diagrams. Closed response loops of a single propagator, on the other hand, vanish by antisymmetry of the integrand

$$= \propto \int d^d k' \, \frac{\boldsymbol{k}\cdot\boldsymbol{k}'}{h|\boldsymbol{k}'|^2 + r} = 0 \ , \tag{3.98}$$

with $\boldsymbol{k}$ the external momentum. Dashes indicating spatial derivatives have been left implicit in Eqs. (3.97) and (3.98). A more thorough analysis of the role of Faddeev-Popov ghosts in static response-field theories is beyond the scope of the current work but will be essential in order to be able to explore theories characterised by multiplicative noise beyond tree level.

3.B.7 Beyond tree level II: Ward identities

While the appearance of new interactions upon carrying out the field shift $\phi_i \to \phi_i + N^{-1}$ at the level of Eq. (3.57) might suggest a proliferation of independent couplings, γ' and γ'' are in fact related to γ by two Ward identities [39] in such a way that their renormalisation flows are strongly constrained. These Ward identities are derived by considering the behaviour of the action $\mathcal{A} = \mathcal{A}_0 + \mathcal{A}_{\text{int}}$ under an infinitesimal shift of ϕ_i,

$$\begin{aligned}
\mathcal{A}' &= \mathcal{A}([\phi_i + \Sigma, \tilde{\phi}, J, \tilde{J}, \xi, \bar{\xi}]; \gamma, \gamma', \gamma'', \kappa, \kappa', \kappa'', \sigma, \sigma', \sigma'', \pi, \pi', \chi, \chi') \\
&= \mathcal{A}([\phi_i, \tilde{\phi}, J, \tilde{J}, \xi, \bar{\xi}]; \quad \gamma, \gamma' + 2\Sigma\gamma, \gamma'' + \Sigma^2\gamma + \sigma\gamma', && (3.99) \\
&\qquad\qquad \kappa, \kappa' + 2\Sigma\kappa, \kappa'' + \Sigma^2\kappa + \Sigma\kappa', && (3.100) \\
&\qquad\qquad \sigma, \sigma' + 2\Sigma\sigma, \sigma'' + \Sigma^2\sigma + \Sigma\sigma, && (3.101) \\
&\qquad\qquad \pi, \pi' + \Sigma\pi, \chi, \chi' + \Sigma\chi) + \sum_{i=1}^{N} r\Sigma\tilde{\phi}_i \ . && (3.102)
\end{aligned}$$

Denoting $\langle\cdots\rangle_{\mathcal{A}}$ and $\langle\cdots\rangle_{\mathcal{A}'}$ expectations with respect to the original and shifted action, respectively, and letting $\mathcal{A}'' = \mathcal{A}' - \sum_i r\Sigma\tilde{\phi}_i$, it must be the case that, for $k \neq 0$,

$$\begin{aligned}
\langle \Phi_k \Phi_{-k} \rangle_{\mathcal{A}} &= \langle (\Phi_k + \Sigma\delta_{k0})(\Phi_{-k} + \Sigma\delta_{k0}) \rangle_{\mathcal{A}'} \\
&= \langle \Phi_k \Phi_{-k} e^{-r\Sigma\tilde{\Phi}_0} \rangle_{\mathcal{A}''} + 2\Sigma\delta_{k0} \langle \Phi_k e^{-r\Sigma\tilde{\Phi}_0} \rangle_{\mathcal{A}''} + \Sigma^2\delta_{k0} \\
&= \langle \Phi_k \Phi_{-k} e^{-r\Sigma\tilde{\Phi}_0} \rangle_{\mathcal{A}''} && (3.103)
\end{aligned}$$

and

$$\begin{aligned}
&\langle \Phi_k \Phi_{-k} (rN^{-1}\tilde{\Phi}_0)\rangle_{\mathcal{A}} \\
&= \langle (\Phi_k + \Sigma\delta_{k0})(\Phi_{-k} + \Sigma\delta_{k0})(rN^{-1}\tilde{\Phi}_0)\rangle_{\mathcal{A}'} \\
&= \langle \Phi_k \Phi_{-k} (rN^{-1}\tilde{\Phi}_0) e^{-r\Sigma\tilde{\Phi}_0}\rangle_{\mathcal{A}''} + 2\Sigma\delta_{k0}\langle \Phi_k (rN^{-1}\tilde{\Phi}_0) e^{-r\Sigma\tilde{\Phi}_0}\rangle_{\mathcal{A}''} + \Sigma^2\delta_{k0}\langle rN^{-1}\tilde{\Phi}_0\rangle \\
&= \langle \Phi_k \Phi_{-k} (rN^{-1}\tilde{\Phi}_0) e^{-r\Sigma\tilde{\Phi}_0}\rangle_{\mathcal{A}''} \ . \qquad (3.104)
\end{aligned}$$

Since the left-hand sides of Eqs. (3.103) and (3.104) are independent of Σ, it follows that

$$\left.\frac{d}{d\Sigma}\right|_{\Sigma=0} \langle \Phi_k \Phi_{-k}\rangle_{\mathcal{A}} = \left.\frac{d}{d\Sigma}\right|_{\Sigma=0} \langle \Phi_k \Phi_{-k} (rN^{-1}\tilde{\Phi}_0)\rangle_{\mathcal{A}} = 0 \ . \qquad (3.105)$$

Differentiating the right-hand side of the two equations then produces the corresponding Ward identities for the renormalised couplings $\gamma_R, \gamma'_R, \gamma''_R$

$$\left(2\gamma\frac{\partial}{\partial\gamma'} + \gamma'\frac{\partial}{\partial\gamma''} + \chi\frac{\partial}{\partial\chi'}\right)\gamma''_R = \gamma'_R \qquad \text{and} \qquad \left(2\gamma\frac{\partial}{\partial\gamma'} + \gamma'\frac{\partial}{\partial\gamma''} + \chi\frac{\partial}{\partial\chi'}\right)\gamma'_R = \gamma_R \ . \qquad (3.106)$$

Diagrammatically, these identities follow from the renormalisation of γ, γ' and γ'' all being driven by the same set of four-point vertices, as shown below up to two-loop order:

$\gamma_R =$ 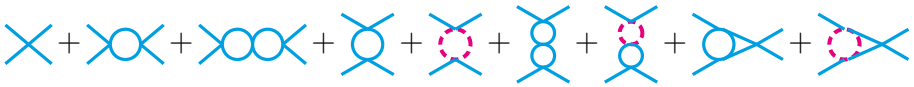 (3.107)

$\gamma'_R =$  (3.108)

$\gamma''_R =$ 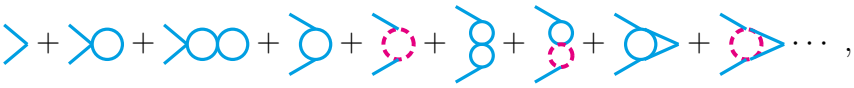 (3.109)

where dashes indicating spatial derivatives have again been left implicit. While in this work we don't perform any formal renormalisation group calculation, and in fact we limit ourselves to tree-level diagrammatics, the observation that the RG flow of the new couplings generated by a trivial shift of the annihilation field are strongly constrained by a set of Ward identities is consistent with these couplings accounting for the same 'physics' as the original coupling in the unshifted theory.

3.C Large L asymptotic form of Eq. (3.18)

We start from Eq. (3.14) for the expectation of the entropy production per mesostate with linear block dimensions L, where $\{\alpha, \beta\}$ is any pair of neighbouring mesostates. Without loss of generality we assume that the interface is a $(d-1)$-dimensional hypercube of constant x coordinate and denote $\{\boldsymbol{i}_\alpha\}$ the set of "boundary" states of α connected to β by a single edge. Denoting $\boldsymbol{e} = (1, 0, \cdots, 0)$ the d-dimensional unit displacement vector along the x axis, let $\{\boldsymbol{i}_\alpha + \boldsymbol{e}\}$ correspond to the set of "boundary" states of β connected to α by a single edge. Inspecting the logarithmic factor on the right-hand side of Eq. (3.14)

$$\ln \frac{j_{\alpha\beta}(L)}{j_{\beta\alpha}(L)} = \ln \frac{\sum_{\{\boldsymbol{i}_\alpha\}} h\bar{\pi} + h\delta\pi_{\boldsymbol{i}} + \pi_{\boldsymbol{i}}\zeta_{\boldsymbol{i},\boldsymbol{i}+\boldsymbol{e}}}{\sum_{\{\boldsymbol{i}_\alpha\}} h\bar{\pi} + h\delta\pi_{\boldsymbol{i}+\boldsymbol{e}} + \pi_{\boldsymbol{i}+\boldsymbol{e}}\zeta_{\boldsymbol{i}+\boldsymbol{e},\boldsymbol{i}}} \tag{3.110}$$

$$= \ln\left(1 + \frac{\sum_{\{\boldsymbol{i}_\alpha\}} h\delta\pi_{\boldsymbol{i}} + \pi_{\boldsymbol{i}}\zeta_{\boldsymbol{i},\boldsymbol{i}+\boldsymbol{e}}}{h\bar{\pi}L^{d-1}}\right) - \ln\left(1 + \frac{\sum_{\{\boldsymbol{i}_\alpha\}} h\delta\pi_{\boldsymbol{i}+\boldsymbol{e}} + \pi_{\boldsymbol{i}+\boldsymbol{e}}\zeta_{\boldsymbol{i}+\boldsymbol{e},\boldsymbol{i}}}{h\bar{\pi}L^{d-1}}\right) \tag{3.111}$$

where we have expanded the steady-state probability about its mean, $\pi_{\boldsymbol{i}} = \bar{\pi} + \delta\pi_{\boldsymbol{i}}$, with $\bar{\pi} = N^{-d}$. Each logarithm in the expression above contains a sum over L^{d-1} zero-mean random variables $h\delta\pi_{\boldsymbol{i}} + \pi_{\boldsymbol{i}}\zeta_{\boldsymbol{i},\boldsymbol{i}+\boldsymbol{e}}$ and $h\delta\pi_{\boldsymbol{i}+\boldsymbol{e}} + \pi_{\boldsymbol{i}+\boldsymbol{e}}\zeta_{\boldsymbol{i}+\boldsymbol{e},\boldsymbol{i}}$, respectively. While the expected value of each sum vanishes by linearity, the typical magnitude can be estimated by computing its standard deviation. We thus write down the variance of the sum

$$\begin{aligned}
&\frac{1}{(h\bar{\pi}L^{d-1})^2}\left\langle\left(\sum_{\{\boldsymbol{i}_\alpha\}} h\delta\pi_{\boldsymbol{i}+\boldsymbol{e}} + \pi_{\boldsymbol{i}+\boldsymbol{e}}\zeta_{\boldsymbol{i}+\boldsymbol{e},\boldsymbol{i}}\right)^2\right\rangle \\
&= \frac{1}{(h\bar{\pi}L^{d-1})^2}\sum_{\boldsymbol{i}_\alpha}\left\langle\left(h\delta\pi_{\boldsymbol{i}+\boldsymbol{e}} + \pi_{\boldsymbol{i}+\boldsymbol{e}}\zeta_{\boldsymbol{i}+\boldsymbol{e},\boldsymbol{i}}\right)^2\right\rangle \\
&+ \frac{1}{(h\bar{\pi}L^{d-1})^2}\sum_{\{\boldsymbol{i}_\alpha \neq \boldsymbol{i}'_\alpha\}}\left\langle\left(h\delta\pi_{\boldsymbol{i}+\boldsymbol{e}} + \pi_{\boldsymbol{i}+\boldsymbol{e}}\zeta_{\boldsymbol{i}+\boldsymbol{e},\boldsymbol{i}}\right)\left(h\delta\pi_{\boldsymbol{i}'+\boldsymbol{e}} + \pi_{\boldsymbol{i}'+\boldsymbol{e}}\zeta_{\boldsymbol{i}'+\boldsymbol{e},\boldsymbol{i}'}\right)\right\rangle\ .
\end{aligned} \tag{3.112}$$

The first contribution on the right hand side of Eq. (3.112), associated with the sum of variances, scales like $L^{-(d-1)}$ due to statistical homogeneity and can thus be taken to be small compared to the factor 1 appearing in the logarithm Eq. (3.111) in the

large L regime. The second contribution is associated with cross correlations among the summands. It involves $L^{d-1}(L^{d-1}-1)$ terms so it is at most of order L^0. However, this scaling only applies to infinite-range correlations and the more relevant decay of density as well as noise correlations over large distances will in general produce a scaling L^ν with $\nu < 0$. The second contributions is thus also asymptotically small compared to the factor 1 appearing in the logarithm. For sufficiently large L we can therefore expand Eq. (3.111) to leading order and obtain

$$\begin{aligned}\ln\frac{j_{\alpha\beta}(L)}{j_{\beta\alpha}(L)} &\simeq \frac{1}{h\bar{\pi}L^{d-1}}\sum_{\{\boldsymbol{i}_\alpha\}} h\delta\pi_{\boldsymbol{i}} + \pi_{\boldsymbol{i}}\zeta_{\boldsymbol{i},\boldsymbol{i}+\boldsymbol{e}} - h\delta\pi_{\boldsymbol{i}+\boldsymbol{e}} - \pi_{\boldsymbol{i}+\boldsymbol{e}}\zeta_{\boldsymbol{i}+\boldsymbol{e},\boldsymbol{i}} \\ &= \frac{1}{h\bar{\pi}L^{d-1}}(j_{\alpha\beta}(L) - j_{\beta\alpha}(L)) \ , \end{aligned} \tag{3.113}$$

whence

$$\left\langle (j_{\alpha\beta}(L) - j_{\beta\alpha}(L))\ln\frac{j_{\alpha\beta}(L)}{j_{\beta\alpha}(L)}\right\rangle \simeq \frac{N^d}{hL^{d-1}}\langle (j_{\alpha\beta}(L) - j_{\beta\alpha}(L))^2\rangle \ . \tag{3.114}$$

3.D Asymptotic scaling of integrated currents from correlation function

Here we outline the calculation required to compute the asymptotic variance of the integrated current across a mesostate interface, Eq. (3.16), starting from the spectral density tensor of the probability current vector field, Eq. (3.13). These arguments closely follow the standard treatment of hyperuniform fluctuations , reviewed in [285]. Without loss of generality we assume that the interface, denoted Ω henceforth, is a $d-1$ dimensional hypersurface of constant $x = 0$ coordinate embedded in d dimensional space (see Figure 3.6). We introduce $\tilde{\boldsymbol{r}}$ as the $d-1$ dimensional vector satisfying $\boldsymbol{r} = (r_x, \tilde{\boldsymbol{r}})$. The variance of the integrated current across the interface Ω is thus given by

$$Var(J;\Omega) = \int_\Omega d^{d-1}\tilde{r}' \int_\Omega d^{d-1}\tilde{r}'' \ \langle J_x(0,\tilde{\boldsymbol{r}}')J_x(0,\tilde{\boldsymbol{r}}'')\rangle \tag{3.115}$$

$$= \int_\Omega d^{d-1}\tilde{r}' \int_\Omega d^{d-1}\tilde{r}'' \ C_{xx}(0,\tilde{\boldsymbol{r}}' - \tilde{\boldsymbol{r}}'') \tag{3.116}$$

$$= v_\Omega \int d^{d-1}\tilde{r}' \ C_{xx}(0,\tilde{\boldsymbol{r}}')\gamma(\tilde{\boldsymbol{r}}';\Omega) \tag{3.117}$$

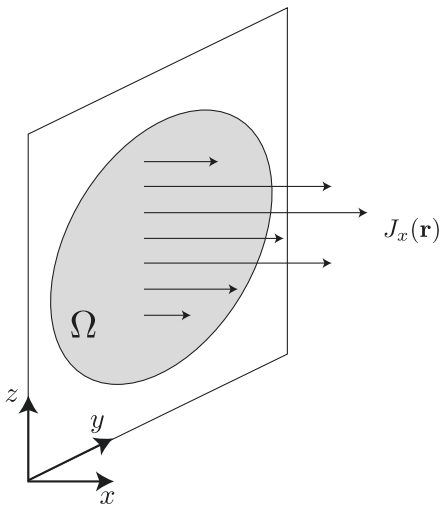

Figure 3.6: Schematic illustration of the setup used for the calculation of the statistics of the integrated current across a mesostate interface Ω, which we assume to be a $d-1$ dimensional hypersurface of constant $x = 0$ coordinate embedded in d dimensional space (here $d = 3$ for the purpose of visualisation). By construction, $J_x(\boldsymbol{r})$ thus corresponds to the projection of the current vector field $\boldsymbol{J}(\boldsymbol{r})$ on the unit vector normal to Ω. The net current is obtained by integrating $J_x(\boldsymbol{r})$ over $\boldsymbol{r} \in \Omega$.

where

$$\gamma(\tilde{\boldsymbol{r}}';\Omega) = \frac{1}{v_\Omega}\int d^{d-1}\tilde{r}''\ \mathcal{I}_\Omega(\tilde{\boldsymbol{r}}'')\mathcal{I}_\Omega(\tilde{\boldsymbol{r}}'+\tilde{\boldsymbol{r}}'') \tag{3.118}$$

is the overlap surface fraction, with $\mathcal{I}_\Omega$ the indicator function over the interface, and v_Ω is the interface surface. What we require to proceed further is therefore an expression for the component C_{xx} of the current correlation function for displacements on the interface. To obtain this, we start from the corresponding component of the spectral density, Eq. (3.95), and introduce $\tilde{\boldsymbol{k}}$ as the $d-1$ dimensional vector satisfying $\boldsymbol{k} = (k_x, \tilde{\boldsymbol{k}})$ to write

$$\langle \mathcal{J}_x(\boldsymbol{k})\mathcal{J}_x(\boldsymbol{k}')\rangle = \langle \mathcal{J}_x(k_x,\tilde{\boldsymbol{k}})\mathcal{J}_x(k_x',\tilde{\boldsymbol{k}}')\rangle = \frac{4\tilde{\lambda}}{V}\frac{|\tilde{\boldsymbol{k}}|^2}{(|\tilde{\boldsymbol{k}}|^2+k_x^2)^{1+\frac{\eta}{2}}}\delta_{\tilde{\boldsymbol{k}}+\tilde{\boldsymbol{k}}',0}\delta_{k_x+k_x',0}\ . \tag{3.119}$$

The correlation function C_{xx} is thus obtained from Eq. (3.119) by Fourier back-transforming according to the convention Eq. (3.11),

$$C_{xx}(0,\tilde{\boldsymbol{r}}) = \langle J_x(0,0)J_x(0,\tilde{\boldsymbol{r}})\rangle \tag{3.120}$$

$$= \frac{1}{V^2}\sum_{k_x,\tilde{\boldsymbol{k}}} e^{i\tilde{\boldsymbol{k}}\cdot\tilde{\boldsymbol{r}}}\langle \mathcal{J}_x(k_x,\tilde{\boldsymbol{k}})\mathcal{J}_x(-k_x,-\tilde{\boldsymbol{k}})\rangle \tag{3.121}$$

$$= \int \text{đ}^{d-1}\tilde{k}\; e^{i\tilde{\boldsymbol{k}}\cdot\tilde{\boldsymbol{r}}}\int \text{đ}k_x\; \frac{4\tilde{\lambda}}{V^2}\frac{|\tilde{\boldsymbol{k}}|^2}{(|\tilde{\boldsymbol{k}}|^2+k_x^2)^{1+\frac{\eta}{2}}} \tag{3.122}$$

$$= \int \text{đ}^{d-1}\tilde{k}\; e^{i\tilde{\boldsymbol{k}}\cdot\tilde{\boldsymbol{r}}}\left[\frac{2\tilde{\lambda}\Gamma\left(\frac{1+\eta}{2}\right)}{V^2\sqrt{\pi}\Gamma\left(1+\frac{\eta}{2}\right)}|\tilde{\boldsymbol{k}}|^{1-\eta}\right]\;, \tag{3.123}$$

where we have approximated sums over momenta, which involve an infrared cutoff at a typical inverse length-scale $V^{-1/d}$, as integrals in the limit of large V on the basis of the infrared convergence of the integral Eq. (3.123) for $\eta < d$. Following the usual convention [318], dashed differentials are a short-hand for $\text{đ}^d k = d^d k/(2\pi)^d$. It is interesting to note that, while the full spectral density Eq. (3.13) is not hyperuniform for $\eta = 0$, the relevant component of the corresponding correlation function is hyperuniform for $\eta < 1$ with hyperuniformity exponent $1-\eta$ when we concentrate on the lower-dimensional object that is the mesostate interface. For the correlation function $C_{xx}(0,\tilde{\boldsymbol{r}})$ origination from Eq. (3.123) to be well-defined in the range $\eta < d$, the Fourier back-transform needs to be regularised in the ultraviolet. Here, we do so by introducing a soft cutoff, suggestive of the introduction of a microscopic lattice spacing of typical length scale $\beta = \ell$. Denoting $C^R_{xx}(0,\tilde{\boldsymbol{r}};\beta)$ the regularised correlation function, we write

$$C^R_{xx}(0,\tilde{\boldsymbol{r}};\beta) = \int \text{đ}^{d-1}\tilde{k}\; e^{i\tilde{\boldsymbol{k}}.\tilde{\boldsymbol{r}}}\left[\frac{2\tilde{\lambda}\Gamma\left(\frac{1+\eta}{2}\right)}{V^2\sqrt{\pi}\Gamma\left(1+\frac{\eta}{2}\right)}|\tilde{\boldsymbol{k}}|^{1-\eta}\right] e^{-\beta|\tilde{\boldsymbol{k}}|} \tag{3.124}$$

$$= \mathcal{N}(\eta,d;\tilde{\lambda},V)\int_0^\pi d\theta\; (\sin(\theta))^{d-3}\int_0^\infty d\tilde{k}\; e^{i\tilde{k}\cos(\theta)|\tilde{\boldsymbol{r}}|-\beta\tilde{k}}\;\tilde{k}^{d-1-\eta} \tag{3.125}$$

$$\propto \sum_{n=0}^{\infty}\frac{(-1)^n}{(2n)!}|\tilde{\boldsymbol{r}}|^{2n}\frac{\Gamma\left(\frac{d}{2}-1\right)\Gamma\left(n+\frac{1}{2}\right)}{\Gamma\left(n+\frac{d}{2}-1\right)}\int_0^\infty d\tilde{k}\; e^{-\beta\tilde{k}}\tilde{k}^{d-1-\eta+2n} \tag{3.126}$$

$$\propto \sqrt{\pi}\frac{\Gamma\left(d-\eta\right)\Gamma\left(\frac{d-2}{2}\right)}{\Gamma\left(\frac{d-1}{2}\right)}\beta^{-d+\eta}\;{}_2F_1\left(\frac{d-\eta}{2},\frac{d-\eta+1}{2},\frac{d-1}{2};-\frac{|\tilde{\boldsymbol{r}}|^2}{\beta^2}\right)\;. \tag{3.127}$$

for $\eta < d$ and $d > 2$, where ${}_2F_1(a, b, c; z)$ denotes the hypergeometric function [22]. We note for later use that ${}_2F_1(a, b, c; z)$ has the asymptotic expansion

$$ {}_2F_1(a, b, c; z) = \lambda_1 z^{-a} + \lambda_2 z^{-b} + \mathcal{O}(z^{-a-1}, z^{-b-1}) \tag{3.128} $$

with

$$ \lambda_1 = \frac{\sqrt{\pi}\Gamma\left(\frac{d-1}{2}\right)}{\Gamma\left(\frac{\eta-1}{2}\right)\Gamma\left(\frac{d+1-\eta}{2}\right)} \tag{3.129} $$

at large $|z|$ unless $a - b$ is an integer [22]. To go from Eq. (3.124) to (3.125) we first perform a change of variable to spherical coordinates using

$$ \int d^n\tilde{k} = \int_0^\infty d\tilde{k} \int_0^\pi d\theta d\phi_1 ... d\phi_{n-3} \int_0^{2\pi} d\phi_{n-2}\, \tilde{k}^{n-1} \sin^{n-2}(\theta) \sin^{n-3}(\phi_1) ... \sin(\phi_{n-3}) \tag{3.130} $$

for $n = d - 1$ and $n > 1$, with $\tilde{k} = |\tilde{\boldsymbol{k}}|$ the wavenumber and $\theta = \arccos[(\tilde{\boldsymbol{k}}/|\tilde{\boldsymbol{k}}|) \cdot (\tilde{\boldsymbol{r}}/|\tilde{\boldsymbol{r}}|)]$ the angle between the wavevector $\tilde{\boldsymbol{k}}$ and the displacement $\tilde{\boldsymbol{r}}$. Since the integrand of Eq. (3.124) is a function only of $\tilde{k}$ and θ, the remaining angular coordinates can be integrated out. To go from Eq. (3.125) to (3.126) we perform a second change of variable $u(\theta) = \cos(\theta)$ and expand the ensuing trigonometric functions as power series in $\tilde{k}u|\tilde{\boldsymbol{r}}|$ before carrying out the integral over u. In the following, we shall ignore the numerical prefactor

$$ \mathcal{N}(\eta, d; \tilde{\lambda}, V) = \frac{1}{(2\pi)^{d-1}} \frac{2\tilde{\lambda}\Gamma\left(\frac{1+\eta}{2}\right)}{V^2\sqrt{\pi}\Gamma\left(1+\frac{\eta}{2}\right)} \frac{2\pi^{\frac{d-2}{2}}}{\Gamma\left(\frac{d-2}{2}\right)} \tag{3.131} $$

in Eq. (3.125), since is independent of both θ and k and thus irrelevant for the window size scaling. The case $d = 2$ needs to be treated separately and produces for $\eta < d$:

$$ C^R_{xx}(0, \tilde{\boldsymbol{r}}; \beta) \propto \Gamma(2-\eta)\beta^{-2+\eta} \left(1 + \frac{|\tilde{\boldsymbol{r}}|^2}{\beta^2}\right)^{\frac{\eta-2}{2}} \cos\left[(2-\eta)\arctan\left(\frac{|\tilde{\boldsymbol{r}}|}{\beta}\right)\right] , \tag{3.132} $$

which is characterised by the same leading order asymptotic scaling with $|\tilde{\boldsymbol{r}}|$ at $|\tilde{\boldsymbol{r}}|/\beta \gg 1$ as Eq. (3.127) for $d \to 2$.

Taking the interface as a hypersphere of radius $\mathcal{L} = L\ell$, whence $v_\Omega \sim \mathcal{L}^{d-1}$, it was

shown [285] that, for $|\tilde{\boldsymbol{r}}| < 2\mathcal{L}$,

$$\gamma(\tilde{\boldsymbol{r}};\Omega) = 1 - c(d)\left(\frac{|\tilde{\boldsymbol{r}}|}{\mathcal{L}}\right) + c(d)\sum_{n=2}^{\infty}(-1)^n \frac{(d-1)(d-3)...(d-2n+3)}{(2n-1)![2\cdot 4\cdot 6...(2n-2)]}\left(\frac{|\tilde{\boldsymbol{r}}|}{\mathcal{L}}\right)^{2n-1} \tag{3.133}$$

with $c(d) = 2\Gamma(1+d/2)/(\sqrt{\pi}\Gamma((d+1)/2))$. Ref. [155] explores the effect of changing the interface shape. Overall

$$Var(J;\Omega) = v_\Omega \int_\Omega d^{d-1}\tilde{r}\; C_{xx}(0,\tilde{\boldsymbol{r}})\left[1 - c(d)\left(\frac{|\tilde{\boldsymbol{r}}|}{\mathcal{L}}\right) + c(d)\sum_{n=2}^{\infty}(-1)^n \frac{(d-1)(d-3)...(d-2n+3)}{(2n-1)![2\cdot 4\cdot 6...(2n-2)]}\left(\frac{|\tilde{\boldsymbol{r}}|}{\mathcal{L}}\right)^{2n-1}\right]. \tag{3.134}$$

The term in Eq. (3.134) originating from the zeroth order in the series expansion of γ approaches, in the asymptotic limit of $\mathcal{L} \to \infty$, the value of the spectral density, Eq. (3.123), at $\tilde{\boldsymbol{k}} = 0$,

$$\lim_{\mathcal{L}\to\infty}\int_\Omega d^{d-1}\tilde{r}\; C_{xx}(0,\tilde{\boldsymbol{r}}) = \lim_{\tilde{\boldsymbol{k}}\to 0}\left[\frac{2\tilde{\lambda}\Gamma\left(\frac{1+\eta}{2}\right)}{V^2\sqrt{\pi}\Gamma\left(1+\frac{\eta}{2}\right)}|\tilde{\boldsymbol{k}}|^{1-\eta}\right] \tag{3.135}$$

and thus vanishes when the latter is hyperuniform, namely for $\eta < 1$.

Based on the expansion Eq. (3.128), the behaviour of the correlation function, Eq. (3.127), for $|\tilde{\boldsymbol{r}}|/\beta \gg 1$ is $C^R_{xx}(0,\tilde{\boldsymbol{r}};\beta) \sim |\tilde{\boldsymbol{r}}|^{\eta-d}$ therefore each term in the integrand in the right-hand side of Eq. (3.134) behaves like $|\tilde{\boldsymbol{r}}|^{\eta-2+m}$ with $m \in \{0,1,3,...\}$. The scaling of the variance with window size $\mathcal{L}$ is thus controlled by the infrared divergence as $\mathcal{L} \to \infty$. For $\eta < 1-m$, the integrals are infrared convergent, which allows us to let $\Omega \to \mathbb{R}^{d-1}$ without modifying the leading order asymptotic scaling with $\mathcal{L}$. Proceeding case by case:

- $\boldsymbol{0 < \eta < d}$: For $\eta > 1$, the relevant integrals are infrared divergent. For $0 < \eta < 1$ the term originating from the zeroth order in the expansion of γ is removed by the cancellation Eq. (3.135). For $\eta = 1$, based on Eq. (3.123), the correlation function C_{xx} takes the form of a Dirac delta in real space so that the term originating from the zeroth order in the expansion of γ is finite but $\mathcal{L}$ independent and

does not contribute to the scaling. Overall, the scaling is dominated by the infrared divergent behaviour at large $|\tilde{\boldsymbol{r}}|$. Substituting Eq. (3.127) together with the asymptotic expansion (3.128) into Eq. (3.134) and performing a change of variable $\tilde{\boldsymbol{r}} \to \tilde{\boldsymbol{r}}/\mathcal{L}$ to isolate the $\mathcal{L}$ dependence, we arrive at $Var(J;\Omega) \sim \mathcal{L}^{d-2+\eta}$ for $0 < \eta < d$.

- $\boldsymbol{\eta = 0}$: The case of $\eta = 0$ needs to be treated separately because the integral of the first order term in the expansion of $\gamma(\tilde{\boldsymbol{r}};\Omega)$ is logarithmically divergent. Substituting Eq. (3.127) for the regularised correlation function into Eq. (3.134) and setting $\eta = 0$ we are left with integrals of the form

$$\mathcal{I}_m(\mathcal{L}) = v_\Omega \int_\Omega d^{d-1}\tilde{r}\ {}_2F_1\left(\frac{d}{2}, \frac{d+1}{2}, \frac{d-1}{2}; -\frac{|\tilde{\boldsymbol{r}}|^2}{\beta^2}\right)\left(\frac{|\tilde{\boldsymbol{r}}|}{\mathcal{L}}\right)^m \ . \tag{3.136}$$

for $m \geq 1$. For $m > 1$ and based on the expansion Eq. (3.128), the $\tilde{\boldsymbol{r}}$ integral is dominated by the behaviour of the integrand in the large $|\tilde{\boldsymbol{r}}|$ regime and we recover the $\mathcal{L}^{d-2}$ scaling obtained upon setting $\eta = 0$ in the scaling law for the case $0 < \eta < d$. For $m = 1$ we exploit the spherical symmetry of the integral to write

$$\int_\Omega d^{d-1}\tilde{r}\ f(|\tilde{\boldsymbol{r}}|) = \int_0^{\mathcal{L}} d|\tilde{\boldsymbol{r}}|\ \frac{2\pi^{\frac{d-1}{2}}}{\Gamma(\frac{d-1}{2})}|\tilde{\boldsymbol{r}}|^{d-2} f(|\tilde{\boldsymbol{r}}|) \tag{3.137}$$

and invoke the asymptotic expansion Eq. (3.128) to obtain the leading order behaviour

$$\mathcal{I}_{m=1}(\mathcal{L}) = \frac{v_\Omega}{\mathcal{L}} \int_0^{\mathcal{L}} \frac{d|\tilde{\boldsymbol{r}}|}{\beta}\ \lambda_1 \frac{2\pi^{\frac{d-1}{2}}\Gamma(d)}{\Gamma(\frac{d-1}{2})}\left(\frac{|\tilde{\boldsymbol{r}}|}{\beta}\right)^{-1} \sim \mathcal{L}^{d-2}\log(\mathcal{L}/\beta)\ , \tag{3.138}$$

which dominates the asymptotic scaling with $\mathcal{L}$. The variance of the integrated current thus scales like $Var(J;\Omega) \sim \mathcal{L}^{d-2}\log(\mathcal{L}/\beta)$ for $\eta = 0$.

- $\boldsymbol{\eta < 0}$: Finally, we consider the case of $\eta < 0$. Substituting once again Eq. (3.127) into Eq. (3.134), we obtain

$$\mathcal{I}_m(\mathcal{L}) = v_\Omega \int_\Omega d^{d-1}\tilde{r}\ {}_2F_1\left(\frac{d-\eta}{2}, \frac{d-\eta+1}{2}, \frac{d-1}{2}; -\frac{|\tilde{\boldsymbol{r}}|^2}{\beta^2}\right)\left(\frac{|\tilde{\boldsymbol{r}}|}{\mathcal{L}}\right)^m \ . \tag{3.139}$$

for $m \in \{1, 3, 5, ...\}$. When $m < 1 - \eta$ this integral is infrared convergent and we can take $\Omega \to \mathbb{R}^{d-1}$ without affecting the leading order scaling with $\mathcal{L}$. Upon

taking this limit, the $\mathcal{L}$ dependence is limited to the prefactors and we straightforwardly obtain $\mathcal{I}_m(\mathcal{L}) \sim \mathcal{L}^{d-1-m}$. When $m = 1 - \eta$ the integral is logarithmically divergent and we obtain $\mathcal{I}_m(\mathcal{L}) \sim \log(\mathcal{L}/\beta)\mathcal{L}^{d-2+\eta}$ along the lines of Eq. (3.138). Finally, when $m > 1 - \eta$, the integral is infrared divergent, whereby we invoke the asymptotic expansion, Eq. (3.128), to obtain $\mathcal{I}_m(\mathcal{L}) \sim \mathcal{L}^{d-2+\eta}$. Overall, the scaling is dominated by the $m = 1$ term and follows $Var(J;\Omega) \sim \mathcal{L}^{d-2}$ for $\eta < 0$.

Combining the results that we just derived into a single expression and making the dependence on the model parameters $\tilde{\lambda}$ and V appearing in the prefactor Eq. (3.131) explicit, we thus have

$$Var(J;\Omega) \sim \begin{cases} \tilde{\lambda}V^{-2}\mathcal{L}^{d-2}, & \text{for } \eta < 0 \\ \tilde{\lambda}V^{-2}\mathcal{L}^{d-2}\ln(\mathcal{L}/\beta), & \text{for } \eta = 0 \\ \tilde{\lambda}V^{-2}\beta^{-\eta}\mathcal{L}^{d-2+\eta}, & \text{for } 0 < \eta < d \end{cases} . \tag{3.140}$$

Substituting into Eq. (3.15) with $\beta = \ell$,

$$\left\langle \dot{s}_i^{(\text{meso})} \right\rangle (\mathcal{L}) \sim \begin{cases} \tilde{\lambda}\ell^{3}V^{-1}h^{-1}\mathcal{L}^{-1}, & \text{for } \eta < 0 \\ \tilde{\lambda}\ell^{3}V^{-1}h^{-1}\mathcal{L}^{-1}\ln(\mathcal{L}/\ell), & \text{for } \eta = 0 \\ \tilde{\lambda}\ell^{3-\eta}V^{-1}h^{-1}\mathcal{L}^{-1+\eta}, & \text{for } 0 < \eta < d \end{cases} , \tag{3.141}$$

which constitutes our main result.

ACKNOWLEDGMENTS

LC would like to thank Rosalba Garcia-Millan, Salvatore Torquato, Nikolai Antonov and Polina Kakin for fruitful discussion at various stages of this work. LC and GS acknowledge support from the Francis Crick Institute, which receives its core funding from Cancer Research UK (FC001317), the UK Medical Research Council (FC001317), and the Wellcome Trust (FC001317).

4

Particle Entity in the Doi-Peliti and Response-Field Formalisms

M. Bothe, L. Cocconi, Z. Zhen, G. Pruessner

Preprint arXiv:2205.10409 (2022) [42]
Submitted 19 May 2022

Overview We have seen in the previous Chapter that coarse graining can have a non-trivial effect on our ability to estimate dissipation and thus to infer the degree to which a particular non-equilibrium process breaks time-reversal symmetry. In the context of active matter, which is often concerned with the collective behaviour of a large number of interacting single-particle units, one feature of microscopically resolved models that is generally lost under coarse graining is what we refer to in the following as "particle entity". We say that a mathematical formalism describing interacting units possesses particle entity if, at any given time, the distribution of "stuff" in space is consistent with a set of localised, point-like particles. The standard diffusion equation, for example, does not possess particle entity, since a localised peak of density will eventually spread

into an ever broadening cloud. While for many purposes the loss of particle entity is not a source of concern, for the purpose of entropy production calculations this is still a matter of debate [193, 111]. As a necessary first step in addressing this problem, we have developed a procedure to probe a field-theoretic formalism for particle entity and applied it to the Doi-Peliti path integral, as well as the Martin-Siggia-Rose field theory derived from Dean's equation. While both formalisms indeed possess particle entity, and are in fact promising candidates for further development of field-theoretic tools for the calculation of entropy production, they do so through very different mechanisms. In the case of Dean's equation, particle entity is enforced through a fine-tuned multiplicative noise, suggesting that perturbative treatments of the latter might have direct consequences on particle entity.

Author contributions: GP introduced the chosen signature of particle entity and demonstrated the connection between particle entity and the commutation relations in the Doi-Peliti formalism. LC suggested the reformulation of the signature in terms of full and connected moments. MB performed the induction over connected diagrams presented in Appendix 4.A. MB, LC and ZZ performed the rest of the analysis and wrote the original draft of the manuscript. GP supervised the project throughout and edited the draft at various stages.

Abstract

We introduce a procedure to test a theory for point particle entity, that is, whether said theory takes into account the discrete nature of the constituents of the system. We then identify the mechanism whereby particle entity is enforced in the context of two field-theoretic frameworks designed to incorporate the particle nature of the degrees of freedom, namely the Doi-Peliti field theory and the response field theory that derives from Dean's equation. While the Doi-Peliti field theory encodes the particle nature at a very fundamental level that is easily revealed, demonstrating the same for Dean's equation is more involved and results in a number of surprising diagrammatic identities. We derive those and discuss their implications. These results are particularly pertinent in the context of active matter, whose surprising and often counterintuitive phenomenology rests wholly on the particle nature of the agents and their degrees of freedom as particles.

4.1 Introduction

The mathematical description of non-equilibrium many-particle systems typically requires a choice of scale at which their behaviour is resolved. When the focus is on the collective dynamics of a large ensemble of particles, it can be convenient to disregard some of the microscopic information and to rely on a coarse-grained description in terms of densities $\rho(x,t)$, which are continuous in space. What is generally lost upon such coarse-graining is "particle entity", namely the familiar attribute of classical point particles whose initial property of being localised at one point only is preserved under the dynamics, in other words that individual particles can only exist at one position in space at any given time. The distinction between effective and microscopically resolved theories has recently been debated in the context of active matter and, more specifically, entropy production [202, 64, 109, 51], where different levels of description grant access to different types of information about the degree of irreversibility of a stochastic process [98]. More generally, the study of sparse collections of interacting particles [121, 271, 266] can make it necessary to equip theories with a notion of "granularity" of their constituents. Field theories have traditionally been the most successful approach to capture the physics and mathematics of phenomena emerging from the interaction of many degrees of freedom [171, 135, 289]. The Doi-Peliti formalism , which has a discrete number-state master equation as its starting point, is perhaps the best known example of a path-integral approach that preserves particle entity [56, 227]. Another, less familiar example is the response field or Martin-Siggia-Rose-Janssen-De Dominicis [195, 146, 81] field theory [133] that derives from Dean's equation [75, 114, 292]. While it is generally accepted that these theories correctly describe the behaviour of physical point particles by construction and that they are, in fact, equivalent [175], the precise mechanism whereby this property is enforced, as well as a general procedure to determine whether a given field theory possesses particle entity, have not been identified. We fill this gap in the following by introducing a signature of particle entity, Eq. (4.69), that draws solely on the moments of the integrated number density in a patch Ω of space. These moments can be computed by standard Feynman diagrammatic techniques.

This work is organised as follows. In Section 4.2, we set the scene by introducing the Doi-Peliti field theory and the response field formalism. As an illustrative example, we compute the two-point correlation function of the number density of n_0 non-interacting

diffusive particles, thus highlighting some of the key similarities and differences between the two approaches. In Section 4.3 we formalise the concept of single-particle entity and derive different observables to probe it. This signature of particle entity is then applied to the Doi-Peliti field theory (Section 4.4) and the response field formalism of Dean's equation without interaction (Section 4.5), confirming that both are indeed valid descriptions of physical point particles. In this last section we also discuss the role of integer particle numbers and relate some of the results to a more intuitive probabilistic picture. Finally, in Section 4.6, we summarise our findings and highlight some open questions. Some of the technical details are relegated to the appendices.

4.2 Setting up the formalisms

4.2.1 Doi-Peliti field theory

A Doi-Peliti field theory, sometimes referred to as a coherent-state path integral, is a standard procedure to cast the discrete-state, continuous-time master equation of reaction-diffusion processes in a second quantised form that is amenable to a perturbative treatment [56, 227, 279]. Its derivation starts from the master equation for the probability $P(\{n_i\}, t)$ to find the system in state $\{n_i\} = \{n_0, n_1, ...\}$, that is to find precisely n_i particles at each site i, which is then written in a second quantised form by introducing a Fock space vector $|\{n_i\}\rangle$, together with the ladder operators $a_i^\dagger$ and a_i for creation and annihilation on each lattice site i. The operators satisfy the commutation relations

$$[a_i, a_j^\dagger] = \delta_{ij}, \quad [a_i, a_j] = [a_i^\dagger, a_j^\dagger] = 0 \tag{4.1}$$

and act on $|\{n_i\}\rangle$ according to

$$a_j|\{n_i\}\rangle = n_j|\{n_j - 1\}\rangle, \quad a_j^\dagger|\{n_i\}\rangle = |\{n_j + 1\}\rangle \ , \tag{4.2}$$

so that $a_i^\dagger a_i$ is the number operator counting the number of particles at site i. The notation $\{n_j + 1\}$ and similar is a suggestive shorthand to indicate that this is the same particle number state as $\{n_i\}$ except that the count at site j is increased by one. The

state of the system is thus described by the mixed state

$$|\Psi(t)\rangle = \sum_{\{n_i\}} P(\{n_i\},t)|\{n_j\}\rangle \ , \tag{4.3}$$

which evolves in time according to an imaginary-time Schrödinger equation of the form [56, 227]

$$\partial_t|\Psi(t)\rangle = \hat{A}(a,a^\dagger)|\Psi(t)\rangle \ . \tag{4.4}$$

For a simple diffusive process on a one-dimensional lattice with homogeneous hopping rate h and extinction rate r, the operator $\hat{A}$ reads

$$\hat{A}(a,a^\dagger) = \sum_i h(a_{i+1}^\dagger + a_{i-1}^\dagger - 2a_i^\dagger)a_i - r(a_i^\dagger - 1)a_i \ . \tag{4.5}$$

The formal solution of Eq. (4.4), $|\Psi(t)\rangle = e^{\hat{A}t}|\Psi(0)\rangle$, can then be cast into path-integral form, whereby the creation and annihilation operators are converted to time-dependent fields, denoted $\psi_i^\dagger(t)$ and $\psi_i(t)$, respectively. For technical reasons discussed extensively elsewhere [56, 227], it is convenient at this stage to introduce the so-called Doi-shifted creation field, $\tilde{\psi}_i(t)$, according to the convention $\psi_i^\dagger(t) = 1 + \tilde{\psi}_i(t)$. For the case of simple diffusion, Eq. (4.5), generalised to d dimensions, the action functional of the resulting field theory reads, upon taking the continuum limit,

$$A[\tilde{\psi}(\mathbf{x},t),\psi(\mathbf{x},t)] = \int \mathrm{d}^d x \mathrm{d}t \, \tilde{\psi}(\mathbf{x},t)(\partial_t - D\Delta + r)\psi(\mathbf{x},t) \tag{4.6}$$

and is fully bilinear. In momentum and frequency space it reads

$$A[\tilde{\psi}(\mathbf{k},\omega),\psi(\mathbf{k},\omega)] = \int \text{đ}^d k \, \text{đ}\omega \, \tilde{\psi}(\mathbf{k},\omega)(-\imath\omega + D\mathbf{k}^2 + r)\psi(-\mathbf{k},-\omega) \tag{4.7}$$

where we have used the convention

$$\psi(\mathbf{x},t) = \int \text{đ}^d k \, \text{đ}\omega \ e^{\imath\mathbf{k}\cdot\mathbf{x}} e^{-\imath\omega t}\psi(\mathbf{k},\omega) \quad \text{and} \quad \psi(\mathbf{k},\omega) = \int \mathrm{d}^d x \mathrm{d}t \ e^{-\imath\mathbf{k}\cdot\mathbf{x}} e^{\imath\omega t}\psi(\mathbf{x},t) \, , \tag{4.8}$$

with $\text{đ}^d k \ = \mathrm{d}^d k \, /(2\pi)^d$ and $\text{đ}\omega \ = \mathrm{d}^d\omega \, /(2\pi)$ (similarly for $\tilde{\psi}$). We will change freely between different representations.

The diffusive propagator can be obtained by Gaussian integration and reads in k, ω

$$\langle \psi(\mathbf{k},\omega)\tilde{\psi}(\mathbf{k}',\omega')\rangle = \frac{\delta(\omega+\omega')\delta(\mathbf{k}+\mathbf{k}')}{-\mathring{\imath}\omega + D\mathbf{k}^2 + r} \hat{=} \quad \mathbf{k},\omega \quad \underline{\mathbf{k}',\omega'} \quad , \tag{4.9}$$

with $\delta(\mathbf{k}) = (2\pi)\delta(\mathbf{k})$ and $\delta(\omega) = (2\pi)\delta(\omega)$. Henceforth we will use the symbol $\hat{=}$ to indicate equivalence between diagrams and other mathematical expressions. All diagrams are to be read from right to left. Expressing fields in x, t, the propagator reads

$$\langle \psi(\mathbf{x},t)\tilde{\psi}(\mathbf{x}',t')\rangle = \theta(t-t')\left(\frac{1}{4\pi D(t-t')}\right)^{d/2} \exp\left(-\frac{(\mathbf{x}-\mathbf{x}')^2}{4D(t-t')}\right) \ , \tag{4.10}$$

for $r \to 0^+$, with the Heaviside theta function $\theta(t)$ enforcing causality. The mass r has solely the role to regularise the large t behaviour and establish causality. In the following, we may take the limit $r \to 0^+$ whenever convenient. For completeness, the propagator in mixed momentum-time representation reads

$$\langle \psi(\mathbf{k},t)\tilde{\psi}(\mathbf{k}',t')\rangle = \theta(t-t')\delta(\mathbf{k}+\mathbf{k}')e^{-Dk^2(t-t')} \ . \tag{4.11}$$

A general observable $\mathcal{O}(\{n_i\})$ in the Doi-Peliti formalism corresponds to a composite operator $\hat{\mathcal{O}}(a_i, a_i^\dagger)$, which we assume to be normal ordered, and which is defined by acting on the pure state $|\{n_i\}\rangle$ according to $\hat{\mathcal{O}}(a_i, a_i^\dagger)|\{n_i\}\rangle = \mathcal{O}(\{n_i\})|\{n_i\}\rangle$. Its expectation translates into a path integral according to the following procedure [215]

$$\begin{aligned}
\langle \mathcal{O} \rangle &= \sum_{\{n_i\}} \mathcal{O}(\{n_i\}) P(\{n_i\},t)|\{n_j\}\rangle && (4.12)\\
&= \langle \text{⛭}|\hat{\mathcal{O}}(a_i, a_i^\dagger)e^{\tilde{A}t}|\Psi(0)\rangle && (4.13)\\
&= \int \mathcal{D}\psi\mathcal{D}\tilde{\psi}\ \hat{\mathcal{O}}(\psi(t),\tilde{\psi}(t)+1)\ e^{A[\tilde{\psi},\psi]}\mathbb{I}(\tilde{\psi}(0)+1) && (4.14)
\end{aligned}$$

where we have introduced the coherent state,

$$\langle \text{⛭}| = \sum_{\{n_i\}} \langle \{n_i\}| \tag{4.15}$$

with $\sum_{\{n_i\}}\langle\{n_i\}|$ summing over all n-particle occupation number states, as well as the

initialisation operator $\mathbb{I}(a_i^\dagger)$, which satisfies $\mathbb{I}(a_i^\dagger)|0\rangle = |\Psi(0)\rangle$, with $|0\rangle$ the vacuum state. For an initial condition where m_i particles are placed at each site i at time $t = 0$, the initialisation appears within the path integral Eq. (4.14) as

$$\mathbb{I}(\tilde{\psi}(0) + 1) = \prod_i (\tilde{\psi}_i(0) + 1)^{m_i} = \prod_i \sum_{k=0}^{m_i} \binom{m_i}{k} \tilde{\psi}_i^k(0) \ . \tag{4.16}$$

4.2.2 Dean's equation in the response field formalism

Dean's equation [75] is a stochastic differential equation of the Itô type obeyed by the number density function $\rho(\mathbf{x}, t)$ for a system of Langevin processes interacting via a pairwise potential. It is an exact mapping of, and thus contains the same information as, the full set of Langevin equations for the individual "single particle" processes. It reads

$$\partial_t \rho(\mathbf{x}, t) = \nabla \cdot \left(\rho \nabla \left. \frac{\delta F[\rho]}{\delta \rho} \right|_{\rho(\mathbf{x},t)} \right) + \nabla \cdot (\rho^{1/2} \boldsymbol{\eta}(\mathbf{x}, t)) + \sum_i n_i \delta(t - t_i) \delta(\mathbf{x} - \mathbf{x}_i) \tag{4.17}$$

where $F[\rho]$ denotes the free energy functional, defined as

$$F[\rho(\mathbf{x})] = \int \mathrm{d}^d x \, \rho(\mathbf{x}) \left(V(\mathbf{x}) + D \log(\rho(\mathbf{x})) + \int \mathrm{d}^d y \, U(\mathbf{x} - \mathbf{y}) \rho(y) \right) \ , \tag{4.18}$$

with $V(\mathbf{x})$ a general single-particle potential and $U(\mathbf{x} - \mathbf{y})$ a translationally invariant pairwise interaction potential. The last term on the right-hand side of Eq. (4.17) describes the initialisation of $n_i \in \mathbb{Z}$ particles in state $\mathbf{x}_i$ at time t_i so that $\lim_{t \to -\infty} \rho(\mathbf{x}, t) = 0$. We will make the simplifying assumption of having only a single non-zero n_i, namely n_0, and generalise our result in Appendix 4.B. The vector-valued noise $\boldsymbol{\eta}(\mathbf{x}, t) \in \mathbb{R}^d$ is an uncorrelated white noise with covariance

$$\langle \eta_\mu(\mathbf{x}, t) \eta_\nu(\mathbf{x}', t') \rangle = 2D \delta_{\mu\nu} \delta(t - t') \delta(\mathbf{x} - \mathbf{x}') \ , \tag{4.19}$$

for $\mu, \nu = 1, 2, ..., d$. The unique feature of Dean's formalism is the nature of the noise term in Eq. (4.17), $\nabla \cdot (\rho^{1/2} \boldsymbol{\eta})$, which is both conservative and Itô-multiplicative, thus conserving the total particle number while preventing fluctuations from producing regions of negative density. Following the standard procedure [133, 289], which requires

special attention due to the multiplicative nature of the noise [139, 292], Dean's equation (4.17) for the time and space dependent field $\rho(\mathbf{x}, t)$ can be cast as a response field, or Martin-Siggia-Rose-Janssen-De Dominicis, field theory with action

$$A[\rho, \tilde{\rho}] = \int \mathrm{d}^d x \mathrm{d}t \, \tilde{\rho} \left(\partial_t \rho - \nabla \cdot \rho \nabla \left. \frac{\delta F[\rho]}{\delta \rho} \right|_{\rho(\mathbf{x},t)} \right) - \rho D (\nabla \tilde{\rho})^2 - \tilde{\rho} \sum_i n_i \delta(t - t_i) \delta(\mathbf{x} - \mathbf{x}_i) \, , \tag{4.20}$$

which simplifies to

$$A[\rho, \tilde{\rho}] = \int \mathrm{d}^d x \mathrm{d}t \, \tilde{\rho}(\mathbf{x}, t) \left(\partial_t \rho(\mathbf{x}, t) - D \Delta \rho(\mathbf{x}, t) \right) - \tilde{\rho} \sum_i n_i \delta(t - t_i) \delta(\mathbf{x} - \mathbf{x}_i) - \rho D (\nabla \tilde{\rho})^2 \tag{4.21}$$

$$= \int \mathrm{đ}^d k \, \mathrm{đ}\omega \, \tilde{\rho}(-\mathbf{k}, -\omega)(-\mathring{\imath}\omega + D\mathbf{k}^2) \rho(\mathbf{k}, \omega) - \tilde{\rho}(\mathbf{k}, \omega) \sum_i n_i e^{\mathring{\imath}\mathbf{k}\cdot\mathbf{x}_i} e^{-\mathring{\imath}\omega t_i}$$

$$+ \int \mathrm{đ}^d k \mathrm{đ}^d k' \, \mathrm{đ}\omega \, \mathrm{đ}\omega' \, D(\mathbf{k} \cdot \mathbf{k}') \tilde{\rho}(\mathbf{k}, \omega) \tilde{\rho}(\mathbf{k}', \omega') \rho(-(\mathbf{k} + \mathbf{k}'), -(\omega + \omega')) \tag{4.22}$$

in the case of non-interacting particles undergoing simple diffusion without external potential. Unlike the Doi-Peliti path integral, Eq. (4.14), the initialisation here shows up as a term in the action. In a diagrammatic perturbation theory, these n_i particles starting from positions $\mathbf{x}_i$, or, as a matter of fact, only one such position, $\mathbf{x}_0$ with n_0 particles starting from there, will be shown as a small, filled circle acting as a source,

 . (4.23)

The presence of the source spoils translational invariance and as a result, the hallmark δ-function as it normally multiplies any correlation function, say $\delta(\mathbf{k}_0 + \mathbf{k}_1 + \ldots + \mathbf{k}_n)$ will be replaced by

$$\int \mathrm{đ}^d k_0 \, \exp\{\mathring{\imath}\mathbf{k}_0 \cdot \mathbf{x}_0\} \delta(\mathbf{k}_0 + \mathbf{k}_1 + \ldots + \mathbf{k}_n) = \exp\{\mathring{\imath}(\mathbf{k}_1 + \ldots + \mathbf{k}_n) \cdot \mathbf{x}_0\} \, . \tag{4.24}$$

Where readability is improved by it, we will retain the integral.

The expectation value of a field-dependent observable $\mathcal{O}[\rho]$ can then be computed via the path integral

$$\langle \mathcal{O}[\rho] \rangle = \int \mathcal{D}\rho \mathcal{D}\tilde{\rho} \, \mathcal{O}[\rho] \exp\{-A[\rho, \tilde{\rho}]\} \tag{4.25}$$

where $\tilde{\rho}$ is the purely imaginary response field. The normalisation is chosen such that $\langle 1 \rangle = 1$. The action A is then split into a bilinear and an interacting part, denoted A_0 and A_{int} respectively, according to

$$A_0[\rho, \tilde{\rho}] = \int \mathrm{d}^d x \mathrm{d}t \, \tilde{\rho} \left(\partial_t \rho - D \Delta \rho \right) \tag{4.26}$$

and

$$\begin{aligned} A_{\text{int}}[\rho, \tilde{\rho}] = - \int \mathrm{d}^d x \mathrm{d}t \Bigg\{ & \rho(\mathbf{x}, t) D (\nabla \tilde{\rho}(\mathbf{x}, t))^2 \\ & + \tilde{\rho}(\mathbf{x}, t) \nabla_{\mathbf{x}} \cdot \left(\rho(\mathbf{x}, t) \nabla_{\mathbf{x}} \left[V(\mathbf{x}) + \int \mathrm{d}^d y \;\; U(\mathbf{x} - \mathbf{y}) \rho(\mathbf{y}, t) \right] \right) \\ & + \tilde{\rho}(\mathbf{x}, t) \sum_i n_i \delta(\mathbf{x} - \mathbf{x}_i) \delta(t - t_i) \Bigg\} \end{aligned} \tag{4.27}$$

$$\begin{aligned} = & \int \text{đ}^d k_{1,2,3} \;\; \text{đ}\omega_{1,2,3} \, \text{đ}(\mathbf{k}_1 + \mathbf{k}_2 + \mathbf{k}_3) \text{đ}(\omega_1 + \omega_2 + \omega_3) \\ & \Big\{ \rho(\mathbf{k}_1, \omega_1) D (\mathbf{k}_2 \cdot \mathbf{k}_3) \tilde{\rho}(\mathbf{k}_2, \omega_2) \tilde{\rho}(\mathbf{k}_3, \omega_3) \\ & + \tilde{\rho}(\mathbf{k}_1, \omega_1) ((\mathbf{k}_2 + \mathbf{k}_3) \cdot \mathbf{k}_3) \rho(\mathbf{k}_2, \omega_2) \Big[V(\mathbf{k}_3) \text{đ}(\omega_3) + U(\mathbf{k}_3) \rho(\mathbf{k}_3, \omega_3) \Big] \Big\} \\ & - \int \text{đ}^d k \;\; \text{đ}\omega \, \tilde{\rho}(\mathbf{k}, \omega) \sum_i n_i \exp\{ \mathring{\imath} \mathbf{k} \cdot \mathbf{x}_i \} \exp\{ - \mathring{\imath} \omega t_i \} \end{aligned} \tag{4.28}$$

Finally, expectations are computed in a perturbation theory about the bilinear theory using

$$\langle \mathcal{O}[\rho] \rangle = \sum_{n=0}^{\infty} \left\langle \frac{(-A_{\text{int}}[\rho, \tilde{\rho}])^n}{n!} \mathcal{O}[\rho] \right\rangle_0 \;\; , \tag{4.29}$$

where

$$\langle \bullet \rangle_0 = \int \mathcal{D}\rho \, \mathcal{D}\tilde{\rho} \;\, \bullet \exp\{ - A_0[\rho, \tilde{\rho}] \} \tag{4.30}$$

denotes expectation with respect to the bilinear action, Eq. (4.26). The right hand side of Eq. (4.29) involves products of fields and the Wick-Isserlis theorem [171] can be

invoked to express these in terms of the bare propagator,

$$G(\mathbf{x}-\mathbf{x}',t-t') = \langle \rho(\mathbf{x},t)\tilde{\rho}(\mathbf{x}',t')\rangle_0 \mathrel{\hat{=}} \quad \underset{\mathbf{x},t}{\bullet}\!\!-\!\!\!-\!\!\!-\!\!\!-\!\!\bullet_{\mathbf{x}',t'} \quad , \tag{4.31}$$

obtained from the bilinear action. In d dimensions, the bare propagator reads

$$G(\mathbf{x}-\mathbf{x}',t-t') = \theta(t-t')\left(\frac{1}{4\pi D(t-t')}\right)^{d/2} \exp\left(-\frac{(\mathbf{x}-\mathbf{x}')^2}{4D(t-t')}\right) \ , \tag{4.32}$$

with the Heaviside theta function $\theta(t)$ enforcing causality. This propagator is identical to that of the corresponding Doi-Peliti field theory, Eq. (4.10). For later use, we recall the form of the propagator in momentum-frequency representation,

$$\langle \rho(\mathbf{k},\omega)\tilde{\rho}(\mathbf{k}',\omega')\rangle_0 = \frac{\delta(\mathbf{k}+\mathbf{k}')\delta(\omega+\omega')}{-\mathring{\imath}\omega + D\mathbf{k}^2 + r} \ , \tag{4.33}$$

which we have amended by a mass $r \to 0^+$ to enforce causality, as Eq. (4.9). Further, we introduce the mixed momentum-time representation,

$$\langle \rho(\mathbf{k},t)\tilde{\rho}(\mathbf{k}',t')\rangle_0 = \theta(t-t')\delta(\mathbf{k}+\mathbf{k}')\exp\left\{-D(t-t')\mathbf{k}^2\right\} \ , \tag{4.34}$$

see Eq. (4.11). For non-interacting particles in a flat potential, $\nabla V(\mathbf{x}) = 0$, $\nabla U(\mathbf{x}) = 0$, the bare propagator equals the full propagator,

$$\langle \rho(\mathbf{k},t)\tilde{\rho}(\mathbf{k}',t')\rangle = \langle \rho(\mathbf{k},t)\tilde{\rho}(\mathbf{k}',t')\rangle_0 \tag{4.35}$$

as the only non-linear term in the action is the amputated three-point vertex

$$-\rho D(\nabla\tilde{\rho})^2 \mathrel{\hat{=}} \tag{4.36}$$

with the dashes on the propagators denoting spatial derivatives acting on the response fields and the dotted line the scalar product of these derivatives. The presence of such a vertex in the free particle case is a non-trivial feature of Dean's equation and clashes somewhat with the notion of 'interaction' associated with terms of order higher than bilinear [289]. As we will demonstrate below, Eq. (4.36), which we will refer to interchangeably as *Dean's vertex* or a *virtual branching* vertex, is the term that implements the particle nature of the degrees of freedom within the Dean framework. In

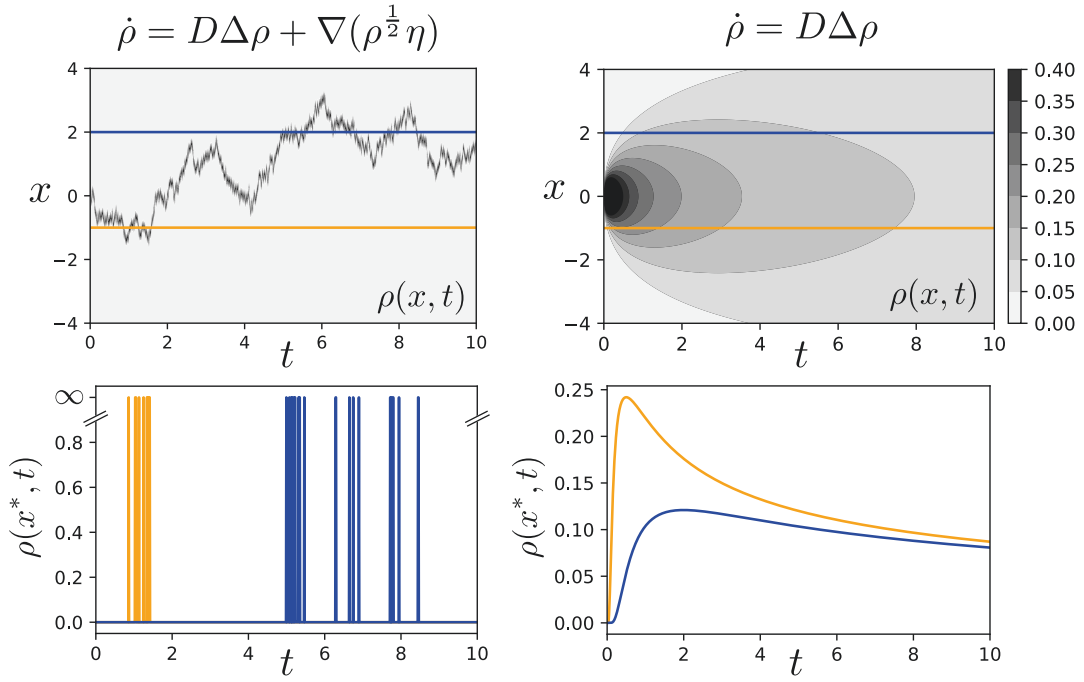

Figure 4.1: The time-dependent number density $\rho(x,t)$ for a physical point particle undergoing diffusion is expected to remain localised under the dynamics, indicating that the particle can only occupy one position in space at any given time. While this property is preserved under Dean's dynamics (left column), it is generally lost when resorting to effective descriptions, such as the classical diffusion equation (right column). This difference is most obvious when measuring the instantaneous particle number density at two points a finite distance away from each other (bottom row).

contrast to Doi-Peliti, particle entity in the response field formalism of Dean's equation is a perturbative feature. The effect of Dean's vertex is illustrated in Fig. 4.1 by comparison with the standard diffusion equation, which lacks particle entity.

The Doi-Peliti field theory and the response field field theory derived from Dean's equation can be mapped onto each other by means of a Cole-Hopf transformation of the fields [175],

$$\psi^\dagger \to e^{\tilde{\rho}}, \quad \psi \to \rho e^{-\tilde{\rho}} \, . \tag{4.37}$$

This equivalence implies that the two formalisms should be equally capable of capturing particle entity. The precise mechanisms by which each does so, however, turn out to be very different, as we will see in detail in Sections 4.4 and 4.5.

4.2.3 Example: the two-point density correlation function

To illustrate the similarities and differences between the two formalisms introduced above, we now calculate the two-point correlation function of the particle number density for n_0 non-interacting diffusive particles in a flat potential, $\nabla V(\mathbf{x}) = 0$ and $\nabla U(\mathbf{x}) = 0$, all initialised at the same position x_0 and time t_0, first in the Doi-Peliti scheme and then using Dean's equation. While the result of this detailed calculation is somewhat trivial and can be derived by straightforward probabilistic arguments, its derivation elucidates certain formalism-specific cancellation mechanisms that will play an important role in the remainder of this work. The reader interested in the generic definition of particle entity but not in the details of the field theoretic approach can skip directly to Section 4.3.

We first use the parameterisation of the field theories in $\mathbf{k}$ and ω, which is very commonly used in field theories. In real-space and time, the two-point correlation function $C(\mathbf{x}_1, \mathbf{x}_2, t_1, t_2)$ in the Doi-Peliti framework is the observable [289, 56]

$$
\begin{aligned}
C(\mathbf{x}_1, \mathbf{x}_2, t_1, t_2) &= \left\langle \left(\psi^\dagger(\mathbf{x}_2, t_2)\psi(\mathbf{x}_2, t_2)\right)\left(\psi^\dagger(\mathbf{x}_1, t_1)\psi(\mathbf{x}_1, t_1)\right)\psi^{\dagger n_0}(\mathbf{x}_0, t_0)\right\rangle && (4.38)\\
&= \binom{n_0}{1}\left\langle \psi(\mathbf{x}_2, t_2)\widetilde{\psi}(\mathbf{x}_1, t_1)\right\rangle\left\langle \psi(\mathbf{x}_1, t_1)\widetilde{\psi}(\mathbf{x}_0, t_0)\right\rangle && (4.39)\\
&\quad + \binom{n_0}{1}\left\langle \psi(\mathbf{x}_1, t_1)\widetilde{\psi}(\mathbf{x}_2, t_2)\right\rangle\left\langle \psi(\mathbf{x}_2, t_2)\widetilde{\psi}(\mathbf{x}_0, t_0)\right\rangle\\
&\quad + 2\binom{n_0}{2}\left\langle \psi(\mathbf{x}_2, t_2)\widetilde{\psi}(\mathbf{x}_0, t_0)\right\rangle\left\langle \psi(\mathbf{x}_1, t_1)\widetilde{\psi}(\mathbf{x}_0, t_0)\right\rangle
\end{aligned}
$$

$$
\hat{=}\binom{n_0}{1}\ \mathbf{x}_2, t_2 \xrightarrow{\quad\mathbf{x}_1, t_1\quad} \mathbf{x}_0, t_0 \qquad + \qquad \binom{n_0}{1}\ \mathbf{x}_1, t_1 \xrightarrow{\quad\mathbf{x}_2, t_2\quad} \mathbf{x}_0, t_0 \qquad + \qquad 2\binom{n_0}{2}\ \begin{matrix}\mathbf{x}_1, t_1 \quad \mathbf{x}_0, t_0\\ \mathbf{x}_2, t_2 \quad \mathbf{x}_0, t_0\end{matrix} \tag{4.40}
$$

where we assume $\mathbf{x}_1 \neq \mathbf{x}_2$ to avoid the special case of non-commutation of the operators. The high number of terms in Eq. (4.38) is due to the Doi-shift, which splits each daggered creator field in two terms, $\psi^\dagger = 1 + \widetilde{\psi}$. This turns the contribution of the initial particles into $\psi^{\dagger n_0} = \sum_k^{n_0} \binom{n_0}{k}\widetilde{\psi}^{n_0}$. The vertices made from a crossed circle in Eq. (4.40) are meant to indicate an annihilation field at the indicated position and time with immediate re-creation. Eq. (4.38) has the generic form of a two-point correlation

function in the Doi-Peliti framework without interaction.

Eq. (4.39) is still expressed in real space and direct time and needs to be Fourier-transformed to write it in the common $\mathbf{k}, \omega$ parameterisation. Each of the three terms in Eq. (4.39) requires four integrals in $\mathbf{k}$ and four in ω, for example

$$n_0 \quad \underset{\mathbf{x}_2, t_2}{\overset{\mathbf{x}_1, t_1}{\otimes}} \quad \mathbf{x}_0, t_0 \tag{4.41}$$

$$\hat{=} n_0 \int \mathrm{đ}^d k_2 \mathrm{đ}^d k_1' \mathrm{đ}^d k_1 \mathrm{đ}^d k_0 \, \mathrm{đ}\omega_2 \, \mathrm{đ}\omega_1' \, \mathrm{đ}\omega_1 \, \mathrm{đ}\omega_0 \, \frac{\delta(\mathbf{k}_2 + \mathbf{k}_1')\delta(\omega_2 + \omega_1')}{-\mathring{\imath}\omega_2 + D\mathbf{k}_2^2 + r} \frac{\delta(\mathbf{k}_1 + \mathbf{k}_0)\delta(\omega_1 + \omega_0)}{-\mathring{\imath}\omega_1 + D\mathbf{k}_1^2 + r} \tag{4.42}$$

$$\times \exp\{\mathring{\imath}(\mathbf{k}_2 \cdot \mathbf{x}_2 + \mathbf{k}_1' \cdot \mathbf{x}_1 + \mathbf{k}_1 \cdot \mathbf{x}_1 + \mathbf{k}_0 \cdot \mathbf{x}_0)\} \exp\{-\mathring{\imath}(\omega_2 t_2 + \omega_1' t_1 + \omega_1 t_1 + \omega_0 t_0)\}$$

drawing on the propagator introduced in Eq. (4.9). Using the δ-functions, the integrals in each term are immediately reduced to only two, all differing solely in the arguments of the exponentials:

$$\begin{aligned} C(\mathbf{x}_1, \mathbf{x}_2, t_1, t_2) = \int \mathrm{đ}^d k_2 \mathrm{đ}^d k_1 \, \mathrm{đ}\omega_2 \, \mathrm{đ}\omega_1 \, \frac{1}{-\mathring{\imath}\omega_2 + D\mathbf{k}_2^2 + r} \frac{1}{-\mathring{\imath}\omega_1 + D\mathbf{k}_1^2 + r} \\ \times \Big\{ n_0 \exp\{\mathring{\imath}(\mathbf{k}_2 \cdot (\mathbf{x}_2 - \mathbf{x}_1) + \mathbf{k}_1 \cdot (\mathbf{x}_1 - \mathbf{x}_0))\} \exp\{-\mathring{\imath}(\omega_2(t_2 - t_1) + \omega_1(t_1 - t_0))\} \\ + n_0 \exp\{\mathring{\imath}(\mathbf{k}_2 \cdot (\mathbf{x}_2 - \mathbf{x}_0) + \mathbf{k}_1 \cdot (\mathbf{x}_1 - \mathbf{x}_2))\} \exp\{-\mathring{\imath}(\omega_2(t_2 - t_0) + \omega_1(t_1 - t_2))\} \\ + n_0(n_0 - 1) \exp\{\mathring{\imath}(\mathbf{k}_2 \cdot (\mathbf{x}_2 - \mathbf{x}_0) + \mathbf{k}_1 \cdot (\mathbf{x}_1 - \mathbf{x}_0))\} \exp\{-\mathring{\imath}(\omega_2(t_2 - t_0) + \omega_1(t_1 - t_0))\} \Big\} \end{aligned} \tag{4.43}$$

with $r \to 0^+$ still to be taken. The first of the three terms in the integrand describes the propagation of any of n_0 particles from $\mathbf{x}_0$ at t_0 to $\mathbf{x}_1$ at t_1 and from there to $\mathbf{x}_2$ at t_2. This term will contribute only if $t_2 \geq t_1 \geq t_0$. The second term describes a similar process, from $\mathbf{x}_0$ at t_0 to $\mathbf{x}_2$ at t_2 and from there to $\mathbf{x}_1$ at t_1, contributing only if $t_1 \geq t_2 \geq t_0$. The last term describes the propagation of two independent particles from $\mathbf{x}_0$ at t_0 to $\mathbf{x}_1$ at t_1 and another one from $\mathbf{x}_0$ at t_0 to $\mathbf{x}_2$ at t_2. There are $n_0(n_0 - 1)$ such pairs. If $n_0 \leq 1$, the last term vanishes, leaving only the first two terms, both of which vanish if $t_1 = t_2$ and $\mathbf{x}_1 \neq \mathbf{x}_2$ as we will show below, because a *particle* cannot possibly be found at two different places simultaneously. Eq. (4.43) completes the derivation of the correlation function in the Doi-Peliti framework.

To derive the correlation function in Dean's framework, we use the action as stated in Eq. (4.21) with both the interaction and the source treated perturbatively. The role of

the creator fields in the field theory of Dean's equation is very different from Doi-Peliti. In the Dean framework, the two-point correlation function is

$$C(\mathbf{x}_1,\mathbf{x}_2,t_1,t_2) = \langle \rho(\mathbf{x}_2,t_2)\rho(\mathbf{x}_1,t_1)\rangle \mathrel{\hat{=}}$$

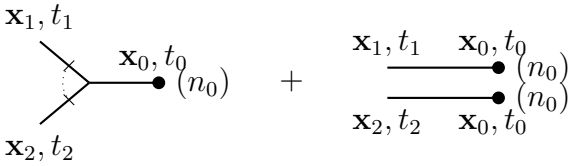

(4.44)

as every field $\rho(\mathbf{x},t)$ can be matched with a creator field from the perturbative part of the action, shown as a small filled circle at the right end of the incoming propagators. Each such creator field appears with a *coupling* n_0, which we have highlighted by writing it in brackets behind each source in the diagram. While the second term in Eq. (4.44) is structurally identical to the last term in Eq. (4.40) and indeed captures the same process, the pre-factors of the two differ by n_0. The first two terms in Eq. (4.40) on the other hand seem to be absent from Eq. (4.44). In turn, the first diagram of Eq. (4.44), is solely due to the Dean-vertex Eq. (4.36) and therefore absent in Doi-Peliti, Eq. (4.40). Writing this term in $\mathbf{k},\omega$ gives

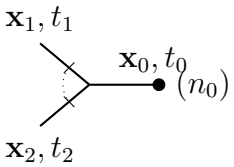

$$\begin{aligned}
&\hat{=} \int \text{đ}^d k_2 \text{đ}^d k_1 \, \text{đ}\omega_2 \, \text{đ}\omega_1 \\
&\exp\{\mathring{\imath}(\mathbf{k}_2\cdot(\mathbf{x}_2-\mathbf{x}_0)+\mathbf{k}_1\cdot(\mathbf{x}_1-\mathbf{x}_0))\}\exp\{-\mathring{\imath}(\omega_2(t_2-t_0)+\omega_1(t_1-t_0))\} \\
&\times(-2n_0 D\mathbf{k}_1\cdot\mathbf{k}_2)\frac{1}{-\mathring{\imath}\omega_2+D\mathbf{k}_2^2+r}\frac{1}{-\mathring{\imath}\omega_1+D\mathbf{k}_1^2+r}\frac{1}{-\mathring{\imath}(\omega_1+\omega_2)+D(\mathbf{k}_1+\mathbf{k}_2)^2+r}
\end{aligned} \tag{4.45}$$

using Eq. (4.33) for the propagator and where the factor $(-2n_0 D\mathbf{k}_1\cdot\mathbf{k}_2)$ is due to the sign of the interaction term in the action Eq. (4.21), including a factor 2 from symmetry.

The second term in Eq. (4.44) can be read off from Eqs. (4.40) and (4.43). Its pre-factor

of n_0^2 has to be split into $n_0^2 = n_0(n_0-1)+n_0$ to reveal the cancellation mechanism,

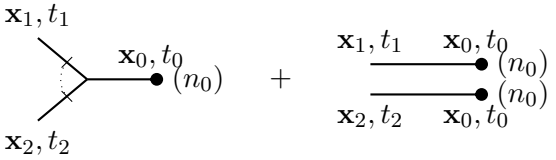

(4.46)

$$\hat{=} \int \text{đ}^d k_2 \text{đ}^d k_1 \, \text{đ}\omega_2 \, \text{đ}\omega_1$$

$$\exp\{\mathring{\imath}(\mathbf{k}_2 \cdot (\mathbf{x}_2 - \mathbf{x}_0) + \mathbf{k}_1 \cdot (\mathbf{x}_1 - \mathbf{x}_0))\} \exp\{-\mathring{\imath}(\omega_2(t_2 - t_0) + \omega_1(t_1 - t_0))\} \tag{4.47}$$

$$\times \frac{1}{-\mathring{\imath}\omega_2 + D\mathbf{k}_2^2 + r} \frac{1}{-\mathring{\imath}\omega_1 + D\mathbf{k}_1^2 + r} \left(\frac{-2n_0 D \mathbf{k}_1 \cdot \mathbf{k}_2}{-\mathring{\imath}(\omega_1+\omega_2) + D(\mathbf{k}_1+\mathbf{k}_2)^2 + r} + n_0 + n_0(n_0-1) \right) \tag{4.48}$$

$$= \int \text{đ}^d k_2 \text{đ}^d k_1 \, \text{đ}\omega_2 \, \text{đ}\omega_1$$

$$\exp\{\mathring{\imath}(\mathbf{k}_2 \cdot (\mathbf{x}_2 - \mathbf{x}_0) + \mathbf{k}_1 \cdot (\mathbf{x}_1 - \mathbf{x}_0))\} \exp\{-\mathring{\imath}(\omega_2(t_2 - t_0) + \omega_1(t_1 - t_0))\} \tag{4.49}$$

$$\times \Big\{ n_0 \frac{1}{-\mathring{\imath}(\omega_1+\omega_2) + D(\mathbf{k}_1+\mathbf{k}_2)^2 + r} \tag{4.50}$$

$$\times \left(\frac{1}{-\mathring{\imath}\omega_2 + D\mathbf{k}_2^2 + r} + \frac{1}{-\mathring{\imath}\omega_1 + D\mathbf{k}_1^2 + r} - \frac{r}{(-\mathring{\imath}\omega_1 + D\mathbf{k}_1^2 + r)(-\mathring{\imath}\omega_2 + D\mathbf{k}_2^2 + r)} \right)$$

$$+ n_0(n_0-1) \frac{1}{-\mathring{\imath}\omega_2 + D\mathbf{k}_2^2 + r} \frac{1}{-\mathring{\imath}\omega_1 + D\mathbf{k}_1^2 + r} \Big\} \, .$$

The term proportional to r in the numerator eventually vanishes when $r \to 0$. To see now that Eq. (4.50) is in fact identical to the first two terms in Eqs. (4.40) and (4.43) requires a simple substitution of the dummy variables, for example $\mathbf{k}_1 + \mathbf{k}_2$ becoming

$\mathbf{k}_1$,

$$\int \text{đ}^d k_2 \text{đ}^d k_1 \, \text{đ}\omega_2 \, \text{đ}\omega_1$$

$$\exp\{\mathring{\imath}(\mathbf{k}_2 \cdot (\mathbf{x}_2 - \mathbf{x}_0) + \mathbf{k}_1 \cdot (\mathbf{x}_1 - \mathbf{x}_0))\} \exp\{-\mathring{\imath}(\omega_2(t_2 - t_0) + \omega_1(t_1 - t_0))\} \tag{4.51}$$

$$\times \frac{1}{-\mathring{\imath}(\omega_1 + \omega_2) + D(\mathbf{k}_1 + \mathbf{k}_2)^2 + r} \frac{1}{-\mathring{\imath}\omega_2 + D\mathbf{k}_2^2 + r} \tag{4.52}$$

$$= \int \text{đ}^d k_2 \text{đ}^d k_1 \, \text{đ}\omega_2 \, \text{đ}\omega_1$$

$$\exp\{\mathring{\imath}(\mathbf{k}_2 \cdot (\mathbf{x}_2 - \mathbf{x}_1) + \mathbf{k}_1 \cdot (\mathbf{x}_1 - \mathbf{x}_0))\} \exp\{-\mathring{\imath}(\omega_2(t_2 - t_1) + \omega_1(t_1 - t_0))\} \tag{4.53}$$

$$\times \frac{1}{-\mathring{\imath}\omega_1 + D\mathbf{k}_1^2 + r} \frac{1}{-\mathring{\imath}\omega_2 + D\mathbf{k}_2^2 + r} \, . \tag{4.54}$$

In summary, after pairing in Eq. (4.50) the interaction term of Dean's equation with the two independent propagators, the field theory of Dean's equation reproduces the two-point correlation function as the Doi-Peliti framework, Eq. (4.43), except for a term proportional to r which vanishes in the limit of $r \to 0$:

$$C(\mathbf{x}_1, \mathbf{x}_2, t_1, t_2) = \langle \rho(\mathbf{x}_2, t_2) \rho(\mathbf{x}_1, t_1) \rangle \mathrel{\hat{=}}$$

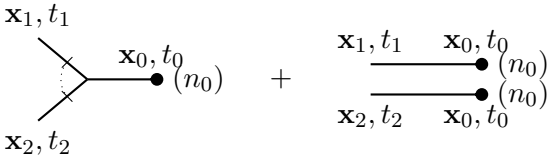

(4.55)

$$\mathrel{\hat{=}} \int \text{đ}^d k_2 \text{đ}^d k_1 \, \text{đ}\omega_2 \, \text{đ}\omega_1 \, \frac{1}{-\mathring{\imath}\omega_2 + D\mathbf{k}_2^2 + r} \frac{1}{-\mathring{\imath}\omega_1 + D\mathbf{k}_1^2 + r} \tag{4.56}$$

$$\times \Big\{ n_0 \exp\{\mathring{\imath}(\mathbf{k}_2 \cdot (\mathbf{x}_2 - \mathbf{x}_1) + \mathbf{k}_1 \cdot (\mathbf{x}_1 - \mathbf{x}_0))\} \exp\{-\mathring{\imath}(\omega_2(t_2 - t_1) + \omega_1(t_1 - t_0))\}$$

$$+ n_0 \exp\{\mathring{\imath}(\mathbf{k}_2 \cdot (\mathbf{x}_2 - \mathbf{x}_0) + \mathbf{k}_1 \cdot (\mathbf{x}_1 - \mathbf{x}_2))\} \exp\{-\mathring{\imath}(\omega_2(t_2 - t_0) + \omega_1(t_1 - t_2))\}$$

$$- n_0 \frac{r}{-\mathring{\imath}(\omega_1 + \omega_2) + D(\mathbf{k}_1 + \mathbf{k}_2)^2 + r}$$

$$\times \exp\{\mathring{\imath}(\mathbf{k}_2 \cdot (\mathbf{x}_2 - \mathbf{x}_0) + \mathbf{k}_1 \cdot (\mathbf{x}_1 - \mathbf{x}_0))\} \exp\{-\mathring{\imath}(\omega_2(t_2 - t_0) + \omega_2(t_1 - t_0))\}$$

$$+ n_0(n_0 - 1) \exp\{\mathring{\imath}(\mathbf{k}_2 \cdot (\mathbf{x}_2 - \mathbf{x}_0) + \mathbf{k}_1 \cdot (\mathbf{x}_1 - \mathbf{x}_0))\} \exp\{-\mathring{\imath}(\omega_2(t_2 - t_0) + \omega_1(t_1 - t_0))\} \Big\} \, .$$

This concludes the demonstration that the Doi-Peliti framework and Dean's equation produce identical results for the two-point correlation function. Eq. (4.50) illustrates the central cancellation mechanism, which we generalise to the relevant observables

below, in particular Appendix 4.A. As Eq. (4.36) is a perturbative term, the resulting branching diagrams in Eq. (4.55) *discount* contributions due to independent particle movement, shown as two parallel propagators in Eq. (4.55), of which there are n_0^2 rather than $n_0(n_0-1)$.

Performing the calculation above immediately in direct time and real space is most easily done assuming a particular time ordering, say $t_2 > t_1 > t_0$. In that case, Doi-Peliti produces

$$\begin{aligned} C(\mathbf{x}_1,\mathbf{x}_2,t_1,t_2) = n_0 \frac{e^{-\frac{(\mathbf{x}_2-\mathbf{x}_1)^2}{4D(t_2-t_1)}}}{(4\pi D(t_2-t_1))^{d/2}} \frac{e^{-\frac{(\mathbf{x}_1-\mathbf{x}_0)^2}{4D(t_1-t_0)}}}{(4\pi D(t_1-t_0))^{d/2}} \\ + n_0(n_0-1) \frac{e^{-\frac{(\mathbf{x}_1-\mathbf{x}_0)^2}{4D(t_1-t_0)}}}{(4\pi D(t_1-t_0))^{d/2}} \frac{e^{-\frac{(\mathbf{x}_2-\mathbf{x}_0)^2}{4D(t_2-t_0)}}}{(4\pi D(t_2-t_0))^{d/2}} \end{aligned} \tag{4.57}$$

directly from Eq. (4.40) using the propagator Eq. (4.10). As $t_2 > t_1$, only the first and the last diagrams of Eq. (4.40) contribute, the first due to a particle travelling from $\mathbf{x}_0$ to $\mathbf{x}_1$ and then to $\mathbf{x}_2$ and the last due to two particles travelling independently. In the limit of $t_2 \downarrow t_1$ the first term, proportional to n_0, becomes $n_0\delta(\mathbf{x}_2-\mathbf{x}_1)(4\pi D(t_1-t_0))^{-d/2}\exp\{-(\mathbf{x}_1-\mathbf{x}_0)^2/(4\pi D(t_1-t_0)\}$, vanishing if $\mathbf{x}_1 \neq \mathbf{x}_2$ as the same particle cannot be at two different places simultaneously. Fig. 4.1 provides a visual illustration of this property.

Although this approach no longer requires regularisation by a mass r, it is somewhat more demanding to perform the calculation of the correlation function within Dean's equation in direct time and real space using Eq. (4.32), because the Dean-vertex requires a convolution over the time and the position where the virtual branching takes place,

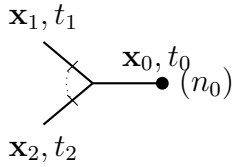

(4.58)

$$\hat{=} 2n_0 \int \mathrm{d}^d x' \mathrm{d}t' \left(\nabla_{\mathbf{x}'} G(\mathbf{x}_2-\mathbf{x}', t_2-t')\right) \cdot \left(\nabla_{\mathbf{x}'} G(\mathbf{x}_1-\mathbf{x}', t_1-t')\right) G(\mathbf{x}'-\mathbf{x}_0, t'-t_0) \ .$$

After some algebra, Dean's equation produces of course the same correlation function Eq. (4.57) as Doi-Peliti.

In explicit calculations below, notably Appendix 4.A, we will make use of a mixed momentum-time, k, t, parameterisation, for which we briefly outline the cancellation mechanism in the following. In Doi-Peliti, the diagrams Eq. (4.40) can immediately be written as

$$
\begin{aligned}
C(\mathbf{x}_1, \mathbf{x}_2, t_1, t_2) = &\int \mathrm{đ}^d k_2 \mathrm{đ}^d k_1 && (4.59)\\
&\times \Big\{ n_0 \exp\{\mathring{\imath}(\mathbf{k}_2 \cdot (\mathbf{x}_2 - \mathbf{x}_1) + \mathbf{k}_1 \cdot (\mathbf{x}_1 - \mathbf{x}_0))\} \theta(t_2 - t_1)\theta(t_1 - t_0) \\
&\qquad \times \exp\big\{ -D\mathbf{k}_2^2 (t_2 - t_1) - D\mathbf{k}_1^2 (t_1 - t_0)) \big\} && (4.60)\\
&+ n_0 \exp\{\mathring{\imath}(\mathbf{k}_2 \cdot (\mathbf{x}_2 - \mathbf{x}_0) + \mathbf{k}_1 \cdot (\mathbf{x}_1 - \mathbf{x}_2))\} \theta(t_1 - t_2)\theta(t_2 - t_0) \\
&\qquad \times \exp\big\{ -D\mathbf{k}_1^2 (t_1 - t_2) - D\mathbf{k}_2^2 (t_2 - t_0)) \big\} && (4.61)\\
&+ n_0(n_0 - 1) \exp\{\mathring{\imath}(\mathbf{k}_2 \cdot (\mathbf{x}_2 - \mathbf{x}_0) + \mathbf{k}_1 \cdot (\mathbf{x}_1 - \mathbf{x}_0))\} \theta(t_2 - t_0)\theta(t_1 - t_0) \\
&\qquad \times \exp\big\{ -D\mathbf{k}_2^2 (t_2 - t_0) - D\mathbf{k}_1^2 (t_1 - t_0)) \big\} \Big\} && (4.62)
\end{aligned}
$$

by replacing each of the bare propagators of Eq. (4.39) by Eq. (4.11) and making use of the δ-functions on the momenta, or by direct interpretation of the diagrams.

Dean's equation, Eq. (4.44), on the other hand, produces

$$
\begin{aligned}
&C(\mathbf{x}_1, \mathbf{x}_2, t_1, t_2) \\
&= \int \mathrm{đ}^d k_2 \mathrm{đ}^d k_1 \mathrm{đ}^d k_0 \, \exp\{\mathring{\imath}\mathbf{k}_2 \cdot \mathbf{x}_2\} \exp\{\mathring{\imath}\mathbf{k}_1 \cdot \mathbf{x}_1\} \exp\{\mathring{\imath}\mathbf{k}_0 \cdot \mathbf{x}_0\} \delta(\mathbf{k}_2 + \mathbf{k}_1 + \mathbf{k}_0) \\
&\times \Big\{ (-2n_0 D\mathbf{k}_1 \cdot \mathbf{k}_2) \int_{-\infty}^{\infty} \mathrm{d}t' \, \theta(t_2 - t') \exp\big\{ -D\mathbf{k}_2^2 (t_2 - t') \big\} \\
&\qquad \times \theta(t_1 - t') \exp\big\{ -D\mathbf{k}_1^2 (t_1 - t') \big\} \theta(t' - t_0) \exp\big\{ -D\mathbf{k}_0^2 (t' - t_0) \big\} \Big\} && (4.63)\\
&+ \int \mathrm{đ}^d k_2 \mathrm{đ}^d k_1 \, \exp\{\mathring{\imath}\mathbf{k}_2 \cdot (\mathbf{x}_2 - \mathbf{x}_0)\} \exp\{\mathring{\imath}\mathbf{k}_1 \cdot (\mathbf{x}_1 - \mathbf{x}_0)\} && (4.64)\\
&\qquad \times \Big\{ n_0^2 \theta(t_2 - t_0) \exp\big\{ -D\mathbf{k}_2^2 (t_2 - t_0) \big\} \theta(t_1 - t_0) \exp\big\{ -D\mathbf{k}_1^2 (t_1 - t_0) \big\} \Big\} \, ,
\end{aligned}
$$

with the convolution over t', the time of the virtual branching in the first diagram. While the lower limit of this integral is fixed to t_0 by $\theta(t' - t_0)$, the upper limit is $t_{\min} = \min(t_1, t_2)$ via the product of two Heaviside θ-functions. Its two possible values generate two terms as in Eq. (4.40), conditioned by θ-functions. Using the δ-function in the first line of Eq. (4.63) to eliminate the integral over $\mathbf{k}_0$, the n_0 branching terms

each produce

$$\int_{t_0}^{t_{\min}} \mathrm{d}t' \, \exp\{-D\mathbf{k}_2^2(t_2-t')\} \exp\{-D\mathbf{k}_1^2(t_1-t')\} \exp\{-D(\mathbf{k}_1+\mathbf{k}_2)^2(t'-t_0)\}$$
$$= \exp\{-D\mathbf{k}_2^2(t_2-t_0)\} \exp\{-D\mathbf{k}_1^2(t_1-t_0)\} \left(1-\exp\{-2D\mathbf{k}_1\cdot\mathbf{k}_2(t_{\min}-t_0)\}\right) \frac{1}{2D\mathbf{k}_1\cdot\mathbf{k}_2} \,. \tag{4.65}$$

The 1-term in the bracket is independent of $t_{\min}$ and cancels with n_0 of the n_0^2 disconnected terms. The remaining terms can be simplified using for example

$$\begin{aligned} &\exp\{-D\mathbf{k}_1^2(t_1-t_0)\} \exp\{-2D\mathbf{k}_1\cdot\mathbf{k}_2(t_1-t_0)\} \\ &= \exp\{-D(\mathbf{k}_1+\mathbf{k}_2)^2(t_1-t_0)\} \exp\{D\mathbf{k}_2^2(t_1-t_0)\} \end{aligned} \tag{4.66}$$

in the case of $t_{\min} = t_1$ and, after a shift in $\mathbf{k}_i$, such as $\mathbf{k}_1 + \mathbf{k}_2 \to \mathbf{k}_1$ in the example above, reproduce the result from Doi-Peliti, Eq. (4.59). This concludes the illustration.

To summarise this section, the correlation function of the particle position of n_0 non-interacting particles is not a single term, as it needs to capture multiple scenarios of particles moving, while keeping track of the particle nature of the constituent degrees of freedom. Both frameworks result in the same expressions, such Eqs. (4.43), (4.56), (4.57) and (4.59). A cancellation mechanism such as Eq. (4.48) in the $\mathbf{k}, \omega$ parameterisation and the convolution in Eq. (4.65) for $\mathbf{k}, t$, connects Doi-Peliti and Dean, revealing that the perturbative, virtual branching in Dean's framework is in fact a sum of sequential propagation of a single particle and independent propagation of two distinct ones.

The calculation in this preliminary section suggests that the interaction vertex Eq. (4.36) in Dean's formalism contains the same information as the commutation relation of the Doi-Peliti ladder operators. The importance of this observation will become evident in Sections 4.4 and 4.5, where we analyse the particle nature in greater detail.

4.3 Probing for particle entity

Within the Dean framework $\rho(\mathbf{x}, t)$ denotes the instantaneous particle number density in state $\mathbf{x}$ at time t. We define particle entity as a property of the evolution equation

for $\rho(\mathbf{x}, t)$ whereby this time-dependent random variable can be written as a finite sum of "single particle densities" with integer coefficients. In the case of a discrete phase space, the single-particle density for a particle in state $\bar{\mathbf{x}}$ is the Kronecker-delta with unit prefactor, $\delta_{\mathbf{x},\bar{\mathbf{x}}}$. For continuous degrees of freedom, the single-particle density for a particle in state $\bar{\mathbf{x}}$ is the Dirac-delta distribution normalised to unity, $\delta(\mathbf{x} - \bar{\mathbf{x}})$. Correspondingly,

$$\rho(\mathbf{x}, t) = \begin{cases} \sum_i n_i(t)\delta_{\mathbf{x},\bar{\mathbf{x}}_i}, & \text{for discrete states} \\ \sum_i n_i(t)\delta(\mathbf{x} - \bar{\mathbf{x}}_i), & \text{for continuous states} \end{cases} \tag{4.67}$$

where $n_i(t) \in \mathbb{N}$. It follows from this requirement that the integral of the particle number density $\rho(\mathbf{x}, t)$ over any (sub-)volume Ω of the space is an integer-valued random variable,

$$\forall \Omega \subset \mathbb{R}^d : \sum\!\!\!\!\!\!\int_{\Omega} \mathrm{d}^d x \, \rho(\mathbf{x}, t) \in \mathbb{N} \; . \tag{4.68}$$

For discrete states, Eq. (4.68) also implies Eq. (4.67), i.e. there can be no densities satisfying Eq. (4.68) that are not a sum of Kronecker deltas with integer coefficient. We leave the proof that this equivalence also holds in the continuum for future work. Such a proof will surely draw on the arbitrariness of Ω, which can be used to include or exclude from the integral in Eq. (4.68) any part of $\rho(\mathbf{x}, t)$. In the case of stochastic dynamics, it is convenient to re-express the condition Eq. (4.68) in terms of an expectation value as

$$\left\langle \exp\left(2\pi \mathring{i} \int_{\Omega} \mathrm{d^d x} \, \rho(\mathbf{x}, \mathrm{t}) \right) \right\rangle = 1 \; , \tag{4.69}$$

which needs to be satisfied for any volume Ω and all times t. Eq. (4.69) will play the role of a signature of particle entity in the following.

Obviously, Eq. (4.68) implies Eq. (4.69). Yet, expressing the particle entity condition as an expectation might appear less stringent than demanding it at the level of individual trajectories. However, rewriting Eq. (4.69) as $\langle \cos\big(2\pi \int \mathrm{d}^d x \, \rho(\mathbf{x}, t)\big) \rangle = 1$ on the basis of $\rho(\mathbf{x}, t)$ being real, shows that the integral must be integer valued almost surely, because $\mathbb{R} \ni \cos(x) \leq 1$ for $x \in \mathbb{R}$.

In order to ease the calculation of the left-hand side of Eq. (4.69) for a particular field theory of interest, we can expand the complex exponential as a Taylor series and invoke

linearity of the expectation to obtain the particle entity signature,

$$\sum_{n=0}^{\infty} \frac{(2\pi\mathring{\imath})^n}{n!}$$ 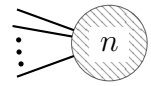

$$\hat{=} \sum_{n=0}^{\infty} \frac{(2\pi\mathring{\imath})^n}{n!} \left\langle \left(\int_\Omega \mathrm{d}^d x\, \rho(\mathbf{x},t) \right)^n \right\rangle = \left\langle \exp\left(2\pi\mathring{\imath} \int_\Omega \mathrm{d^d x}\, \rho(\mathbf{x},\mathrm{t}) \right) \right\rangle = 1 \ , \tag{4.70}$$

where the left-hand side is now a function of the nth full moment of the integrated particle number density, $\left\langle \left(\int_\Omega \mathrm{d}^d x\, \rho(\mathbf{x},t) \right)^n \right\rangle$. In Eq. (4.70) we have also introduced the diagrammatic notation for the nth full moment of the *integrated* particle number density. The hatched vertex henceforth indicates generally a sum of possibly disconnected diagrams involving an arbitrary amount of sources. More specifically, here it is the n-fold spatial integral of a sum of products of connected diagrams. An example for such a sum is Eq. (4.44). These moments are perfectly suited for being calculated in both Doi-Peliti and response field field theories, as done in the following.

An alternative form of our particle entity signature can be obtained by recognising that the left hand side of Eq. (4.69) is also the moment-generating function $\langle \exp\{zX\} \rangle$ of the random variable $X = \int_\Omega \mathrm{d}\mathbf{x}\, \rho(\mathbf{x},t)$ evaluated at $z = 2\pi\mathring{\imath}$. It is a well-known result from the field-theoretic literature on equilibrium critical phenomena [171, 31] that the generating function of the full moments $\langle X^n \rangle$ can be expressed as the exponential of the generating function of the so-called connected moments, denoted $\langle X^n \rangle_c$. Outside the field-theoretic literature, connected moments are usually referred to as cumulants [291]. While one would normally expect source fields $j(\mathbf{x},t)$ to be introduced corresponding to a conjugate variable z at each point in space and time, in the present context a single variable suffices, as in Eq. (4.70) every field $\rho(\mathbf{x},t)$ is integrated over the same volume Ω. Diagrammatically,

$$\sum_{n=0}^{\infty} \frac{z^n}{n!}$$ 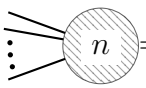

$$\hat{=} \sum_{n=0}^{\infty} \frac{z^n}{n!} \left\langle \left(\int_\Omega \mathrm{d}^d x\, \rho(\mathbf{x},t) \right)^n \right\rangle = \left\langle \exp\left(z \int_\Omega \mathrm{d}^d x\, \rho(\mathbf{x},t) \right) \right\rangle$$

$$= \exp\left(\sum_{n=1}^{\infty} \frac{z^n}{n!} \left\langle \left(\int_\Omega \mathrm{d}^d x\, \rho(\mathbf{x},t) \right)^n \right\rangle_c \right) = \exp\left(\sum_{n=1}^{\infty} \frac{z^n}{n!}$$ 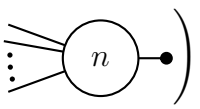

$$\right) \ , \tag{4.71}$$

where we have introduced the notation for the nth *connected* moment of the integrated particle number density, shown as a circular vertex on the right, which differs from that

of the corresponding full moment also by the presence of an explicit, single, ingoing propagator emerging from a single source, shown as a filled circle, the only possible form of a connected diagram contributing to moments of the density. In equilibrium statistical mechanics, this relationship provides the connection between the partition function and the Helmholtz free energy [171, 31]. Generating functions of observables such as n-point correlation functions of $\rho(\mathbf{x}, t)$ can be reduced to those of connected diagrams as long as the observables can be written as (functional) derivatives of an exponential and provided that each resulting diagram can be written as a product of connected diagrams. Under these conditions, Eq. (4.71) does all the right accounting.

Evaluating Eq. (4.71) at $z = 2\pi\mathring{\imath}$, according to Eq. (4.70) one can write

$$\exp\left(\sum_{\mathrm{n}=1}^{\infty} \frac{(2\pi\mathring{i})^{\mathrm{n}}}{\mathrm{n}!} \left\langle \left(\int_{\Omega} \mathrm{d}^{\mathrm{d}}\mathrm{x}\, \rho(\mathbf{x}, \mathrm{t}) \right)^{\mathrm{n}} \right\rangle_{\mathrm{c}} \right) = 1 \ , \tag{4.72}$$

or, equivalently,

$$\sum_{n=1}^{\infty} \frac{(2\pi\mathring{i})^{n}}{n!} \quad \hat{=} \sum_{n=1}^{\infty} \frac{(2\pi\mathring{i})^{n}}{n!} \left\langle \left(\int_{\Omega} \mathrm{d}^{d}x\, \rho(\mathbf{x}, t) \right)^{n} \right\rangle_{c} = 2\pi\mathring{\imath}\ell \tag{4.73}$$

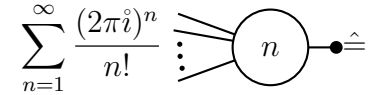

for some integer $\ell \in \mathbb{Z}$, on the basis of the connected moments of the particle number, to be compared to the particle signature on the basis of the full moments, Eq. (4.70).

4.4 Particle entity in Doi-Peliti

Doi-Peliti field theories are designed to respect particle entity and they do indeed do so on a rather fundamental level. To probe for particle entity, we want to use Eq. (4.69) with $\rho(\mathbf{x}, t)$ replaced by an object suitable for a Doi-Peliti field theory. In such a field theory, the instantaneous particle number at any position $\mathbf{x}$ is probed by the number operator $\hat{n}(\mathbf{x}) = a^{\dagger}(\mathbf{x})a(\mathbf{x})$. The expected particle number at position $\mathbf{x}$ and time t is therefore

$$\langle n(\mathbf{x}, t) \rangle = \langle \text{☼} |\, a^{\dagger}(\mathbf{x})a(\mathbf{x})\, | \Psi(t) \rangle \ , \tag{4.74}$$

using a continuum version of the notation introduced in Section 4.2, in particular Eq. (4.3). While this expectation might be any non-negative real, the instantaneous $a^{\dagger}(\mathbf{x})a(\mathbf{x})$ is an integer. As already discussed in Section 4.3, Eq. (4.69), we therefore

expect

$$\langle ☼| \exp\big(2\pi \mathring{\imath} a^\dagger(\mathbf{x}) a(\mathbf{x})\big) |\Psi(t)\rangle = 1 \tag{4.75}$$

to hold for every $\mathbf{x}$, as $\exp\{2\pi \mathring{\imath} n\} = 1$ for any $n \in \mathbb{Z}$. If this holds for every point $\mathbf{x}$, it also holds for every patch Ω, since

$$\langle ☼| \exp\left(2\pi \mathring{\imath} \sum_{\mathbf{x}\in\Omega} a^\dagger(\mathbf{x}) a(\mathbf{x})\right) |\Psi(t)\rangle = \langle ☼| \prod_{\mathbf{x}\in\Omega} \exp\big(2\pi \mathring{\imath} a^\dagger(\mathbf{x}) a(\mathbf{x})\big) |\Psi(t)\rangle \ , \tag{4.76}$$

where we have used that operators at different $\mathbf{x}$ commute. In the continuum, one might argue that the particle number at $\mathbf{x}$ can only ever be 0 or 1, possibly leading to some simplifications, but on the lattice occupation is not bound to be sparse in this sense.

To show that Eq. (4.75) is indeed satisfied in general Doi-Peliti field theories, we follow the standard procedure, outlined in Eq. (4.14), to express the operator $\exp\big(2\pi \mathring{\imath} a^\dagger(\mathbf{x}) a(\mathbf{x})\big)$ in terms of scalar fields $\psi(\mathbf{x}, t)$ and $\psi^\dagger(\mathbf{x}, t)$. The simple mapping of operator to field applies as soon as the operators are normal ordered,

$$\exp\big(z a^\dagger(\mathbf{x}) a(\mathbf{x})\big) = \sum_{n=0}^{\infty} \frac{1}{n!} z^n \left(a^\dagger(\mathbf{x}) a(\mathbf{x})\right)^n \tag{4.77}$$

$$= \sum_{n=0}^{\infty} \frac{1}{n!} z^n \sum_{k=0}^{n} \left\{ {n \atop k} \right\} \left(a^\dagger(\mathbf{x})\right)^k a(\mathbf{x})^k \tag{4.78}$$

where we have replaced $2\pi \mathring{\imath}$ by z to improve readability and used [215] to normal order $\left(a^\dagger(\mathbf{x}) a(\mathbf{x})\right)^n$. In terms of fields, the observable Eq. (4.76) is thus

$$\mathcal{O} = \langle ☼| \exp\left(z \sum_{x\in\Omega} \left(a^\dagger(\mathbf{x})\right)^k a(\mathbf{x})^k\right) |\Psi(\mathbf{x}, t)\rangle \tag{4.79}$$

$$= \langle ☼| \prod_{x\in\Omega} \sum_{n=0}^{\infty} \frac{1}{n!} z^n \sum_{k=0}^{n} \left\{ {n \atop k} \right\} \left(a^\dagger(\mathbf{x})\right)^k a(\mathbf{x})^k |\Psi(\mathbf{x}, t)\rangle \tag{4.80}$$

$$= \left\langle \prod_{x\in\Omega} \sum_{n=0}^{\infty} \frac{1}{n!} z^n \sum_{k=0}^{n} \left\{ {n \atop k} \right\} \psi^k(\mathbf{x}, t) \right\rangle \tag{4.81}$$

$$= \left\langle \exp\left(\sum_{x\in\Omega} \psi(\mathbf{x}, t)(e^z - 1)\right) \right\rangle \tag{4.82}$$

as $\langle \text{☼} | \, (a^\dagger(\mathbf{x}))^k = \langle \text{☼} |$ [227]. From Eq. (4.81) to (4.82), we draw on the the mixed bivariate generating function for the Stirling numbers of the second kind [68],

$$\sum_{n=0}^{\infty} \sum_{k=0}^{n} \left\{ {n \atop k} \right\} \frac{1}{n!} z^n y^k = \exp(y(\exp\{z\} - 1)) \ . \tag{4.83}$$

For $z = 2\pi \mathring{\imath}$, and any integer multiple thereof, Eq. (4.82) indeed produces $\mathcal{O} = 1$ as required by Eq. (4.69). Because this calculation never draws on any particular action, but rather on the fundamentals of normal ordering, Doi-Peliti field theories respect particle entity universally in the presence of any interactions and potentials.

4.5 Particle entity in response field theories: Dean's equation

Demonstrating that the response field theory derived from Dean's equation possesses particle entity turns out to be a much more challenging task, which requires us to compute explicitly the connected moments of the integrated particle number density to arbitrary order. This calculation draws on the specific action Eq. (4.21) and (4.22) as we perform it here for the case of non-interacting diffusive particles without external potential. This is done most conveniently by first computing the connected moments of the density in the mixed momentum-time representation, where Dean's action reads

$$\begin{aligned} A[\rho, \tilde{\rho}] = &\int \mathrm{đ}^d k \mathrm{d}t \, \tilde{\rho}(\mathbf{k}, t)(\partial_t + D\mathbf{k}^2)\rho(-\mathbf{k}, t) - \tilde{\rho}(\mathbf{k}, t) \sum_i n_i e^{\mathring{\imath}\mathbf{k}\cdot\mathbf{x}_i} \delta(t - t_i) \\ &+ \int \mathrm{đ}^d k \mathrm{đ}^d k' \mathrm{d}t \, D(\mathbf{k} \cdot \mathbf{k}') \tilde{\rho}(\mathbf{k}, t) \tilde{\rho}(\mathbf{k}', t) \rho(-(\mathbf{k} + \mathbf{k}'), t). \end{aligned} \tag{4.84}$$

In this parametrisation, we find (Appendix 4.A, Eq. (4.146))

$$\begin{aligned} \langle \rho(\mathbf{k}_1, t) ... \rho(\mathbf{k}_n, t) \rangle_c = n_0 \theta(t - t_0) \exp\{\mathring{\imath}(\mathbf{k}_1 + ... \mathbf{k}_n) \cdot \mathbf{x}_0\} \sum_{m=1}^{n} (-1)^{m-1} (m-1)! \\ \times \sum_{\{\mathbb{P}_1, ..., \mathbb{P}_m\} \in \mathcal{P}(\{1,...,n\}, m)} \exp\left\{ -T(t - t_0) \sum_{i=1}^{m} \mathbf{K} \left(\mathbb{P}_i\right)^2 \right\}. \end{aligned} \tag{4.85}$$

with $\mathcal{P}\left(\{1, \ldots, n\}, m\right)$ the set of all partitions of the set $\{1, \ldots, n\}$ into m non-empty, distinct subsets $\mathbb{P}_i$ with $i = 1, ..., m$, *i.e.* $\cup_{i=1}^{m} \mathbb{P}_i = \{1, 2, \ldots, n\}$ and $\mathbb{P}_i \cap \mathbb{P}_j = \emptyset$ for

$i \neq j$. The sum thus runs over all possible partitions of {1,2,...,n} into m non-empty sets. There is one partition for $m = n$ and n for $m = 1$. The vector featuring in the right-most exponential of Eq. (4.85)

$$\mathbf{K}\left(\mathbb{P}_i\right) = \sum_{p \in \mathbb{P}_i} \mathbf{k}_p \tag{4.86}$$

is the total momentum given by the indices in the subset $\mathbb{P}_i$, *i.e.* it is the total momentum of the subset $\mathbb{P}_i$, and by linearity, $\mathbf{K}\left(\mathbb{A}\right) + \mathbf{K}\left(\mathbb{B}\right) = \mathbf{K}\left(\mathbb{A} \cup \mathbb{B}\right)$. For example, one partition into two of $\{1, 2, 3, 4\}$ is $\{\mathbb{P}_1 = \{1, 2, 4\}, \mathbb{P}_2 = \{3\}\}$, which is one of 7 elements of $\mathcal{P}\left(\{1, 2, 3, 4\}, 2\right)$. In this example, the momenta of the subsets are $\mathbf{K}\left(\mathbb{P}_1\right) = \mathbf{k}_1 + \mathbf{k}_2 + \mathbf{k}_4$ and $\mathbf{K}\left(\mathbb{P}_2\right) = \mathbf{k}_3$. Diagrammatically, the right-hand side of Eq. (4.85) is obtained by summing over all connected, topologically distinct diagrams with a single incoming propagator and n outgoing propagators labelled by the external momenta $\mathbf{k}_i$ $(i = 1, ..., n)$, where we need to account for all non-equivalent permutations of the latter.

The connected moments of the integrated particle number density in a patch Ω are then obtained by Fourier back-transforming Eq. (4.85) into position-time representation and integrating over the probing locations $\mathbf{x}_i \in \Omega$,

$$\left\langle \int_\Omega \mathrm{d}^d x_1 \, ... \, \mathrm{d}^d x_n \, \rho(\mathbf{x}_1, t) ... \rho(\mathbf{x}_n, t) \right\rangle_c \tag{4.87}$$

$$= \int_\Omega \prod_{i=1}^{n} \mathrm{d}^d x_i \int \prod_{j=0}^{n} \text{đ}^d k_j \, \exp\left(-\mathring{\imath} \sum_{\ell=1}^{n} \mathbf{k}_\ell \cdot \mathbf{x}_\ell \right) \left\langle \rho(\mathbf{k}_1, t) ... \rho(\mathbf{k}_n, t) \right\rangle_c \tag{4.88}$$

$$= \int_\Omega \prod_{i=1}^{n} \mathrm{d}^d x_i \int \prod_{j=1}^{n} \text{đ}^d k_j \, \exp\left(-\mathring{\imath} \sum_{\ell=1}^{n} \mathbf{k}_\ell \cdot (\mathbf{x}_\ell - \mathbf{x}_0) \right) \tag{4.89}$$

$$\times \, n_0 \theta(t - t_0) \sum_{m=1}^{n} (-1)^{m-1} (m-1)! \sum_{\{\mathbb{P}_1, ..., \mathbb{P}_m\} \in \mathcal{P}(\{1,...,n\}, m)} \exp\left\{ -D(t - t_0) \sum_{p=1}^{m} \mathbf{K}\left(\mathbb{P}_p\right)^2 \right\} .$$

The integrals in Eq. (4.89) can be carried out partition by partition, by taking the integration inside the summation over $m = 1, \ldots, n$ and the partitions $\{\mathbb{P}_1, \ldots\} \in \mathcal{P}\left(\{1, \ldots, n\}, m\right)$. As $\mathbf{x}_i$ and $\mathbf{k}_j$ are both dummy variables, we may think of subset $\mathbb{P}_p$ containing indices $1, \ldots, a$ with $a = |\mathbb{P}_p|$, so that the integrals to be carried out for each

$p = 1, \ldots, m$ are

$$J_p = \int_\Omega \prod_{i=1}^{a} \mathrm{d}^d x_i \int \prod_{j=1}^{a} \text{đ}^d k_j \, \exp\left(-\mathring{\imath} \sum_{\ell=1}^{a} \mathbf{k}_\ell \cdot (\mathbf{x}_\ell - \mathbf{x}_0) \right) \exp\left\{ -D(t-t_0) \mathbf{K}\left(\mathbb{P}_p\right)^2 \right\} . \tag{4.90}$$

In this indexing we have $\mathbf{K}\left(\mathbb{P}_p\right) = \mathbf{k}_1 + \cdots + \mathbf{k}_a$ which simplifies to $\tilde{\mathbf{k}}_1$ after suitable shifting of the origin in the integration over $\mathbf{k}_1 = \tilde{\mathbf{k}}_1 - (\mathbf{k}_2 + \cdots + \mathbf{k}_a)$, so that

$$\begin{aligned} J_p &= \int_\Omega \prod_{i=1}^{a} \mathrm{d}^d x_i \int \text{đ}^d \tilde{k}_1 \, \exp\left\{ -\mathring{\imath} \tilde{\mathbf{k}}_1 \cdot (\mathbf{x}_1 - \mathbf{x}_0) \right\} \exp\left\{ -D(t-t_0) \tilde{\mathbf{k}}_1^2 \right\} && \text{(4.91a)} \\ &\quad \times \int \prod_{j=2}^{a} \text{đ}^d k_j \, \exp\left(-\mathring{\imath} \sum_{\ell=2}^{a} \mathbf{k}_\ell \cdot (\mathbf{x}_\ell - \mathbf{x}_1) \right) \\ &= \int_\Omega \prod_{i=1}^{a} \mathrm{d}^d x_i \, G(\mathbf{x}_1 - \mathbf{x}_0, t - t_0) \delta(\mathbf{x}_2 - \mathbf{x}_1) ... \delta(\mathbf{x}_a - \mathbf{x}_1) && \text{(4.91b)} \\ &= I_\Omega(t - t_0) && \text{(4.91c)} \end{aligned}$$

where we have used Eqs. (4.32) and (4.34) in Eq. (4.91b) and introduced

$$I_\Omega(t - t_0) = \int_\Omega \mathrm{d}^d x \, G(\mathbf{x} - \mathbf{x}_0, t - t_0) \ , \tag{4.92}$$

in Eq. (4.91c), which is the probability to find a particle at time t within the volume Ω that had at time t_0 been placed at $\mathbf{x}_0$. We may drop the time-dependence of I_Ω where that improves readability.

As J_p is independent of the specific partition, the sum over partitions $\{\mathbb{P}_1, \ldots, \mathbb{P}_m\} \in \mathcal{P}\left(\{1, \ldots, n\}, m\right)$ in Eq. (4.89) amounts to multiplying a product of m such integrals by the number of partitions, given by the Stirling numbers of the second kind. Overall,

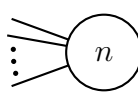

$$\hat{=} \left\langle \left(\int_\Omega \mathrm{d}^d x \, \rho(\mathbf{x}, t) \right)^n \right\rangle_c = -n_0 \theta(t - t_0) \sum_{m=1}^{n} \left(-I_\Omega \right)^m \left\{ {n \atop m} \right\} (m-1)! \ , \tag{4.93}$$

which provides us with the information we need to probe the theory for particle entity. It is a key result of the present work. Its derivation is generalised to distinct initial positions in Appendix 4.B.

Using the particle entity signature based on connected diagrams, Eq. (4.73), confronts us with some undesirable hurdles due to convergence. We therefore turn our attention to the full moments, which can be constructed from the connected moments via Eq. (4.71), so that for $t > t_0$,

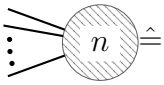

$$\hat{=} \left\langle \left(\int_\Omega \mathrm{d}^d x \, \rho(\mathbf{x}, t) \right)^n \right\rangle \tag{4.94}$$

$$= \left. \frac{d^n}{dz^n} \right|_{z=0} \exp\left(\sum_{m=1}^{\infty} \frac{z^m}{m!} \left\langle \left(\int_\Omega \mathrm{d}^d x \, \rho(\mathbf{x}, t) \right)^m \right\rangle_c \right) \tag{4.95}$$

$$= \left. \frac{d^n}{dz^n} \right|_{z=0} \exp\left(\sum_{m=1}^{\infty} \frac{z^m}{m!} (-n_0) \sum_{\ell=1}^{m} (-I_\Omega)^\ell \left\{ {m \atop \ell} \right\} (\ell - 1)! \right) \tag{4.96}$$

$$= \left. \frac{d^n}{dz^n} \right|_{z=0} \exp\left(-n_0 \sum_{\ell=1}^{\infty} (-I_\Omega)^\ell (\ell - 1)! \sum_{m=\ell}^{\infty} \frac{z^m}{m!} \left\{ {m \atop \ell} \right\} \right) , \tag{4.97}$$

where we have changed the order of summation in the exponential to arrive at the final equality. This step deserves further scrutiny below. Using in Eq. (4.97) the generating function of the Stirling numbers [68] in the form

$$\sum_{m=\ell}^{\infty} \frac{z^m}{m!} \left\{ {m \atop \ell} \right\} = \frac{(e^z - 1)^\ell}{\ell!} , \tag{4.98}$$

as used previously in the Doi-Peliti field theory, Eq. (4.83), leads to

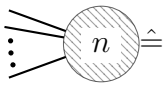

$$\hat{=} \left. \frac{d^n}{dz^n} \right|_{z=0} \exp\left(-n_0 \sum_{\ell=1}^{\infty} (-I_\Omega)^\ell \frac{(e^z - 1)^\ell}{\ell} \right) . \tag{4.99}$$

We briefly return to the change of the order of summation from Eq. (4.96) to (4.97). To justify this, we require *absolute* convergence

$$\sum_{\ell=1}^{\infty} \sum_{m=\ell}^{\infty} \frac{|z|^m}{m!} I_\Omega^\ell \left\{ {m \atop \ell} \right\} (\ell - 1)! < \infty \tag{4.100}$$

for $I_\Omega \in [0, 1]$ and z within a finite vicinity around the origin, given the repeated differentiation in Eq. (4.99). As Eq. (4.98) holds for all $z \in \mathbb{C}$, we require $\sum_{\ell=1}^{\infty} I_\Omega^\ell (\exp(|z|) - 1)^\ell / \ell < \infty$ and thus $|z| < \ln(2)$ by the ratio test.

Rewriting the exponent in Eq. (4.99) for any $|z| < \ln(2)$ as a logarithm,

$$\sum_{l=1}^{\infty} \frac{(-x)^l}{l} = -\log(1+x)\,, \tag{4.101}$$

we have

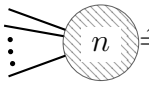

$$\hat{=} \left.\frac{d^n}{dz^n}\right|_{z=0} (1 + (e^z - 1)I_\Omega)^{n_0} \tag{4.102}$$

$$= \left.\frac{d^n}{dz^n}\right|_{z=0} \sum_{k=0}^{n_0} \binom{n_0}{k} (e^z - 1)^k I_\Omega^k \tag{4.103}$$

$$= \sum_{k=0}^{n_0} \binom{n_0}{k} I_\Omega^k \left.\frac{d^n}{dz^n}\right|_{z=0} \sum_{j=0}^{k} \binom{k}{j} (-1)^j e^{z(k-j)} \tag{4.104}$$

$$= \sum_{k=0}^{n_0} \binom{n_0}{k} I_\Omega^k \sum_{j=0}^{k} \binom{k}{j} (-1)^j (k-j)^n\,, \tag{4.105}$$

and using the definition of the Stirling numbers of the second kind [68]

$$\sum_{g=0}^{k} \binom{k}{g} (-1)^g (k-g)^n = k! \left\{ {n \atop k} \right\}, \tag{4.106}$$

we finally arrive at

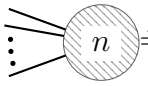

$$\hat{=} \sum_{k=0}^{n_0} \binom{n_0}{k} I_\Omega^k k! \left\{ {n \atop k} \right\}. \tag{4.107}$$

This is the central result of the present section.

The nth full moment, in the form of the right hand side Eq. (4.107), has an instructive physical interpretation drawing on n_0 being integer. To see this, we write the nth moment of the particle number as

$$\left\langle \left(\int_\Omega \mathrm{d}^d x\, \rho(\mathbf{x}, t) \right)^n \right\rangle = \int_\Omega \mathrm{d}^d x_1' \mathrm{d}^d x_2' \ldots \mathrm{d}^d x_n' \, \langle \rho(\mathbf{x}_1', t) \rho(\mathbf{x}_2', t) \ldots \rho(\mathbf{x}_n', t) \rangle \tag{4.108}$$

with each density $\rho(\mathbf{x}_i', t)$ considered a random variable as a function of the positions

$x_j(t)$ of n_0 particles indexed by $j = 1, 2, \ldots, n_0$

$$\rho(\mathbf{x}'_i, t) = \sum_{j=1}^{n_0} \delta(\mathbf{x}'_i - \mathbf{x}_j(t)) \ , \tag{4.109}$$

generating n_0^n terms of products of δ-functions in Eq. (4.108). To calculate the right-hand side of Eq. (4.108) on the basis of Eq. (4.109) using Eq. (4.92) in the form

$$\int_\Omega \mathrm{d}^d x' \ \langle \delta(\mathbf{x}' - \mathbf{x}_j(t) \rangle = I_\Omega(t - t_0) \tag{4.110}$$

requires careful bookkeeping of how often each particle coorrdinate $\mathbf{x}_j(t)$ is repeated. For example

$$\int_\Omega \mathrm{d}^d x'_1 \mathrm{d}^d x'_2 \ \langle \delta(\mathbf{x}'_1 - \mathbf{x}_1(t)) \delta(\mathbf{x}'_2 - \mathbf{x}_2(t)) \rangle = I_\Omega^2 \tag{4.111a}$$

$$\int_\Omega \mathrm{d}^d x'_1 \mathrm{d}^d x'_2 \ \langle \delta(\mathbf{x}'_1 - \mathbf{x}_1(t)) \delta(\mathbf{x}'_2 - \mathbf{x}_1(t)) \rangle = I_\Omega \tag{4.111b}$$

as particle coordinates are independent in Eq. (4.111a), but not in Eq. (4.111b), where in fact $\delta(\mathbf{x}'_1 - \mathbf{x}_1(t))\delta(\mathbf{x}'_2 - \mathbf{x}_1(t)) = \delta(\mathbf{x}'_1 - \mathbf{x}_1(t))\delta(\mathbf{x}'_2 - \mathbf{x}'_1)$. To calculate the right-hand side of Eq. (4.108) thus is a matter of allowing for $k = 1, 2, \ldots, n$ distinct particle coordinates $x_j(t)$ from each of the n sums Eq. (4.109). There are $n_0(n_0 - 1) \cdot \ldots \cdot (n_0 - k + 1) = \binom{n_0}{k} k!$ such choices. As each of the $\rho(\mathbf{x}'_i, t)$ is a function of a different dummy variable, they have to be distributed among the k distinct particle coordinates. There are $\left\{ {n \atop k} \right\}$ choices for that. The integration produces I_Ω^k depending on the number k of distinct particle coordinates following the reasoning for Eq. (4.111). In summary, we arrive at

$$\left\langle \left(\int_\Omega \mathrm{d}^d x \, \rho(\mathbf{x}, t) \right)^n \right\rangle = \sum_{k=0}^{n} \binom{n_0}{k} I_\Omega^k k! \left\{ {n \atop k} \right\} \ , \tag{4.112}$$

including $k = 0$ in the summation to cover the special case of $n = 0$. Eq. (4.112) is subtly different from Eq. (4.107), as the upper limit of the sum in Eq. (4.107) is n_0, while it is n in Eq. (4.112). However, $\left\{ {n \atop k} \right\}$ in Eq. (4.107) vanishes if k exceeds n and $\binom{n_0}{k}$ in Eq. (4.107) vanishes if *integer* k exceeds *integer* n_0, *i.e.* in both sums the upper limit may be replaced by $\min(n, n_0)$, provided only n_0 is integer. We conclude that the full moment Eq. (4.107) has a sensible interpretation in terms of particle numbers only

if n_0 is integer.

A second form of Eq. (4.107) can be derived, which offers a more immediate physical interpretation. To this end, we draw on the identity

$$\sum_{k=0}^{n_0} \binom{n_0}{k} (1-x)^{n_0-k} x^k k^n = \sum_{\ell=0}^{n_0} \binom{n_0}{\ell} x^\ell \ell! \left\{ n \atop \ell \right\} \tag{4.113}$$

which can be obtained by resolving the binomial $(1-x)^{n_0-k}$ on the left into a sum, collecting terms of order x^ℓ and then using $\binom{n_0}{k}\binom{n_0-k}{\ell-k} = \binom{n_0}{\ell}\binom{\ell}{k}$ to arrive at an expression that simplifies to the final sum by means of Eq. (4.106).

Using Eq. (4.113) in Eq. (4.107) gives

$$\left\langle \left(\int_\Omega \mathrm{d}^d x\, \rho(\mathbf{x}, t) \right)^n \right\rangle = \sum_{k=0}^{n_0} \binom{n_0}{k} \Big(1 - I_\Omega(t-t_0)\Big)^{n_0-k} \Big(I_\Omega(t-t_0)\Big)^k k^n \ , \tag{4.114}$$

which has a rather simple physical interpretation: of the (integer) n_0 particles, k can be found in the volume Ω, each independently with probability I_Ω, so that the probability of such a configuration is that of a repeated Bernoulli trial, $\binom{n_0}{k}(1-I_\Omega)^{n_0-k} I_\Omega^k$. As k particles are in the relevant volume, the contribution to the nth particle number moment is k^n.

In the form Eq. (4.114), the particle number moments can be used in our particle entity signature Eq. (4.70),

$$\sum_{n=0}^{\infty} \frac{(2\pi \mathring{\imath})^n}{n!}$$
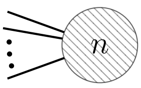

$$= \sum_{n=0}^{\infty} \frac{(2\pi \mathring{\imath})^n}{n!} \sum_{k=0}^{n_0} \binom{n_0}{k} (1-I_\Omega)^{n_0-k} I_\Omega^k k^n \tag{4.115}$$

$$= \sum_{k=0}^{n_0} \binom{n_0}{k} (1-I_\Omega)^{n_0-k} I_\Omega^k \left(\sum_{n=0}^{\infty} \frac{(2\pi \mathring{\imath})^n}{n!} k^n \right) = 1 \ , \tag{4.116}$$

where we have used $e^{2\pi \mathring{\imath} k} = 1$ for $k \in \mathbb{Z}$ in the last bracket and the normalisation of a binomial distribution. To change the order of summation going from Eq. (4.115) to (4.116) we draw on the absolute convergence of the last line Eq. (4.116). This concludes the proof of particle entity on the basis of Eq. (4.70) in the Dean formalism.

We have seen how the falling factorials $n_0(n_0-1)\cdot\ldots\cdot(n_0-k+1) = \binom{n_0}{k}k!$ emerge in

Dean's theory by computing the connected moments, Eq. (4.107) and also Eq. (4.112), explicitly. This structure is another signature of particle entity, in the sense that it highlights the special role played by the integer nature of the initial particle number n_0. Unsurprisingly, it similarly emerges in Doi-Peliti. In particular, the full moments of the particle number at position $\mathbf{x}$ are given by

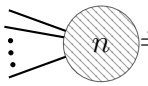

$$\hat{=} \langle \text{☼} | \left(a^\dagger(\mathbf{x}) a(\mathbf{x}) \right)^n \exp\Big\{ \hat{A}(t - t_0) \Big\} \left(a^\dagger(\mathbf{x}_0) \right)^{n_0} |0\rangle \ , \tag{4.117}$$

where $\hat{A}$ denotes the time evolution operator of Eq. (4.4). We then use

$$\left(a^\dagger(\mathbf{x}_0) \right)^{n_0} = \left(\tilde{a}(\mathbf{x}_0) + 1 \right)^{n_0} = \sum_{k=0}^{n_0} \binom{n_0}{k} \left(\tilde{a}(\mathbf{x}_0) \right)^k \tag{4.118}$$

together with [108]

$$\langle \text{☼} | \left(a^\dagger(\mathbf{x}) a(\mathbf{x}) \right)^n = \sum_{\ell=0}^{n} \left\{ {n \atop \ell} \right\} \langle \text{☼} | \left(a(\mathbf{x}) \right)^\ell \tag{4.119}$$

to rewrite the right-hand side of Eq. (4.117) as

$$\begin{aligned}
&\langle \text{☼} | \left(a^\dagger(\mathbf{x}) a(\mathbf{x}) \right)^n \exp\Big\{ \hat{A}(t - t_0) \Big\} \left(a^\dagger(\mathbf{x}_0) \right)^{n_0} |0\rangle \\
&= \sum_{\ell=0}^{n} \left\{ {n \atop \ell} \right\} \sum_{k=0}^{n_0} \binom{n_0}{k} \langle \text{☼} | \left(a(\mathbf{x}) \right)^\ell \exp\Big\{ \hat{A}(t - t_0) \Big\} \left(\tilde{a}(\mathbf{x}_0) \right)^k |0\rangle \qquad (4.120) \\
&= \sum_{\ell=0}^{n_0} \left\{ {n \atop \ell} \right\} \binom{n_0}{\ell} \ell! \, \langle \text{☼} | \, a(\mathbf{x}) \exp\Big\{ \hat{A}(t - t_0) \Big\} \tilde{a}(\mathbf{x}_0) \, |0\rangle^\ell \qquad (4.121)
\end{aligned}$$

where we have used $\langle \text{☼} | \left(a(\mathbf{x}) \right)^\ell \exp \hat{A}(t - t_0)) (\tilde{a}(\mathbf{x}_0))^k \, |0\rangle = \delta_{k\ell} \ell! \, \langle \text{☼} | \, a(\mathbf{x}) \exp \hat{A}(t - t_0)) \tilde{a}(\mathbf{x}_0) \, |0\rangle^\ell$ in the absence of interactions. The final expression corresponds to the one we found via the Dean route, Eq. (4.107), with $I_\Omega(t - t_0)$ replaced by the Doi-Peliti propagator $\langle \text{☼} | \, a(\mathbf{x}) \exp A(t - t_0)) \tilde{a}(\mathbf{x}_0) \, |0\rangle$.

4.6 Conclusion

To the best of our knowledge, this paper presents the first formalisation and systematic study of the concept of particle entity in the context of statistical field theory. Focusing on two well-known field theoretic formalisms applied to the study of stochastic processes, namely the Doi-Peliti [289] and the Martin-Siggia-Rose-Janssen-De Dominicis [195, 146, 81] response field theories, we have demonstrated that particle entity is enforced in a formalism-specific way. In Doi-Peliti field theories, particle entity is built into its foundation, namely in the commutation relation of the ladder operators, Eq. (4.1). In the response field field theory derived from Dean's equation, particle entity is a perturbative feature that relies on the precise form of the interaction vertex, Eq. (4.36). This "Dean vertex" originates from the Itô-multiplicative noise term in the original Langevin equation Eq. (4.17). It compensates for some overcounting that occurs in the bilinear part of the field theory Eq. (4.26), a mechanism that was already identified in an earlier work on the statistics of the non-interacting Brownian gas [292]. As a result, one is faced with more complicated branching diagrams in the response field formalism equipped with particle entity via Dean's equation compared to the Doi-Peliti formalism, *cf.* Eqs. (4.38) and (4.44) or Eqs. (4.57) and (4.58).

To test for particle entity, we introduced the condition Eq. (4.69), that we rewrote in terms of particle number moments, Eq. (4.70), and, on the basis of the identity Eq. (4.71), in terms of connected moments, Eq. (4.73).

In Section 4.4, we were able to show in a few lines that particle entity according to Eq. (4.70) generally holds in Doi-Peliti field theories, Eq. (4.82). This finding is independent of the specifics of the action. To demonstrate particle entity for non-interacting, diffusive field theories on the basis of Dean's equation, we used in Section 4.5 our key result on the connected particle number moments, Eq. (4.93), before constructing the main result Eq. (4.116) on the basis of the full moments, with some of the more cumbersome calculations relegated to Appendix 4.A.

It is interesting to speculate whether our derivation simplifies further by exploiting the well-known identity [171] relating the Legendre transform of the generating function of the connected moments and the effective action, which only depends on the one-particle irreducible (1PI) diagrams. Since 1PIs represent a relatively small subset of all connected diagrams, a particle entity signature of this type might be more easily

applicable to theories involving pair interactions, which are beyond the scope of the present analysis.

4.A Induction over connected diagrams

We want to prove that the connected moments of the particle number density in the response field field theory derived from Dean's equation obey Eq. (4.85) to all orders of n, restated here for convenience:

$$\langle \rho(\mathbf{k}_1,t)...\rho(\mathbf{k}_n,t)\rangle_c = n_0\theta(t-t_0)\exp\{\mathring{\imath}(\mathbf{k}_1+...\mathbf{k}_n)\cdot\mathbf{x}_0\}\sum_{m=1}^{n}(-1)^{m-1}(m-1)! \quad (4.122)$$
$$\times \sum_{\{\mathbb{P}_1,...,\mathbb{P}_m\}\in\mathcal{P}(\{1,...,n\},m)} \exp\left\{-D(t-t_0)\sum_{i=1}^{m}\mathbf{K}\left(\mathbb{P}_i\right)^2\right\}.$$

For this we have to consider all diagrams with a single incoming leg and an arbitrary number n of outgoing legs, the first four orders of which are depicted in Eqs. (4.123), (4.124), (4.125) and (4.126).

$\langle \rho(\mathbf{k}_1,t)\rangle_c \mathrel{\hat{=}}$ 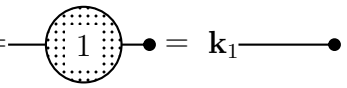 (4.123)

$\langle \rho(\mathbf{k}_1,t)\rho(\mathbf{k}_2,t)\rangle_c \mathrel{\hat{=}}$ 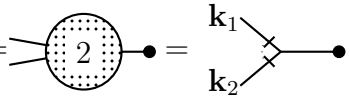 (4.124)

$\langle \rho(\mathbf{k}_1,t)\rho(\mathbf{k}_2,t)\rho(\mathbf{k}_3,t)\rangle_c \mathrel{\hat{=}}$ 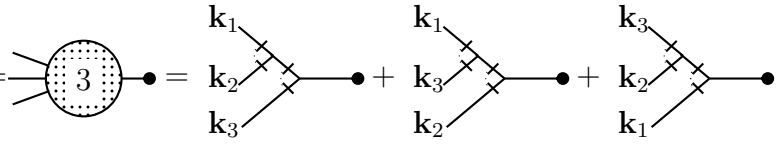 (4.125)

$$\langle \rho(\mathbf{k}_1,t)\rho(\mathbf{k}_2,t)\rho(\mathbf{k}_3,t)\rho(\mathbf{k}_4,t)\rangle_c \hat{=}$$

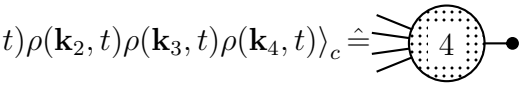

$$=$$

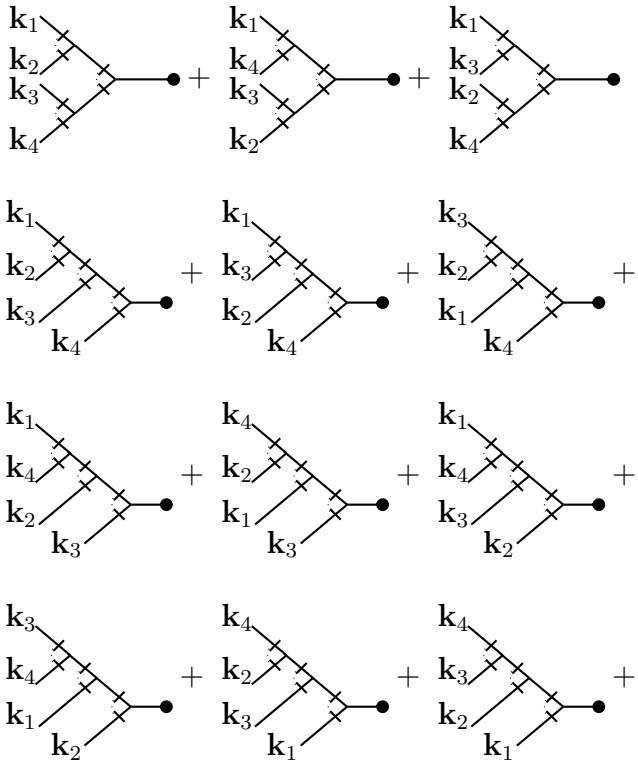

. (4.126)

The shading of the circular vertices above is meant as a visual reminder that we are now dealing with connected moments of the local number *density*, which depend on an unordered set of n external momenta $\mathbf{k}_1, ..., \mathbf{k}_n$, as opposed to connected moments of the *integrated* number density in a patch Ω (cf. Eq. (4.85) and Eq. (4.89)). The shaded diagrams are by construction invariant under permutations of the momenta $\mathbf{k}_1, ..., \mathbf{k}_n$.

We proceed by determining some of the shaded diagrams. The trivial case, $n = 1$ shown in Eq. (4.123), is given by the propagator Eq. (4.34) and the perturbative contribution from the source Eq. (4.22) with coupling n_0. Through direct computation in the mixed

momentum-time representation, see Eq. (4.84), we find for the $n = 2$ case Eq. (4.124):

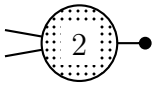

$$\begin{aligned}
&\hat{=} n_0 \Theta(t - t_0) \exp\{\mathring{i}(\mathbf{k}_1 + \mathbf{k}_2) \cdot \mathbf{x}_0\} \\
&\quad \times \int_{t_0}^{t} \mathrm{d}t' \, (-2D\mathbf{k}_1 \cdot \mathbf{k}_2) \exp\big\{-D(t - t')\mathbf{k}_1^2\big\} \exp\big\{-D(t - t')\mathbf{k}_2^2\big\} \exp\big\{-D(t' - t_0)\mathbf{k}_0^2\big\} \\
&= n_0 \exp\{\mathring{i}(\mathbf{k}_1 + \mathbf{k}_2) \cdot \mathbf{x}_0\} \left[\exp\big\{-D(t - t_0)(\mathbf{k}_1 + \mathbf{k}_2)^2\big\} - \exp\big\{-D(t - t_0)(\mathbf{k}_1^2 + \mathbf{k}_2^2)\big\}\right] ,
\end{aligned} \tag{4.127}$$

where the integral over t arises from representing the Dean vertex Eq. (4.36) in k-t-space. Each Dean vertex comes with a symmetry factor of 2. A factor of $(-2\mathbf{k}_1 \cdot \mathbf{k}_2)^{-1}$ that arises in the t integration precisely cancels with the vertex prefactor $-2D\mathbf{k}_1 \cdot \mathbf{k}_2$, which simplifies the result Eq. (4.127) considerably. A similar calculation for the $n = 3$ case Eq. (4.125) yields

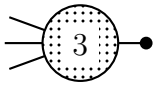

$$\begin{aligned}
&\hat{=} n_0 \Theta(t - t_0) \exp\{\mathring{i}(\mathbf{k}_3 + \mathbf{k}_2 + \mathbf{k}_1) \cdot \mathbf{x}_0\} \left[\exp\big\{-D(t - t_0)(\mathbf{k}_1 + \mathbf{k}_2 + \mathbf{k}_3)^2\big\}\right. \\
&- \exp\big\{-D(t - t_0)((\mathbf{k}_1 + \mathbf{k}_2)^2 + \mathbf{k}_3^2)\big\} - \exp\big\{-D(t - t_0)((\mathbf{k}_1 + \mathbf{k}_3)^2 + \mathbf{k}_2^2)\big\} \\
&\left. - \exp\big\{-D(t - t_0)((\mathbf{k}_3 + \mathbf{k}_2)^2 + \mathbf{k}_1^2)\big\} + 2\exp\big\{-D(t - t_0)(\mathbf{k}_1^2 + \mathbf{k}_2^2 + \mathbf{k}_3^2)\big\}\right] .
\end{aligned} \tag{4.128}$$

The left-hand side of Eq. (4.128) contains the sum over all distinct ways to assign the external momenta to the outgoing legs, as shown in (4.125). The whole sum of the terms is necessary for the coefficients of the Dean vertices to cancel with the k-dependent factor coming down from the t-integrations. We will see that this mechanism is instrumental in performing the induction later on.

Based on Eq. (4.127) and (4.128) we conjecture and indeed show below that a general

connected moment has the form Eq. (4.85),

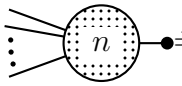

$$\hat{=} \langle \rho(\mathbf{k}_1,t)\rho(\mathbf{k}_1,t)\dots\rho(\mathbf{k}_n,t)\rangle$$

$$= n_0\theta(t-t_0)\exp\{\mathring{i}(\mathbf{k}_1+\dots)\cdot\mathbf{x}_0\}\sum_{m=1}^{n}(-1)^{m-1}(m-1)! \qquad (4.129)$$

$$\times \sum_{\{\mathbb{P}_1,\dots,\mathbb{P}_m\}\in\mathcal{P}(\{1,\dots,n\},m)} \exp\left\{-D(t-t_0)\sum_{i=1}^{m}\mathbf{K}\left(\mathbb{P}_i\right)^2\right\},$$

with $\mathcal{P}\left(\{1,\dots,n\},m\right)$ the set of all partitions of the set $\{1,\dots,n\}$ into m non-empty, distinct subsets $\mathbb{P}_i$ with $i=1,2,\dots,m$ so that $\cup_{i=1}^{m}\mathbb{P}_i=\{1,2,\dots,n\}$, as introduced after Eq. (4.85). The second sum $\sum_{\{\mathbb{P}_1,\dots,\mathbb{P}_m\}\in\mathcal{P}(\{1,\dots,n\},m)}$ in Eq. (4.129) thus runs over all distinct partitions of $\{1,2,\dots,n\}$ into m subsets $\mathbb{P}_1,\dots,\mathbb{P}_m$. There is no order to the subsets, so that the partition $\{\{1\},\{2\}\}$ of $\{1,2\}$ is identical to $\{\{2\},\{1\}\}$ and thus considered the same in $\mathcal{P}\left(\{1,2\},2\right)$. We use $\mathbf{K}\left(\mathbb{P}\right)$ to denote sums over momenta given by the indices in set $\mathbb{P}$, Eq. (4.86), $\mathbf{K}\left(\mathbb{P}\right)=\sum_{p\in\mathbb{P}}\mathbf{k}_p$. Eq. (4.129) is a function of the *set* of momenta $\{\mathbf{k}_1,\dots,\mathbf{k}_n\}$, or simply the indices $\{1,\dots,n\}$ alone, and invariant under their permutation.

Eq. (4.129) will be our induction hypothesis, with the induction to be taken in n, the number of outgoing legs. The base cases $n=1$, $n=2$ and $n=3$ are immediately verified, as $\mathcal{P}\left(\{1\},1\right)=\{\,\{\{1\}\}\,\}$ reduces Eq. (4.129) trivially to Eq. (4.34), $\mathcal{P}\left(\{1,2\},1\right)=\{\,\{\{1,2\}\}\,\}$ and $\mathcal{P}\left(\{1,2\},2\right)=\{\,\{\{1\},\{2\}\}\,\}$ to Eq. (4.127) and $\mathcal{P}\left(\{1,2,3\},1\right)=\{\,\{\{1,2,3\}\}\,\}$, $\mathcal{P}\left(\{1,2,3\},2\right)=\{\,\{\{1\},\{2,3\}\},\{\{2\},\{3,1\}\},\{\{3\},\{1,2\}\}\,\}$ and $\mathcal{P}\left(\{1,2,3\},3\right)=\{\,\{\{\{1\},\{2\},\{3\}\}\}\,\}$ to Eq. (4.128).

We want to show that if Eq. (4.129) holds for all strictly positive $n\leq m-1$ then it also holds for $n=m$. To this end we consider two distinct subsets of indices $\mathbb{A}$ and $\mathbb{B}$ with cardinality $|\mathbb{A}|>0$ and $|\mathbb{B}|>0$ respectively, so that $\mathbb{A}\cap\mathbb{B}=\emptyset$, $\mathbb{A}\cup\mathbb{B}=\{1,\dots,n\}$ and thus $|\mathbb{A}|+|\mathbb{B}|=n$. Each of these sets enters as the argument of diagrams

that have $|\mathbb{A}|$ and $|\mathbb{B}|$ external legs respectively, each parameterised by the momenta given by the subsets, $\{\mathbf{k}_q|q\in\mathbb{A}\}$ and $\{\mathbf{k}_q|q\in\mathbb{B}\}$ respectively. These diagrams can be

"stitched together" via the Dean vertex, Eq. (4.36), so that

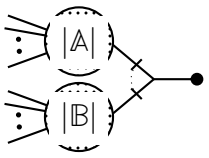

$$
\begin{aligned}
&\hat{=} n_0\theta(t-t_0)\exp\{\mathring{\imath}(\mathbf{k}_1+\ldots+\mathbf{k}_n)\cdot\mathbf{x}_0\}\int_{t_0}^{t}\mathrm{d}t'\ (-2D\mathbf{K}(\mathbb{A})\cdot\mathbf{K}(\mathbb{B}))e^{-D(t'-t_0)(\mathbf{k}_1+\ldots+\mathbf{k}_n)^2}\\
&\times\left[\sum_{a=1}^{|\mathbb{A}|}(-1)^{a-1}(a-1)!\sum_{\{\mathbb{P}_1,\ldots,\mathbb{P}_a\}\in\mathcal{P}(\mathbb{A},a)}\exp\left\{-D(t-t')\sum_{i=1}^{a}\mathbf{K}(\mathbb{P}_i)^2\right\}\right] \qquad (4.130)\\
&\times\left[\sum_{b=1}^{|\mathbb{B}|}(-1)^{b-1}(b-1)!\sum_{\{\mathbb{Q}_1,\ldots,\mathbb{Q}_b\}\in\mathcal{P}(\mathbb{B},b)}\exp\left\{-D(t-t')\sum_{j=1}^{b}\mathbf{K}(\mathbb{Q}_j)^2\right\}\right]\\
&=n_0\theta(t-t_0)\exp\{\mathring{\imath}(\mathbf{k}_1+\ldots+\mathbf{k}_n)\cdot\mathbf{x}_0\}\sum_{a=1}^{|\mathbb{A}|}\sum_{b=1}^{|\mathbb{B}|}(-1)^{a+b}(a-1)!(b-1)!(-2D\mathbf{K}(\mathbb{A})\cdot\mathbf{K}(\mathbb{B}))\\
&\times\sum_{\{\mathbb{P}_1,\ldots\}\in\mathcal{P}(\mathbb{A},a)}\sum_{\{\mathbb{Q}_1,\ldots\}\in\mathcal{P}(\mathbb{B},b)}\\
&\times\exp\big\{D(\mathbf{k}_1+\ldots+\mathbf{k}_n)^2t_0\big\}\exp\left\{-Dt\sum_{i=1}^{a}\mathbf{K}(\mathbb{P}_i)^2\right\}\exp\left\{-Dt\sum_{j=1}^{b}\mathbf{K}(\mathbb{Q}_j)^2\right\}\\
&\times\int_{t_0}^{t}\mathrm{d}t'\ \exp\left[Dt'\left(\sum_{i=1}^{a}\mathbf{K}(\mathbb{P}_i)^2+\sum_{j=1}^{b}\mathbf{K}(\mathbb{Q}_j)^2-(\mathbf{k}_1+\cdots+\mathbf{k}_n)^2\right)\right]\ .
\end{aligned}
$$

On the left is a diagram with $|\mathbb{A}|+|\mathbb{B}|$ legs and on the right we use Eq. (4.129) for diagrams with fewer legs, because neither $\mathbb{A}$ nor $\mathbb{B}$ can be empty. If we can show that the sum of all diagrams on the left obeys Eq. (4.129), then the induction step is completed.

Since $\cup_{i=1}^{a}\mathbb{P}_i=\mathbb{A}$, we have from Eq. (4.86) that $\sum_{i=1}^{a}\mathbf{K}(\mathbb{P}_i)=\mathbf{K}(\mathbb{A})$ and similarly $\sum_{j=1}^{b}\mathbf{K}(\mathbb{Q}_j)=\mathbf{K}(\mathbb{B})$ and further $\mathbf{K}(\mathbb{A})+\mathbf{K}(\mathbb{B})=\mathbf{K}(\{1,\ldots,n\})=\mathbf{k}_1+\ldots\mathbf{k}_n$, so that the exponent in square brackets appearing within the t' integral in the last line of

Eq. (4.130) can be rearranged as follows:

$$\sum_{i=1}^{a} \mathbf{K}\left(\mathbb{P}_i\right)^2 + \sum_{j=1}^{b} \mathbf{K}\left(\mathbb{Q}_j\right)^2 - \left(\mathbf{k}_1 + \cdots + \mathbf{k}_n\right)^2$$
$$= -2\left(\mathbf{K}\left(\mathbb{A}\right)\cdot\mathbf{K}\left(\mathbb{B}\right) + \sum_{i=1}^{a}\sum_{e=i+1}^{a} \mathbf{K}\left(\mathbb{P}_i\right)\cdot\mathbf{K}\left(\mathbb{P}_e\right) + \sum_{j=1}^{b}\sum_{f=j+1}^{b} \mathbf{K}\left(\mathbb{Q}_j\right)\cdot\mathbf{K}\left(\mathbb{Q}_f\right)\right) , \tag{4.131}$$

with the nested double summations generating all cross-terms once. In fact, the bracket on the right hand side of Eq. (4.131) is the sum of the vector products of all $ab + a(a-1)/2 + b(b-1)/2 = (a+b)(a+b-1)/2$ distinct pairs of vectors generated with Eq. (4.86) from the $a+b$ sets $\{\mathbb{P}_1, \ldots, \mathbb{P}_a, \mathbb{Q}_1, \ldots, \mathbb{Q}_b\}$. With Eq. (4.131) we arrive at

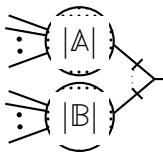

$$\hat{=} n_0\theta(t-t_0)\exp\{\mathring{i}(\mathbf{k}_1 + \ldots + \mathbf{k}_n)\cdot\mathbf{x}_0\}\sum_{a=1}^{|\mathbb{A}|}\sum_{b=1}^{|\mathbb{B}|}(-1)^{a+b}(a-1)!(b-1)!$$
$$\times \sum_{\{\mathbb{P}_1,\ldots\}\in\mathcal{P}(\mathbb{A},a)} \sum_{\{\mathbb{Q}_1,\ldots\}\in\mathcal{P}(\mathbb{B},b)} \frac{\mathbf{K}\left(\mathbb{A}\right)\cdot\mathbf{K}\left(\mathbb{B}\right)}{\mathbf{K}\left(\mathbb{A}\right)\cdot\mathbf{K}\left(\mathbb{B}\right) + \sum_{i=1}^{a}\sum_{e=i+1}^{a} \mathbf{K}\left(\mathbb{P}_i\right)\cdot\mathbf{K}\left(\mathbb{P}_e\right) + \sum_{j=1}^{b}\sum_{f=j+1}^{b} \mathbf{K}\left(\mathbb{Q}_j\right)\cdot\mathbf{K}\left(\mathbb{Q}_f\right)} \tag{4.132}$$
$$\times \left[e^{-D(t-t_0)(\mathbf{k}_1+\ldots+\mathbf{k}_n)^2} - e^{-D(t-t_0)\left(\sum_{i=1}^{a}\mathbf{K}(\mathbb{P}_i)^2 + \sum_{j=1}^{b}\mathbf{K}(\mathbb{Q}_j)^2\right)}\right] .$$

The main obstacle to simplify Eq. (4.132) further at this point is the fraction of scalar products of $\mathbf{K}\left(\cdot\right)$'s. Similar to the 3-point case, Eq. (4.128), this will simplify only once we consider the sum over all diagrams with non-equivalent permutations of the external momenta. Since the expressions inserted for sub-diagrams already take care of permutations within each subdiagram we need to consider only different partitionings of the indices $1, ..., n$ into subsets $\mathbb{A}$ and $\mathbb{B}$. Diagrammatically, for $n \geq 2$,

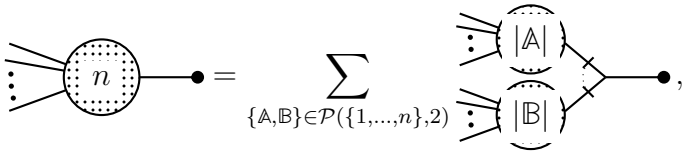

$$= \sum_{\{\mathbb{A},\mathbb{B}\}\in\mathcal{P}(\{1,\ldots,n\},2)} , \tag{4.133}$$

where $\mathbb{A}$ and $\mathbb{B}$ are again the sets of indices of the momenta associated with each part

of the partition. The external fields of the sub-diagram labelled $|\mathbb{A}|$ have momenta $\mathbf{k}_a$ with $a \in \mathbb{A}$ and correspondingly for the other sub-diagram. The cardinality $|\mathbb{A}|$ of the non-empty partition $\mathbb{A}$, ranges from 1 to $n-1$. The cardinality of the non-empty partition $\mathbb{B}$ is then given by $|\mathbb{B}| = n - |\mathbb{A}|$. Using Eq. (4.132) for the diagrams summed over in Eq. (4.133), we re-organise the partitioning, as explained below, and rewrite it as

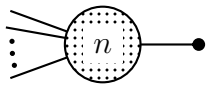

$$\hat{=} \sum_{\{\mathbb{A},\mathbb{B}\}\in\mathcal{P}(\{1,\ldots,n\},2)} \sum_{a=1}^{|\mathbb{A}|} \sum_{\{\mathbb{P}_1,\ldots\}\in\mathcal{P}(\mathbb{A},a)} \sum_{b=1}^{|\mathbb{B}|} \sum_{\{\mathbb{Q}_1,\ldots\}\in\mathcal{P}(\mathbb{B},b)} \mathcal{F}(\{\mathbb{P}_1,\ldots,\mathbb{P}_a\},\{\mathbb{Q}_1,\ldots,\mathbb{Q}_b\}) \tag{4.134a}$$

$$= \sum_{m=2}^{n} \sum_{\{\mathbb{W}_1,\ldots,\mathbb{W}_m\}\in\mathcal{P}(\{1,\ldots,n\},m)} \left[\sum_{\{\mathbb{T}_A,\mathbb{T}_B\}\in\mathcal{P}(\{1,\ldots,m\},2)} \mathcal{F}\left(\bigcup_{t\in\mathbb{T}_A} \{\mathbb{W}_t\}, \bigcup_{t\in\mathbb{T}_B} \{\mathbb{W}_t\} \right) \right] , \tag{4.134b}$$

where $\mathcal{F}$ is given by

$$\begin{aligned} &\mathcal{F}(\{\mathbb{P}_1,\ldots,\mathbb{P}_a\},\{\mathbb{Q}_1,\ldots,\mathbb{Q}_b\}) \\ &= \frac{n_0\theta(t-t_0)\exp\{\mathring{\imath}(\mathbf{k}_1+\ldots+\mathbf{k}_n)\cdot\mathbf{x}_0\}(-1)^{a+b}\,(a-1)!\,(b-1)!\,\mathbf{K}\left(\bigcup_{i=1}^{a}\mathbb{P}_i\right)\cdot\mathbf{K}\left(\bigcup_{i=1}^{b}\mathbb{Q}_i\right)}{\mathbf{K}\left(\bigcup_{i=1}^{a}\mathbb{P}_i\right)\cdot\mathbf{K}\left(\bigcup_{i=1}^{b}\mathbb{Q}_i\right) + \sum_{i=1}^{a}\sum_{e=i+1}^{a}\mathbf{K}(\mathbb{P}_i)\cdot\mathbf{K}(\mathbb{P}_e) + \sum_{j=1}^{b}\sum_{f=j+1}^{b}\mathbf{K}(\mathbb{Q}_j)\cdot\mathbf{K}(\mathbb{Q}_f)} \\ &\qquad \times\left[e^{-D(t-t_0)(\mathbf{k}_1+\ldots+\mathbf{k}_n)^2} - e^{-D(t-t_0)\left(\sum_{i=1}^{a}\mathbf{K}(\mathbb{P}_i)^2+\sum_{j=1}^{b}\mathbf{K}(\mathbb{Q}_j)^2\right)}\right] . \end{aligned} \tag{4.135}$$

The parameters a and b are the cardinalities of the first and the second partition in the argument of $\mathcal{F}$. This function depends on two partitions of two sets, $\mathbb{A}$ and $\mathbb{B}$, and it is invariant under exchange of its two arguments, which are sets of sets. On the basis of the partitions and the globally known $\mathbf{k}_1,\ldots,\mathbf{k}_n$, all the vectors on the right of Eq. (4.135) can be constructed, so that $\mathcal{F}$ is solely a function of the two partitions.

Both sides of Eq. (4.134) are performing the same summation, based on the five sums from Eqs. (4.132) and (4.133). Both summations generate all possible ways of partitioning the n external legs into two or more subsets. In fact there is a one-to-one correspondence between every term in the two sums, as we will demonstrate below. The first sum in Eq. (4.134a) considers all partitions $\mathcal{P}(\{1,\ldots,n\},2)$ of the full set of

indices $\{1,\ldots,n\}$ into two sets, $\mathbb{A}$ and $\mathbb{B}$. These indicate the momenta the two subdiagrams shown in Eqs. (4.132) and (4.133) depend on. To calculate these two subdiagrams all partitions of $\mathbb{A}$ and $\mathbb{B}$ need to be summed over, which is done in the remaining four sums. The right-hand side Eq. (4.134b) of Eq. (4.134) performs the same summation, but first produces all partitions of all $\{1,\ldots,n\}$ into $m = 2,\ldots,n$ non-empty subsets $\{\mathbb{W}_1,\ldots,\mathbb{W}_m\}$. In the rightmost sum, these subsets are distributed among the upper and the lower subdiagram by perfoming a partition into two subsets $\mathbb{T}_A$ and $\mathbb{T}_B$ on the indexing $\{1,\ldots,m\}$ of the subsets $\mathbb{W}_t$. These selections of subsets enter into the function $\mathcal{F}$, with, for example, the upper diagram being parameterised by the collection of sets

$$\bigcup_{t\in\mathbb{T}_A}\{\mathbb{W}_t\} = \{\mathbb{W}_{t_1},\mathbb{W}_{t_2},\ldots\} \neq \bigcup_{t\in\mathbb{T}_A}\mathbb{W}_t \quad \text{for} \quad \mathbb{T}_A = \{t_1,t_2,\ldots\}\ . \tag{4.136}$$

Both summations of Eq. (4.134) generate all partitions of the indices and their division into an upper and a lower subdiagram. Any term appearing on the left can be found on the right and vice versa. A set of parameters $\{\mathbb{P}_1,\ldots,\mathbb{P}_a\}$ and $\{\mathbb{Q}_1,\ldots,\mathbb{Q}_b\}$ on the left is found on the right when $m = a+b$ and $\{\mathbb{W}_1,\ldots,\mathbb{W}_m\} = \{\mathbb{P}_1,\ldots,\mathbb{P}_a\}\cup\{\mathbb{Q}_1,\ldots,\mathbb{Q}_b\}$ are the same partition of $\{1,\ldots,n\}$, with exactly one of the partitions $\mathbb{T}_A,\mathbb{T}_B$ of the elements of $\{\mathbb{W}_1,\ldots\}$ such that $\cup_{t\in\mathbb{T}_A}\{\mathbb{W}_t\} = \{\mathbb{P}_1,\ldots,\mathbb{P}_a\}$ and $\cup_{t\in\mathbb{T}_B}\{\mathbb{W}_t\} = \{\mathbb{Q}_1,\ldots,\mathbb{Q}_b\}$ or equivalenty $\cup_{t\in\mathbb{T}_A}\{\mathbb{W}_t\} = \{\mathbb{Q}_1,\ldots,\mathbb{Q}_b\}$ and $\cup_{t\in\mathbb{T}_B}\{\mathbb{W}_t\} = \{\mathbb{P}_1,\ldots,\mathbb{P}_a\}$. Similarly, the term generated by the partition $\cup_{t\in\mathbb{T}_A}\{\mathbb{W}_t\},\cup_{t\in\mathbb{T}_B}\{\mathbb{W}_t\}$ on the right, can be identified on the left, as the one where $\mathbb{A} = \cup_{t\in\mathbb{T}_A}\mathbb{W}_t$ and $\mathbb{B} = \cup_{t\in\mathbb{T}_B}\mathbb{W}_t$ or vice versa, which are both sets, not partitions. They need to be partitioned subsequently, for example $\mathbb{A}$ into $\{\mathbb{P}_1,\ldots,\mathbb{P}_a\} = \cup_{t\in\mathbb{T}_A}\mathbb{W}_t$ and $\mathbb{B}$ into $\{\mathbb{P}_1,\ldots,\mathbb{P}_b\} = \cup_{t\in\mathbb{T}_B}\mathbb{W}_t$ or equally $\mathbb{A}$ into $\{\mathbb{P}_1,\ldots,\mathbb{P}_a\} = \cup_{t\in\mathbb{T}_B}\mathbb{W}_t$ and $\mathbb{B}$ into $\{\mathbb{P}_1,\ldots,\mathbb{P}_b\} = \cup_{t\in\mathbb{T}_A}\mathbb{W}_t$.

Writing $\mathbb{T}_A = \{\alpha_1,\alpha_2,\ldots,\alpha_a\}$ and $\mathbb{T}_B = \{\beta_1,\beta_2,\ldots,\beta_b\}$, the parameterisation of the right-hand side of Eq. (4.134) allows us to express the denominator of $\mathcal{F}$, Eq. (4.135),

succinctly in terms of the new partition $\{\mathbb{W}_1, \ldots, \mathbb{W}_m\}$,

$$\begin{aligned}
&\mathbf{K}\left(\cup_{t\in\mathbb{T}_A}\{\mathbb{W}_t\}\right)\cdot\mathbf{K}\left(\cup_{t\in\mathbb{T}_B}\{\mathbb{W}_t\}\right)\\
&\qquad+\sum_{i=1}^{a}\sum_{e=i+1}^{a}\mathbf{K}\left(\mathbb{W}_{\alpha_i}\right)\cdot\mathbf{K}\left(\mathbb{W}_{\alpha_e}\right)+\sum_{j=1}^{b}\sum_{f=j+1}^{b}\mathbf{K}\left(\mathbb{W}_{\beta_j}\right)\cdot\mathbf{K}\left(\mathbb{W}_{\beta_f}\right)\\
&\qquad\qquad=\sum_{u=1}^{m}\sum_{v=u+1}^{m}\mathbf{K}\left(\mathbb{W}_u\right)\cdot\mathbf{K}\left(\mathbb{W}_v\right)
\end{aligned}\tag{4.137}$$

as this is the sum of all cross-terms in the square of $\sum_{t=1}^{m}\mathbf{K}\left(\mathbb{W}_t\right)$, as alluded to after Eq. (4.131). Further, the sum of the squares in the exponent of the right-most exponential in Eq. (4.135) can be written as

$$\sum_{i=1}^{a}\mathbf{K}\left(\mathbb{W}_{\alpha_i}\right)^2+\sum_{j=1}^{b}\mathbf{K}\left(\mathbb{W}_{\beta_j}\right)^2=\sum_{u=1}^{m}\mathbf{K}\left(\mathbb{W}_u\right)^2\tag{4.138}$$

as $\mathbb{T}_A\cup\mathbb{T}_B=\{1,\ldots,m\}$. Because the right-hand sides of Eqs. (4.137) and (4.138) are independent of the partitioning of $\{\mathbb{W}_1,\ldots,\mathbb{W}_m\}$ via $\mathbb{T}_A$ and $\mathbb{T}_B$, they can be taken outside the sum over these partitions together with $(-1)^{|\mathbb{T}_A|+|\mathbb{T}_B|}=(-1)^m$,

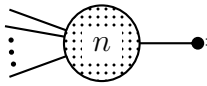

$$\hat{=}n_0\theta(t-t_0)\exp\{\mathring{\imath}(\mathbf{k}_1+\ldots+\mathbf{k}_n)\cdot\mathbf{x}_0\}\tag{4.139}$$

$$\times\sum_{m=2}^{n}(-1)^m\sum_{\{\mathbb{W}_1,\ldots,\mathbb{W}_m\}\in\mathcal{P}(\{1,\ldots,n\},m)}\frac{e^{-D(t-t_0)(\mathbf{k}_1+\ldots+\mathbf{k}_n)^2}-e^{-D(t-t_0)\left(\sum_{u=1}^{m}\mathbf{K}(\mathbb{W}_u)^2\right)}}{\sum_{u=1}^{m}\sum_{v=u+1}^{m}\mathbf{K}\left(\mathbb{W}_u\right)\cdot\mathbf{K}\left(\mathbb{W}_v\right)}$$

$$\times\left[\sum_{\{\mathbb{T}_A,\mathbb{T}_B\}\in\mathcal{P}(\{1,\ldots,m\},2)}(|\mathbb{T}_A|-1)!\;(|\mathbb{T}_B|-1)!\,\bar{\mathbf{K}}_A\cdot\bar{\mathbf{K}}_B\right],$$

where we use the shorthands

$$\bar{\mathbf{K}}_A=\mathbf{K}\left(\bigcup_{t\in\mathbb{T}_A}\{\mathbb{W}_t\}\right)=\sum_{t\in\mathbb{T}_A}\mathbf{K}\left(\mathbb{W}_t\right)\tag{4.140a}$$

$$\bar{\mathbf{K}}_B=\mathbf{K}\left(\bigcup_{t\in\mathbb{T}_B}\{\mathbb{W}_t\}\right)=\sum_{t\in\mathbb{T}_B}\mathbf{K}\left(\mathbb{W}_t\right)\;.\tag{4.140b}$$

Next we want to simplify the sum in square brackets in Eq. (4.139). Since it is over all ways to partition $\{1,\ldots,m\}$ into the two distinct sets that define $\bar{\mathbf{K}}_A$ and $\bar{\mathbf{K}}_B$, we know that the sum over the products $\bar{\mathbf{K}}_A \cdots \bar{\mathbf{K}}_B$ will involve every cross-term $\mathbf{K}(\mathbb{W}_u)\cdot\mathbf{K}(\mathbb{W}_v)$ with $u \neq v$ at least once and by symmetry equally often. The sum will therefore cancel with the denominator up to a pre-factor. In order to determine it, we pick a particular scalar product, $\mathbf{K}(\mathbb{W}_u)\cdot\mathbf{K}(\mathbb{W}_v)$ for some fixed $u \neq v$ and consider those terms in the sum that contain $\mathbf{K}(\mathbb{W}_u)\cdot\mathbf{K}(\mathbb{W}_v)$:

$$\begin{aligned} C_{u,v} &= \mathbf{K}(\mathbb{W}_u)\cdot\mathbf{K}(\mathbb{W}_v) \\ &\times \sum_{\{\mathbb{T}_A,\mathbb{T}_B\}\in\mathcal{P}(\{1,\ldots,m\},2)} \mathcal{I}\Big((u\in\mathbb{T}_A \wedge v\in\mathbb{T}_B)\vee(u\in\mathbb{T}_B\wedge v\in\mathbb{T}_A)\Big)\,(|\mathbb{T}_A|-1)!\,(|\mathbb{T}_B|-1)!\;, \end{aligned} \tag{4.141}$$

where $\mathcal{I}(\ldots)$ is an indicator function that is 1 only if indices u and v are in different subsets and 0 otherwise, so that the square bracket in Eq. (4.139) becomes $\sum_{u=1}^{m}\sum_{v=u+1}^{m} C_{u,v}$. We may therefore simply sum over all partitions where u and v indeed *are* in different subsets, for example u in $\mathbb{T}_A$ and v in $\mathbb{T}_B$ — there is no need to separately consider the case $u\in\mathbb{T}_B$ and $v\in\mathbb{T}_A$, as the resulting partitions are identical. The make-up of the subsets enters only in as far as their cardinalities are concerned, which feature in the factorial. If $n_A = |\mathbb{T}_A| > 0$ is the cardinality of $\mathbb{T}_A$, that leaves $n_B = m - n_A > 0$ elements for $\mathbb{T}_B$. With one "seat" in $\mathbb{T}_A$ given to u, there are $n_A - 1$ further elements to be chosen from the $m-2$ elements in $\{1,\ldots,m\}\setminus\{u,v\}$,

$$\begin{aligned} C_{u,v} &= \mathbf{K}(\mathbb{W}_u)\cdot\mathbf{K}(\mathbb{W}_v)\sum_{n_A=1}^{m-1}\binom{m-2}{n_A-1}(n_A-1)!\,(m-n_A-1)! \\ &= \mathbf{K}(\mathbb{W}_u)\cdot\mathbf{K}(\mathbb{W}_v)\sum_{n_A=1}^{m-1}(m-2)! = (m-1)!\,\mathbf{K}(\mathbb{W}_u)\cdot\mathbf{K}(\mathbb{W}_v)\;, \end{aligned} \tag{4.142}$$

which means that the square bracket in Eq. (4.139) cancels with the denominator in the preceding fraction up to a factor $(m-1)!$, which can be taken outside the second

sum,

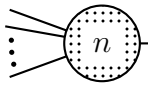

$$\hat{=} n_0\theta(t-t_0)\exp\{\mathring{\imath}(\mathbf{k}_1+\ldots+\mathbf{k}_n)\cdot\mathbf{x}_0\} \tag{4.143}$$
$$\times\sum_{m=2}^{n}(-1)^m\,(m-1)!\sum_{\{\mathbb{W}_1,\ldots,\mathbb{W}_m\}\in\mathcal{P}(\{1,\ldots,n\},m)}\left(e^{-D(t-t_0)(\mathbf{k}_1+\ldots+\mathbf{k}_n)^2}-e^{-D(t-t_0)\left(\sum_{u=1}^{m}\mathbf{K}(\mathbb{W}_u)^2\right)}\right)\,.$$

The first exponential in the final bracket is independent of the partition, so that the sum degenerates into the count of the ways a set of n elements can be partitioned into m non-empty sets, given by the Stirling number of the second kind, $\left\{{n \atop m}\right\}$. We find with the help of [122, 9.745.1]

$$\sum_{m=2}^{n}(-1)^m\,(m-1)!\sum_{\{\mathbb{W}_1,\ldots,\mathbb{W}_m\}\in\mathcal{P}(\{1,\ldots,n\},m)}1=\sum_{m=2}^{n}(-1)^m\,(m-1)!\left\{{n \atop m}\right\}=1\,. \tag{4.144}$$

With that in place, we rewrite Eq. (4.143) as

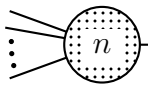

$$\hat{=} n_0\theta(t-t_0)\exp\{\mathring{\imath}(\mathbf{k}_1+\ldots+\mathbf{k}_n)\cdot\mathbf{x}_0\} \tag{4.145}$$
$$\times\left\{e^{-D(t-t_0)(\mathbf{k}_1+\ldots+\mathbf{k}_n)^2}+\sum_{m=2}^{n}(-1)^{m-1}\,(m-1)!\sum_{\{\mathbb{W}_1,\ldots,\mathbb{W}_m\}\in\mathcal{P}(\{1,\ldots,n\},m)}e^{-D(t-t_0)\left(\sum_{u=1}^{m}\mathbf{K}(\mathbb{W}_u)^2\right)}\right\}\,.$$

The exponential of $-D(t-t_0)(\mathbf{k}_1+...+\mathbf{k}_n)^2$ in the curly brackets is the summand of the subsequent sum running over $m\geq 2$ evaluated for $m=1$, because the only partition of $\{1,\ldots,n\}$ into $m=1$ subsets is $\mathbb{W}_1=\{1,\ldots,n\}$ which produces the vector $\mathbf{K}(\mathbb{W}_1)=\mathbf{k}_1+...+\mathbf{k}_n$. It follows that

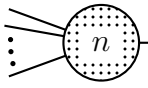

$$\hat{=} n_0\theta(t-t_0)\exp\{\mathring{\imath}(\mathbf{k}_1+\ldots+\mathbf{k}_n)\cdot\mathbf{x}_0\} \tag{4.146}$$
$$\times\sum_{m=1}^{n}(-1)^{m-1}\,(m-1)!\sum_{\{\mathbb{W}_1,\ldots,\mathbb{W}_m\}\in\mathcal{P}(\{1,\ldots,n\},m)}\left(e^{-D(t-t_0)\left(\sum_{u=1}^{m}\mathbf{K}(\mathbb{W}_u)^2\right)}\right)\,,$$

which is Eq. (4.129). We have thus demonstrated that if Eq. (4.129) holds for all diagrams with fewer than $n\geq 2$ legs, as they enter into Eq. (4.130), then Eq. (4.129) also holds for the diagrams with n legs. This concludes the induction step and together

with the base case $n = 1$ proves Eqs. (4.129) and (4.85) for all $n \geq 1$.

4.B Multiple starting points

We generalise our calculation of the connected and full moments of the integrated particle number density in Dean's formalism, Section 4.5, to the case where a total of n_0 particles are initialised at $H \leq n_0$ distinct sites. We upgrade the previous derivation by replacing in the action Eqs. (4.22) and (4.84) and correspondingly in Eqs. (4.24) and (4.85)

$$n_0 \exp\{i\mathbf{k}_0\mathbf{x}_0\} \qquad \text{by} \qquad \sum_{h=1}^{H} n_{0,h} \exp\{i\mathbf{k}_0\mathbf{x}_{0,h}\} \tag{4.147}$$

where $x_{0,h}$ for $h = 1, ..., H$ denote the $n_{0,h} \in \mathbb{N}$ particles' initial positions such that

$$\sum_{h=1}^{H} n_{0,h} = n_0 \ . \tag{4.148}$$

In Section 4.5 and Appendix 4.A we were entirely concerned with connected diagrams, where $n_0 \exp\{\mathring{i}\mathbf{x}_0 \cdot \mathbf{k}_0\}$ only ever enters linearly. Replacing it according to Eq. (4.147) renders each such diagram a sum over the H distinct locations, each such sum still to be considered a single *connected* diagram. This equally applies to the central result Eq. (4.93), which now reads

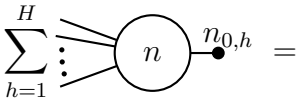

$$= -\sum_{h=1}^{H} n_{0,h}\theta(t-t_0) \sum_{m=1}^{n} \left(I_{\Omega,h}(t-t_0)\right)^m (m-1)! \left\{ {n \atop m} \right\} \tag{4.149}$$

where $I_{\Omega,h}(t - t_0)$ denotes the transition probability from the starting point $x_{0,h}$ into the set Ω.

The full moments of the integrated particle number density for distinct starting points can also be derived straighforwardly following the calculation in Eqs. (4.95)–(4.105).

Using Eq. (4.149) for the associated connected moments, we arrive at

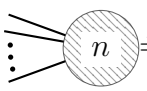

$$\hat{=} \left.\frac{d^n}{dz^n}\right|_{z=0} \prod_{h=1}^{H} \left[1 + (e^z - 1) I_{\Omega,h})\right]^{n_{0,h}} \tag{4.150}$$

$$= \sum_{j_1+\ldots+j_H=n} \binom{n}{j_1, \ldots, j_H} \prod_{h=1}^{H} \left.\frac{d^{j_h}}{dz^{j_h}}\right|_{z=0} \left[1 + (e^z - 1) I_{\Omega,h}\right]^{n_{0,h}} \tag{4.151}$$

$$= \sum_{j_1+\ldots+j_H=n} \binom{n}{j_1, \ldots, j_H} \prod_{h=1}^{H} \sum_{k_h=0}^{n_{0,h}} \binom{n_{0,h}}{k_h} \left(I_{\Omega,h}\right)^{k_h} k_h! \left\{ {j_h \atop k_h} \right\} , \tag{4.152}$$

where we have used the generalised product rule to go from Eq. (4.150) to Eq. (4.151) by swapping the differential operator into the product, as well as the intermediate result Eqs. (4.102)–(4.107) for the last step. One can easily verify that Eq. (4.152) reduces to Eq. (4.107) when $H = 1$, *i.e.* when all particles are initialised at the same point.

To show particle entity we use a similar procedure as in the single source case from Eq. (4.107) to (4.116),

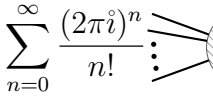

$$\sum_{n=0}^{\infty} \frac{(2\pi\mathring{i})^n}{n!} \hat{=} \sum_{n=0}^{\infty} \sum_{j_1+\ldots+j_H=n} \frac{(2\pi\mathring{i})^n}{j_1!\ldots j_H!} \prod_{h=1}^{H} \sum_{k_h=0}^{n_{0,h}} \binom{n_{0,h}}{k_h} \left(I_{\Omega,h}\right)^{k_h} k_h! \left\{ {j_h \atop k_h} \right\} , \tag{4.153}$$

where the second sum on the right runs over all non-negative integers $j_1, j_2, \ldots, j_H$ which sum to n. We now use that $\sum_{n=0}^{\infty} \sum_{j_1+\ldots+j_H=n} = \sum_{j_1=0}^{\infty} \ldots \sum_{j_H=0}^{\infty}$ as the sums

converge individually and absolutely, and Eq. (4.113) to obtain

$$\sum_{n=0}^{\infty} \frac{(2\pi\mathring{\imath})^n}{n!} \; \hat{=} \sum_{j_1=0}^{\infty} \dots \sum_{j_H=0}^{\infty} \frac{(2\pi\mathring{\imath})^{j_1+\dots+j_H}}{j_1!\dots j_H!} \prod_{h=1}^{H} \sum_{k_h=0}^{n_{0,h}} \binom{n_{0,h}}{k_h} (1-I_{\Omega,h})^{n_{0,h}-k_h} (I_{\Omega,h})^{k_h} k_h^{j_h} \tag{4.154}$$

$$= \prod_{h=1}^{H} \left(\sum_{j_h=0}^{\infty} \sum_{k_h=0}^{n_{0,h}} \binom{n_{0,h}}{k_h} (1-I_{\Omega,h})^{n_{0,h}-k_h} (I_{\Omega,h})^{k_h} \frac{(2\pi\mathring{\imath}k_h)^{j_h}}{j_h!} \right) \tag{4.155}$$

$$= \prod_{h=1}^{H} \left(\sum_{k_h=0}^{n_{0,h}} \binom{n_{0,h}}{k_h} (1-I_{\Omega,h})^{n_{0,h}-k_h} (I_{\Omega,h})^{k_h} e^{2\pi\mathring{\imath}k_h} \right) \tag{4.156}$$

$$= \prod_{h=1}^{H} (1) \tag{4.157}$$

$$= 1\,. \tag{4.158}$$

This completes the derivation of particle entity according to the criterion Eqs. (4.70) for particles initialised as multiple origins, *cf.* Eq. (4.116).

4.C Entropy production from Dean's equation

As already mentioned in the introduction to this Chapter, our interest in the concept of particle entity originates in part from the debate surrounding the use of path integral approaches to compute the thermodynamic dissipation in effective field theories of active matter, following the influential work of Nardini and collaborators [202]. In short, it is unclear whether the coarse-graining step implicit in the derivation of many continuum theory of collective active motion renders inaccessible certain microscopic features of the dynamics which could in principle have a non-trivial impact on the thermodynamic characterisation of these models [111]. This is why, more recently, the denomination of *informational* entropy production was introduced in this context, to distinguish between measures of time-reversal symmetry breaking versus dissipation [98, 193]. Field theories that retain particle entity, and are thus accurate descriptions of collective dynamics down to the single-particle scale, such as those studied in this work, are promising candidates to explore this issue further.

In this spirit, we derive here the expression for the entropy production for a system of indistinguishable Langevin processes interacting via a pairwise potential in a path integral representation of Dean's equation [75], as introduced in Section 4.2. We restate for convenience Dean's equation for the particle number density $\rho(x,t)$

$$\partial_t \rho(x,t) = \nabla \left(\rho \nabla \left. \frac{\delta F}{\delta \rho} \right|_{\rho(x,t)} \right) + \nabla(\rho^{1/2}\eta(x,t)) \tag{4.159}$$

where F is the free energy functional, defined as

$$F[\rho(x)] = \int \mathrm{dx}\ \rho(x) \left(V(x) + D\log(\rho(x)) + \int \mathrm{dy}\ U(x-y)\rho(y) \right) \tag{4.160}$$

with $V(x)$ a general single-particle potential, D the diffusion coefficient and $U(x-y)$ a translationally-invariant pairwise interaction potential. Neither V nor U are assumed to be binding potentials. The noise $\eta = (\eta^1, ..., \eta^d)$ entering the second term of Eq. (4.159) is a global uncorrelated vector white noise with covariance

$$\langle \eta^\mu(x,t)\eta^\nu(x',t')\rangle = 2D\delta(t-t')\delta(x-x')\delta^{\mu\nu}\ . \tag{4.161}$$

By formally rearranging Eq. (4.159) we can also write the noise η as

$$\eta = \rho^{-1/2}\nabla^{-1} \left(\partial_t \rho - \nabla \left(\rho \nabla \left. \frac{\delta F}{\delta \rho} \right|_{\rho(x,t)} \right) \right) \tag{4.162}$$

where the integral operator ∇^{-1} is the functional inverse of the gradient operator. The definition of ∇^{-1} requires a choice of gauge [202], which however is immaterial to the present derivation. Following the Onsager-Machlup construction [211], we substitute Eq. (4.162) directly into the expression for the probability of the forward and backwards noise path to obtain

$$P_F[\rho(x,t)] \propto \exp\left\{ \frac{1}{2D} \int \mathrm{dx\ dt}\ \rho^{-1} \left[\nabla^{-1} \left(\partial_t \rho - \nabla \left(\rho \nabla \left. \frac{\delta F}{\delta \rho} \right|_{\rho(x,t)} \right) \right) \right]^2 \right\} \tag{4.163}$$

and

$$P_B[\rho(x,t)] \propto \exp\left\{\frac{1}{2D}\int \mathrm{dx\ dt}\ \rho^{-1}\left[\nabla^{-1}\left(\partial_t\rho + \nabla\left(\rho\nabla\left.\frac{\delta F}{\delta\rho}\right|_{\rho(x,t)}\right)\right)\right]^2\right\}\ , \quad (4.164)$$

respectively. Note that we have omitted the Jacobian of the field transformation $\eta[\phi]$, which depends on the particular choice of time discretisation and is thus directly affected by the time-reversal operation implicit in Eq. (4.164) [72]. To sidestep this issue we interpret here Eq. (4.159) as a Stratonovich stochastic differential equation, so that the Jacobian is invariant under such reversal and thus cancels when ratios of probabilities are computed. We now substitute for these probabilities into the definition of the path-wise entropy production rate [64] in the limit of infinite path duration

$$\dot{S}_i = -\lim_{\tau\to\infty}\frac{1}{\tau}\log\frac{P_F[\rho(x,t)]}{P_B[\rho(x,t)]} \quad (4.165)$$

and obtain

$$\dot{S}_i = \lim_{\tau\to\infty}\frac{-1}{D\tau}\int \mathrm{dx\ dt}\ \rho^{-1}(\nabla^{-1}\partial_t\rho)\nabla^{-1}\nabla(\rho\nabla\frac{\delta F}{\delta\rho})\ . \quad (4.166)$$

After noticing that $\nabla^{-1}\nabla = 1$ by definition, the ρ^{-1} term originating from the multiplicative nature of the noise cancels out and we are left with

$$\dot{S}_i = \lim_{\tau\to\infty}\frac{-1}{D\tau}\int \mathrm{dx\ dt}\ (\nabla^{-1}\partial_t\rho)\nabla\frac{\delta F}{\delta\rho} = \lim_{\tau\to\infty}\frac{-1}{D\tau}\int \mathrm{dx\ dt}\ \partial_t\rho\frac{\delta F}{\delta\rho}\ , \quad (4.167)$$

where to obtain the second equality we have integrated by parts with respect to the position x. As already pointed out in [202], in the Stratonovich discretisation the usual chain rule of differentiation applies, $\partial_t\rho\delta F/\delta\rho = \partial_t F$, so that the integral above is equal to the free energy difference $\Delta F = F(x(\tau)) - F(x(0))$. For stable potentials U and V, the free energy function $F(x)$ is bounded below and $\dot{S}_i$ vanishes upon taking the limit $\tau\to\infty$ on the right hand side, as expected for relaxational equilibrium dynamics. It is instructive to explicitly expand the functional derivative of the free energy into its various contributions, namely

$$\frac{\delta F}{\delta\rho} = V(x) + D(1+\log(\rho(x))) + \int \mathrm{dy}\ U(x-y)\rho(y)\ . \quad (4.168)$$

Substituting into (4.167),

$$\dot{S}_i = \lim_{\tau\to\infty} \frac{-1}{D\tau} \int \mathrm{dx\ dt}\ \partial_t \rho(x) \left(V(x) + D(1 + \log(\rho(x))) + \int \mathrm{dy}\ U(x-y)\rho(y) \right) . \tag{4.169}$$

We see that the term coming from the single-particle potential $V(x)$ has the same form as the entropy production for a single Langevin process in a potential, where the potential might originate from a constant self-propulsion force, e.g. $V(x) = \pm\nu x$. Note, however, that in the usual derivation [256] the density $\rho(x,t)$ is a probability, specifically the solution to the deterministic Fokker-Planck equation associated with the Langevin dynamics, while here it represents a fluctuating particle number density. The second term in Eq. (4.169) comes from the entropic part of the free energy and accounts for ρ being an actual density of particles, rather than a probability density for a single particle. It vanishes upon integration by part in the continuum, where the probability to find two particles at the same position x at any given time vanishes. Finally, the third terms accounts for the change in free energy associated with relative displacement of the individual particles.

ACKNOWLEDGMENTS

GP would like to thank Rohit Jain for interesting discussions and sparking his interest in Dean's equation. LC acknowledges support from the Francis Crick Institute, which receives its core funding from Cancer Research UK (FC001317), the UK Medical Research Council (FC001317), and the Wellcome Trust (FC001317).

5

Dynamically accelerated cover times

G. Maziya, L. Cocconi, G. Pruessner, N. Moloney

PRR **2**, 023421 (2020) [196]
Published 30 June 2020
DOI 10.1103/PhysRevResearch.2.023421

Overview Starting with this Chapter, we step away from the stochastic thermodynamics and into the wider realm of the statistical mechanics of non-equilibrium processes. The Coupon Collector problem (CCP) and its spatial generalisation, the Cover Time problem (CTP), both originate as problems in probability theory [136] (where they are examples of urn problems) but have found applications in a number of other contexts, from epidemics to polymer physics. The CCP and CTP deal with the statistics of the time/number of attempts required to sample every item in a set at least once given a particular sampling procedure, always with replacement. For example, how many attempts are required on average to sample all cards in a standard 52-card deck at least once, assuming cards are picked at random one at a time and mixed back into the deck after every sampling? Naturally, the probability of sampling a previously unseen item decreases over time as the fraction of unseen items decreases, leading to the completion time scaling superlinearly with the cardinality N of the set, in particular as

$N \log N$ for large N. In this sense, we can say that collection processes exhibits ageing, a feature of many non-equilibrium systems such as glasses. The CTP, where locations in some finite space are visited sequentially by local exploration, has attracted particular attention in the context of ecology. Here, previously unvisited locations can be thought of as untapped pools of resources/nutrients. While the search process is usually assumed to be homogeneous in time, mostly for the sake of simplicity, it is natural to imagine that realistic search strategies could be 'tweaked' in response to successful collection events (e.g. through a reward/penalty mechanism). In this Chapter we explore how the statistics of the standard CCP and CTP are modified upon introducing such dynamical acceleration/deceleration rules. We find that the resulting probability distributions for the completion time ranges from Gaussian for highly accelerated searches to exponential for highly decelerated ones. In the next Chapter, we will revisit the CCP through the lens of statistical field theory, in particular by casting it as a reaction-diffusion process on a graph and invoking the Doi-Peliti formalism (already introduced in Chapter 3) to extract a number useful observables.

Author contributions: NM identified the connection between CCP acceleration and the roughness of $1/f^{\alpha}$ signals and wrote the original draft of the manuscript. GM performed numerical experiments on the accelerated process. LC performed numerical experiments on the trajectory block-shuffling and teleportation. GP and NM supervised the project.

Abstract

Among observables characterising the random exploration of a graph or lattice, the cover time, namely the time to visit every site, continues to attract widespread interest. Much insight about cover times is gained by mapping to the (spaceless) coupon-collector problem, which amounts to ignoring spatio-temporal correlations, and an early conjecture that the limiting cover time distribution of regular random walks on large lattices converges to the Gumbel distribution in $d \geq 3$ was recently proved rigorously. Furthermore, a number of mathematical and numerical studies point to the robustness of the Gumbel universality to modifications of the *spatial* features of the random search processes (e.g. introducing persistence and/or intermittence, or changing the graph topology). Here we investigate the robustness of the Gumbel universality to dynamical modification of the *temporal* features of the search, specifically by allowing the random

walker to “accelerate" or “decelerate" upon visiting a previously unexplored site. We generalise the mapping mentioned above by relating the statistics of cover times to the roughness of $1/f^{\alpha}$ Gaussian signals, leading to the conjecture that the Gumbel distribution is but one of a family of cover time distributions, ranging from Gaussian for highly accelerated cover, to exponential for highly decelerated cover. While our conjecture is confirmed by systematic Monte Carlo simulations in dimensions $d > 3$, our results for acceleration in $d = 3$ challenge the current understanding of the role of correlations in the cover time problem.

5.1 Introduction

How long does it take to collect N distinct objects that are sampled uniformly with replacement? This is the so-called coupon collector problem [136]. Depending on the context, the objects may represent stickers in a football album, vertices on a fully-connected graph, or people in an epidemic. Close analogies to the coupon collector can be found in a toy model for the build-up of strain in a seismic fault [1], the random deposition of k-mers on a substrate [287], the infection of nodes on a network [15], or the parasitization of hosts [320]. More generally, the coupon collector belongs to the family of urn problems [150, 137]. An early result, proved by Erdős and Rényi [90], is that the coupon collection time follows a Gumbel distribution.

Often, the N objects to be collected are not sampled uniformly at any given time. For example, a random walker exploring a lattice can only “collect” nearest-neighbour sites. In this context, the total time to visit every site on a graph or lattice is known as the cover time. Cover times have been intensely studied since the 1980s [5, 2, 299]. For example, an early conjecture [3] that the cover time for a $d \geq 3$ torus is also Gumbel distributed was recently proved rigorously [24]. The manner in which a random walker covers a lattice [47, 48, 103] is encoded in the trace of the walk, i.e. the walk’s history, and this non-trivial random object has received much attention in the mathematics literature [276, 83]. Qualitatively, an important distinction is between walks that are transient ($d > 2$) versus recurrent ($d \leq 2$), even if the walk is restricted to a finite torus, in which case every site will eventually be visited.

In this paper, we are interested in modifying the cover process in time. Thus, we study the consequences of accelerating or decelerating the random walker upon visiting a new

site. In this way, we show that the Gumbel distribution is but one of a family of cover time distributions, ranging from Gaussian for highly accelerated cover, to exponential for highly decelerated cover. Coincidentally, this family of distributions describes the roughness of $1/f^{\alpha}$ Gaussian signals [10].

Our motivation for dynamically modifying the cover process is to further investigate some of the assumptions underlying the mapping of the cover time problem in $d \geq 3$ to the coupon collector problem, specifically those relating to the irrelevance of spatio-temporal correlations. The specific procedure we implement is also inspired by transport behavior in e.g. cellular environments, in which a molecule may aggregate or fragment in the course of its diffusion, thereby altering its diffusion constant in time [69, 134]. Alternatively, in the context of search problems [27], the random walker could be "rewarded" or "penalized" upon acquiring new targets, thereby enhancing or inhibiting future search.

The structure of the paper is as follows: In Sec. 5.2 we review basic results of the coupon collector problem. In Sec. 5.3 we describe how we accelerate or decelerate the dynamics, and identify the distribution of collection times. In Sec. 5.4 we turn our attention to cover times on a torus, and present numerical results for accelerated and decelerated random walkers in Secs. 5.5 and 5.6. We summarize our findings in Sec. 5.7.

5.2 Coupon collector problem

In this section we review the basic properties of the coupon collector problem [90]. The probability p_i of collecting a new coupon, given that i have already been collected, is

$$p_i = 1 - i/N, \quad i = 0, 1, \ldots, N-1. \tag{5.1}$$

Qualitatively, the first coupons are collected rapidly, while the last coupons are collected very slowly. Let n_i be the number of coupons drawn between collecting the ith and $(i+1)$th distinct coupon. Then the total number of draws C_N to collect N coupons is

$$C_N = \sum_{i=0}^{N-1} n_i, \tag{5.2}$$

where n_i are independent but non-identical geometric random variables with mean $1/p_i$. Using angular brackets to denote expectation, the mean of C_N is therefore

$$\langle C_N \rangle = \sum_{i=0}^{N-1} \langle n_i \rangle \tag{5.3}$$

$$= \sum_{i=0}^{N-1} \frac{1}{1 - i/N} = N \sum_{k=1}^{N} \frac{1}{k}, \tag{5.4}$$

which behaves like $N \log N$ for large N, i.e. collecting the full set of N coupons is slower than linear in N. Similarly, it can be shown that the variance of C_N is proportional to N^2. Erdős and Rényi derived the full distribution of C_N, showing it to be Gumbel [90].

Before giving a heuristic derivation of this distribution, it is convenient to embed the coupon collector in continuous time, such that coupons arrive at unit rate in the manner of a Poisson point process [3]. Thus, rather than the discrete unit steps representing the number of coupon draws, consider instead the amount of continuous time elapsed since collection began. In this perspective, the collection time H_j for any particular coupon j is an exponential random variable with mean N,

$$\mathbb{P}(H_j \leq t) = 1 - \exp(-t/N). \tag{5.5}$$

The total collection time is the maximum of all the individual coupon collection times. Since these times are identical and independent

$$\mathbb{P}(C_N \leq t) = \mathbb{P}(\max\{H_1, H_2, \ldots, H_N\} \leq t) \tag{5.6}$$

$$= \mathbb{P}(H_1 \leq t, H_2 \leq t, \ldots, H_N \leq t) \tag{5.7}$$

$$= \mathbb{P}(H_1 \leq t)\mathbb{P}(H_2 \leq t) \cdots \mathbb{P}(H_N \leq t) \tag{5.8}$$

$$= [1 - \exp(-t/N)]^N \tag{5.9}$$

$$\to \exp[-N \exp(-t/N)], \quad \text{as } N \to \infty. \tag{5.10}$$

After centering and rescaling,

$$\mathbb{P}\left(\frac{C_N - N \log N}{N} \leq t\right) = \exp(-\exp(-t)), \tag{5.11}$$

which is recognized as the Gumbel distribution from extreme value statistics [172].

5.3 Accelerated and decelerated coupon collector

The waiting time T_i between collecting the ith and $(i+1)$th distinct coupon is a sum over a random number n_i of unit exponential random variables. Since n_i is a geometric random variable, T_i is, in fact, also exponentially distributed with mean $1/p_i$ [70]. Thus, the total collection time can be written as

$$C_N = \sum_{i=0}^{N-1} T_i = N \sum_{k=1}^{N} \frac{\varepsilon_k}{k}, \tag{5.12}$$

where ε_k are independent and identically distributed exponential random variables with unit mean.

We now manipulate the arrival rate of random coupons which, in turn, alters the rate at which distinct coupons are collected. For example, if coupons arrive at rate $\rho_i = 1/p_i = 1/(1 - i/N)$ all the while i coupons have been collected, then the waiting time between distinct coupons has unit mean. Thus, by accelerating the arrival of coupons to compensate for the decreasing likelihood of obtaining a distinct coupon, distinct coupons are collected at unit rate. This acceleration protocol is depicted schematically in Fig 5.1: the piecewise constant rates ρ_i increase each time a distinct coupon is collected.

In order to accommodate a variety of acceleration-deceleration protocols, we generalize the rates ρ_i according to

$$\rho_i(\alpha) = p_i^{\alpha-1}, \quad \alpha \geq 0. \tag{5.13}$$

This leads to the collection time

$$C_N(\alpha) = N^\alpha \sum_{k=1}^{N} \frac{\varepsilon_k}{k^\alpha}, \tag{5.14}$$

where the unaccelerated coupon collector is recovered for $\alpha = 1$, i.e. Eq. (5.12), and the accelerated version just discussed above corresponds to $\alpha = 0$. For large N, the

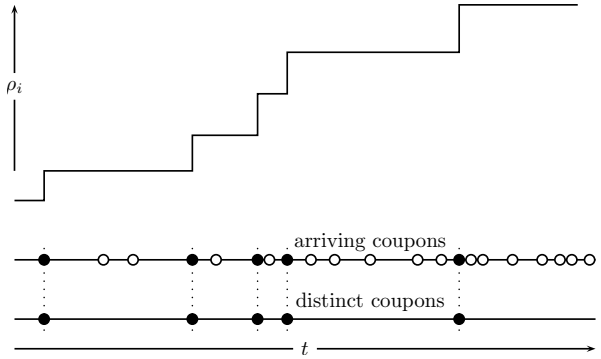

Figure 5.1: Schematic illustration of an acceleration protocol. The intensity of coupon arrivals (middle) is increased as distinct coupons are acquired (filled circles). The piecewise constant and increasing intensity profile (top) gives rise to a point process of distinct coupon arrivals (bottom) whose intensity can be adjusted.

mean of $C_N(\alpha)$ scales as

$$\langle C_N(\alpha) \rangle \sim \begin{cases} N, & 0 \leq \alpha < 1, \\ N \log N, & \alpha = 1, \\ N^\alpha, & \alpha > 1, \end{cases} \tag{5.15}$$

so that coupon collecting is accelerated for $0 \leq \alpha < 1$, and decelerated for $\alpha > 1$, as compared to the original unaccelerated process with $\alpha = 1$.

Apart from the N^α prefactor, the exact same sum in Eq. (5.14) describes the roughness of periodic Gaussian $1/f^\alpha$ signals [10], as outlined in the Appendix. In that context, $\alpha = 0, 1, 2, 4$ correspond respectively to white noise, $1/f$ noise [298], a steady-state Edwards-Wilkinson interface [87], and a steady-state curvature-driven interface [200].

When $\alpha = 0$, $C_N(0)$ in Eq. (5.14) is a sum over independent and identically distributed random exponential variables, which, after rescaling, is described by the central limit theorem. As shown in the Appendix, the Lindeberg condition extends the central limit theorem to non-identical random variables, such that the rescaled distribution of $C_N(\alpha)$ remains Gaussian for all $\alpha \leq 1/2$. For $\alpha = 2$, the distribution is Kolmogorov-Smirnov, i.e. the distribution of the test statistic in the Kolmogorov-Smirnov goodness-of-fit test [159]. This distribution reoccurs in many Brownian problems [100, 30], branching processes [101], aggregation [41], and statistics [297]. For $\alpha = 4$, the distribution of $C_N(4)$ has been calculated in [184]. Finally, in the limit $\alpha \to \infty$, $C_N(\infty)$ is exponentially

distributed, since only the first term in Eq. 5.14 contributes. A full discussion of the properties of $C_N(\alpha)$ can be found in [10]. In summary, the Gumbel distribution is one of a family of distributions of sums of weighted exponential random variables.

5.4 Cover times on a torus

If one identifies coupons with sites, then coupon collecting is similar in spirit to covering a lattice or graph, that is, visiting each and every site at least once. However, if the lattice exploration is undertaken by a random walker, it is far from obvious that coupon collecting describes the statistics of covering: at any given time coupons are sampled uniformly, whereas a random walker samples nearest neighbour sites. This non-uniform sampling is illustrated in Fig. 5.2, showing a portion of the trace of a random walk as it covers a lattice in $d = 3$.

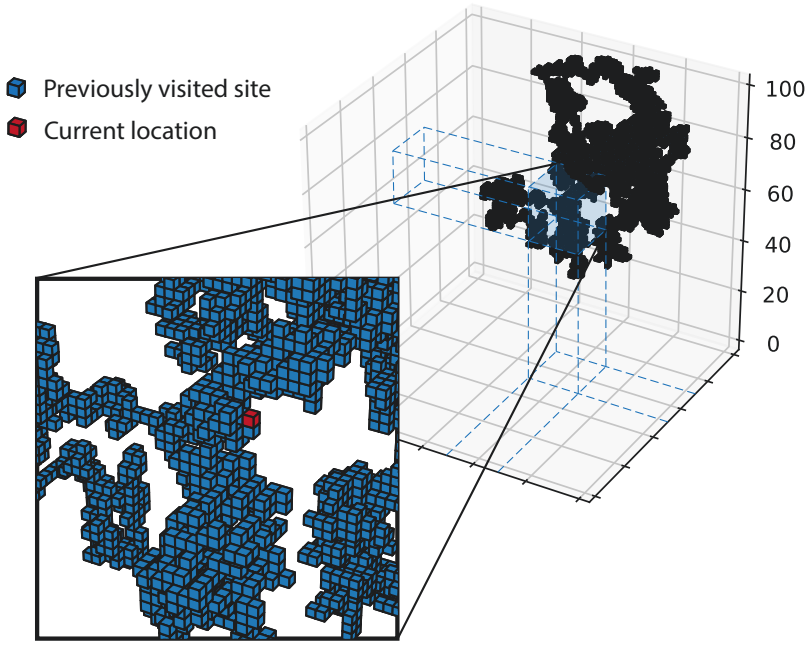

Figure 5.2: (Color online) Portion of the trace of a random walk in $d = 3$, showing the sites visited as the walker covers the lattice.

On a fully-connected graph all sites are nearest neighbours. Therefore covering a fully-

connected graph via a random walk is almost identical to coupon collecting, with the irrelevant difference that the random walker must necessarily leave the site most recently visited (assuming self-loops are excluded). Meanwhile, for random graphs cover times have been actively studied by mathematicians [2, 4] and physicists [319, 188], among others. If the probability distribution of the random walker location converges to the uniform distribution sufficiently fast, the same $N \log N$ scaling as Eq. (5.4) often describes the mean cover time. A graph-dependent constant prefactor will reflect the fact that the walker has to diffuse across the graph to cover it. This constant can be expressed in terms of the mean time spent at the origin [5].

For random walks on a torus (i.e., a regular lattice with periodic boundary conditions), cover times depend on dimension. In $d = 1$, the cover time (equivalent to the first-passage time of the range process) is not Gumbel distributed [144], while in $d \geq 3$ it is [24]. The $d = 2$ cover time, posed as the "white screen problem" [299], is not completely resolved to this day. Dembo *et al.* have established rigorously that the mean cover time converges to $4L^2(\log L)^2/\pi$ as the side length L of the simple cubic lattice tends to infinity, although there are practical difficulties in observing this behaviour in numerics [123]. Subleading order corrections to Dembo *et al.*'s result have been explored in the mathematics literature [25]. In the physics literature, numerical evidence suggests that $d = 2$ cover times are approximately Gumbel-distributed [63].

For this reason, in the following we restrict our attention to $d \geq 3$, where it is rigorously known that the cover time is Gumbel distributed [24] (already anticipated heuristically in [3]). The technical proof of this result relies on the transience of a random walker in $d \geq 3$, and the approximately Poisson distribution of unvisited sites at the late stage of the cover process [24]. Remarkably, the coupon collector scaling carries over to the cover time, even though the first-passage times $\{H_1, H_2, \ldots, H_N\}$ to each of the N sites are clearly not independent random variables, although they are approximately exponential. The appropriately scaled cover time now takes the form

$$\frac{C_N - g(0)N \log N}{g(0)N}, \tag{5.16}$$

which is identical to the coupon collector apart from a factor $g(0)$. This factor is the Green function for the unrestricted random walker evaluated at the origin, which is equivalent to the mean time spent at the origin. For example, for the simple cubic

lattice in $d = 3$ [116]

$$g(0) = \frac{4\sqrt{6}}{\pi^2}\Gamma\left(\frac{1}{24}\right)\Gamma\left(\frac{5}{24}\right)\Gamma\left(\frac{7}{24}\right)\Gamma\left(\frac{11}{24}\right)$$
$$= 1.516... \tag{5.17}$$

Thus, random walk covering is approximately 50% slower on a simple-cubic lattice compared to a fully-connected graph.

5.5 Accelerated and decelerated cover

In the coupon collector, the waiting times between coupon arrivals is exponential, and acceleration or deceleration is effected by changing its rate. Analogously, the cover process is accelerated or decelerated by changing the rate of the exponential waiting times between random walk steps. Thus, if we employ the acceleration-deceleration protocol as described in Eq. (5.13), we might conjecture that, for $d \geq 3$, the cover time in Eq. (5.14) is generalized to

$$C_N(\alpha) = g(0)N^\alpha \sum_{k=1}^{N} \frac{\varepsilon_k}{k^\alpha}, \tag{5.18}$$

where ε_k are again iid exponential random variables, and the effect of the underlying lattice is incorporated by the Green function $g(0)$. This generalization assumes that the correlations that were carefully accounted for in the standard cover problem [24] continue to play a minor role for $\alpha \neq 1$. In the case $\alpha = 1$, it is known that the first-passage times $H_{\mathbf{x}}$ and $H_{\mathbf{y}}$ of sites $\mathbf{x}$ and $\mathbf{y}$ respectively are correlated such that

$$\mathrm{Cov}(\mathbf{1}(H_{\mathbf{x}} > t), \mathbf{1}(H_{\mathbf{y}} > t)) \sim |\mathbf{x} - \mathbf{y}|^{-(d-2)}, \quad d \geq 3, \tag{5.19}$$

where $\mathbf{1}(H_{\mathbf{x}} > t)$ indicates that site $\mathbf{x}$ has been visited at a time greater than t. Eq. (5.19) is an asymptote in large system size N with t proportional to that size [48, 83]. For $\alpha \neq 1$, on the other hand, the nature of the correlations is unknown to us.

We numerically test the conjecture of Eq.(5.18) in the following by rescaling the observed

probability density $p(C_N(\alpha))$ by the mean

$$\phi_1(x) = \langle C_N(\alpha)\rangle \, p\left(x\langle C_N(\alpha)\rangle\right) \tag{5.20}$$

or by the standard deviation after centering,

$$\phi_2(x) = \sigma_{C_N(\alpha)} \, p\left(x\sigma_{C_N(\alpha)} + \langle C_N(\alpha)\rangle\right) \ . \tag{5.21}$$

5.5.1 Deceleration, $\alpha = 2$

For $\alpha = 2$, we conjecture that $C_N(2)$ is described by the Kolmogorov-Smirnov distribution, with Laplace transform [100, 30]

$$\langle e^{-sC_N(2)}\rangle = \frac{\sqrt{\pi^2 g(0) N^2 \, s}}{\sinh \sqrt{\pi^2 g(0) N^2 \, s}} \tag{5.22}$$

for large N, and first two moments

$$\langle C_N(2)\rangle = \frac{\pi^2 g(0)}{6} \, N^2, \quad \langle C_N^2(2)\rangle = \frac{7\pi^4 g^2(0)}{180} \, N^4. \tag{5.23}$$

The Laplace transform in Eq. (5.22) can be inverted to recover a series expansion for the probability density $p(C_N(2))$ which, after rescaling by the mean, reads [100]

$$\phi_1(x) = \frac{\pi^2}{3} \sum_{k=1}^{N} (-1)^{k+1} k^2 \exp\bigl(-\pi^2 k^2 x/6\bigr). \tag{5.24}$$

The sum converges fast, so that the cover time density of relatively small systems is very close to the asymptotic density as $N \to \infty$. Figs 5.3 and 5.4 show excellent agreement between empirical cover time densities and Eq. (5.24) in $d = 3, 4$.

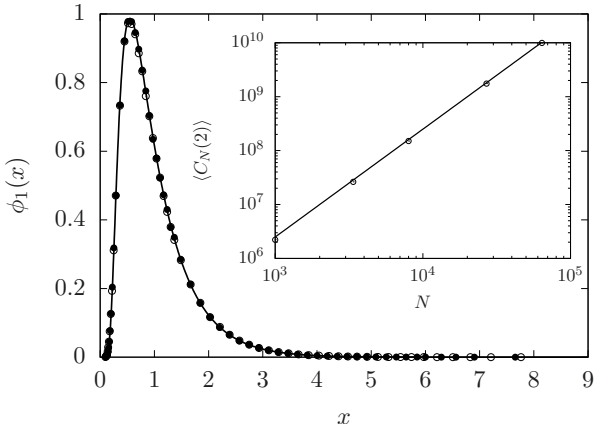

Figure 5.3: Rescaled cover time density, $\phi_1(x)$, for $\alpha = 2$ in $d = 3$ with $N = 30^3$ (empty circles), and $d = 4$ with $N = 15^4$ (filled circles), over an ensemble of 10^6 independent realizations. The conjectured density (solid line) is given by Eq. (5.24). Inset: Scaling of moments $\langle C_N(2)\rangle$ in $d = 3$ (empty circles). The conjectured behavior (solid line) is given by Eq. (5.23). Standard errors are smaller than the symbols.

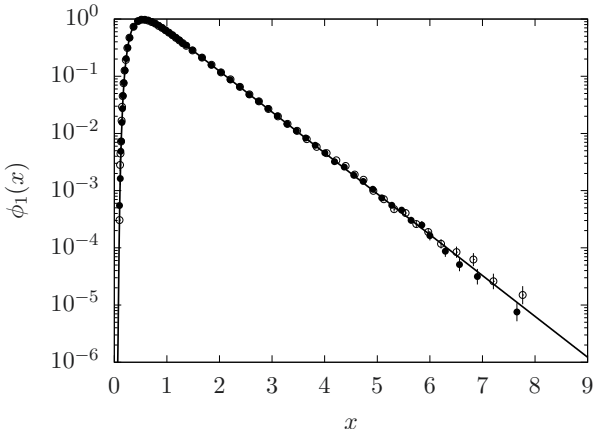

Figure 5.4: Same as Fig 5.3 but with a logarithmic y-axis. Error bars denote standard errors of histogram bins.

5.5.2 Deceleration, $\alpha = 4$

For $\alpha = 4$, we conjecture that $C_N(4)$ has the same distribution as the roughness of a curvature-driven interface, with Laplace transform [184]

$$\langle e^{-sC_N(4)}\rangle = \sqrt{4\pi^4 g(0) N^4 s} \times \frac{1}{\sinh[(4\pi^4 g(0) N^4 s)^{1/4}] - \cos[(4\pi^4 g(0) N^4 s)^{1/4}]} \tag{5.25}$$

and first two moments

$$\langle C_N(4)\rangle = \frac{\pi^4 g(0)}{90}\, N^4, \quad \langle C_N^2(4)\rangle = \frac{13\pi^8 g^2(0)}{56700}\, N^8. \tag{5.26}$$

The Laplace transform in Eq. (5.25) can be inverted to recover a series expansion for the probability density $p(C_N(4))$ which, after rescaling by the mean, reads [184]

$$\phi_1(x) = \frac{2\pi^5}{45} \sum_{k=1}^{N} \frac{(-1)^{k+1} k^5}{\sinh(\pi k)} \exp\bigl(-\pi^4 k^4 x/90\bigr). \tag{5.27}$$

Figs 5.5 and 5.6 show excellent agreement between empirical cover time densities and Eq. (5.27) in $d = 3, 4$.

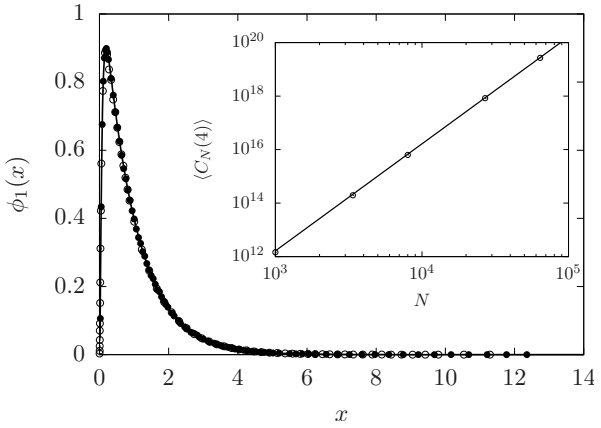

Figure 5.5: Rescaled cover time density, $\phi_1(x)$, for $\alpha = 4$ in $d = 3$ with $N = 30^3$ (empty circles), and $d = 4$ with $N = 15^4$ (filled circles), over an ensemble of 10^6 independent realizations. The conjectured density (solid line) is given by Eq. (5.27). Inset: Scaling of moments $\langle C_N(4)\rangle$ in $d = 3$ (empty circles). The conjectured behavior (solid line) is given by Eq. (5.26). Standard errors are smaller than the symbols.

5.5.3 Acceleration, $0 \le \alpha \le 1/2$, $d \ge 4$

For $0 \le \alpha \le 1/2$, Eq. (5.18) falls under the scope of the central limit. Therefore, the conjectured statistics of $C_N(\alpha)$ normalised to zero mean and unit standard deviation are described by a Gaussian distribution

$$\phi_2(z) = \frac{1}{\sqrt{2\pi}} e^{-z^2/2}. \tag{5.28}$$

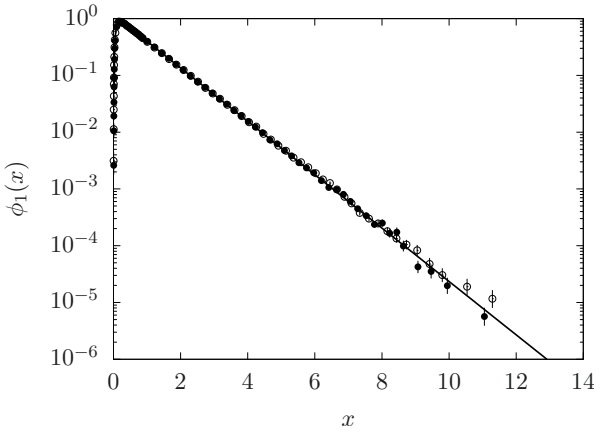

Figure 5.6: Same as Fig 5.5 but with a logarithmic y-axis. Error bars denote standard errors of histogram bins.

In the presence of correlations, the central limit theorem need no longer apply. Indeed, we find that our conjecture breaks down for accelerated cover in $d = 3$, and we discuss that case separately in Section 5.6. For $d \geq 4$, however, our conjecture continues to agree well with numerics. Fig 5.7 shows empirical cover time densities for $\alpha = 0, 1/4$ and $d = 4$. The small asymmetric discrepancies from Gaussian behaviour in the tails in $d = 4$ (Fig 5.7) disappear altogether in $d = 5$, as seen in Fig 5.8. This is in keeping with the general notion that correlations weaken with increasing dimension — also suggested by Eq. (5.19).

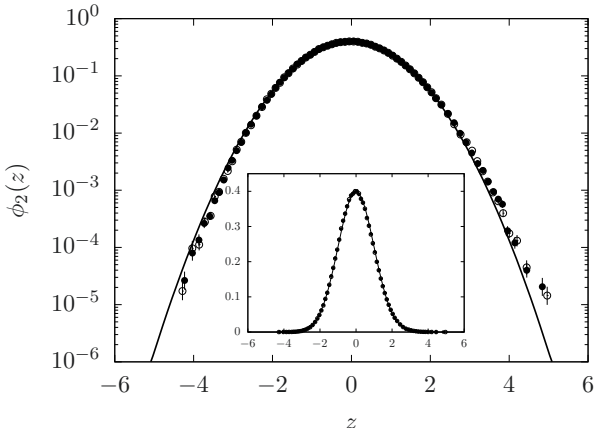

Figure 5.7: Rescaled cover time density, $\phi_2(z)$, for $\alpha = 0$ (empty circles) and $\alpha = 1/4$ (filled circles) in $d = 4$ with $N = 15^4$, over an ensemble of 10^6 independent realizations, compared with the Gaussian conjecture (solid line). Error bars denote standard errors of histogram bins. Inset: $\phi_2(z)$ on linear axes.

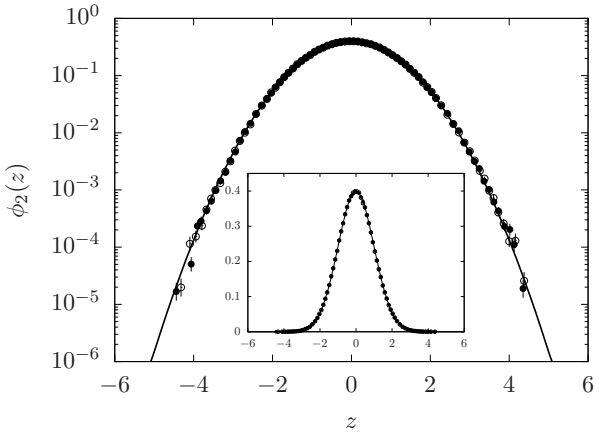

Figure 5.8: Rescaled cover time density, $\phi_2(z)$, for $\alpha = 0$ (empty circles) and $\alpha = 1/4$ (filled circles) in $d = 5$ with $N = 10^5$, over an ensemble of 10^6 independent realizations, compared with the Gaussian conjecture (solid line). Error bars denote standard errors of histogram bins. Inset: $\phi_2(z)$ on linear axes.

5.5.4 Acceleration, $\alpha = 3/4$

As explained in [10], for $1/2 < \alpha < 1$ the rescaled cover time densities $\phi_2(z)$ can be expanded as

$$\phi_2(z) = \sqrt{\zeta(2\alpha)} \sum_{k=1}^{\infty} k^{\alpha} Y(\alpha, k) \exp\Big(-k^{\alpha}\sqrt{\zeta(2\alpha)}\, z - 1\Big), \tag{5.29}$$

where ζ is the Riemann zeta function, and

$$Y(\alpha, k) = \prod_{n=1, \neq k}^{\infty} \frac{e^{(-k/n)^{\alpha}}}{1 - (k/n)^{\alpha}}. \tag{5.30}$$

Eq. (5.29) defines an α-dependent family of distributions with exponential right tails. For the representative case of $\alpha = 3/4$, Fig 5.9 shows good agreement with our conjecture, with small discrepancies in $d = 3$ disappearing altogether in $d = 4$.

5.6 Acceleration, $\alpha = 0$, $d = 3$

In all cases considered so far, the conjecture that the cover time $C_N(\alpha)$ is described statistically by Eq. (5.18) is successfully verified empirically. However, the conjecture fails in the case $\alpha = 0$ in $d = 3$. According to Eq. (5.18), the cover time is predicted to

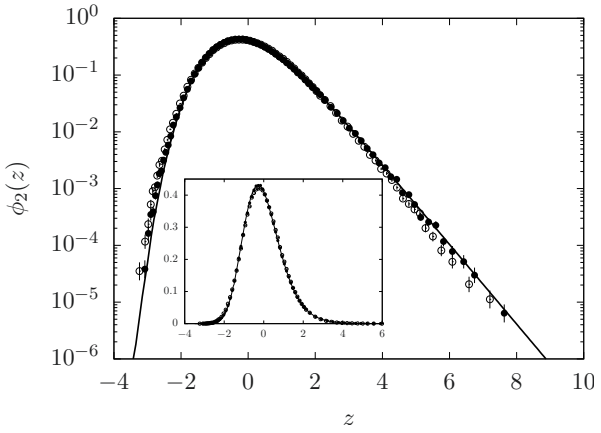

Figure 5.9: Rescaled cover time density, $\phi_2(z)$, for $\alpha = 3/4$ in $d = 3$ with $N = 30^3$ (empty circles), and $d = 4$ with $N = 15^4$ (filled circles), over an ensemble of 10^6 independent realizations. The conjectured density (solid line) is given by Eq. (5.29). Error bars denote standard errors of histogram bins. Inset: $\phi_2(z)$ on linear axes.

be statistically equivalent to a sum of independent and identical exponential random variables, therefore falling under the scope of the central limit theorem. The only feature correctly predicted by Eq. (5.18) is that the mean cover time $\langle C_N(0)\rangle$ still behaves as $g(0)N$, as shown in Fig 5.10. However, the standard deviation $\sigma_{C_N(0)}$ does not scale as $N^{1/2}$. Instead, for system sizes $N \geq 10^3$ it is well approximated by

$$\sigma_{C_N(0)} = Ag(0)N^{\gamma}, \tag{5.31}$$

where we note that the fitted values of the amplitude $A = 0.44(2)$ and exponent $\gamma = 0.6608(12)$ are close to $\sqrt{2} - 1 = 0.414\ldots$ and $2/3$, respectively.

The rescaled cover time density $\phi_2(z)$ is also not Gaussian, as shown in Figs 5.11 and 5.12. We are not able to identify the empirical density, although a Tracy-Widom density for the largest eigenvalue from the Gaussian orthogonal ensemble of random matrices gives a reasonable approximation. Given the discrepancies in the right tail of the density, and the behaviour of the skewness and kurtosis as shown in Fig 5.13, we cannot claim conclusive support for the Tracy-Widom density and offer this curious near coincidence as an open problem.

While we cannot identify the empirical density of cover times for $\alpha = 0$ and $d = 3$, we can nevertheless investigate the breakdown of our conjecture, Eq (5.18), which naively expresses the cover time as a sum over exponential waiting times ε_k. Since we do not

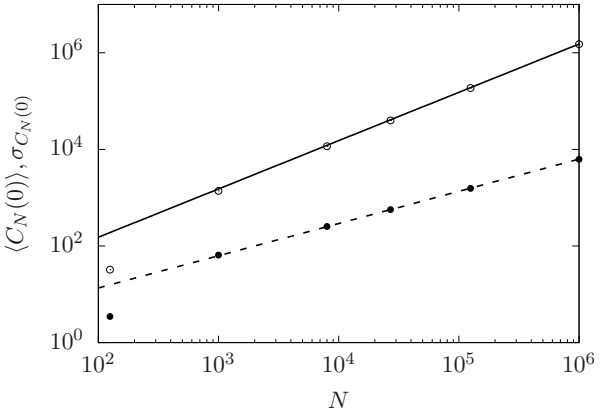

Figure 5.10: Scaling of the mean $\langle C_N(0)\rangle$ (empty circles) and standard deviation $\sigma_{C_N(0)}$ (filled circles) for $\alpha = 0$ in $d = 3$. The mean follows the conjectured behavior $g(0)N$ (solid line), but the standard deviation appears to scale as $N^{2/3}$ (dashed line Eq. (5.31)), rather than $N^{1/2}$. Standard errors are smaller than the symbols.

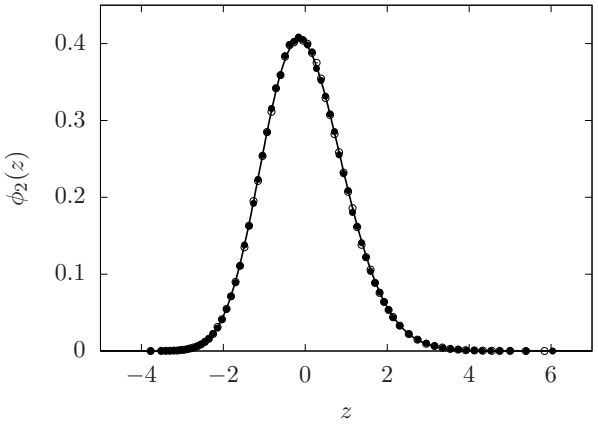

Figure 5.11: Rescaled cover time density, $\phi_2(z)$, for $\alpha = 0$ in $d = 3$ with $N = 100^3$ (empty circles) and $N = 50^3$ (filled circles), over an ensemble of 10^6 independent realizations. A Tracy-Widom density from the Gaussian orthogonal ensemble is plotted for comparison (solid line).

recover the anticipated Gaussian distribution, we are led to conclude that the random variables ε_k are either sufficiently non-identical, or non-independent (or both).

To isolate these question, we perform a shuffling operation across (independent) members of the ensemble from which we collect statistics of cover times. Specifically, we choose one member of the ensemble at random, i.e. one realisation of the cover process, and sum the first of its b waiting times $\{\varepsilon_k^{(1)}\}_{k=1}^{b}$. Then we pick another realisation at random, and sum the next b waiting times from that process $\{\varepsilon_k^{(2)}\}_{k=b+1}^{2b}$, and so on. We continue this operation N/b times, so that we accumulate the shuffled cover time

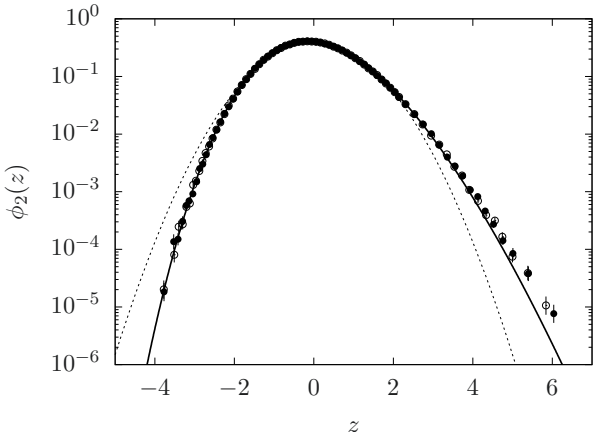

Figure 5.12: Same as Fig 5.11 but with a logarithmic y-axis. Error bars denote standard errors of histogram bins. For comparison, a Gaussian density is also plotted (dotted line).

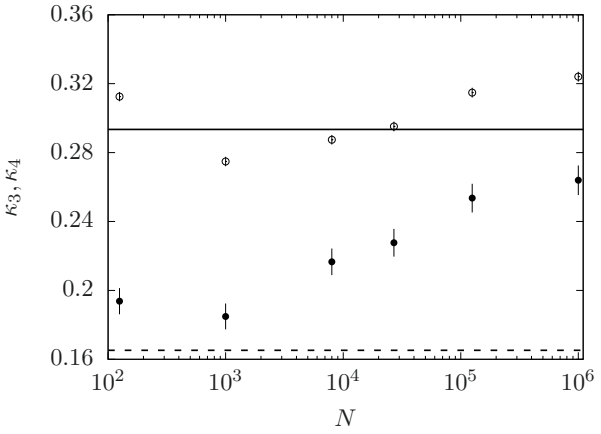

Figure 5.13: Skewness κ_3 (empty circles) and kurtosis κ_4 (filled circles) for $\alpha = 0$ in $d = 3$. Error bars denote jackknife standard errors. The Tracy-Widom skewness (solid line) and kurtosis (dashed line) are plotted for comparison.

process

$$C_N^{\text{shuff.}}(0) = \sum_{k=1}^{b} \varepsilon_k^{(1)} + \sum_{k=b+1}^{2b} \varepsilon_k^{(2)} + \cdots + \sum_{k=N-b+1}^{N} \varepsilon_k^{(N/b)}. \tag{5.32}$$

By this operation, we generate an ensemble of cover times from processes that have been block-shuffled. If the block length $b = N$, then the original cover process is left intact and no shuffling occurs. Meanwhile, if $b = 1$, then each waiting time ε_k is drawn randomly from the ensemble distribution of waiting times to the kth unvisited site. More generally, the block length plays the role of a "high-pass" filter that destroys correlations with characteristic scale larger than b. Thus, for $b = 1$, the block-shuffled

cover time $C_N^{\text{shuff.}}(0)$ is a sum of waiting times from independent realizations. The resulting $C_N^{\text{shuff.}}(0)$ could only be non-Gaussian if the ε_k were sufficiently non-identical.

As a measure of discrepancy between the empirical density $\phi_2(z)$ of shuffled cover times and a standard Gaussian density $g(z)$, we compute the Kullback-Leibler divergence from $\phi_2(z)$ to $g(z)$

$$D_{\text{KL}}(g||\phi_2) = \int \mathrm{d}z\, g(z) \log \frac{g(z)}{\phi_2(z)} \tag{5.33}$$

for different block lengths b. Figure 13 shows that a comparatively large block length of $b \lesssim 5\times 10^3 = N/25$ is enough to recover Gaussian cover time behaviour, thus suggesting that long-range correlations are at play.

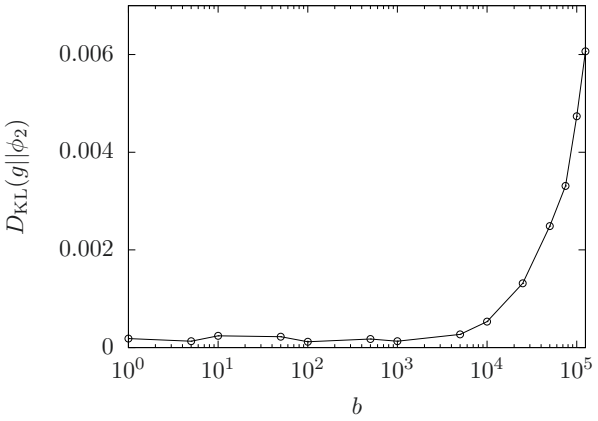

Figure 5.14: Kullback-Leibler divergence from a Gaussian distribution for the rescaled cover time, as a function of block length b, with $N = 50^3$ over an ensemble of 10^5 realizations.

It is instructive to consider another modification of the cover process (also implemented in [63] in the unaccelerated case). Instead of splicing together blocks of cover from independent realizations, we intermittently allow the random walker to "teleport" to a randomly chosen site. Thus, the walker performs a teleportation jump with probability p, and a nearest-neighbour step with probability $(1-p)$. If $p = 0$, the original cover process is recovered. If $p = 1$, the walker effectively explores a fully-connected graph. Fig 5.15 shows that a teleportation probability of approximately $p \gtrsim 0.1$ is enough to recover Gaussian cover time behavior.

In conclusion, we attribute the non-Gaussianity of $\alpha = 0$ accelerated cover times in $d = 3$ to correlations in the sequence of sites visited as the lattice is covered. However, we are not able to explain why such correlations can be ignored for $d \geq 4$, or for

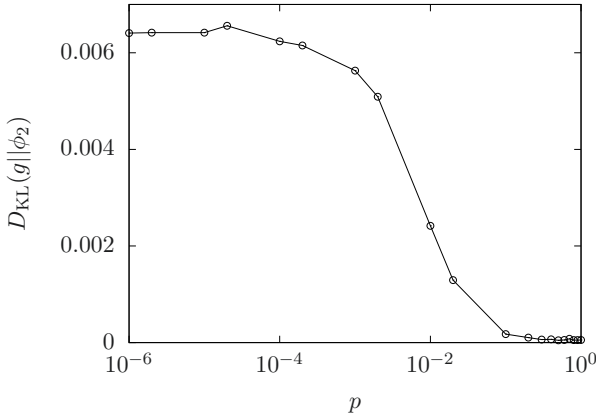

Figure 5.15: Kullback-Leibler divergence from a Gaussian density for the rescaled cover time, as a function of teleportation probability p, with $N = 50^3$ over an ensemble of 10^6 independent realizations.

deceleration protocols with $\alpha > 1$.

5.7 Conclusion

We have studied the cover times of accelerated and decelerated random walks on a torus in dimensions $d \geq 3$. Building on the work of Aldous [3] and Belius [24], we conjecture a generalized cover time which agrees well with numerics for a range of acceleration-deceleration protocols and dimensions. The α-indexed family of cover time distributions are in fact those describing the roughness of $1/f^{\alpha}$ Gaussian signals [10], which include Gaussian ($0 \leq \alpha \leq 1/2$), Gumbel $\alpha = 1$ and exponential ($\alpha \to \infty$) distributions, to name a few.

A notable exception to our conjecture is for $\alpha = 0$ in $d = 3$, where we find a cover time distribution somewhat resembling a Tracy-Widom distribution from the Gaussian orthogonal ensemble of random matrices. Although the numerics do not support this identification conclusively, it is interesting to speculate whether a connection between accelerated cover in $d = 3$ and random matrices exists, e.g. via mappings to KPZ interfaces [278], Gaussian free fields [79, 106], or spin glasses [57].

This study leaves a number of open questions, such as the identification of the cover time distribution for $\alpha = 0$ in $d = 3$, and why this distribution is particular to $d = 3$.

5.A Roughness of $1/f^\alpha$ Gaussian signals

A $1/f^\alpha$ signal $h(x)$ of length L is sampled over N Fourier modes according to

$$h(x) \propto \sum_{k=1}^{N} \frac{1}{k^{\alpha/2}} \left[a_k \sin(2\pi kx/L) + b_k \cos(2\pi kx/L) \right], \tag{5.34}$$

where the amplitudes a_k and b_k are independent standard Gaussian random variables [10]. By construction, the signal is periodic with zero mean, and its power spectrum decays as $1/k^\alpha$. The integrated power spectrum

$$w^2(\alpha) \propto \frac{1}{L} \int_0^L \mathrm{d}x\, h^2(x) \tag{5.35}$$

$$\propto \sum_{k=1}^{N} \frac{1}{k^\alpha} (a_k^2 + b_k^2) \tag{5.36}$$

by Parseval's theorem. Since the sum of two Gaussian squared random variables is exponentially distributed,

$$w^2(\alpha) \propto \sum_{k=1}^{N} \frac{\varepsilon_k}{k^\alpha}. \tag{5.37}$$

Hence, apart from an N^α prefactor, the integrated power spectrum of $1/f^\alpha$ signals has the same distribution as the coupon collection time $S_N(\alpha)$ discussed in the main text.

In the language of interfaces, Eq. (5.34) describes a periodic steady-state height profile, and the integrated power spectrum is equivalent to the profile's roughness [16]. A review of $1/f^\alpha$ signals can be found in [10].

5.B Lindeberg condition

Given a collection of independent but not necessarily identical random variables $\{X_k\}_{k=1}^N$ with (finite) variances $\{\sigma_k^2\}_{k=1}^N$, the Lindeberg condition [231] guarantees that their rescaled sum is still Gaussian-distributed, provided that

$$\frac{\max\limits_{1 \le k \le N} \sigma_k^2}{\sum_{k=1}^N \sigma_k^2} \to 0, \quad N \to \infty. \tag{5.38}$$

In our context, the collection of random variables ε_k/k^α have variances $1/k^{2\alpha}$. Therefore, satisfying Eq. (5.38) requires

$$\sum_{k=1}^{N} \frac{1}{k^{2\alpha}} \to \infty, \quad N \to \infty, \tag{5.39}$$

i.e. that $0 \leq \alpha \leq 1/2$.

ACKNOWLEDGMENTS

The authors thank Andy Thomas for computer support. GM thanks LML and Imperial College for financial support via the LML-Roth scholarship.

6

Of Hogs and Truffles: a Doi-Peliti Field Theory of the Coupon Collector Problem

L. Cocconi, G. Maziya, N. Moloney, G. Pruessner

Overview The Coupon Collector (CCP) and Cover Time (CTP) problems have historically been studied mainly by probabilistic methods, leading to a number of important results (see Chapter 5 and references therein). In this Chapter, we demonstrate that path integral methods, in particular the Doi-Peliti formalism, offer a valid alternative approach to exploring specific features as well as novel variations of these problems. As already discussed at length in Chapter 4, this formalism retains particle entity and it is thus particularly suited for setups where transitions between discrete states need to be precisely resolved. In fact, in recent years, various works have successfully expanded the scope of such field theories to address, among others, first-passage time problems and the short-time statistical features of self-propelled active particles [109, 312, 43, 236, 294]. The spirit of these works is perhaps in contrast with the impression one might get by a superficial look at the field-theoretic literature in non-equilibrium statistical physics, where path integral methods are typically applied to study asymptotic features of continuum, coarse-grained theories, often drawing on the

toolkit of the Renormalisation Group. Notably, the modularity and flexibility of the Doi-Peliti approach makes it possible to 'mix and match' interactions that were originally introduced in separate studied, thus in principle granting access to a wide variety of composite stochastic processes. For example, we will see in the following that stochastic resetting is easily implemented in the CCP by augmenting the Doi-Peliti action with a suitable term, whence the standard renewal equation follows straightforwardly.

Author contributions: LC derived the field theory, performed the analysis and wrote the current draft of the manuscript. All authors discussed the results at various stages of the project.

Abstract

We cast the Cover Time problem on a generic graph as a two-species reaction diffusion process involving a diffusible species (the hogs) interacting on-site with an immobile species (the truffles) by permanently removing the latter from the system. Cover is defined to occur when the last truffle is removed. We apply the Doi-Peliti formalism to cast the corresponding master equations as a coherent-state path integral, which we compute exactly for the case of a trivial zero-dimension graph, where the Cover Time problem reduces to the spaceless Coupon Collector problem, to recover the full cover time distribution (Gumbel statistics). We show that a suitable choice for the ensemble of initial conditions, specifically one with Poisson statistics for the number of uncollected truffles at initialisation, can streamline the derivation of the Coupon Collector statistics compared to the standard probabilistic derivation. We characterise for the first time the avalanche shape of the process and subsequently generalise it by separately introducing stochastic resetting (conditioned on completion not having been achieved yet) and collection by a stochastically evolving population of hogs.

6.1 Introduction

We study the Coupon Collector problem by means of field theoretic techniques based on the Doi-Peliti path-integral formalism. This is a standard formalism employed in the study of stochastic processes described at the microscopic level by discrete-state, continuous-time master equations. Unlike other path-integral techniques, such as

the Martin-Siggia-Rose Janssen-De Dominicis formalism [289], which has a mesoscopic Langevin equations as its starting point, the capability of Doi-Peliti to resolve single particle identity makes it particularly suitable for the study of probabilistic and, more specifically, extreme-value problems [39, 204, 293]. The derivation of this formalism has been reviewed by various authors [215, 56, 227, 175] and won't be covered here for the sake of brevity.

We consider here a stochastic lattice process involving a single diffusive particle (the 'hog') interacting on-site with immobile particles (the 'truffles') by permanently removing them from the system. The process is initialised by spawning a diffusive particle and some number of immobile particles in the system, possibly at different locations. Denoting the occupation number of hogs and truffles at site i by n_i and m_i, respectively, we can write down the following master equation for the occupation probability $P(n_i, m_i)$

$$\begin{aligned}\partial_t P(n_i, m_i) = &+ \eta\ n_i(m_i+1)P(n_i, m_i+1)\\ &- \eta\ n_i m_i P(n_i, m_i)\\ &+ h(n_i+1)P(n_i+1, n_{i+1}-1, m_i)\\ &+ h(n_i+1)P(n_i+1, n_{i-1}-1, m_i)\\ &- 2hn_i P(n_i, m_i)\end{aligned} \tag{6.1}$$

where η is the interaction (collection) rate and h is the hopping rate. Following the standard second quantisation procedure, we arrive at the corresponding Hamiltonian, written in terms of creation and annihilation operators $\{a_i^\dagger, a_i\}$ and $\{b_i^\dagger, b_i\}$ for hogs and truffles, respectively, at each lattice site

$$H_{ij} = \eta(a_i^\dagger b_i^\dagger a_i b_i - a_i^\dagger a_i b_i)\delta_{ij} + h(a_{i+1}^\dagger + a_{i-1}^\dagger - 2a_i^\dagger)a_i \tag{6.2}$$

This is often the stage at which one takes the continuum limit of the lattice spacing going to zero, so that $\{a_i^\dagger, a_i\} \to \{\phi^\dagger(x), \phi(x)\}$, $\{b_i^\dagger, b_i\} \to \{\psi^\dagger(x), \psi(x)\}$. While dealing with such continuous fields is often technically convenient, it is important here that we retain the discreteness, as well as finiteness, of the underlying lattice, since the observables we are interested in are intimately linked to the recurrence/transience of the random walk

performed by the searcher. With this in mind, we proceed by performing the Doi-shift of the creation fields $\phi_i^\dagger \to (1+\tilde{\phi}_i)$, $\psi_i^\dagger \to (1+\tilde{\psi}_i)$. The harmonic part of the resulting Liouvillian $\mathcal{L} = \mathcal{L}_0 + \mathcal{L}_1$ then reads

$$\mathcal{L}_0 = \tilde{\phi}\partial_t\phi + \tilde{\psi}\partial_t\psi + D\nabla\tilde{\phi}\nabla\phi + r_a\tilde{\phi}\phi + r_b\tilde{\psi}\psi \tag{6.3}$$

where we have introduced spontaneous decay rates $r_{a,b}$ for the two species for the purpose of infrared regularisation in later calculations. These decay rates will eventually be sent to zero. The non-linear part of the Liouvillian instead reads

$$\mathcal{L}_1 = \kappa\tilde{\psi}\psi\tilde{\phi}\phi + \lambda\tilde{\psi}\psi\phi \tag{6.4}$$

with $\kappa = \lambda = \eta$ at bare level. The two non-linear terms in $\mathcal{L}_1$ define the two vertices available for perturbative calculations by means of Feynman diagrams. Assuming for the shifted fields $[\tilde{\phi}] = [\tilde{\psi}] = 1$ and imposing $[D] = 1$ to preserve diffusion on all scales, dimensional analysis in the continuum limit indicates $d_c = 2$ as the upper critical dimension for the theory. This is a signature of the random walk performed by the searcher becoming transient in $d > 2$, resulting in a finite probability that a particular site in never visited by the searcher. While this makes the non-linear part of the Liouvillian "dimensionally irrelevant" in the Renormalisation Group sense, in the absence of a diverging time-scale (e.g. for finite systems), these interactions are still to be accounted for in $d > d_c$.

6.2 Observables

In the following we will consider observables such as the probability of a certain number M of truffles surviving for a time t after N are initialised (with $0 \leq M \leq N$). Extracting this observable from the field theory involves a projection at time t on the desired Fock state. In particular, the probability of the system containing exactly M particles can be written

$$P_M(t) = \langle M|e^{-Ht}a^\dagger(b^\dagger)^N|0\rangle \tag{6.5}$$

However, by construction of Doi-Peliti formalism, path integrals of the form

$$\langle \mathcal{O} \rangle = \int \mathcal{D}\left[\tilde{\phi}, \phi, \tilde{\psi}, \psi\right] \mathcal{O} e^{-\int dt dx \mathcal{L}} \tag{6.6}$$

imply a projection on the coherent state, such that

$$\langle \mathcal{O}(t) \rangle = \langle \sleepy | \mathcal{O} e^{-Ht} | \Psi(0) \rangle \tag{6.7}$$

where $\langle \sleepy | = \langle 0 | e^{\phi + \psi} = \sum_i \langle i |$. The correct field theoretic observable corresponding to the probability of a number M of truffles being alive at time t is therefore

$$P_M(t) = \langle M | e^{-H(t-t_0)} | \Psi(t_0) \rangle = \langle e^{-\psi} \psi^M ... \rangle / M! \ . \tag{6.8}$$

with the dots indicating an arbitrary initialisation at $t_0 \leq t$. A general initialisation can be written operatorially as

$$\mathcal{I}(t_0, \{n_i, m_i\}) = \prod_i (a_i^\dagger(t_0))^{n_i} (b_i^\dagger(t_0))^{m_i} \ . \tag{6.9}$$

Rather than the probability $P_M(t)$ of a certain number of coupons not having been collected (or sites not having been visited) after some time t, the literature often focuses on the probability density for the M^{th} distinct coupon to be picked at a particular time t. Denoting this probability density as $\tilde{P}_M(t)$ and noting that it corresponds to the influx of probability into the $|N-M\rangle$ particle number state (or, equivalently, the outflux from $|N-M+1\rangle$), we obtain

$$\partial_t P_M(t) = \begin{cases} -\tilde{P}_1(t), & \text{for } M = N \\ \tilde{P}_M(t) - \tilde{P}_{M+1}(t), & \text{for } 0 < M < N \\ \tilde{P}_N(t), & \text{for } M = 0 \end{cases} \tag{6.10}$$

for $0 \leq M \leq N$. In other words, $\tilde{P}_{M+1}(t)$ can be found by differentiating $P_M(t)$ with respect to time and, starting from $M = 0$ or $M = N$, working our way into the bulk of the process in a recursive manner by means of substitution.

6.3 Results for the spaceless case ($d = 0$)

We consider the simplest case, in which truffles and hogs coexist at a single lattice site and diffusion is switched off (i.e. the Coupon Collector Problem). We will refer to this set-up as a zero-dimensional field theory and drop any site indices for now. The corresponding bare propagators in direct time representation read

$$\langle \phi(t)\tilde{\phi}(t_0)\rangle_0 = \quad = e^{-r_a(t-t_0)} \tag{6.11}$$

$$\langle \psi(t)\tilde{\psi}(t_0)\rangle_0 = \quad = e^{-r_b(t-t_0)} \, . \tag{6.12}$$

The interaction (collection) rate η introduced in Eq. (6.1) corresponds here to the true rate with which distinct coupons are collected, which is understood to scale like $1/N$ in the original setup but here is generally independent of N. The corresponding diagrammatic notation for the interaction vertices is

$$\kappa = \quad \text{and} \quad \lambda = \tag{6.13}$$

6.3.1 Poisson initialisation

We first consider a Poisson initialisation for the truffles with density ρ. We thus let the probability for a number M of truffles being spawned at initial time t_0 be given by $P_M(t_0) = e^{-\rho}\rho^M/M!$ and write the initial mixed state

$$\begin{aligned} |\Psi(t_0)\rangle &= \sum_{M=0}^{\infty} \frac{e^{-\rho}\rho^M}{M!} (\psi^\dagger(t_0))^M |0\rangle \\ &= e^{-\rho} e^{\rho\psi^\dagger(t_0)}|0\rangle = e^{\rho\tilde{\psi}(t_0)}|0\rangle \end{aligned} \tag{6.14}$$

While this is not standard initialisation used in the probabilistic approach to the Coupon Collector problem, we will find that such a choice saves us from having to perform any time rescaling and from having to take the limit $N \to \infty$ explicitly. This in turn suggests that the Poissonian initialisation might capture some important feature of the asymptotic distribution of uncollected coupons, at least at late times.

We now proceed by calculating the relevant observable as defined in the previous section, namely

$$\begin{aligned} P_M(t) &= \frac{1}{M!}\langle e^{-\psi(t)}\psi^M(t)\phi^\dagger(t_0)e^{\rho\tilde{\psi}(t_0)}\rangle \\ &= \frac{1}{M!}\sum_{n=0}^{\infty}\sum_{m=0}^{\infty}\frac{(-1)^n\rho^m}{n!m!}\langle\psi^{n+M}\phi^\dagger\tilde{\psi}^m\rangle \end{aligned} \tag{6.15}$$

We now note from Equation (6.4) that none of the vertices available allows for a change in the number of the truffle propagators, thus imposing $m = n + M$ in the above. We thus obtain

$$P_M(t) = \frac{1}{M!}\sum_{n=0}^{\infty}\frac{(-1)^n\rho^{n+M}}{n!(n+M)!}\langle\psi^{n+M}\phi^\dagger\tilde{\psi}^{n+M}\rangle \ . \tag{6.16}$$

It is convenient here to work in direct time representation, noting that in the limit $r_a, r_b \to 0$ the contribution from the exponential decay of both propagator types reduces to a factor of unity. To demonstrate the consequences of this observation, we calculate the expectation $\langle\psi(t)\phi^\dagger(t_0)\tilde{\psi}(t_0)\rangle = 1 + \langle\psi\tilde{\phi}\tilde{\psi}\rangle$ in direct time explicitly. We find

$\langle\psi\tilde{\phi}\tilde{\psi}\rangle =$  $+ \cdots$

$$\begin{aligned} &= e^{-r_b(t-t_0)}\sum_{n=0}^{\infty}\prod_{m=0}^{n} -\eta\int_{t_m}^{t} dt_{m+1}e^{-r_a(t_{m+1}-t_m)} \\ &= e^{-r_b(t-t_0)}\sum_{n=1}^{\infty}(-\eta)^n\int_{t_0}^{t} dt'\frac{(t'-t_0)^{n-1}}{(n-1)!}e^{-r_a(t'-t_0)} \end{aligned} \tag{6.17}$$

Taking the limit $r_a, r_b \to 0$, we obtain

$$\lim_{r_a,r_b\to 0}\langle\psi\phi^\dagger\tilde{\psi}\rangle = e^{-\eta(t-t_0)} \ . \tag{6.18}$$

This result shows that, in the presence of a hog, each truffle acquires an additional *effective* mass equal to the interaction rate, i.e. it disappears from the system with rate η. Calculating the expectation (6.18) is particularly simple in $d = 0$ because each

truffle interacts independently and at all times with the hog.
While the limit $r_a, r_b \to 0$ that we have taken above matches the absence of spontaneous decay for either particle species in the conventional formulation of the coupon collector problem, it is interesting to consider how the result (6.18) changes when the masses r_a and r_b do not vanish. For starters, it can be directly checked from (6.17) that a positive truffle mass $r_b > 0$, signature of spontaneous decay, carries through to the renormalised propagator in the presence of a hog, namely

$$\lim_{r_a \to 0} \langle \psi \phi^\dagger \tilde{\psi} \rangle = e^{-(\eta + r_b)(t - t_0)} \ . \tag{6.19}$$

The case of a non-vanishing hog mass is richer. In this case, the renormalised propagator (6.17) does not have a closed form and instead reads

$$\langle \psi \tilde{\phi} \tilde{\psi} \rangle = e^{-r_b(t-t_0)} \sum_{n=0}^{\infty} \sum_{m=0}^{\infty} \frac{(-\eta)^n (-r_a)^m (t - t_0)^{n+m}}{m!(n-1)!(n+m)} \tag{6.20}$$

$$= \sum_{m=0}^{\infty} \left(-\frac{r_a}{\eta} \right)^m \frac{\Gamma(1+m, \eta(t-t_0)) - \Gamma(1+m)}{\Gamma(1+m)} \tag{6.21}$$

where $\Gamma(z)$ is the Euler gamma function and $\Gamma(z,k)$ is the upper incomplete gamma function

$$\Gamma(z,k) = \int_k^\infty dt \ t^{z-1} e^{-t} \ , \tag{6.22}$$

which admits the asymptotic expansion

$$\lim_{k \to \infty} \frac{\Gamma(z,k)}{z^{k-1} e^{-z}} = 1 \ . \tag{6.23}$$

Thus, the asymptotic behaviour of the renormalised truffle propagator in the presence of a hog is

$$\langle \psi \tilde{\phi} \tilde{\psi} \rangle \simeq -\frac{\eta}{\eta + r_a} + \mathcal{O}(e^{-\eta(t-t_0)}) \ , \tag{6.24}$$

whence the survival probability $\langle \psi \phi^\dagger \psi^\dagger \rangle \sim r_a/(r_a + \eta)$. Since truffle collection and hog decay are effectively concurrent Poisson processes, the asymptotic survival probability is the probability that decay occurs before collection.

The calculation of the observable $\langle \psi^k \phi^\dagger \tilde{\psi}^k \rangle$ required to make progress with Eq. (6.16)

follows along the same lines (with some extra care taken in accounting correctly for the symmetry factors) and we obtain

$$\lim_{r_a,r_b\to 0}\langle\psi^\ell\phi^\dagger\tilde{\psi}^\ell\rangle = \ell!\sum_{n=1}^{\infty}(-\eta\ell)^n\int_{t_0}^{t}dt'\frac{(t'-t_0)^{n-1}}{(n-1)!}$$
$$= \ell!\lim_{r_a,r_b\to 0}\langle\psi\phi^\dagger\tilde{\psi}\rangle^\ell\ . \tag{6.25}$$

Since both the hog and truffle bare propagators are massless, what we need to keep track of in the diagrammatics of (6.25) is only the 'temporal positioning' of the interaction vertices. This was done along the lines of (6.17) by integrating over the times $t_m \in [t_0, t]$ assigned to each vertex, with the difference that every interaction now carries a symmetry factor of ℓ accounting for the multiplicity of truffle propagators it can be attached to. This multiplicity is thus at the origin of the exponent ℓ appearing in the right-hand side of (6.25). Finally, one last symmetry factor needs to be identified, which comes from the contraction of the two sets of equal-time external truffle fields, $\psi(t)$ and $\tilde{\psi}(t_0)$, leading to the combinatorial prefactor $\ell!$. We note in passing that the calculations above can be extended straightforwardly to the case of multiple hogs being created at initialisation, thanks to the absence of interactions amongst them. In particular, in the presence of m hogs, each truffle acquires an effective mass equal to m times the interaction rate, i.e. the presence of multiple hogs can be captured by the rescaling of the interaction rate $\eta \to m\eta$. The proportionality between the effective mass of a truffle and the number of hogs present is a signature of removals occurring in the manner of concurring Poisson processes.

Substituting Eq. (6.25) into (6.16) we arrive at the expression

$$P_M(t) = \frac{1}{M!}\rho^M e^{-M\eta(t-t_0)-\rho e^{-\eta(t-t_0)}} \tag{6.26}$$

We can immediately check that this expression is consistent by setting $t = t_0$, for which $P_M(0) = \rho^M e^{-\rho}/M!$, which is indeed the Poisson distribution describing the system at initialisation. Finally, by taking the time derivative of $P_M(t)$ and using Equation (6.10) we find

$$\tilde{P}_{M+1}(t) = \frac{1}{M!}e^{-\eta(M+1)(t-t_0)-e^{-\eta(t-t_0)}} \tag{6.27}$$

which is the known result for the full order statistics, also referred to as generalised Gumbel distribution.

The moments of the full time-dependent truffle number probability distribution can also be obtained straightforwardly. In this case what we need to calculate is

$$\langle [\psi^\dagger(t)\psi(t)]^N \rangle = \langle [\psi^\dagger(t)\psi(t)]^N \phi^\dagger(t_0) e^{\rho\tilde{\psi}(t_0)} \rangle \ . \tag{6.28}$$

Using [108]

$$\langle \sun | [\psi^\dagger(t)\psi(t)]^N = \sum_{\ell=0}^{N} \left\{ {N \atop \ell} \right\} \langle \sun | \psi^\ell(t) \ , \tag{6.29}$$

where $\left\{ {N \atop \ell} \right\}$ denotes the Stirling number of the second kind for ℓ out of N, we obtain

$$\langle [\psi^\dagger(t)\psi(t)]^N \rangle = \sum_{\ell=0}^{N} \sum_{k=0}^{\infty} \left\{ {N \atop \ell} \right\} \frac{\rho^k}{k!} \langle \psi^\ell(t) \phi^\dagger(t_0) \tilde{\psi}^k(t_0) \rangle \tag{6.30}$$

$$= \sum_{\ell=0}^{N} \left\{ {N \atop \ell} \right\} \frac{\rho^\ell}{\ell!} \langle \psi^\ell(t) \phi^\dagger(t_0) \tilde{\psi}^\ell(t_0) \rangle \tag{6.31}$$

where we have used $\langle \psi^\ell \phi^\dagger \tilde{\psi}^k \rangle \propto \delta_{\ell k}$, with $\delta_{\ell k}$ the Kroneker delta. Substituting 6.18 and 6.25 into the expression above, we thus arrive at

$$\langle [\psi^\dagger(t)\psi(t)]^N \rangle = \sum_{\ell=0}^{N} \left\{ {N \atop \ell} \right\} \rho^\ell e^{-\eta\ell(t-t_0)} \tag{6.32}$$

$$= B_N(\rho e^{-\eta(t-t_0)}) \ , \tag{6.33}$$

with $B_n(x)$ the nth Bell polynomial in x. At initialisation, $t = t_0$, the nth moment of the distributions is thus $B_n(\rho)$, consistent with Dobiński's formula [26] and the fact that the distribution is Poisson.

Calculating the moments of time-dependent probability distribution of the number of collected truffles is slightly more involved due to the number of truffles at initialisation

not being constant. The relevant field theoretic observable reads

$$\langle [\hat{N}_\psi(t_0) - \hat{N}_\psi(t)]^N \rangle = \langle [\hat{N}_\psi(t_0) - \hat{N}_\psi(t)]^N \phi^\dagger(t_0) e^{\rho\tilde{\psi}(t_0)} \rangle \ , \tag{6.34}$$

where $\hat{N}_\psi(t) = \psi^\dagger(t)\psi(t)$ denotes the truffle number operator. In order to proceed we expand the Nth power of the difference in truffle number on the basis of the binomial theorem and use the identity

$$\hat{N}_\psi(t_0) e^{\rho\tilde{\psi}(t_0)}|0\rangle = \rho\psi^\dagger(t_0) e^{\rho\tilde{\psi}(t_0)}|0\rangle \ , \tag{6.35}$$

which can be proved starting from the power series Eq. 6.14. Using Eq. 6.29 to further simplify the resulting expression, the right hand side of Eq. 6.34 reduces to

$$\begin{aligned}
&\sum_{n=0}^{N}\sum_{\ell=0}^{n} \binom{N}{n} \left\{ {n \atop \ell} \right\} (-1)^n \rho \langle \psi^\ell(t)\psi^\dagger(t_0)\phi^\dagger(t_0) e^{\rho\tilde{\psi}(t_0)} \rangle \\
&= \sum_{n=1}^{N}\sum_{\ell=1}^{n} \binom{N}{n} \left\{ {n \atop \ell} \right\} (-1)^n \rho \left[\frac{\rho^\ell}{\ell!} \langle \psi^\ell(t)\phi^\dagger(t_0)\tilde{\psi}^\ell(t_0) \rangle + \frac{\rho^{\ell-1}}{(\ell-1)!} \langle \psi^\ell(t)\phi^\dagger(t_0)\tilde{\psi}^\ell(t_0) \right] \\
&= \sum_{n=1}^{N}\sum_{\ell=1}^{n} \binom{N}{n} \left\{ {n \atop \ell} \right\} (-1)^n \rho^\ell (\rho + \ell) e^{-\eta\ell(t-t_0)} \ ,
\end{aligned} \tag{6.36}$$

which does not appear to simplify further.

6.3.2 Initialisation with N indistinguishable truffles

We have seen above that in $d = 0$ a Poissonian initialisation for the immobile species gives Gumbel 'for free', meaning that no rescaling of time is required. However, the probabilistic derivation usually assumes a finite number N of coupons and produces a Gumbel distribution in the limit $N \to \infty$ only upon suitable rescaling of time. This

route is available in the field theory as well and proceeds as follows:

$$\begin{aligned} P_0(t) &= \left\langle e^{-\psi(t)} \left(\psi^\dagger(t_0)\right)^N \phi^\dagger(t_0) \right\rangle \\ &= \left\langle \sum_{n=0}^{\infty} \frac{(-\psi(t))^n}{n!} \sum_{m=0}^{N} \binom{N}{m} (\tilde{\psi}(t_0))^m \phi^\dagger(t_0) \right\rangle \\ &= \left(1 - \langle \psi \phi^\dagger \tilde{\psi} \rangle\right)^N \end{aligned} \tag{6.37}$$

We now rescale time as $t \to t' + \ln N/\eta$,which happens to be the same rescaling used in the probabilistic derivation. Using Equation (6.18) to replace the expectation, we obtain

$$P_0(t') = \left(1 - \frac{e^{-\eta(t'-t'_0)}}{N}\right)^N \tag{6.38}$$

The expression has now a non-trivial $N \to \infty$ limit, which corresponds to the cumulative Gumbel distribution $P_0(t') = \exp(-\exp(-\eta(t' - t'_0)))$.

6.3.3 Avalanche shape

An interesting observable that the field theory gives us access to is the so-called avalanche shape [108], which can be used to characterise the dynamics of the CCP conditioned on completion at a particular time after initialisation. The avalanche shape, denoted $V(t, \tau)$, is here defined as the expected number of un-sampled coupons at time t after initialisation conditioned on the last un-sampled coupon being sampled at time τ. Equivalently,

$$V(t, \tau) := \frac{\frac{d}{d\tau}\langle N(t)|N(\tau) = 0\rangle}{\frac{d}{d\tau}P_0(\tau)} \ , \tag{6.39}$$

where the denominator is required to normalise the joint probability over the given sub-ensemble of trajectories, so that

$$\int_0^\infty d\tau \ \frac{\frac{d}{d\tau}\langle N(t)|N(\tau) = 0\rangle}{\frac{d}{d\tau}P_0(\tau)} = \langle N(t)\rangle \ . \tag{6.40}$$

In order to calculate the avalanche shape we first need to compute $\langle N(t)|N(\tau) = 0\rangle$ and for this we are required to make a choice of initialisation. We choose to initialise

the system with N indistinguishable truffles at time $t = 0$. Thus, in the field theory

$$\begin{aligned}\langle N(t)|N(\tau)=0\rangle &= \langle e^{-\psi(\tau)}\psi^\dagger(t)\psi(t)(\psi^\dagger(0))^N\phi^\dagger(0)\rangle \\ &= \sum_{m=1}^{N}\frac{(-1)^{m-1}}{(m-1)!}\binom{N}{m}m!e^{-\eta\tau}(e^{\eta(\tau-t)}-1) \\ &= \frac{N(1-e^{-\eta\tau})^N}{e^{\eta\tau}-1}(e^{\eta(\tau-t)}-1)\ . \end{aligned} \tag{6.41}$$

As expected, the expression we just found for $\langle N(t)|N(\tau)=0\rangle$ vanishes as t approaches τ from below and equals N when $t = 0$ and the limit $\tau \to \infty$ is taken. Differentiating once the conditional probability with respect to τ we obtain

$$\begin{aligned}&\frac{d}{d\tau}\langle N(t)|N(\tau)=0\rangle \\ &= \frac{\eta N\left(1-e^{-\eta\tau}\right)^N\left(e^{\eta\tau}+(N-1)e^{\eta(\tau-t)}-N\right)}{\left(e^{\eta\tau}-1\right)^2}\ . \end{aligned} \tag{6.42}$$

Finally, using Eq. (6.37) for the probability of all coupons having been collected by time τ, the denominator of Eq. (6.39) reads

$$\frac{dP_0(\tau)}{d\tau} = N\eta e^{-\eta\tau}(1-e^{-\eta\tau})^{N-1}\ . \tag{6.43}$$

Substituting into Eq. (6.39), the avalanche shape is thus

$$V(t,\tau) = \frac{e^{\eta\tau}+(N-1)e^{\eta(\tau-t)}-N}{e^{\eta\tau}-1}\ . \tag{6.44}$$

As expected, $V(0,\tau) = N$ since the expected number of particles at initialisation is fixed and independent of τ. Similarly, $\lim_{t\to\tau^-} V(t,\tau) = 1$, consistent with the last uncollected coupon being removed at time τ. It is also interesting to consider the regime $\eta\tau \ll 1$, i.e. one where we impose 'premature extinction' compared with the typical timescale of collection. In this case we find

$$V(t,\tau) \simeq N(1-t/\tau)\ , \tag{6.45}$$

which decays linearly in time.

6.3.4 Time-inhomogeneous collection

The collection rate parametrising the interaction between the hog and the truffles need not be homogeneous in time. In fact, we have explored the effect of acceleration on the cover time statistics in a recent paper [196]. We briefly consider the case where the rate with which the hog removes a truffle from the system is a function of time, $\eta(t) \geq 0$. Focusing on the case $M = 0$ with Poissonian initialisation and a single hog, i.e. the original Coupon Collector problem, a similar calculation to the one performed above yields

$$\langle \psi(t)\phi^\dagger(t_0)\psi(t_0)\rangle = e^{-\langle\eta\rangle_t(t-t_0)} \ , \tag{6.46}$$

whence

$$P_0[\eta(t),t] = \tilde{P}_1[\eta(t),t] = e^{-\rho e^{-\langle\eta\rangle_t(t-t_0)}} \ , \tag{6.47}$$

where we defined the running average

$$\langle\eta\rangle_t = \frac{1}{t-t_0}\int_{t_0}^{t} dt'\eta(t') \ . \tag{6.48}$$

The consistency with (6.27) for the case of a constant interaction rate $\eta(t) = \eta$ can be checked straighforwardly. Eq. (6.47) demonstrates that introducing a time-dependent interaction rate effectively amounts to an inhomogeneous rescaling of time, which is intuitively clear. Nonetheless, it is interesting to note that any non-trivial acceleration protocol that depends only on time elapsed since initalisation 'breaks' Gumbel statistics for the completion time $\tilde{P}_1(t)$ in such a way that

$$P_0[\eta(t),t] = P_0[\nu(t),t] \iff \eta(t) = \nu(t) \ . \tag{6.49}$$

This should be compared to the case of piece-wise acceleration following a successful collection event, for which a continuous family of strategies produces Gaussian statistics [196].

6.3.5 Resetting

The formalism above can be extended to include stochastic resetting of the coupons to the initial number N with a Poisson rate γ. We condition this resetting to at least one coupon not having been collected by the time resetting is triggered. Mathematically, this additional process is captured by augmenting the master equation (6.1) in its spaceless version by

$$\partial_t P(n) = \cdots - \gamma(1-\delta_{n0})P(n) + \delta_{nN}\sum_{m=1}^{N}\gamma P(m) \tag{6.50}$$

with δ_{nm} the Kroneker delta of n and m. This terms represent a leakage of probability with rate γ out of all number states $|n\rangle$ with $n > 1$ and into $|N\rangle$. Unlike the original removal process, where the transition rates were proportional to the particle number of the associated Fock state, here the conversion into operator form requires us to contruct these operators implicitly by means of projectors $|k\rangle\langle k|$. After some manipulation we arrive at the modified second quantised form of the master equation

$$|\dot{\Psi}(t)\rangle = \cdots - \gamma|\Psi\rangle + \gamma(|0\rangle\langle 0| - |N\rangle\langle 0| + |N\rangle\langle \text{☼}|)|\Psi\rangle \tag{6.51}$$

which can be formally integrated to obtain

$$|\Psi(t)\rangle = e^{-\gamma t + \gamma\int_0^t dt'\hat{R}(t')+\cdots}|\Psi(0)\rangle \tag{6.52}$$

where we have introduced the shorthand

$$\hat{R}(t') = |0\rangle\langle 0| - |N\rangle\langle 0| + |N\rangle\langle \text{☼}| \tag{6.53}$$

with operators defined at time t'. To proceed further, we expand the new exponential term in the formal solution to obtain

$$|\Psi(t)\rangle = \sum_{n=0}^{\infty}\frac{(\gamma t)^n e^{-\gamma t}}{n!}\left(\frac{1}{t}\int_0^t dt'\hat{R}(t')\right)^n|\Psi(0)\rangle\ , \tag{6.54}$$

where we identify the first term in the sum as a Poisson probability associated with a number n of resetting events having happened in a time interval of duration t given a rate

γ. To calculate the coupon collector observable we introduce the conditional probability $P_0^{(n)}(t)$ for all coupons having been collected by time t given exactly n resetting event, such that $P_0^{(0)}$ corresponds to the cumulative Gumbel distribution derived earlier for $\gamma = 0$. This is given by

$$P_0^{(n)}(t) = \langle e^{-\psi(t)} \left(\frac{1}{t} \int_0^t dt' \hat{O}(t') \right)^n \psi^\dagger(0)(\psi^\dagger(0))^N \rangle \tag{6.55}$$

$$= \frac{1}{t} \int_0^t dt' P_0^{(n-1)}(t') + P_0^{(0)}(t-t')(1 - P_0^{(n-1)}(t')) \ , \tag{6.56}$$

which reads like a renewal equation with the first term corresponding to the probability of having already collected the last coupon by the time the nth reset occurs and the second corresponding to the probability of completing the collection after the nth resetting occurs.
While we don't expect full observable

$$P_0(t) = \sum_{n=0}^{\infty} \frac{(\gamma t)^n e^{-\gamma t}}{n!} P_0^{(n)}(t) \tag{6.57}$$

to have a simple form, we can still proceed a little further by noticing that the integral equation Eq. (6.56) can be rewritten in terms of the generating function

$$H(z,t) = \sum_{n=0}^{\infty} \frac{z^n e^{-z}}{n!} P_0^{(n)}(t) \ , \tag{6.58}$$

with $H(\gamma t, t) = P_0(t)$, as a differential equation

$$(t\partial_t \partial_z + \partial_z - 1) H(z,t) + P_0^{(0)}(t) = 0 \ . \tag{6.59}$$

with boundary conditions $H(0,t) = P_0^{(0)}(t)$ and $H(z,0) = 0$. While more compact, this representation also appears to have no closed form solution.

6.3.6 Coupon Collection by Stochastic Process

As a variation on the theme of the spaceless Coupon Collector Problem, it is possible to 'embellish' the dynamics of the collector while leaving the interaction between collectors and coupons unaffected. This gives us access to a whole family of problems but for the sake of simplicity here we only consider the extension to collectors increasing in number over time in the manner of a spontaneous creation process with Poisson rate s. Our starting point is the expression

$$\langle \psi(t)\phi^\dagger(t_0)\tilde{\psi}(t_0)\rangle = \left\langle \exp\left(-\int_{t_0}^{t} dt'\ \eta(t)\phi^\dagger(t')\phi(t')\right)\right\rangle \ . \tag{6.60}$$

which we prove in Appendix 6.A. Assuming $\eta(t) = \eta$, the expression reduces to

$$\langle \psi\phi^\dagger\tilde{\psi}\rangle = \sum_{n=0}^{\infty} \frac{(-\eta)^n}{n!} \int dt^{(1)} \dots dt^{(n)} \ \left\langle \prod_{i=1}^{n} \phi^\dagger(t^{(i)})\phi(t^{(i)}) \right\rangle \tag{6.61}$$

and so the problem reduces to computing the n-th order correlation functions of the collector number operator $\hat{N}_\phi = \phi^\dagger\phi$ for the desired process. The first expression has inhomogeneous collection by a single collector as a limiting case (see relevant section above). For spontaneous creation with Poisson rate s, the correlation functions of all order of the collector number can be obtained in close form,

$$\left\langle \prod_{i=1}^{n} \phi^\dagger(t^{(i)})\phi(t^{(i)})\phi^\dagger(t_0) \right\rangle = \prod_{i=1}^{n}(1 + s(t^{(i)} - t_0)) \ . \tag{6.62}$$

Plugging this expression back into (6.61) we get

$$\langle \psi\phi^\dagger\tilde{\psi}\rangle = \exp\left(-\eta(t - t_0)\left(1 + \frac{s}{2}(t - t_0)\right)\right) \ . \tag{6.63}$$

For $s(t - t_0) \ll 1$, the effective mass of the coupons is unaffected by the Poisson source and corresponds to the value η found previously. At long times, collection is dominated by the newly spawned collectors and the survival probability decays super-exponentially. Finally, using (6.25) we get the modified probability of M coupons having survived up

to time t, which is given by

$$P_M(t;s) = \frac{\rho^M}{M!} \exp\left(M\eta q(t-t_0;s) - \rho e^{-\eta q(t-t_0;s)}\right) \tag{6.64}$$

where $q(\tau;s) = \tau(1+s\tau)$ for the sake of compactness.

6.4 Discussion

In this Chapter we have developed a field-theoretic approach to the Coupon Collector Problem based on the Doi-Peliti coherent state path integral. While here we concern ourselves with the spaceless case only, the theory is able to account for hopping on a generic graph and can thus in principle be applied to the study of Cover Time Problems, which are in some sense a generalisation of the CCP to dimensions $d > 0$. It is understood, however, that extending the calculations presented here to the spatial case is highly non-trivial. Among known results, such as the generalised Gumbel probability density for the Mth distinct coupon to be picked at a particular time t, the flexibility and modularity of the Doi-Peliti formalism allows us to obtain various new ones. In particular, the avalanche shape, the introduction of resetting and the case of collection by a generic stochastic particle process have to the best of our knowledge not been considered in the literature before.

This work adds to a growing body of field-theoretic literature [109, 312, 43, 236, 294] exploiting the microscopic exactness of the Doi-Peliti formalism to address problems in the realm of stochastic processes, such as first passage and extreme value statistics, that are traditionally solved via probabilistic methods. Interestingly, the power of field theory comes here from the convenient handling (via Feynman diagrams) of combinatorial factors, rather than from application of Renormalisation Group methods, which tend to be concerned with asymptotic 'bulk' behaviour, rather than the finite-time, finite-size extremes probed here.

6.A Derivation of Eq. (6.60)

The relation between the effective propagator in the presence of collectors

$$\langle \psi(t)\phi^\dagger(t_0)\tilde{\psi}(t_0)\rangle = \left\langle \exp\left(-\int_{t_0}^{t} dt'\ \eta(t)\phi^\dagger(t')\phi(t')\right)\phi^\dagger(t_0)\right\rangle\ , \tag{6.65}$$

given the interaction terms Eq. (6.4) between the coupon field ψ and the collector field ϕ can be proved as follows. First of all, we note that, upon performing the Doi shift and assuming that the truffles are massless, $\langle \psi(t)\phi^\dagger(t_0)\tilde{\psi}(t_0)\rangle = 1 + \langle \psi(t)\tilde{\phi}(t_0)\tilde{\psi}(t_0)\rangle$. By carrying out the perturbative expansion explicitly, we have

$$\begin{aligned}
&\langle \psi(t)\tilde{\phi}(t_0)\tilde{\psi}(t_0)\rangle \\
&= \sum_{n=0}^{\infty}\frac{1}{n!}\left\langle \psi(t)\Big[\underbrace{\int_{t_0}^{t} dt_f\ \eta(t_f)\phi(t_f)\tilde{\psi}(t_f)\psi(t_f)}\Big]\right. \\
&\qquad \left.\times\Big[\underbrace{\prod_{i=0}^{n}\int_{t_0}^{t_f} dt_i\ \eta(t_i)\tilde{\phi}(t_i)\phi(t_i)\tilde{\psi}(t_i)\psi(t_i)}\Big]\tilde{\psi}(t_0)\tilde{\phi}(t_0)\right\rangle\ .
\end{aligned} \tag{6.66}$$

with $t_f > t_i$ for all $i = 1, ..., n$. Since the truffle propagators are causal and massless, there is only one way of Wick-contracting the coupons fields in pairs such that the resulting diagram has a non-zero contribution (namely according to time ordering) and in this case the overall contribution from the truffle fields is a factor of unity. Consequently, the expression above can be simplified by removing the explicit dependence on

the $\tilde{\psi}$ and ψ fields, thus arriving at

$$\begin{aligned}
&\langle \psi(t)\tilde{\phi}(t_0)\tilde{\psi}(t_0)\rangle \\
&= \sum_{n=0}^{\infty} \frac{1}{n!} \left\langle \int_{t_0}^{t} dt_f \ \eta(t_f)\phi(t_f) \left[\prod_{i=0}^{n} \int_{t_0}^{t_f} dt_i \ \eta(t_i)\tilde{\phi}(t_i)\phi(t_i) \right] \tilde{\phi}(t_0) \right\rangle \qquad (6.67) \\
&= \sum_{n=1} \frac{1}{n!} \left\langle \left[\int_{t_0}^{t} dt' \ \eta(t')\phi^{\dagger}(t')\phi(t') \right]^n \right\rangle \qquad (6.68) \\
&= \left\langle \exp\left(- \int_{t_0}^{t} dt' \ \eta(t)\phi^{\dagger}(t')\phi(t') \right) \phi^{\dagger}(t_0) \right\rangle - 1 \ . \qquad (6.69)
\end{aligned}$$

7

Morphogen gradient formation with leakage and multiple co-receptors

K. Stapornwongkul, M. De Gennes, L. Cocconi, G. Salbreux, J. P. Vincent

Science **370**, 321-327 (2020) [273]
Published 16 October 2020
DOI 10.1126/science.abb8205

OVERVIEW Morphogenesis refers to the fundamental developmental process in multicellular organisms whereby tissues and organs acquire their target shape in accordance to the organism's genetic program. Successful morphogenesis typically relies on a combination of external cues (e.g. maternal gradients) and spontaneous self-organisation through local signalling, and it is eventually enacted by internally generated mechanical forces that are able to evolve the simple geometry of early embryos into the rich variety of forms that we are familiar with from our everyday experience of the natural world. A typical example is that of gastrulation, a developmental stage common to most animals during which the embryo invaginates to form a multilayered structure, thus breaking its original spherical symmetry [268]. Needless to say, morphogenesis is a fundamentally non-equilibrium process, not just because of the obvious energy expen-

diture underlying cell proliferation and mechanical force generation, but also because of the multiple layers of signal processing and error correction that are required to map a disordered "ball" of undifferentiated cells into the highly reproducible patterns typical of fully developed individuals.

One of the ways in which morphogenesis is orchestrated is through medium-to-long range signalling mediated by *morphogens*. These are secreted proteins that typically spread from a localised source to form gradients of concentration, which is then read out by target cells to trigger downstream signalling which eventually results in cell fate specification. To form stable gradients in tissues of finite size, transport needs to occur alongside degradation, either by actual protein degradation, active endocytosis or e.g. by leakage out of the tissue. The concept of morphogens was first introduced theoretically by Turing [288] and Crick later [71] suggested a simple source-sink mechanism for the formation of linear morphogen gradients. In terms of the downstream signalling, the simplest mechanism of morphogen action is Wolpert's "French Flag Model" [302], where cells autonomously differentiate in stripes parallel to a hypothetical morphogen source stripe depending on the absolute level of morphogen. An important concept in this context is that of *positional information* of the gradient, i.e. the mutual information between the fluctuating morphogen concentration (or the expression level of one of its target genes) and the position of a given cell in the tissue. [85].

Over the past few decades, *drosophila melanogaster* has proved a key model system to further our understanding of morphogenesis, and more specifically morphogen gradients. In particular, extensive work has been dedicated to disentangling the complex network of morphogenetic signals occurring in the *wing imaginal disc*, a conveniently quasi-2d group of cells which acts as the precursor to the adult wing and most of the notum (the dorsal portion of the thoracic segment) [286]. During the $\sim 140h$ of larval development, the wing disc grows from about 30 to more than 30000 cells, at which point a pulse of the steroid hormone *Ecdysone* triggers eversion (balooning of the wing disc bulk which eventually leads to the formation of the wing blade) [304]. The bulk of the disc, known as the pouch, is an epithelium of undifferentiated columnar cells which is exposed on the basal side to the haemolymph, the insect's "blood", with which it exchanges nutrients, oxygen as well as any other diffusible species which is allowed to "leak" in and out of the tissue. See schematic in Fig. 7.1, panels A and B. The haemolymph thus also acts as a channel of communication between the wing disc and other tissues

that are in contact with it, such as the fat body, a large adipose tissue which will be relevant in the following. On the apical side, the pouch is instead in contact with the peripodial space, a smaller enclosed lumen that is separated from the lateral part of the tissue by impermeable tight junctions. In addition to the apico-basal axis, the disc is spanned by the anterior-posterior (AP) and dorsal-ventral (DV) axes, along which two key morphogens, respectively *Decapentaplegic* (*Dpp*) and *Wingless* (*Wg*), are known to form concentration gradients.

In this brief overview, we focus for the sake of brevity on the Dpp signalling network. Dpp is the Drosophila homolog (a gene originating from a common ancestor) of the vertebrate bone morphogenetic proteins (BMPs), a family of growth factors which control, amongst others, the formation of bones and cartilage. In the wing disc, Dpp secretion is triggered by *Hedgehog* (*hh*) signalling in a stripe of cells at the boundary between the anterior and posterior compartments [61]. For later reference, it is worth mentioning that *hh* is only secreted in the posterior compartment, such that artificially replacing the endogenous *hh* for a protein of one's choice leads to the latter's expression in half of the disc only. Once produced at the A-P boundary, Dpp then spreads away from the source region and eventually binds to its signalling receptor Thickveins (Tkv) to initiate signalling in the form of phosphorilated Mad (pMad), which acts as a transcription factor on a number of target genes. Dpp can also bind with lower affinity to other non-signalling receptors, such as *Dally*, which further differs from Tkv by the absence of a transmembrane domain and thus a higher diffusivity on the cell membrane. In the wing disc, the main downstream targets of Dpp signalling is Brinker (Brk), which in turn represses expression of Optomotor-blind (Omb) and Spalt (Sal). As a result, while Brk is transcriptionally downregulated by pMad and is thus expressed in an inverse concentration gradients increasing away from the Dpp source, Omb and Sal form broad bands of high expression around the Dpp source. These genes act in concert to pattern the future wing blade by positioning, among others, the L2 and L5 veins. Interestingly, Brk also appears to control growth by reducing cell proliferation towards the edges of the wing disc, thus "flattening" the otherwise inhomogeneous growth profile [252].

Notwithstanding the apparent simplicity of the underlying mechanism, the shape and patterning of the adult wing are surprisingly robust to artificial perturbations, such as changes in the source production rate or modifications in the spatial expression of receptors [209, 130]. These observations are suggestive of a number of feedback mech-

anisms being at play. A still poorly understood such mechanism is that controlling gradient scaling [296], namely the observed progressive increase in gradient characteristic length during growth which maintains the relative position of the target boundaries approximately constant. This feature of morphogen gradients has also been studied extensively in the Drosophila embryo, where Bicoid and other morphogens form overlapping gradients which control expression of the "gap" genes responsible for body segment determination [179].

Whether we are interested in error correction, scaling or the temporal dynamics of target gene expression, a key fact that needs to be established is the precise mode of transport of morphogens, on which secondary mechanisms are then likely to act. Surprisingly, and partly due to the difficulty of visualising single molecule motion in vivo (however, see [162] for recent related work), this has been a somewhat controversial topic [274]. It has been suggested that Dpp spreads by planar transcytosis or on special filopodia (membrane protrusions) called cytonemes; however, direct evidence for these specialised processes remains limited. On the other hand, hindered diffusion in the extracellular space, whereby single Dpp molecules repeatedly bind and unbind from receptors before eventually being degraded, offers a simpler alternative. In this Chapter, we present a mathematical model of morphogen transport by hindered diffusion in the presence of multiple extracellular binders based on a set of experiments carried out by our collaborators in which Dpp was replaced by an inert fluorescent protein (GFP) [273]. Remarkably, engineering the Dpp receptors to be able to bind GFP with high affinity – specifically by fusing an anti-GFP nanobody (Nb^{high}) to the former – leads to the establishment of a functional GFP gradient. Furthermore, near-wild-type patterning quality is achieved upon concomitant expressions of low affinity non-signalling receptors (Nb^{low}). Interestingly, the observed levels of bound GFP in the disc are affected by the expression of high-affinity binders in different tissues, specifically the fat body, that are not in direct contact with the disc, suggesting that leakage into and back-flow from the haemolymph might play a non-trivial role in morphogen transport. Together, these results support the view that Dpp transport occurs via non-specific, signal-agnostic processes such as hindered diffusion.

Author contributions: KS performed all the experiment, collected the data presented the the published article and wrote the first draft of the main body. MDG, LC and GS developed the mathematical model and wrote the Supplementary Material. In particular, MDG focused on the diffusion-degradation models with a single receptor,

while LC focused on the role of multiple receptors and receptor diffusion. JPV and GS supervised the project throughout.

Abstract

In this Chapter (which originally appeared as the supplementary document of the associated paper [273]), we derive equations describing the formation of a morphogen gradient with leakage (section 7.1). In addition to considering the consequences of leakage, we discuss the effect of varying receptor density on the shape of the morphogen gradient and on the domains of target activation inferred from the gradient. We show that a maximal range of target activation is achieved for intermediate values of the density of receptors. We then describe a model gradient with two types of receptors: one type of signaling receptor, and one type of non-signaling receptor which is allowed to undergo a hopping process between neighbouring cells (section 7.2). We study how introducing a hopping non-signaling receptor can allow for modulation of the gradient range.

Abstract of original paper *

Morphogen gradients provide positional information during development. To uncover the minimal requirements for morphogen gradient formation, we have engineered a synthetic morphogen in Drosophila wing primordia. We show that an inert protein, green fluorescent protein (GFP), can form a detectable diffusion-based gradient in the presence of surface-associated anti-GFP nanobodies, which modulate the gradient by trapping the ligand and limiting leakage from the tissue. We next fused anti-GFP nanobodies to the receptors of Dpp, a natural morphogen, to render them responsive to extracellular GFP. In the presence of these engineered receptors, GFP could replace Dpp to organize patterning and growth in vivo. Concomitant expression of glycosylphosphatidylinositol (GPI)–anchored nonsignaling receptors further improved patterning, to near–wild-type quality. Theoretical arguments suggest that GPI anchor-

*Here we make a distinction between the abstract of the Chapter and that of the original paper on which the former is based due to the difference in focus (theoretical in the first, experimental in the second).

age could be important for these receptors to expand the gradient length scale while at the same time reducing leakage.

7.1 Ligand diffusion and inferred signaling activity with one receptor

7.1.1 Model description

We discuss here a description of basolateral ligand gradients with leakage. The ligand is GFP and binders are anti-GFP nanobodies expressed only in the posterior compartment. This is meant to match the experimental setup, where the DNA encoding the GFP binder was knocked into the *hedgehog* (*hh*) locus. We consider leakage occurring towards the hemolymph, basal to the epithelium. The ligand is produced in a source of width L_S (Fig. 7.1). It can diffuse in a tissue of total width $2L$, bind and unbind to receptors at the cell surface, and be degraded. Degradation can occur in two ways: the ligand can be internalised after binding to a receptor, or it can diffuse out of the tissue to the underlying hemolymph. For simplicity we assume translational invariance in the direction tangential to the source, and we consider homogeneous concentrations in the tissue along the apico-basal axis, so that all quantities only vary with x, the coordinate perpendicular to the source. We choose the reference position $x = 0$ to denote the boundary between the source and the posterior compartment. The density of unbound receptors at the cell surface is denoted n_u, the density of bound receptors is denoted n_b. These densities are taken per surface of intercellular junctions and are twice as large as the cell membrane density, as each intercellular junction includes two cell membranes facing each other. The concentration of freely diffusing ligand in the tissue, within the intercellular space, is denoted by c. The concentration of ligand in the hemolymph is assumed to be uniform, and is denoted c_H. We do not take into account the potential role of advection due to tissue growth.

The concentration of extracellular ligand in the posterior part of the tissue is then given by:

$$\partial_t c = D\partial_x^2 c + \frac{1}{h}\left[-k_\mathrm{on} n_\mathrm{u} c + k_\mathrm{off} n_\mathrm{b}\right] - \frac{1}{H} j_\mathrm{TH} - k_d c, \quad 0 \leq x < L \ , \tag{7.1}$$

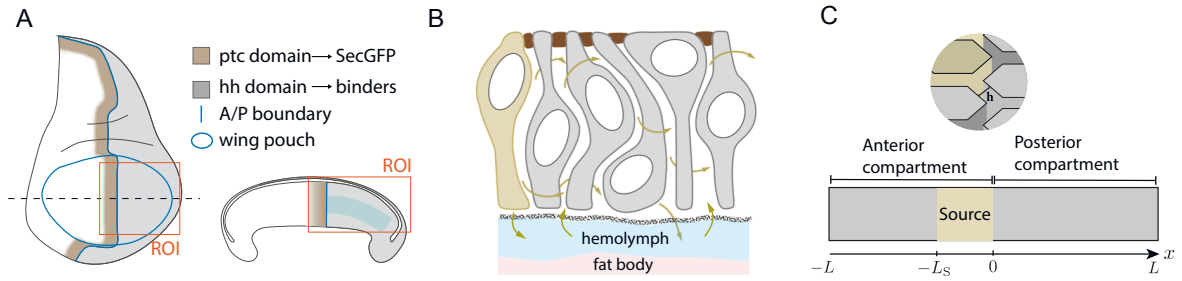

Figure 7.1: (A) Schematic representation of a wing imaginal disc of Drosophila. In the set of experiments reported in [273], a secreted form of GFP (SecGFP) is expressed under the control of the patched (ptc) promoter (brown), and a membrane-tethered anti-GFP nanobody is expressed under the control of the hedgehog (hh) promoter (gray). (B) Schematic representation of the paths a diffusing protein can take following secretion (diffusion through the basolateral space and exchange with the hemolymph). The fat body is a large adipose tissue with extensive contact with the hemolymph. (C) Schematic of one-dimensional model geometry. The mean intercellular distance is denoted h (upper schematic). The width of the source is denoted L_S, the width of the anterior and posterior compartments L (lower schematic).

where D is the free GFP diffusion constant, $k_{\rm on}$ is the rate of binding to receptors, $k_{\rm off}$ the rate of unbinding from receptors, h is the width of the intercellular space (Fig. 7.1), $j_{\rm TH}$ is the local flux of GFP to the hemolymph, H is the tissue height, and k_d is the rate of dilution associated with tissue growth. In the following we will assume that the contribution of dilution to the dynamics of free GFP is negligible compared to other processes, such as diffusion. We further assume that the GFP flux from the tissue to the hemolymph can be written as:

$$j_{\rm TH} = H\kappa(c - c_{\rm H}) \ , \tag{7.2}$$

with κ an effective leakage rate in between the tissue and hemolymph. The dynamics of the unbound and bound receptor densities is given in the posterior compartment ($0 \leq x < L$) by:

$$\partial_t n_{\rm u} = -k_{\rm on} n_{\rm u} c + k_{\rm off} n_{\rm b} - k n_{\rm u} + j_{\rm r}, \tag{7.3}$$

$$\partial_t n_{\rm b} = k_{\rm on} n_{\rm u} c - k_{\rm off} n_{\rm b} - k n_{\rm b} \ , \tag{7.4}$$

where $j_{\rm r}$ is the rate of increase of free receptor surface density, following from receptors biosynthesis and export to the membrane. $k = k_{\rm int} + k_d$ is the total rate of degradation of receptors, which could arise from cell internalisation and degradation (with rate $k_{\rm int}$) or from dilution due to cell growth (with rate k_d). In this part we assume that

ligand binding to the receptors does not affect receptor degradation. In the anterior compartment, receptors are not expressed and $n_{\mathrm{b}} = n_{\mathrm{u}} = 0$.

The GFP concentration within the source changes according to diffusion, production from source cells and losses from fluxes to the hemolymph:

$$\frac{dc}{dt} = D\partial_x^2 c + j - \kappa(c - c_{\mathrm{H}}) \ , -L_{\mathrm{S}} < x < 0 \ , \tag{7.5}$$

where j is the rate of GFP secretion in the source (defined as the rate of increase of extracellular free GFP concentration per unit time). In the anterior compartment, outside of the source, the GFP concentration follows the equation

$$\frac{dc}{dt} = D\partial_x^2 c - \kappa(c - c_{\mathrm{H}}) \ , -L < x \leq -L_{\mathrm{S}} \ . \tag{7.6}$$

We postulate the following evolution of the concentration of GFP in the hemolymph:

$$\frac{dc_{\mathrm{H}}}{dt} = \frac{\phi w}{V_{\mathrm{H}}} \int_{-L}^{L} j_{\mathrm{TH}} dx - k_{\mathrm{H}} c_{\mathrm{H}} \ , \tag{7.7}$$

where V_{H} is an effective volume of the hemolymph, w the transverse width of the tissue (orthogonal to the antero-posterior direction) and k_{H} is the ligand degradation rate in the hemolymph. Here we have introduced the intercellular volume fraction $\phi \simeq h/R$ with R the radius of a cell in the plane of the tissue; the total influx from the tissue to the hemolymph is proportional to ϕ. In vivo, ligands and receptors production does not occur only in wing imaginal discs. We assume that the contribution of the other imaginal discs and the larval epidermis can be captured by modulating the effective volume V_{H}; this approximation is discussed more extensively in section 7.1.6. At steady-state Eq. (7.7) becomes, using Eq. (7.2),

$$\langle c \rangle = \left(1 + \frac{\bar{k}_{\mathrm{H}}}{\kappa}\right) c_{\mathrm{H}} \tag{7.8}$$

with $\bar{k}_{\mathrm{H}} = \frac{k_{\mathrm{H}} V_{\mathrm{H}}}{2\phi w H L}$ and $\langle c \rangle = \frac{1}{2L} \int_{-L}^{L} c dx$ the average ligand concentration in the tissue. In one of the experimental conditions considered, which we refer to as "fat body trap" in the following, GFP binders were overexpressed in the fat body, resulting in a sponging effect which dramatically reduced c_{H}, thus suppressing GFP backflow into the tissue.

In the model, this perturbation is captured by a modified degradation rate $\bar{k}_{\mathrm{H}}^{\mathrm{FB}} > \bar{k}_{\mathrm{H}}$.

In addition we assume that there is no free GFP flux at the anterior and posterior boundaries of the tissue:

$$\partial_x c(-L) = \partial_x c(L) = 0 \ . \tag{7.9}$$

7.1.2 Steady state

At steady state, we obtain the density of bound and unbound receptors by solving Eqs. (7.3) and (7.4):

$$n_{\mathrm{b}} = n_{\mathrm{T}} \frac{k_{\mathrm{on}} c}{k + k_{\mathrm{off}} + k_{\mathrm{on}} c} \tag{7.10}$$

$$n_{\mathrm{u}} = n_{\mathrm{T}} \frac{k + k_{\mathrm{off}}}{k + k_{\mathrm{off}} + k_{\mathrm{on}} c} \tag{7.11}$$

$$n_{\mathrm{T}} = n_{\mathrm{b}} + n_{\mathrm{u}} = \frac{j_r}{k} \ . \tag{7.12}$$

The density of bound receptors depends on the extracellular ligand concentration, with possible receptor saturation effects for large concentrations, $c > (k + k_{\mathrm{off}})/k_{\mathrm{on}}$. Using Eq. (7.1), the steady-state concentration profile of the free ligand in the posterior part of the tissue is given by:

$$D\partial_x^2 c - \frac{k n_{\mathrm{T}}}{h} \frac{k_{\mathrm{on}} c}{k + k_{\mathrm{off}} + k_{\mathrm{on}} c} - \kappa(c - c_{\mathrm{H}}) = 0 \ . \tag{7.13}$$

7.1.3 Results for low production rate of ligand (no receptor saturation)

Steady-state relations at low ligand production rate

If the production of GFP at the source is sufficiently weak, or if the degradation through leakage and internalisation is sufficiently high, $k_{\mathrm{on}} c \ll (k + k_{\mathrm{off}})$, then the term associated with degradation of the bound receptors in Eq. (7.13) becomes linear in the concentration c. This corresponds to a situation where the receptors are nowhere saturated. The concentration of free ligands then takes the simple form, assuming $L \gg \ell$

:

$$c = c_0 \exp\left(-\frac{x}{\ell}\right) + c_{\rm H}\frac{\kappa}{\kappa + k_{\rm r}} \ , \tag{7.14}$$

where we have defined $k_{\rm r}$ the effective ligand degradation rate due to binding to receptors:

$$k_{\rm r} \equiv \frac{k n_T}{h}\frac{k_{\rm on}}{k + k_{\rm off}} = \frac{j_{\rm r}}{h}\frac{k_{\rm on}}{k + k_{\rm off}} \ , \tag{7.15}$$

and ℓ the length scale of the gradient which is given by:

$$\ell \equiv \sqrt{\frac{D}{k_{\rm r} + \kappa}} \ . \tag{7.16}$$

In addition, for low concentrations of ligand, $c \ll (k + k_{\rm off})/k_{\rm on}$, the density of steady-state bound receptors given in Eq. (7.10) becomes:

$$n_{\rm b} = \frac{n_{\rm T} k_{\rm on}}{k + k_{\rm off}} c \ . \tag{7.17}$$

For low receptor degradation $k \ll k_{\rm off}$, Eqs. (7.17) leads to $n_{\rm b} \simeq n_{\rm T} k_{\rm on} c/k_{\rm off}$. Away from the source for $x \gg \ell$, using Eq. (7.14), one then finds the asymptote $n_{\rm b}^{\infty} \simeq n_{\rm T} k_{\rm on} c_{\rm H}/(k_{\rm off}(1 + k_{\rm r}/\kappa))$.

The free ligand concentration at the source c_0 and the hemolymph concentration $c_{\rm H}$ are then determined by solving for the concentration profile in the source and in the anterior compartment, and calculating the total flux towards the hemolymph. Solving Eqs. (7.5) and (7.6), the free GFP concentration profile decays in the anterior compartment on a length scale $\ell_0 = \sqrt{D/\kappa}$ (we assume that $\ell_0 \ll L$, and also note that $\ell < \ell_0$). Matching concentrations and fluxes at the interface between the source and the anterior and posterior parts of the tissue, we then obtain:

$$c_0 = \frac{\ell}{\kappa(\ell + \ell_0)}\left(c_{\rm H}\frac{\kappa k_{\rm r}}{\kappa + k_{\rm r}} + j\left(1 - e^{-\frac{L_{\rm S}}{\ell_0}}\right)\right) \ , \tag{7.18}$$

and calculating the average free ligand concentration in the tissue, we obtain from the

balance equation (7.8) the hemolymph concentration for $L \gg \ell_0$:

$$c_{\rm H} = \frac{j}{L} \frac{L_{\rm S} - (\ell_0 - \ell)\left(1 - e^{-\frac{L_{\rm S}}{\ell_0}}\right)}{2\bar{k}_H + \frac{k_{\rm r}\kappa}{\kappa + k_{\rm r}}} \ . \tag{7.19}$$

We also note that a simple, intuitive condition can be obtained by writing that all GFP produced in the source must, at steady-state, either be degraded in the tissue or in the hemolymph. As a result, with $V_{\rm S} = wL_{\rm S}H$ the volume of the source,

$$\begin{aligned} \phi V_{\rm S} j &= \phi w H k_{\rm r} \int_0^L c(x)dx + V_{\rm H} k_{\rm H} c_{\rm H} \\ L_{\rm S} j &\simeq k_{\rm r} \left[c_0 \ell + L c_{\rm H} \frac{\kappa}{\kappa + k_{\rm r}} \right] + 2L\bar{k}_H c_{\rm H} \ , \end{aligned} \tag{7.20}$$

for $L \gg \ell$. One can verify that this condition is indeed satisfied with the expressions given in Eqs. (7.18) and (7.19) for $L \to \infty$.

Boundaries of expression domains of target genes as a function of the total receptor density

We now discuss the expression domain of a hypothetical target gene activated by ligand-receptor complexes. We ask how the expression domain changes when the total density of receptors $n_{\rm T}$ is varied. We first consider the case where there is strong degradation in the hemolymph, so that $c_{\rm H} = 0$. In that case, using Eqs. (7.14), (7.17), and (7.18), the profile of bound receptors is given by

$$n_{\rm b} = \frac{n_{\rm T} k_{\rm on}}{k + k_{\rm off}} \frac{j\left(1 - e^{-\frac{L_{\rm S}}{\ell_0}}\right)}{\kappa + \sqrt{\kappa(\kappa + k_{\rm r})}} \exp\left(-\frac{x}{\ell}\right) \ . \tag{7.21}$$

We consider that the target is activated above a threshold value of bound receptors, $n_{\rm b} > n_{\rm b}^*$. This sets a domain boundary with position x^* (Fig. 7.2):

$$x^* = \ell \ln \left[\frac{n_{\rm T} k_{\rm on} j \left(1 - e^{-\frac{L_{\rm S}}{\ell_0}}\right)}{n_{\rm b}^* (k + k_{\rm off})(\kappa + \sqrt{\kappa(\kappa + k_{\rm r})})} \right] \ . \tag{7.22}$$

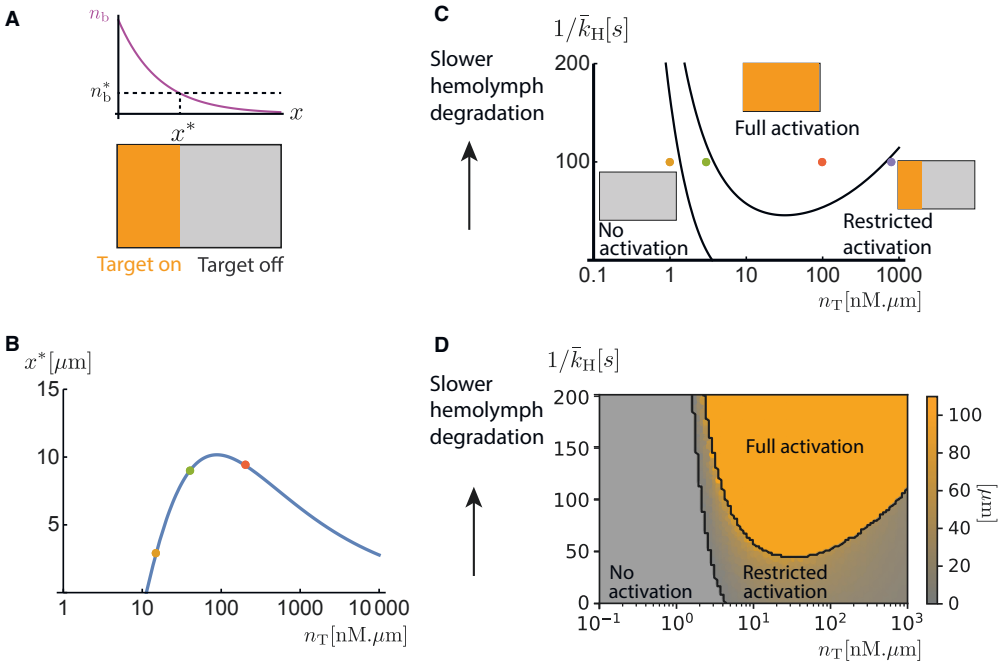

Figure 7.2: (A) A threshold level of surface density of bound receptors n_B^* determines the boundary of the activation domain (x^*) of a hypothetical downstream target (orange). (B) On/off target boundary (x^*) as a function of the total receptor surface density, in the absence of receptor saturation and ligands in the hemolymph. The activation threshold ($n_B^* = 10$nM. μm) was used to determine x^* for different receptor surface density (dots). A maximal target domain size can be found for intermediate values of the total receptor surface density. (C) Phase diagram of target activation domain size, as a function of total receptor surface density and effective ligand degradation rate in the hemolymph. Receptor saturation is not taken into account. At low receptor density level, no activation occurs; at intermediate receptor density and for low enough degradation in the hemolymph, a region of full activation appears; the third domain of parameter space is that of biologically relevant spatially restricted activation. (D) Phase diagram as described for panel F, but with receptor saturation included. Color code corresponds to the size of the activated domain.

Using this expression, we discuss below the limits $n_{\mathrm{T}} \to 0$ and $n_{\mathrm{T}} \to \infty$, at a fixed degradation rate k.

- When the total receptor density is small, $n_{\mathrm{T}} \to 0$, the length scale $\ell \to \ell_0 = \sqrt{D/\kappa}$ (Eq. (7.16)), which depends only on diffusion and leakage. In addition following Eq. (7.21), $n_{\mathrm{b}} \sim n_{\mathrm{T}} \to 0$. Therefore the profile maintains a fixed characteristic length scale and decreases in magnitude as $n_{\mathrm{T}} \to 0$. As a result as n_{T} decreases, x^* first approaches the position of the interface between the posterior compartment and the source, and for small enough n_{T} there is no target activation in the tissue. This occurs when the term within the logarithm in Eq. (7.22) is equal to 1.

- When the total receptors density is large, $n_{\mathrm{T}} \to \infty$, the effective degradation rate k_{r} increases (Eq. (7.15)) and the length scale $\ell \to 0$ (Eq. (7.16)). The decrease in the length scale is due to faster binding and overall degradation of the ligand as a result of a higher number of available receptors. The magnitude of the bound receptors profile ($n_{\mathrm{b}}(x = 0)$) also increases as $\sim \sqrt{n_{\mathrm{T}}}$ as can be seen from Eq. (7.21) in the limit $n_{\mathrm{T}} \to \infty$; so that the profile becomes higher and sharper. Overall the position of the boundary x^* converges to 0 for large n_{T} (Eq. (7.22)).

- In between these two limits, the boundary position x^* exhibits a maximum (Fig. 7.2).

We now take into account a non-zero value of the concentration in the hemolymph. In this case the target gene can be fully activated in the tissue when the ligand concentration at large distance becomes high enough. Using Eqs. (7.14), (7.17) and (7.19), the condition for full activation to occur is given by:

$$\frac{n_{\mathrm{T}} k_{\mathrm{on}}}{k + k_{\mathrm{off}}} \frac{j}{L} \frac{L_{\mathrm{S}} - (\ell_0 - \ell)(1 - e^{-\frac{L_{\mathrm{S}}}{\ell_0}})}{2\bar{k}_{\mathrm{H}} \frac{\kappa + k_{\mathrm{r}}}{\kappa} + k_{\mathrm{r}}} > n_{\mathrm{b}}^* \, . \tag{7.23}$$

As the total receptor density increases, $n_{\mathrm{T}} \to \infty$, two different behaviours can occur. For high enough ligand production, if $jh\kappa \left(L_{\mathrm{S}} - \ell_0 (1 - e^{-\frac{L_s}{\ell_0}}) \right) > Lkn_{\mathrm{b}}^* (2\bar{k}_H + \kappa)$, full activation of the target occurs even for a high number of receptors. If $jh\kappa \left(L_{\mathrm{S}} - \ell_0 \left(1 - e^{-\frac{L_s}{\ell_0}} \right) \right) < Lkn_{\mathrm{b}}^* (2\bar{k}_H + \kappa)$, increasing the total receptor density results in a shrinking expression domain near the source. In general a phase diagram can be drawn in the space of ($\bar{k}_H$,

Parameter	Name	Value	Unit	
Free ligand diffusion constant	D	21	$\mu m^2.s^{-1}$	As measured for Dpp [168]
Thickness of intercellular space	h	20	nm	Estimated from EM
Tissue height	H	53	μm	Measured (n=10 wings)
Length of one AP compartment	L	116	μm	Measured (n=10 wings)
Length of the source	L_S	26	μm	Measured (n=11 wings)
Binding rate of GFP to $Nb1^{high}$ (VHHGFP4)	$k_{on}^{Nb1^{high}}$	7.7×10^{-4}	$nM^{-1}.s^{-1}$	[303]
Unbinding rate of GFP from $Nb1^{high}$ (VHHGFP4)	$k_{off}^{Nb1^{high}}$	1.7×10^{-4}	s^{-1}	[303]
Binding rate of GFP to Nb^{low} (LAG3)	$k_{on}^{Nb^{low}}$	2×10^{-3}	$nM^{-1}.s^{-1}$	[40]
Unbinding rate of GFP from Nb^{low} (LAG3)	$k_{off}^{Nb^{low}}$	5×10^{-2}	s^{-1}	[40]
Ligand production rate in the source	j	0.32	$nM.s^{-1}$	Fitted
Leakage rate to hemolymph	κ	0.074	s^{-1}	Fitted
Rescaled degradation rate in hemolymph	$\bar{k}_H$	0.01	s^{-1}	Fitted
Rescaled degradation rate in hemolymph, fat body experiment	$\bar{k}_H^{FB}$	0.23	s^{-1}	Fitted
Receptor production rate	j_r	0.0027	$nM.\mu m.s^{-1}$	Fitted

Table 7.1: Parameter table for single receptor model (EM stands from electron micrographs).

n_T) with regions of finite activated region, full activation and no activation. For intermediate values of $\bar{k}_H$, increasing the total receptor density can change the activation region from full activation to a spatially restricted activated region (Fig. 7.2C), a result which is confirmed by numerical analysis of the full model with saturation (Fig. 7.2D). Qualitatively, the behaviour of going from full activation to restricted activation with an increasing receptor concentration is observed experimentally for the pMAD expressing region, when increasing the concentration of signaling receptors [273].

7.1.4 Parameters

To compare the model with experimental results, we solved for the steady-state bound receptor density profile n_b. We discuss here the set of parameters used in numerical solutions, listed in Table 7.1. We used the same set of parameters to fit different experiments, since we expect most of the parameters (e.g. those characterising the tissue geometry) to be independent by the level and affinity of the binders; except that the degradation rate of ligands in the hemolymph was assumed to be increased in experiments with the fat body trap (from $\bar{k}_H$ to $\bar{k}_H^{FB}$) and the on and off rates of

ligands to receptors were modified depending on whether the Nb^{low} or Nb^{high} receptors were expressed. Additionally, in one of the conditions included in the dataset, our collaborators quantified the shortening of the bound GFP gradient upon overexpression of Nb^{high}, which we capture by increasing the receptor density by a factor 20. This factor was estimated from *ex vivo* experiments (see Fig. 7.3). Much of the detail regarding the experimental side of this work was left out of the following for the sake of brevity but and extensive discussion can be found in the Materials and Methods, as well as the full Supplementary Text accompanying the original publication [273].

- Measurements of the geometry of the tissue (tissue height H, length of the posterior compartment L, length of the source L_S) are obtained by averaging measurements from cross-sections of wing discs.

- The width of the intercellular space is variable but a reasonable value of $h = 20$nm can be estimated from electron micrographs (C. Rabouille, personal communication).

- The diffusion constant D is the effective diffusion constant of free GFP in the tissue along the antero-posterior direction. An order of magnitude for this value can be obtained by noting that Dpp and GFP are proteins with similar sizes, and that the diffusion constant of extracellular Dpp has been measured in wing imaginal discs by fluorescence correlation spectroscopy to be $\sim 10 - 21\mu m^2/s$ [316]. Here we take $D = 21\mu m^2.s^{-1}$. We discuss below how parameters values vary when D is taken in the range $5 - 45\mu m^2/s$.

- The on and off rates of GFP to the Nb^{high} and Nb^{low} nanobody are obtained from biophysical measurements with purified proteins [241, 104, 161].

- To obtain the parameters j, κ, $\bar{k}_H$, $\bar{k}_H^{FB}$ and j_r, we fitted experimental measurements of fluorescence intensity of bound GFP profiles to the model of diffusion-degradation-leakage (Eqs. (7.10) and (7.13)). We fitted simultaneously profiles obtained with the Nb^{high} receptor with or without the fat body trap, or with the Nb^{low} receptor (Fig. 7.4).

  To estimate the turnover rate of bound receptors, our collaborators performed a pulse-chase experiment where the tissue was exposed *ex vivo* to GFP and subsequently washed, incubated for different durations and imaged. The result suggests

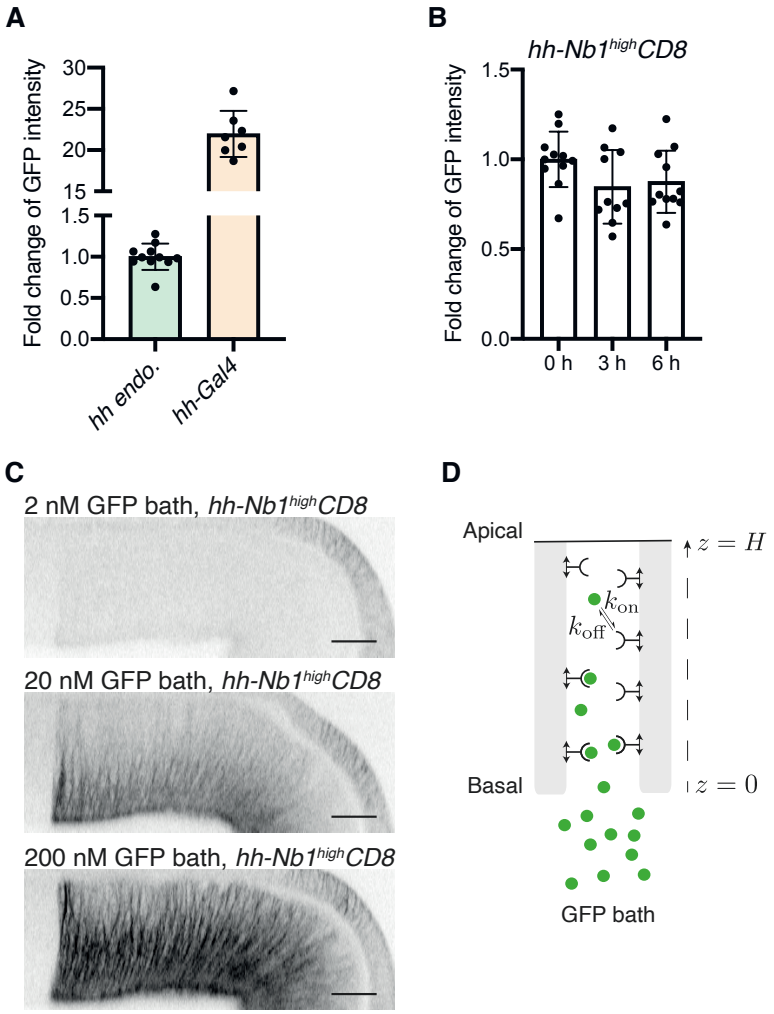

Figure 7.3: (A) Normalized fluorescent GFP intensity in the Nb^{high} condition (hh-$Nb1^{high}$CD8, green bar) and Nb^{high} overexpression condition (hh-Gal4, UAS-$Nb1^{high}$CD8, orange bar) after ex vivo incubation in a GFP bath. The difference in GFP intensity suggests that (Gal4-mediated) overexpression leads to a $\sim$ 20 fold increase in surface receptor levels. (B) Nb^{high}-expressing discs ($Nb1^{high}$CD8 condition) were saturated with GFP on ice, washed, incubated for different durations and imaged. Normalized GFP intensity in hh- $Nb1^{high}$CD8 wing discs decreased by $\sim$25% over the time course of 6 h. Since GFP is quenched in late endosomes due to a low pH (58), this observation suggests that Nb^{high} is degraded only slowly (on the scale of several hours as predicted by modelling). (C) To estimate the concentration of $Nb1^{high}$CD8 at the cell surface, a GFP invasion assay was used. hh-$Nb1^{high}$CD8 discs were incubated in 2 nM, 20 nM and 200 nM GFP baths for 5 min at 25°C. The resulting basal-to-apical GFP gradient in the posterior compartment was imaged and quantified. (D) A simple model of apico-basal gradient formation.

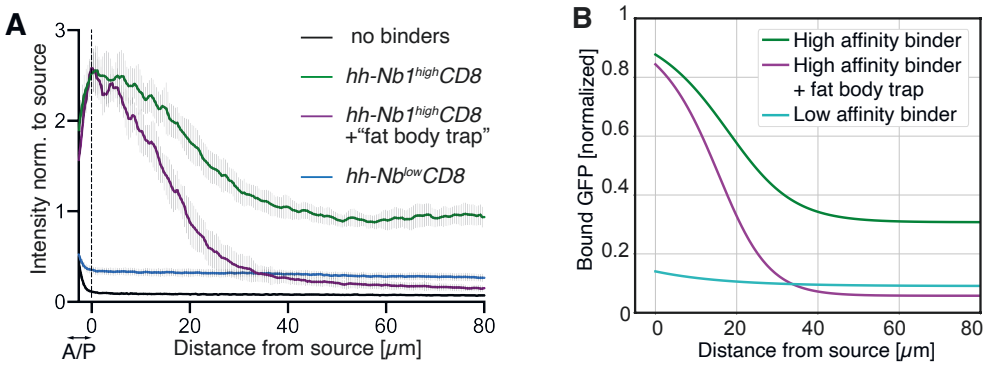

Figure 7.4: (A) Fluorescence intensity profiles of bound GFP obtained for the four experiments of interest, all of which involve GFP production at the AP boundary: no binders expressed in the disc (no binders condition), Nb^{high} expressed in the posterior compartment (hh-Nb1$^{\mathrm{high}}$CD8 condition), concomitant expression of Nb^{high} expressed in the posterior compartment and the fat body (hh-Nb1$^{\mathrm{high}}$CD8+fat body trap condition), Nb^{low} expressed in the posterior compartment (hh-Nb$^{\mathrm{low}}$CD8 condition). The vertical dotted line marks the estimated posterior edge of the source. The numbers of discs analyzed are as follows: no binders, n = 10; hh-Nb1$^{\mathrm{high}}$CD8, n = 11; hh-Nb1$^{\mathrm{high}}$CD8 + fat body trap, n = 7; hh-Nb$^{\mathrm{low}}$CD8, n = 10. Scale bars, 20 μm. (B) Bound GFP profiles normalized to the total concentration of receptors as predicted by our diffusion-degradation model after parameter fitting. The blue and green curves were obtained with the known on- and off-rates for the low- and high-affinity receptors, respectively. The purple curve was obtained by increasing degradation in the hemolymph.

that degradation occurs on a timescale of several hours (Fig. 7.3). This low rate can be rationalized from the lack of specific endocytic signals. Therefore we assume that $k \ll k_{\text{off}}^{\text{Nb}^{\text{high}}}$ and $k \ll k_{\text{off}}^{\text{Nb}^{\text{low}}}$, and we simplify Eqs. (7.10) and (7.13) to obtain:

$$\frac{n_{\text{b}}}{n_{\text{T}}} = \frac{k_{\text{on}} c}{k_{\text{off}} + k_{\text{on}} c} \tag{7.24}$$

$$0 = D\partial_x^2 c - \frac{j_{\text{r}}}{h} \frac{k_{\text{on}} c}{k_{\text{off}} + k_{\text{on}} c} - \kappa(c - c_{\text{H}}) \ . \tag{7.25}$$

using that $j_{\text{r}} = k n_{\text{T}}$ at steady-state. With this simplification, and fitting $n_{\text{b}}/n_{\text{T}}$ to normalized fluorescence intensity profiles, the fitting procedure can be performed for the parameters j, κ, $\bar{k}_{\text{H}}$, $\bar{k}_{\text{H}}^{\text{FB}}$ and j_{r}, without specifying the value of k or n_{T}. We use a least-square minimization performed with the scipy minimization Nelder-Mead method. Experimental and theoretical curves are normalized to the mean of the profile for Nb^{high}. We performed a bootstrapping analysis in order to estimate the robustness of the fitting process. We used a resampling residuals approach to generate 1000 set of artificial data curves, fitted each of them individually, and calculated the standard deviation of the resulting distribution of parameters. We find $j = 0.3 \pm 0.04\text{nM.s}^{-1}$, $\kappa = 0.075 \pm 0.004\text{s}^{-1}$, $\bar{k}_{\text{H}} = 0.01 \pm 0.001\text{s}^{-1}$, $\bar{k}_{\text{H}}^{\text{FB}} = 0.19 \pm 0.02\text{s}^{-1}$, $j_{\text{r}} = 0.0026 \pm 0.0003\text{nM.}\mu\text{m.s}^{-1}$. We also tested the influence on parameters of shifting the assumed position of the AP boundary by $\pm 0.76\mu$m, and found $0.28 < j < 0.34\text{nM.s}^{-1}$, $0.073 < \kappa < 0.078\text{s}^{-1}$, $0.009 < \bar{k}_{\text{H}} < 0.011\text{s}^{-1}$, $0.19 < \bar{k}_{\text{H}}^{\text{FB}} < 0.2\text{s}^{-1}$, $0.0025 < j_{\text{r}} < 0.0028\text{nM.}\mu\text{m.s}^{-1}$.

We note that the ligand production rate we obtain is $j = 0.3$ nM.s^{-1}. For a cell of lateral surface $500\mu\text{m}^2$ producing GFP in an intercellular space of width $h = 0.02\mu$m, this is equivalent to a production rate of ~ 0.9 GFP/cell/s. Here we have counted that each cell contributes specifically in the domain $h/2$ away from its surface. This production rate is in the same range as previously fitted production rates of Dpp (~ 2.7 molecules/cell/s [154]).

In Nb^{high} overexpression experiments, we use a receptor production rate j_{r} increased by a factor 20, as we estimated an increase of fluorescence intensity of 20 in this condition (Fig. 7.3).

In section 7.1.7 we discuss a method based on a GFP invasion experiment, where a wing

disc that does not secrete GFP but expresses Nb^{high} is put in contact *ex vivo* on the basal side with a GFP bath at different concentrations, to estimate the receptor surface density. With this method we find $n_T = 80\text{nM}.\mu\text{m}$ (corresponding to 1600 nM.μm in Nb^{high} overexpression experiments). This corresponds to a single cell surface receptor density of 40nM.μm. This value is smaller but comparable to the surface density of receptors measured in mammalian cells [311] . With the fitted value of j_r (Table 7.1), the relation $n_T = j_r/k$ gives $k \simeq 3.3 \times 10^{-5}\text{s}^{-1}$ or a degradation time scale of ~ 8 hours, consistent with our previous assumption of low receptor degradation rate.

To test how our results depend on an estimate of the diffusion constant D, we first note that in the limit $k \ll k_{\text{off}}$, the steady-state solution c of Eqs. (7.1), (7.5), (7.6) and (7.7) is invariant under the transformation $D \to \alpha D$, $j_r \to \alpha j_r$, $\kappa \to \alpha\kappa$, $k_H \to \alpha k_H$, $j \to \alpha j$ and $n_T \to \alpha n_T$; and the concentration of bound receptors changes by $n_b \to \alpha n_b$. We also found numerically that in the regime of parameters that we explored (including $5 < D < 45\mu\text{m}^2/\text{s}$), the dynamics of c in GFP invasion simulations was approximately quasi-static, $\partial_t c \simeq 0$ (see Eqs. (7.30)-(7.32)). In this limit Eqs. (7.30)-(7.32) are also invariant by $D_f \to \alpha D_f$, $n_T \to \alpha n_T$, $n_b \to \alpha n_b$, $D_r \to D_r$; where D_f is the diffusion constant of free GFP and D_r the diffusion constant of Nb^{high}-CD8 receptors within the surface. Since we only study normalized profiles of the bound concentration n_b in our analysis, we conclude that changing the estimate of D and D_f by a factor α, in the range that we explored, leads to the approximate parameter change $j_r \to \alpha j_r$, $\kappa \to \alpha\kappa$, $k_H \to \alpha k_H$, $j \to \alpha j$, $n_T \to \alpha n_T$, and $D_r \to D_r$.

7.1.5 Effect of replacing Nb^{high} receptor by Nb^{low} receptor

Here we discuss the effect of replacing the Nb^{high} by the Nb^{low} receptor, using results obtained in section 7.1.3 in the regime below receptor saturation. Bound GFP intensity profiles in tissues expressing the Nb^{high} receptor exhibit a non-zero tail, which is reduced by a factor ~ 3 compared to intensity profiles in tissues expressing the Nb^{low} receptor (Fig. 7.4).

With known receptor parameters, this implies that the plateau value of the free GFP concentration profile is actually increased by a factor ~ 30. Indeed, at steady-state and outside the receptor saturation regime, and since $k \ll k_{\text{off}}$, the free GFP density c is

related to the bound GFP density $n_{\rm b}$ by (Eq. (7.17)):

$$c \simeq \frac{k_{\rm off} n_{\rm b}}{k_{\rm on} n_{\rm T}} \ . \tag{7.26}$$

The overall affinity of $\mathrm{Nb}^{\rm low}$ to GFP $k_{\rm on}^{\mathrm{Nb}^{\rm low}}/k_{\rm off}^{\mathrm{Nb}^{\rm low}} = 0.04\mathrm{nM}^{-1}$ is ~ 100 times lower than the affinity of $\mathrm{Nb}^{\rm high}$ to GFP $k_{\rm on}^{\mathrm{Nb}^{\rm high}}/k_{\rm off}^{\mathrm{Nb}^{\rm high}} = 4.53\mathrm{nM}^{-1}$ (Table 7.1). The density of receptors $n_{\rm T}$ should be identical in tissues expressing the $\mathrm{Nb}^{\rm low}$ and $\mathrm{Nb}^{\rm high}$ receptors. Therefore, application of Eq. (7.26) indeed implies that the plateau of free GFP concentration profile c is increased by a factor ~ 30 with the $\mathrm{Nb}^{\rm low}$ receptor compared to the $\mathrm{Nb}^{\rm high}$ receptor.

In addition, one also observes that the $\mathrm{Nb}^{\rm low}$ bound receptor profile is flat, with no detectable gradient, in contrast to the gradient formed with the $\mathrm{Nb}^{\rm high}$ receptor (Fig. 7.4).

To rationalize these observations, we consider the limit of low ligand-receptor affinity, $k_{\rm on}/k_{\rm off} \to 0$, of the steady-state gradient formed outside of the regime of receptor saturation (section 7.1.3), since $\mathrm{Nb}^{\rm low}$ has a smaller affinity to GFP than $\mathrm{Nb}^{\rm high}$. In that limit $k_{\rm r} \ll \kappa$ and also taking $k_{\rm r} \ll \bar{k}_{\rm H}$ for simplicity, the predicted gradient is given by

$$n_{\rm b} = \frac{n_{\rm T} k_{\rm on} j}{2\kappa k_{\rm off}} \left[(1 - e^{-\frac{L_s}{\ell_0}}) e^{-\frac{x}{\ell_0}} + \frac{L_{\rm S}\kappa}{L\bar{k}_{\rm H}} \right] \ , \tag{7.27}$$

where we have assumed $k \ll k_{\rm off}$. In the limit $\frac{L_{\rm S}\kappa}{L\bar{k}_H} \gg 1$, the first term in brackets becomes negligible and the profile of bound receptors becomes flat, as observed experimentally. We note however that with the parameters listed in Table 7.1, we find $\frac{L_{\rm S}\kappa}{L\bar{k}_H} \simeq 1.7$ so that this limit is not exactly reached; indeed the corresponding profile still has a weak gradient for the $\mathrm{Nb}^{\rm low}$ case (Fig. 7.4).

In addition, one can discuss how the free ligand concentration at large distance depends on the receptor affinity for the ligand. In Fig. 7.5, we plot the predicted free GFP concentration when $k_{\rm on}$ and $k_{\rm off}$ are varied around the known $\mathrm{Nb}^{\rm high}$ parameters. The free GFP concentration at large distance increases when $k_{\rm on}$ is reduced or $k_{\rm off}$ is increased. This arises in the model because decreased ligand-receptor affinity leads to a smaller effective degradation in the tissue (rate $k_{\rm r}$). As a result, the concentration $c_{\rm H}$ in the

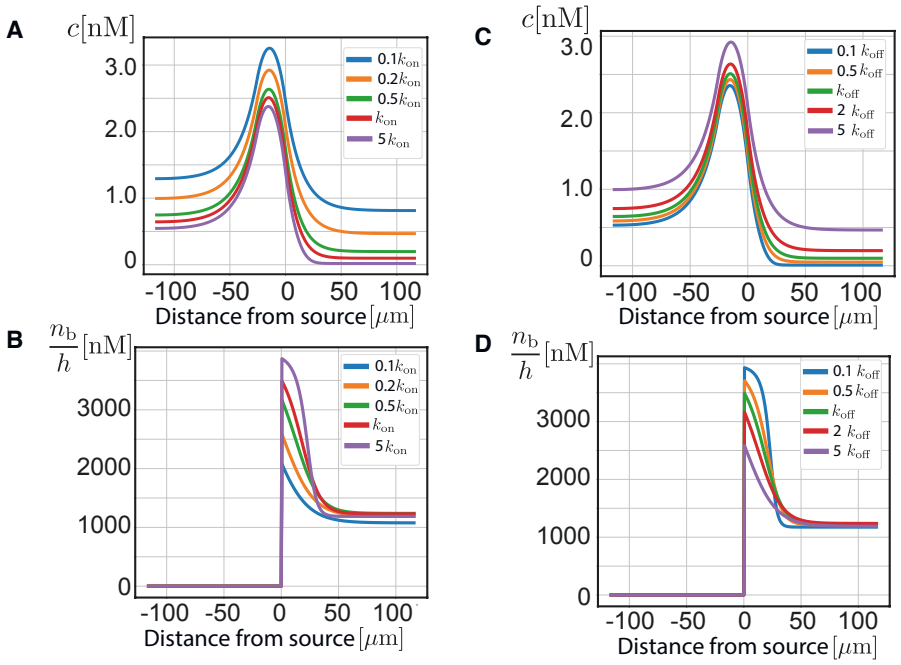

Figure 7.5: Free ligand concentration (A,C) and effective 3D bound receptor concentration (as opposed to membrane density) in the intercellular space (B, D) profiles for different k_{on} (A, B) and, k_{off} values (C, D). The relative levels of free ligand concentration and effective 3D bound receptor concentration indicate that the GFP fluorescence profile is largely dominated by bound receptors. n_T = 80nM.μm, and other parameters as in Table 7.1.

hemolymph is higher, as a larger fraction of produced GFP molecules accumulates in the hemolymph instead of being degraded in the tissue (see Eq. (7.19)). Besides, more ligands coming from the hemolymph can remain in the tissue without binding to a receptor and being degraded (factor $\kappa/(\kappa+k_\mathrm{r})$ in Eq. (7.14)). Overall, our model predicts a larger free ligand concentration far from the source when ligand-receptor affinity is reduced. This is consistent with the reasoning at the beginning of this section, which showed that the free ligand concentration at large distance should be ~ 30 higher for $\mathrm{Nb}^{\mathrm{low}}$ than for $\mathrm{Nb}^{\mathrm{high}}$.

7.1.6 Effect of GFP production and trapping by multiple tissues

The hedgehog and patched genes are active in several tissues besides wing imaginal discs [277, 174, 140, 117, 160]. These tissues are therefore expected to express GFP and binders and hence affect the level of GFP in the hemolymph. Here we assess these contributions.

We consider that $i = 1...N$ different tissues which, as in section 7.1.1, have a cuboidal shape (Fig. 7.1). We assume as before that the concentration of free GFP in the hemolymph is uniform. The equation for the hemolymph concentration (previously Eq. (7.7)) then becomes:

$$\frac{dc_\mathrm{H}}{dt} = \sum_i \frac{V_i \phi_i \kappa_i}{V_\mathrm{H}^\mathrm{tot}} (\langle c \rangle_i - c_\mathrm{H}) - k_\mathrm{H} c_\mathrm{H} \ , \tag{7.28}$$

where $\langle c \rangle_i$ is the average free ligand concentration in tissue i, $V_i = 2L_i w_i H_i$ is the volume of tissue i, ϕ_i is the intercellular volume fraction of tissue i, and κ_i is the leakage rate of tissue i into the hemolymph. If we assume that all regions have the same intercellular volume fraction, leakage rate and average free ligand concentration, we obtain

$$\frac{dc_\mathrm{H}}{dt} = \frac{\kappa \phi (\sum_i V_i)}{V_\mathrm{H}^\mathrm{tot}} (\langle c \rangle - c_\mathrm{H}) - k_\mathrm{H} c_\mathrm{H} \ , \tag{7.29}$$

which is identical to Eq. (7.7), with an effective hemolymph volume $V_\mathrm{H} = V_\mathrm{H}^\mathrm{tot} V / (\sum_i V_i)$ with V the volume of one wing imaginal disc. Here we make the simplifying assumption that this approximation holds. A more detailed description would require, for each tissue, the knowledge of the size of each domains of expression of *patched* and *hh*, and

the cell geometries, in order to solve Eq. (7.28).

7.1.7 Estimate of the receptor surface density from GFP invasion experiments

In Fig. 7.3, we describe GFP invasion experiments. In these experiments, a wing disc that does not secrete GFP but expresses $\mathrm{Nb}^{\mathrm{high}}$ is put in contact *ex vivo* on the basal side with a GFP bath at different concentrations c^{bath}=2nM, 20nM, 200nM. Free GFP then diffuses through the basal membrane into the tissue, along its apico-basal direction, and binds and unbinds to receptors. After $\tau_c = 300$s of contact with the bath, the disc is washed and fixed and the apico-basal profile of GFP intensity is quantified. Here we denote the diffusion constant of free GFP D_{f} and choose $D_{\mathrm{f}} = 2D$. Indeed assuming that GFP diffuses within the small intercellular space, and treating the edge of cells as straight lines with a random orientation, the effective diffusion constant along the antero-posterior axis is $D \simeq \langle \cos^2\theta \rangle D_{\mathrm{f}} = D_{\mathrm{f}}/2$, where the average is over possible junction orientations θ.

We assume that the process of GFP invasion in the tissue can be described using the following equations for the free GFP concentration c, the surface density of bound receptors n_{b} and the surface density of unbound receptors n_{u},

$$\partial_t c = D_{\mathrm{f}} \partial_z^2 c + \frac{1}{h}\left(-k_{\mathrm{on}} c n_{\mathrm{u}} + k_{\mathrm{off}} n_{\mathrm{b}}\right) \ , \tag{7.30}$$

$$\partial_t n_{\mathrm{b}} = D_{\mathrm{r}} \partial_z^2 n_{\mathrm{b}} + k_{\mathrm{on}} c n_{\mathrm{u}} - k_{\mathrm{off}} n_{\mathrm{b}} \ , \tag{7.31}$$

$$\partial_t n_{\mathrm{u}} = D_{\mathrm{r}} \partial_z^2 n_{\mathrm{u}} - k_{\mathrm{on}} c n_{\mathrm{u}} + k_{\mathrm{off}} n_{\mathrm{b}} \ , \tag{7.32}$$

where we denote z the apico-basal coordinate, with $z = 0$ denoting the basal side and $z = H$ the apical side (Fig. 7.3). We assume that on the short time scale of the experiment, receptor production and internalization can be neglected, such that the total receptor density $n_{\mathrm{T}} = n_{\mathrm{b}} + n_{\mathrm{u}}$ is fixed. We also assume that free and bound receptors can diffuse within the cell membrane with a diffusion constant D_{r}. In addition,

we impose the boundary conditions

$$c(z=0,t) = c^{\text{bath}} \tag{7.33}$$

$$\partial_z c(z=H,t) = \partial_z n_{\text{b}}(z=H,t) = \partial_z n_{\text{u}}(z=H,t) = 0 \tag{7.34}$$

$$\partial_z n_{\text{b}}(z=0,t) = \partial_z n_{\text{u}}(z=0,t) = 0 \tag{7.35}$$

Eq. (7.33) arises from the condition that the GFP bath imposes its concentration at the basal side (we assume that there is no barrier between the bath and the basal side of the tissue). Eq. (7.34) arises from the lack of exchange between the basolateral compartment and the apical compartment, such that free GFP or receptors have a vanishing diffusion flux at the apical end of the tissue. Eq. (7.35) arises from the condition that receptors can not leave the cell membrane on the basal side.

Solving for these equations with the initial conditions $c(z,t=0) = n_{\text{b}}(z,t=0) = 0$, we calculate the profile $n_{\text{b}}(z,\tau_c)$ for different values of c^{bath} and compare to experiments. A fit to experimental data is performed by a least-square minimization between the experimental GFP fluorescence and the profile $n_{\text{b}}(z,\tau_c)$, normalizing all curves by the mean of the profile for $c^{\text{bath}} = 200\text{nM}$. From this fitting procedure we find $n_{\text{T}} = 80 \pm 1.8\text{nM}.\mu\text{m}$ and $D_{\text{r}} = 1.36 \pm 0.05\mu\text{m}^2/\text{s}$. Here the uncertainty values are standard deviations, obtained from a bootstrapping method, where we fitted synthetic curves generated by adding errors to the best fit theoretical curve. Errors were taken from a normal distribution with a standard deviation given by the maximal residual between theoretical and experimental curves, for each condition. In section 7.2 we use the rounded value $n_{\text{T}} = 100\text{nM}.\mu\text{m}$ for the receptor surface density.

7.2 Model with second hopping receptor

In this section we introduce a description of gradients that involves a second class of receptors binding to the ligand. We discuss the possibility that this second receptor effectively diffuses in the tissue, through hopping between neighbouring cells. We show that this receptor effective diffusion can lead to gradient expansion, i.e. an increase in the characteristic length scale of the gradient. In this section, we consider receptors which are expressed uniformly in the tissue, including in the source.

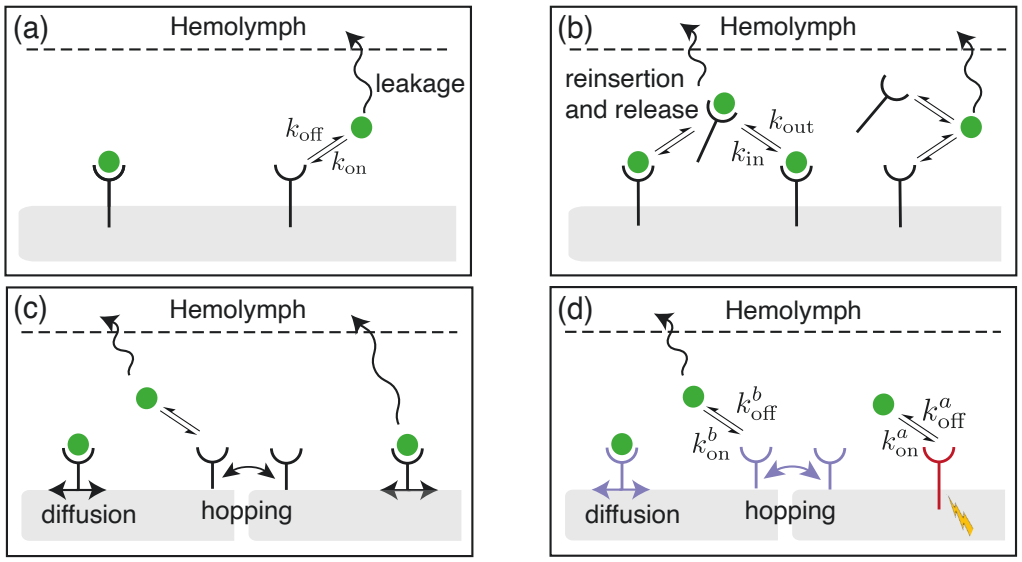

Figure 7.6: Diffusion-leakage-degradation models with one or two receptor types, as discussed in the text: (a) simple model of ligand binding to immobile, membrane-bound receptors. (b) As in (a), but with receptor release from the membrane and subsequent reinsertion. (c) As in (a) but considering effective diffusion of receptors at the surface of the tissue, through membrane diffusion and hopping. (d) As in (c), but with two receptor types: one type of receptor is allowed to hop and diffuse, while the second type remains membrane-bound and immobile. The two receptor types are color-coded according to the same convention for signalling/non-signalling receptors followed in Fig. 7.7B.

7.2.1 Morphogen gradient with receptor release and reinsertion

Simplified model of a single receptors with release and reinsertion

We first discuss a simplified model where a single receptor type can be released from the membrane, diffuse in the inter-cellular space, and reinsert in the membrane of another cell (see Fig. 7.6(b) for a schematic). For simplicity we describe the epithelium as a continuous material and do not describe explicitly discrete cellular interfaces. As in the previous section, we denote c the concentration of freely diffusing ligand, and n_{u} and n_{b}, the concentrations of unbound and ligand-bound membrane receptors. We also introduce the concentrations of unbound and ligand-bound freely-diffusing receptors, c_{u} and c_{b}. The ligand can bind to receptors with on-rate k_{on} and unbind with off-rate

$k_{\rm off}$. The concentration equations read:

$$\partial_t c = D\partial_x^2 c + \frac{1}{h}\left[-k_{\rm on} n_{\rm u} c + k_{\rm off} n_{\rm b}\right] - k_{\rm on} c_{\rm u} c + k_{\rm off} c_{\rm b} - \kappa(c - c_{\rm H}) + j_{\rm S}(x) \tag{7.36}$$

$$\partial_t n_{\rm u} = -k_{\rm on} n_{\rm u} c + k_{\rm off} n_{\rm b} - k n_{\rm u} - k_{\rm out} n_{\rm u} + h k_{\rm in} c_{\rm u} + j_{\rm r} \tag{7.37}$$

$$\partial_t n_{\rm b} = k_{\rm on} n_{\rm u} c - k_{\rm off} n_{\rm b} - k n_{\rm b} - k_{\rm out} n_{\rm b} + h k_{\rm in} c_{\rm b} \tag{7.38}$$

$$\partial_t c_{\rm u} = D_{\rm ru}\partial_x^2 c_{\rm u} + \frac{1}{h} k_{\rm out} n_{\rm u} - k_{\rm in} c_{\rm u} + k_{\rm off} c_{\rm b} - k_{\rm on} c c_{\rm u} - \kappa_{\rm r}(c_{\rm u} - c_{\rm u,H}) \tag{7.39}$$

$$\partial_t c_{\rm b} = D_{\rm rb}\partial_x^2 c_{\rm b} + \frac{1}{h} k_{\rm out} n_{\rm b} - k_{\rm in} c_{\rm b} + k_{\rm on} c c_{\rm u} - k_{\rm off} c_{\rm b} - \kappa_{\rm r}(c_{\rm b} - c_{\rm b,H})\ . \tag{7.40}$$

Here we have introduced the rates of receptor detachment from the membrane $k_{\rm out}$ and reattachment to the membrane $k_{\rm in}$. $D_{\rm rb}$ and $D_{\rm ru}$ are the diffusion constants of untethered ligand-bound and free receptors, respectively; in the following we take these diffusion constants equal to D for simplicity. $j_{\rm S}(x)$ is the ligand secretion rate, which is non-zero and equal to j only in the source. $j_{\rm r}$ is the rate of increase of free receptor surface density, following from receptors biosynthesis and export to the membrane. In this section, $j_{\rm r}$ is uniform within the tissue. $\kappa_{\rm r}$ is the rate of exchange of receptors with the hemolymph, which we assume can be different from the rate of exchange of ligands κ. We also have introduced for completeness the concentrations of freely-diffusing receptors in the hemolymph, $c_{\rm u,H}$ and $c_{\rm b,H}$; in the following we set these concentrations to 0 for simplicity.

At steady-state, $n_{\rm T} = n_{\rm u} + n_{\rm b}$ and $c_{\rm T} = c_{\rm u} + c_{\rm b} = \frac{k_{\rm out}}{h(k_{\rm in}+\kappa_{\rm r})} n_{\rm T}$ are uniform, assuming no flux-boundary conditions for the freely diffusing receptors at both ends of the tissue. Then at steady-state, outside of the source, away from receptor saturation ($c \ll k_{\rm off}/k_{\rm on}$), one obtains, eliminating $c_{\rm b}$ from the steady-state equations:

$$D\partial_x^2 c - \frac{k_{\rm on} n_{\rm T}}{h}\left(1 + \frac{k_{\rm off}}{k_{\rm in}} + \frac{k_{\rm out}}{\kappa_{\rm r} + k_{\rm in}}\right) c - \kappa(c - c_{\rm H}) + \frac{k_{\rm off}}{h k_{\rm in}}(k_{\rm off} + k + k_{\rm in} + k_{\rm out}) n_{\rm b} = 0 \tag{7.41}$$

$$(k_{\rm off} + k + k_{\rm out})(D\partial_x^2 - k_{\rm in} - k_{\rm off} - \kappa_{\rm r}) n_{\rm b} + k_{\rm in} k_{\rm out} n_{\rm b} = k_{\rm on} n_{\rm T}(D\partial_x^2 - k_{\rm in} - k_{\rm off} - \kappa_{\rm r} - \frac{k_{\rm in} k_{\rm out}}{k_{\rm in} + \kappa_{\rm r}}) c\ . \tag{7.42}$$

The concentration profile solution of these equations is a double exponential. For $k_{\rm in} \to$

∞, $k \ll k_{\rm off}$ and $k \ll k_{\rm on} n_{\rm T}/h$, the longer length scale on which the gradient decays, $\tilde{\ell}$, is given by:

$$\tilde{\ell}^2 \simeq \ell^2 \left[1 + \frac{k_{\rm on} k_{\rm out} n_{\rm T}}{k_{\rm in}} \left(\frac{1}{h k_{\rm off}} - \frac{\kappa_{\rm r}}{h\kappa k_{\rm off} + k k_{\rm on} n_{\rm T}} \right) \right] \ , \tag{7.43}$$

with $\ell^2 = D/\left(\kappa + k\frac{k_{\rm on} n_{\rm T}}{h k_{\rm off}}\right)$. The equation above indicates that for $0 < \kappa_{\rm r} < \kappa$, the net effect of receptor detachment in the intercellular space is to enlarge the characteristic length scale of the gradient. For $\kappa_{\rm r} = 0$ (no receptor leakage), the relation above becomes

$$\tilde{\ell}^2 \simeq \ell^2 \left(1 + \frac{k_{\rm out}}{k_{\rm in}} \frac{k_{\rm on} n_{\rm T}}{h k_{\rm off}} \right) \ . \tag{7.44}$$

The non-dimensional factor $\frac{k_{\rm on} n_{\rm T}}{h k_{\rm off}}$ can be large ($\sim 2 \cdot 10^4$ for the $\mathrm{Nb}^{\rm high}$ receptor and ~ 200 for the $\mathrm{Nb}^{\rm low}$ receptor, with $n_{\rm T} = 100\mathrm{nM}.\mu\mathrm{m}$), so that even a small value of $k_{\rm out}/k_{\rm in}$ (corresponding to a small fraction of receptors circulating in the intercellular space) can have a significant effect in extending the length scale of the gradient, if the receptors do not leak.

Effective surface diffusion of receptors

We start from the model described in section 7.2.1, and consider the limit $k_{\rm in}, k_{\rm out} \to \infty$ with $\frac{k_{\rm out}}{k_{\rm in}} \to K_{\rm md}$ being kept constant ($K_{\rm md}$ is the dissociation constant of receptors from the membrane). Starting from Eqs. (7.39) and (7.40) for the intercellular concentration of free and bound receptors, we divide both sides of these equations by $k_{\rm in}$ and obtain in this limit:

$$c_{\rm u} \simeq \frac{K_{\rm md}}{h} n_{\rm u}, \quad c_{\rm b} \simeq \frac{K_{\rm md}}{h} n_{\rm b} \ . \tag{7.45}$$

We now substitute Eq. (7.39) into Eq. (7.37), Eq. (7.40) into (7.38) and use Eq. (7.45) to remove $c_{\rm b}$ and $c_{\rm u}$ from the system of equations. The concentration equation for the

unbound and bound receptors thus reads to zeroth order in $1/k_{\rm in}$:

$$\partial_t n_{\rm u} = \left(\frac{K_{\rm md} D}{1+K_{\rm md}}\right)\partial_x^2 n_{\rm u} - \left(\frac{k+K_{\rm md}\kappa_{\rm r}}{1+K_{\rm md}}\right) n_{\rm u} - k_{\rm on} n_{\rm u} c + k_{\rm off} n_{\rm b} + \frac{j_r}{1+K_{\rm md}}$$
$$\partial_t n_{\rm b} = \left(\frac{K_{\rm md} D}{1+K_{\rm md}}\right)\partial_x^2 n_{\rm b} - \left(\frac{k+K_{\rm md}\kappa_{\rm r}}{1+K_{\rm md}}\right) n_{\rm b} + k_{\rm on} n_{\rm u} c - k_{\rm off} n_{\rm b} \tag{7.46}$$

We conclude that in the limit of fast binding/unbinding to the membrane relative to receptor-ligand dynamics, receptor release and reinsertion in the membrane results in an effective diffusion term for the membrane-bound receptor, with a characteristic diffusion coefficient $D_{\rm r}^{\rm eff} = \frac{K_{\rm md} D}{1+K_{\rm md}}$.

We now consider that in addition, receptors diffuse within the cell membrane, and can directly hop between neighbouring cells (see Fig. 7.6(c) for a schematic). We assume that these processes result in an effective diffusion constant of membrane-bound receptors at the surface of the tissue, $D_{\rm m}$ [36, 143]. One then obtains the following dynamical equations for the receptors:

$$\partial_t n_{\rm u} = D_{\rm r}^{\rm eff}\partial_x^2 n_{\rm u} - \kappa_{\rm r}^{\rm eff} n_{\rm u} - k_{\rm on} n_{\rm u} c + k_{\rm off} n_{\rm b} + \frac{j_r - k n_{\rm u}}{1+K_{\rm md}} \tag{7.47}$$
$$\partial_t n_{\rm b} = D_{\rm r}^{\rm eff}\partial_x^2 n_{\rm b} - \kappa_{\rm r}^{\rm eff} n_{\rm b} + k_{\rm on} n_{\rm u} c - k_{\rm off} n_{\rm b} - \frac{k}{1+K_{\rm md}} n_{\rm b}\ , \tag{7.48}$$

with $D_{\rm r}^{\rm eff} = \frac{D_{\rm m}+K_{\rm md}D}{1+K_{\rm md}}$ an effective diffusion constant and $\kappa_{\rm r}^{\rm eff} = \frac{K_{\rm md}\kappa_{\rm r}}{1+K_{\rm md}}$ is an effective leakage rate. For large $K_{\rm md}$, corresponding to receptors spending a large fraction of their time in the intercellular space, this effective diffusion constant approaches the original diffusion constant of the intercellular species D; conversely for $K_{\rm md} \ll 1$ the diffusion constant approaches $D_{\rm m}$. When freely diffusing intercellular receptors leak into the hemolymph, corresponding to $\kappa_{\rm r} > 0$, the effective leakage rate of receptors is modified by release and reinsertion. For large $K_{\rm md}$ the intercellular receptor leakage constant $\kappa_{\rm r}$ contributes to the overall degradation of receptors. For large affinity of receptors for the cell membrane, $K_{\rm md} \ll 1$, the effective leakage rate $\kappa_{\rm r}^{\rm eff}$ vanishes.

Neglecting for now the role of receptor degradation, Eqs. (7.47) and (7.48) involve a characteristic length scale $\ell_{\rm r} = \sqrt{\frac{D_{\rm r}^{\rm eff}}{\kappa_{\rm r}^{\rm eff}}} = \sqrt{\frac{\kappa}{\kappa_{\rm r}}}\sqrt{1+\frac{D_{\rm m}}{K_{\rm md}D}}\ell_0$, where $\ell_0 = \sqrt{D/\kappa}$ is the length scale set by diffusion and leakage. Considering the characteristic length scales of the steady-state solution of Eqs. (7.36), (7.47), (7.48), outside of saturation, we

find that that receptor diffusion, release and reinsertion in the membrane contribute to expand the gradient when $\ell_r > \ell_0$. For $\kappa_r = \kappa$ and $D_m = 0$, i.e. if receptors leak with the same rate as ligands, and do not diffuse at the surface of the tissue, $\ell_r = \ell_0$ and there is no gradient expansion. Gradient expansion could be achieved however either with a low value of $\kappa_r \ll \kappa$, corresponding to inhibition of receptor leakage; or in the case where $\kappa_r = \kappa$, with a small value of K_{md} together with a sufficiently large value of D_m. In the following, we assume that κ_r^{eff} can be neglected.

Simplified model of one fixed + one diffusing receptor

We now discuss a simplified model involving two receptor species, only one of which can diffuse and hop at the surface of the tissue (see Fig. 7.6(d) for a schematic). We identify the hopping species with the GPI-anchored non-signaling receptors (NR) discussed in the main text, while the non-hopping species is meant to describe the signaling receptors (SR). For simplicity, we absorb the details of the hopping dynamics into a diffusion term for the NR, an approach we discussed in section 7.2.1; and we assume that leakage of intercellular receptors can be neglected and take the limit $\kappa_r \to 0$. Similarly to what was observed in section 7.2.1, we find that NR diffusion always increases the gradient length scale compared to the corresponding system without diffusion. We also derive an exact expression for the threshold receptor diffusion coefficient, above which introduction of NR extends the gradient length scale compared to the SR-only case. We find that this threshold diffusion constant is set by a competition between NR-mediated ligand degradation and hopping.

The concentration equations read for $0 < x < L$, outside of the source:

$$\partial_t c = D\partial_x^2 c + \frac{1}{h}\left[-k^{\text{a}}_{\text{on}} n^{\text{a}}_{\text{u}} c + k^{\text{a}}_{\text{off}} n^{\text{a}}_{\text{b}}\right] + \frac{1}{h}\left[-k^{\text{b}}_{\text{on}} n^{\text{b}}_{\text{u}} c + k^{\text{b}}_{\text{off}} n^{\text{b}}_{\text{b}}\right] - \kappa(c - c_{\text{H}}) \tag{7.49}$$

$$\partial_t n^{\text{a}}_{\text{u}} = -k^{\text{a}}_{\text{on}} n^{\text{a}}_{\text{u}} c + k^{\text{a}}_{\text{off}} n^{\text{a}}_{\text{b}} - k^{\text{a}} n^{\text{a}}_{\text{u}} + j^{\text{a}}_r \tag{7.50}$$

$$\partial_t n^{\text{a}}_{\text{b}} = k^{\text{a}}_{\text{on}} n^{\text{a}}_{\text{u}} c - k^{\text{a}}_{\text{off}} n^{\text{a}}_{\text{b}} - k^{\text{a}} n^{\text{a}}_{\text{b}} \tag{7.51}$$

$$\partial_t n^{\text{b}}_{\text{u}} = D_{\text{r}}\partial_x^2 n^{\text{b}}_{\text{u}} - k^{\text{b}}_{\text{on}} n^{\text{b}}_{\text{u}} c + k^{\text{b}}_{\text{off}} n^{\text{b}}_{\text{b}} - k^{\text{b}} n^{\text{b}}_{\text{u}} + j^{\text{b}}_r \tag{7.52}$$

$$\partial_t n^{\text{b}}_{\text{b}} = D_{\text{r}}\partial_x^2 n^{\text{b}}_{\text{b}} + k^{\text{b}}_{\text{on}} n^{\text{b}}_{\text{u}} c - k^{\text{b}}_{\text{off}} n^{\text{b}}_{\text{b}} - k^{\text{b}} n^{\text{b}}_{\text{b}}\ , \tag{7.53}$$

where superscripts a and b are used to indicate the concentrations of SR and NR, respectively. D_r is the effective diffusion constant of receptors, which was discussed more

extensively in section 7.2.1. Away from receptor saturation ($c \ll \frac{k_{\rm off}}{k_{\rm on}}$), the dynamics become linear; we now take this approximation. At steady-state the total receptor densities $n_{\rm T}^a = n_{\rm u}^a + n_{\rm b}^a = j_{\rm r}^{\rm a}/k^{\rm a}$ and $n_{\rm T}^{\rm b} = n_{\rm u}^{\rm b} + n_{\rm b}^{\rm b} = j_{\rm r}^{\rm b}/k^{\rm b}$ are uniform, assuming no flux-boundary conditions for the freely diffusing receptors at both ends of the tissue. This allows to eliminate $n_{\rm u}^{\rm a}$ and $n_{\rm u}^{\rm b}$ from the system of equations. Finally, we turn (7.49) into a steady-state equation for c only, by multiplying both sides with the operator $(D_{\rm r}\partial_x^2 - k_{\rm off}^{\rm b} - k^{\rm b})$ and performing suitable substitutions. We then obtain the following equation for the concentration profile of free ligand:

$$\left[\frac{D_{\rm r}D}{k^{\rm b}+k_{\rm off}^{\rm b}}\right]\partial_x^4 c - \left[D + \frac{D_{\rm r}}{k^{\rm b}+k_{\rm off}^{\rm b}}\left(\frac{k_{\rm on}^{\rm a} j_{\rm r}^{\rm a}}{h(k^{\rm a}+k_{\rm off}^{\rm a})} + \frac{k_{\rm on}^{\rm b} j_{\rm r}^{\rm b}}{hk^{\rm b}} + \kappa\right)\right]\partial_x^2 c + \left[\frac{k_{\rm on}^{\rm a} j_{\rm r}^{\rm a}}{h(k^{\rm a}+k_{\rm off}^{\rm a})} + \frac{k_{\rm on}^{\rm b} j_{\rm r}^{\rm b}}{h(k^{\rm b}+k_{\rm off}^{\rm b})} + \kappa\right] c - \kappa c_{\rm H} = 0 \ , \tag{7.54}$$

which is then related to the profile of bound SR via

$$n_{\rm b}^{\rm a} = \frac{k_{\rm on}^{\rm a} j_{\rm r}^{\rm a}}{k^{\rm a}(k^{\rm a}+k_{\rm off}^{\rm a})} c \ . \tag{7.55}$$

At large distance away from the source where the derivatives of the concentration profile vanish, the background ligand concentration is given by

$$c_\infty = c_{\rm H}\frac{\kappa}{k_{\rm r}^{\rm ab}+\kappa} \ , \tag{7.56}$$

where we have defined $k_{\rm r}^{\rm ab}$ the effective degradation rate of ligand due to the presence of the two receptor species:

$$k_{\rm r}^{\rm ab} = \frac{k_{\rm on}^{\rm a} j_{\rm r}^{\rm a}}{h(k^{\rm a}+k_{\rm off}^{\rm a})} + \frac{k_{\rm on}^{\rm b} j_{\rm r}^{\rm b}}{h(k^{\rm b}+k_{\rm off}^{\rm b})} \ . \tag{7.57}$$

By comparing this result with the corresponding expression obtained for the single-receptor model (Eq. (7.15)), we notice that the effective ligand degradation rate is in general increased by the introduction of a second receptor. This is not surprising, since adding receptors adds a route for ligand degradation. The introduction of a low-affinity non-signaling receptor could thus allow to vary the effective degradation rate without changing the characteristics of the signaling-receptor.

A further comparison with the single-receptor model presented in section 7.1 suggests that an increase in effective degradation rate due to the introduction of a second receptor also leads to a reduction of the length scale ℓ of the gradient. This is indeed the case when $D_\mathrm{r} = 0$, in which case ℓ is a monotonically decreasing function of j_r^b ($\ell = \sqrt{\frac{D}{k_\mathrm{r}^\mathrm{ab}+\kappa}}$). For $D_\mathrm{r} > 0$, the situation is more complex and, in order to find the new length-scale $\tilde{\ell}$, we need to solve the following polynomial equation

$$\left[\frac{D_\mathrm{r} D}{k^\mathrm{b} + k_\mathrm{off}^\mathrm{b}}\right] - \left[D + \frac{D_\mathrm{r}}{k^\mathrm{b} + k_\mathrm{off}^\mathrm{b}}\left(\frac{k_\mathrm{on}^\mathrm{a} j_\mathrm{r}^\mathrm{a}}{h(k^\mathrm{a} + k_\mathrm{off}^\mathrm{a})} + \frac{k_\mathrm{on}^\mathrm{b} j_\mathrm{r}^\mathrm{b}}{h k^\mathrm{b}} + \kappa\right)\right] \tilde{\ell}^2 + \left[k_\mathrm{r}^\mathrm{ab} + \kappa\right] \tilde{\ell}^4 = 0 \quad (7.58)$$

obtained by plugging an exponential ansatz in Eq. (7.54).

To get a qualitative picture of the effect of finite non-signaling receptor diffusion, we start by treating this equation perturbatively in small D_r. We expand the largest length to linear order, such that $\tilde{\ell} = \ell + \delta\ell$, with $\ell = \sqrt{\frac{D}{k_\mathrm{r}^\mathrm{ab}+\kappa}}$ and $\delta\ell$ a small correction of order D_r. We obtain:

$$\delta\ell = \frac{D_\mathrm{r}}{2\ell(k_\mathrm{r}^\mathrm{ab} + \kappa)(k^\mathrm{b} + k_\mathrm{off}^\mathrm{b})} \frac{k_\mathrm{on}^\mathrm{b} j_\mathrm{r}^\mathrm{b}}{h k^\mathrm{b}} \frac{k_\mathrm{off}^\mathrm{b}}{k^\mathrm{b} + k_\mathrm{off}^\mathrm{b}} > 0 \ . \quad (7.59)$$

We thus conclude that introducing an effective diffusion process of the NR extends the signaling gradient length scale. Assuming slow degradation of this receptor ($k^\mathrm{b} \ll k_\mathrm{off}^\mathrm{b}$) and dividing both sides of (7.59) by ℓ, we can obtain a more transparent expression for the relative increase in gradient length scale:

$$\frac{\delta\ell}{\ell} = \frac{D_\mathrm{r}}{2D} \frac{k_\mathrm{on}^\mathrm{b} n_\mathrm{T}^\mathrm{b}}{h k_\mathrm{off}^\mathrm{b}} \ , \quad (7.60)$$

which has a similar form as Eq. (7.44). In this approximation, the relative increase in gradient length scale is therefore controlled by the ligand affinity to the NR, and the ratio of NR and ligand diffusion coefficients.

We now ask whether this extension is sufficient to counter-balance the effect of the increased degradation brought by the presence of the second receptor, thus allowing for a longer gradient compared to the limiting case where the NR is absent, $j_\mathrm{r}^\mathrm{b} = 0$. For

$D_\mathrm{r} \to \infty$, the larger length scale solution of Eq. (7.58) diverges and is

$$\tilde{\ell} = \sqrt{\frac{D_\mathrm{r}}{k^\mathrm{b} + k^\mathrm{b}_\mathrm{off}}} \sqrt{\frac{\frac{k^\mathrm{a}_\mathrm{on} j^\mathrm{a}_\mathrm{r}}{h(k^\mathrm{a}+k^\mathrm{a}_\mathrm{off})} + \frac{k^\mathrm{b}_\mathrm{on} j^\mathrm{b}_\mathrm{r}}{h k^\mathrm{b}} + \kappa}{k^\mathrm{ab}_\mathrm{r} + \kappa}} \,, \tag{7.61}$$

so that for large enough D_r, gradient expansion is always possible. We then ask for the threshold value of D_r where $\tilde{\ell} = \tilde{\ell}_0 = \lim_{j^\mathrm{b}_\mathrm{r} \to 0} \tilde{\ell} = \sqrt{D/(k^\mathrm{a}_\mathrm{r} + \kappa)}$ with $k^\mathrm{a}_\mathrm{r} = k^\mathrm{a}_\mathrm{on} j^\mathrm{a}_\mathrm{r}/(h(k^\mathrm{a} + k^\mathrm{a}_\mathrm{off}))$. Using Eq. (7.58), we find that $\tilde{\ell} > \tilde{\ell}_0$ for

$$D_\mathrm{r} > D^*_\mathrm{r} = \frac{k^\mathrm{b} D}{k^\mathrm{a}_\mathrm{r} + \kappa} \,. \tag{7.62}$$

We find therefore that the threshold for extension is set by a competition between the additional degradation introduced by the NR and the expansion allowed by its diffusion. The full dependence of $\tilde{\ell}/\tilde{\ell}_0$ on D_r for the set of parameters stated in Table 7.1 can be found by solving Eq. (7.58) numerically and is shown in Fig. 7.7D (blue curve). Steady-state gradients in the different conditions of interest are also shown in Fig. 7.7A, where we have taken $D_\mathrm{r} = 0.1 \mu m^2/\mathrm{s}$ to capture a combination of lateral diffusion in the cell membrane and intercellular hopping (simulation parameters will be discussed more extensively in the next subsection).

7.2.2 Two-receptor model with GFP dimers

In this subsection we outline the numerical implementation of the two-receptor model with GFP dimers that is used to investigate the role of SR and NR coexpression in rescuing near-wild-type patterning [273] (see schematics in Fig. 7.7B). The corresponding plots of the steady-state signalling gradient are presented in Fig. 7.7C and 7.8A. These numerical simulations allow us to explore the dynamics underlying the simplified models presented above, beyond the far-from-receptor-saturation regime. Additionally, they account for the dimeric nature of the artificial ligand by allowing for single as well as double binding to receptors. This last feature allows in principle for the formation of mixed SR-NR bound configurations, a process that we will refer to as handover. We will discuss the effect of handover later in this section. The effect of increased ligand size on its diffusion constant, formalised in the Stokes-Einstein relation, is accounted for by approximating the GFP dimer as a sphere with twice the volume of a GFP

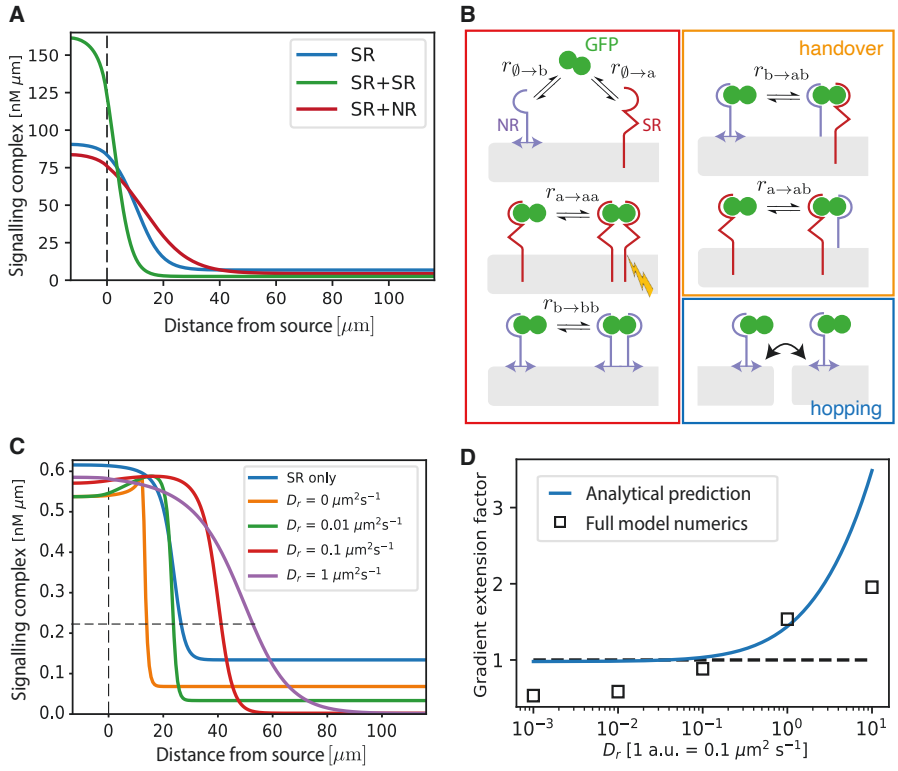

Figure 7.7: Role of hopping and handover of the non-signaling receptor: simulations. (A) Signaling activity profile predicted by the simplified GFP monomer model of Fig. 7.6(d) in the three experimental conditions of interest, namely SR (blue), SR+SR (green), SR+NR (red). These gradients are qualitatively similar to those of the dimer model, shown in Fig. 7.8A. (B) Schematic of the reactions involved in the two-receptor model with GFP dimers. The arrows indicate reversible transitions and have been labelled according to the notation introduced in the text. The colored boxes contain subgraphs corresponding to the different mechanisms at play in the model, namely single and double binding to receptors (red), handover (orange), hopping (blue). (C) Concentration gradient of signaling complex obtained from the two-receptor model with GFP dimer shown in (B), for different choices of effective NR diffusion coefficient K0. Introducing a non-diffusing NR (orange curve) shortens the gradient compared to the case with SR only (blue curve). In line with our analytical calculations, the gradient length scale is however observed to increase with increasing NR diffusion constant D_r. The dotted line indicates 1/e of the maximal value of the SR only profile, used to determine gradient extension factors in panel (D). Other parameters are as described in the text. (D) Blue line: Gradient extension factor as a function of the effective NR diffusion coefficient D_r (other parameters are as described in the text), in the simplified model with two receptors (Fig. 7.6(d)), in the regime far from receptor saturation. The gradient extension factor is defined as the ratio of the longer gradient length scale for a given value of D_r and for $D_r = 0$, with other parameters kept the same. The dashed line indicates no extension of the gradients, and its intersection with the blue line sets the threshold diffusion coefficient D_r^* for gradient extension. Square marks: gradient extension factor obtained with characteristic length scales extracted from the curves in Panel (C), plotted for comparison with the result of the simplified model.

Parameter	Name	Value	Unit	
GFP dimer diffusion constant	D	$21 \times 2^{-\frac{1}{3}}$	$\mu\text{m}^2\text{s}^{-1}$	estimated from D in Table 7.1
Effective NR diffusion constant	D_r	0.1	$\mu\text{m}^2\text{s}^{-1}$	[180, 262]
Degradation rate signaling configuration	k^{aa}	2.1×10^{-3}	s^{-1}	[168]
Degradation rate non-signaling configurations	$k^{\text{a}}, k^{\text{b}}, k^{\text{bb}}, k^{\text{ab}}$	2.7×10^{-5}	s^{-1}	as in Table 7.1
SR production rate	j_r^{a}	2.7×10^{-3}	$\text{nM}.\mu\text{m}.\text{s}^{-1}$	as in Table 7.1
NR production rate	j_r^{b}	2.7×10^{-3}	$\text{nM}.\mu\text{m}.\text{s}^{-1}$	as in Table 7.1

Table 7.2: Parameter table for numerical simulations of the two-receptor models. Unlisted parameters are as in Table 7.1 or given in the text.

monomer (Table 7.2). Since the NR are GPI-anchored in the experimental set up, we explore a possible role for NR hopping and it is therefore included in the model through an effective diffusion term for the membrane NRs. We further assume that leakage of intercellular receptors can be neglected and take the limit $\kappa_\text{r} \to 0$. Finally, although in experiments there are two distinct SR types, for simplicity here we consider a single type of SR which can form dimers when bound to a ligand.

We will maintain the previously introduced notation n_b, n_u to indicate the concentrations of membrane-bound receptor complexes, with superscripts specifying the composition (b = NR, bb = NR-NR, a = SR, aa = SR-SR, ab = SR-NR). As in other sections, the extracellular concentration of GFP is denoted c, the hemolymph GFP concentration c_H. All concentrations equations are solved numerically imposing no flux boundary conditions at $x = -L_\text{S}/2$ (centre of source, a condition arising from an assumed symmetry between each side of the source, in this section) and $x = L$ (end of AP compartment). In our simulations $x = 0$ corresponds to the posterior boundary of the source. The concentration equations for the diffusible species read:

$$\partial_t c = D\partial_x^2 c + j_\text{S}(x) - \frac{1}{h}\left(r_{\emptyset\to\text{a}} + r_{\emptyset\to\text{b}}\right) - \kappa(c - c_\text{H}) \ , \tag{7.63}$$

$$\frac{dc_\text{H}}{dt} = \frac{\phi w}{V_\text{H}} \int_{-L}^{L} H\kappa(c - c_\text{H})dx - k_\text{H} c_\text{H} \ . \tag{7.64}$$

These equations describe ligand diffusion in the tissue and leakage into/out of the hemolymph. The position dependent ligand production term $j_\text{S}(x)$ describes uniform production in the source with rate j and vanishes for $x > 0$ and $x < -L_\text{S}$. The

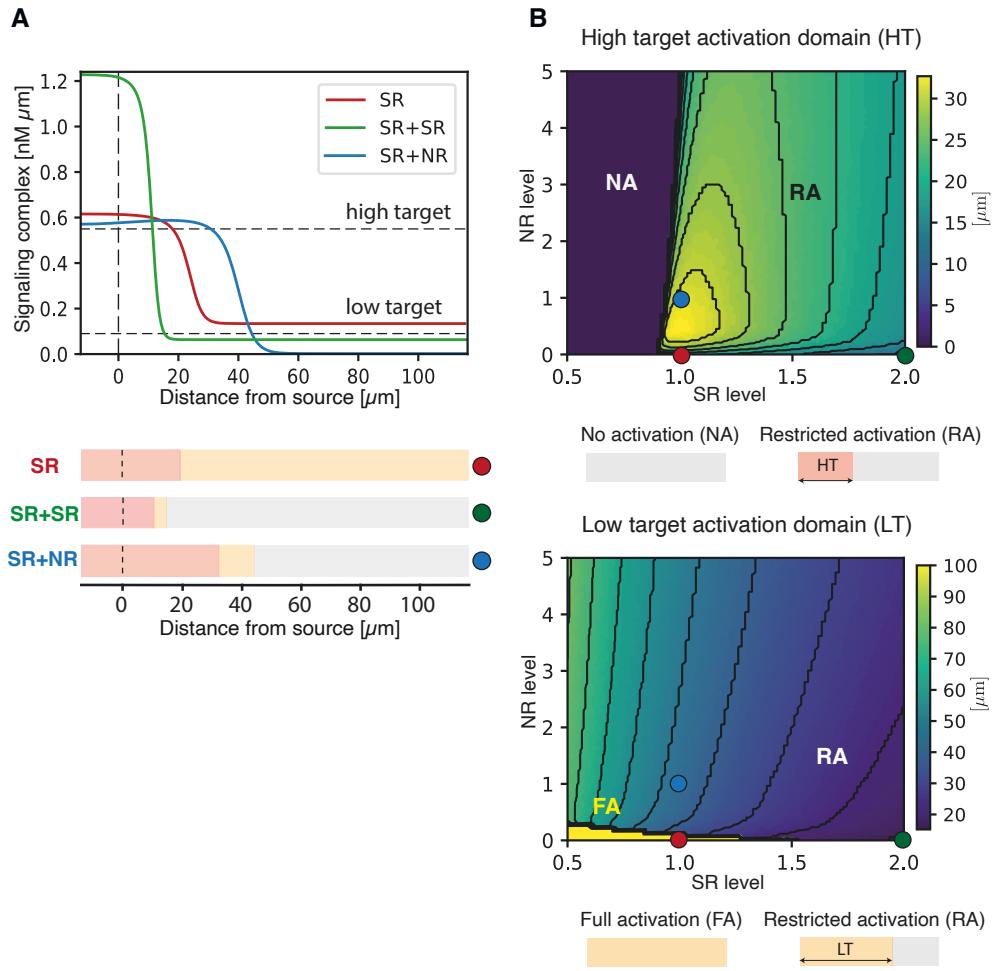

Figure 7.8: Modeling the effect of GPI-anchored nonsignaling receptors on a gradient length scale. (A) Predicted profiles of signaling complexes in three conditions: a reference case with signaling receptors only (SR; red), doubling SR levels (SR + SR; green), and adding nonsignaling receptors (SR + NR; blue). As observed experimentally, doubling SR leads to a steeper gradient, whereas adding NR reduces backflow-induced (GFP^{hemo}) signaling and extends the gradient, due to nonsignaling receptor effective diffusion. For illustration, arbitrary thresholds were chosen to indicate the position where high- and low-level target genes would be activated (tables 7.1 and 7.2 report the parameter values). (B) Width of the high (top) and low (bottom) target activation domains [arbitrary threshold shown in (A)], as a function of normalized levels of SR and NR. Warmer colors indicate a wider target activation domain. Colored dots show parameter combinations used in (B). (Top) For the normalized SR value of 1, increasing NR initially lengthens the high target domain, while a further increase shortens it by preventing access of GFP to SR. (Bottom) For the normalized SR value of 1 and in the absence of NR, GFP^{hemo} signaling dominates and low target gene is activated throughout (bright yellow region). Increasing SR or NR production both lead to a reduction in the low target domain size.

concentration equations for the membrane-bound receptor complexes under the effective diffusion approximation discussed in Section 7.2.1 read:

$$\partial_t n_{\mathrm{u}}^{\mathrm{a}} = -r_{\emptyset\to\mathrm{a}} - r_{\mathrm{a}\to\mathrm{aa}} - r_{\mathrm{b}\to\mathrm{ab}} - k^{\mathrm{a}} n_{\mathrm{u}}^{\mathrm{a}} + j_{\mathrm{r}}^{\mathrm{a}} \tag{7.65}$$

$$\partial_t n_{\mathrm{b}}^{\mathrm{a}} = r_{\emptyset\to\mathrm{a}} - r_{\mathrm{a}\to\mathrm{aa}} - r_{\mathrm{a}\to\mathrm{ab}} - k^{\mathrm{a}} n_{\mathrm{b}}^{\mathrm{a}} \tag{7.66}$$

$$\partial_t n_{\mathrm{b}}^{\mathrm{aa}} = r_{\mathrm{a}\to\mathrm{aa}} - k^{\mathrm{aa}} n_{\mathrm{b}}^{\mathrm{aa}} \tag{7.67}$$

$$\partial_t n_{\mathrm{u}}^{\mathrm{b}} = D_{\mathrm{r}} \partial_x^2 n_{\mathrm{u}}^{\mathrm{b}} - r_{\emptyset\to\mathrm{b}} - r_{\mathrm{b}\to\mathrm{bb}} - r_{\mathrm{a}\to\mathrm{ab}} - k^{\mathrm{b}} n_{\mathrm{u}}^{\mathrm{b}} + j_{\mathrm{r}}^{\mathrm{b}} \tag{7.68}$$

$$\partial_t n_{\mathrm{b}}^{\mathrm{b}} = D_{\mathrm{r}} \partial_x^2 n_{\mathrm{b}}^{\mathrm{b}} + r_{\emptyset\to\mathrm{b}} - r_{\mathrm{b}\to\mathrm{bb}} - r_{\mathrm{b}\to\mathrm{ab}} - k^{\mathrm{b}} n_{\mathrm{b}}^{\mathrm{b}} \tag{7.69}$$

$$\partial_t n_{\mathrm{b}}^{\mathrm{bb}} = D_{\mathrm{r}} \partial_x^2 n_{\mathrm{b}}^{\mathrm{bb}} + r_{\mathrm{b}\to\mathrm{bb}} - k^{\mathrm{bb}} n_{\mathrm{b}}^{\mathrm{bb}} \tag{7.70}$$

$$\partial_t n_{\mathrm{b}}^{\mathrm{ab}} = r_{\mathrm{a}\to\mathrm{ab}} + r_{\mathrm{b}\to\mathrm{ab}} - k^{\mathrm{ab}} n_{\mathrm{b}}^{\mathrm{ab}} \ , \tag{7.71}$$

where, for the sake of readability, we have defined the following reaction rates:

$$r_{\emptyset\to\mathrm{a}} = m k_{\mathrm{on}}^{\mathrm{a}} n_{\mathrm{u}}^{\mathrm{a}} c - k_{\mathrm{off}}^{\mathrm{a}} n_{\mathrm{b}}^{\mathrm{a}} \tag{7.72}$$

$$r_{\emptyset\to\mathrm{b}} = m k_{\mathrm{on}}^{\mathrm{b}} n_{\mathrm{u}}^{\mathrm{b}} c - k_{\mathrm{off}}^{\mathrm{b}} n_{\mathrm{b}}^{\mathrm{b}} \tag{7.73}$$

$$r_{\mathrm{a}\to\mathrm{aa}} = g k_{\mathrm{on}}^{\mathrm{a}} n_{\mathrm{b}}^{\mathrm{a}} n_{\mathrm{u}}^{\mathrm{a}} - k_{\mathrm{off}}^{\mathrm{a}} n_{\mathrm{b}}^{\mathrm{aa}} \tag{7.74}$$

$$r_{\mathrm{b}\to\mathrm{bb}} = g k_{\mathrm{on}}^{\mathrm{b}} n_{\mathrm{b}}^{\mathrm{b}} n_{\mathrm{u}}^{\mathrm{b}} - k_{\mathrm{off}}^{\mathrm{b}} n_{\mathrm{b}}^{\mathrm{bb}} \tag{7.75}$$

$$r_{\mathrm{a}\to\mathrm{ab}} = g k_{\mathrm{on}}^{\mathrm{b}} n_{\mathrm{b}}^{\mathrm{a}} n_{\mathrm{u}}^{\mathrm{b}} - k_{\mathrm{off}}^{\mathrm{b}} n_{\mathrm{b}}^{\mathrm{ab}} \tag{7.76}$$

$$r_{\mathrm{b}\to\mathrm{ab}} = g k_{\mathrm{on}}^{\mathrm{a}} n_{\mathrm{u}}^{\mathrm{a}} n_{\mathrm{b}}^{\mathrm{b}} - k_{\mathrm{off}}^{\mathrm{a}} n_{\mathrm{b}}^{\mathrm{ab}} \ . \tag{7.77}$$

These equations describe GFP (un)binding to receptors as well as receptor production, diffusion and degradation. Although the degradation rates are allowed to be different for different receptor complexes, we will henceforth assume that all non-signaling complexes undergo slow passive degradation with rate $k^{\mathrm{a}} = k^{\mathrm{b}} = k^{\mathrm{bb}} = k^{\mathrm{ab}} \sim 10^{-5} s^{-1}$ (Table 7.2). On the other hand, the SR-SR signaling complex is actively degraded at a rate $k^{\mathrm{aa}} \sim 10^{-3} s^{-1}$ (Table 7.2).

The geometric factor g introduced in Eqs. (7.74)-(7.77) has dimensions of inverse length and it accounts for the enhancement in binding rate due to proximity to the membrane when the GFP dimer is already bound to one receptor. We estimate g as the reciprocal of the typical receptor size ($L_{\mathrm{rec}} \sim 10$ nm [161, 157]) since this is the distance from the membrane within which single-bound GFP is found, whence $g = 100 \mu\mathrm{m}^{-1}$. We neglect further effects of multiple binding on receptor affinities (e.g. the possible stabilisation of

the first bond following a second binding). The factor $m = 2$ appearing in the definition of fluxes $r_{\emptyset\to a}$ and $r_{\emptyset\to b}$ accounts for the multiplicity of binding sites available for the first binding.

Parameters

Most of the parameters entering the two-receptor model are borrowed directly from the single receptor model outlined in section 7.1. In particular, all quantities related to the geometry of the system, as well as the (un)binding rate for the high- and low-affinity nanobodies and leakage rate carry through to this model. The ligand production rate j is controlled by the *patched* promoter in the experiments used to extract the parameters in Table 7.1 and by the *dpp* promoter in the rescue experiments. Since they have similar activities (13 vs 29 a.u [283, 124]), we keep the same parameter value. Similarly, the production rate of non-signaling receptors j_r^b, which controlled by the *dally* promoter in the rescue experiments (38 a.u. in the whole disc, which is roughly equal to that of *hh* [283, 124]) , is fixed to the value of j_r presented in Table 7.1. The signaling receptors are under the control of the *ubi* promoter. The significant difference of reported activities between the endogeneous *hh* and *ubi* promoter (16 a.u. and 359 a.u., respectively [283, 124]) might not apply to our situation because only part of the regulatory region of the *ubi* promoter was used to create the NR-expressing transgene, inserted at a random genomic location. We find that the qualitative features of the experimental gradients are well described by a value of j_r^a comparable to that in Table 7.1. Finally, we set the NR diffusion constant to reported values of diffusion constant of GPI on the membrane [283, 124] , assuming that NR hopping between cells is not limiting for NR diffusion at the surface of the tissue. In Fig. 7.7C, we show how the gradient properties change for different values of the effective receptor diffusion constant D_r, while in Fig. 7.8B we show the effect of modifying the levels of the two types of receptors on the position of hypothetical high and low target activation boundaries. The numerical values of the parameters discussed above are given in Table 7.2.

Effect of handover

Although handover seems to be a natural consequence of the dimeric nature of the artificial morphogen, we would like to disentangle its the effect on gradient formation from that of hopping, which occurs independently of the ligand. To assess the importance of handover we briefly consider a simplified two-receptor model involving a GFP monomer, rather than dimer (Figs. 7.6(d)). This corresponds to the model described in section 7.2.1, and also amounts to setting $g = 0$ and $m = 1$ in Eqs. (7.72)-(7.77). Since SR-SR complexes can no longer form in this model, we identify the single bound SR as the signaling configuration, and we therefore enhance its internalisation rate so that $k^{\mathrm{a}} = k^{\mathrm{aa}} \sim 10^{-3}s^{-1}$ to account for active degradation of the signaling complexes. Leaving all other parameters unchanged, this simplified model still displays a noticeable extension of the signaling gradient upon introduction of NR (Fig. 7.7A). This is in line with our analysis of two single receptors discussed in section 7.2.1. The main difference that is observed when comparing these gradients with those produced by the GFP dimer model concerns the behaviour close to the source. There signalling can be non-monotonous (Fig. 7.7C and 7.8A) and, as a result, the high target could be activated in a stripe located away from the source boundary. In such rare cases, in Fig. 7.8B the boundary position was defined as the distance between the end of the activation domain and the source. Because the monomer gradients do not exhibit the extended saturation region seen in the dimer case, we conclude that handover is not essential to extending the gradient length scale (which controls low-level targets), while it could play a role in setting the high-level target range.

8

Thermodynamics of Information Processing: a Case Study

L. Cocconi, G. Pruessner, G. Salbreux

Overview As we have seen in the previous Chapter, fundamental processes in organism development are often orchestrated through cell-cell signalling. In the case of morphogen gradients, positional information is encoded in the local concentration of a set of specialised proteins, which decreases away from a localised source region. The usefulness of this information for the robust and highly reproducible patterning of a developing tissue, i.e. the extent to which it allows individual cells to infer their relative position, depends fundamentally on how reliable cell machinery is in recording and processing information about the chemical environment [284, 11]. Unicellular organisms capable of performing chemotaxis, i.e. directed migration in response to spatial gradients of specific chemical species, are faced with very similar challenges [166], as are effectively all living systems when required to adapt to environments that are inhomogeneous, either spatially or temporally. Precision, however, comes at a cost and thermodynamic approaches have recently started to shed light on the constraints imposed by the energetics of information processing [34, 301]. In this short Chapter, we

augment the familiar run-and-tumble process in one dimension (introduced in Chapter 1) in a minimal way to allow for binary measurement of the particle's position with respect to a target, upon which the active force is adjusted as to typically propel the particle towards the target. We then apply the methods of Chapter 1 to compute the entropy production and discuss its relation with the variance of the particle position, which measures the localisation of the particle around its target. As expected, we identify a trade-off between precision and dissipation, originating from the constraint that the two cannot be minimised independently.

Author contributions: LC performed the mathematical analysis and wrote the code used to study the model numerically. GP and GS supervised the project.

Abstract

The field of active matter has historically focused on the collective behaviour of self-propelling (motile active) particles in the overdamped regime, whose local dissipation is dominated by viscous contributions. More recently, information processing at the single agent level has been recognised as an important driver of non-equilibrium dynamics. The task of extending the theoretical tool-kit of active matter beyond the paradigm of unbiased active motility, however, is complicated by the non-reciprocal nature of measurement-mediated interactions, as well as by the non-trivial thermodynamic impact of information processing. To explore these issues further, we introduce a minimal model of "adaptive active matter", a proposed new class of models which interpolate between standard active matter models (here, the run-and-tumble particle) and measurement-driven models as a function of the measurement error rate.

8.1 Introduction.

One important open problem in the field of active matter is that of characterising the out-of-equilibrium behaviour of active systems capable of recording and processing information about their environment at the single agent level. The deep relationship between thermodynamics and information theory [301, 213], which has its roots in Maxwell's demon and the Bennet-Landauer bound [176], offers a fascinating perspective on biological active matter, as being able to respond to a changing environment is often chosen as

a criterion to define living systems. New techniques need to be developed to efficiently capture the "adaptive" interactions between information processing units, one common feature of which is non-reciprocity [181], in the sense that unlike potential-type forces they do not respect Newton's third law of action and reaction. Interestingly, information theory also offers a systematic way of distinguishing redundant and synergistic contributions to the correlation structure of multivariate stochastic processes [240], a type of analysis that might elucidate different modes of collective behaviour in adaptive active matter.

Since cyclical information processing is an intrinsically out-of-equilibrium process and thus requires a finite amount of energy to be carried out reliably, it is easy to imagine that living systems might under particular circumstances be faced with the multi-objective optimisation problem of reducing the energetic expenditure as much as possible while maximising some biologically-relevant objective function.

8.2 The Adaptive Run-and-Tumble Model

A simple but illustrative example of how such a trade-off can be explored through the combined tools of stochastic thermodynamics and statistical mechanics is a generalisation of one-dimensional Run-and-Tumble (RnT) motion which we will refer to here as the Adaptive Run-and-Tumble model (ARnT). In the ARnT, the position $x \in \mathbb{R}$ of the self-propelled particle evolves according to the Langevin equation

$$\dot{x}(t) = \nu(t) + \sqrt{2D}\eta(t) \tag{8.1}$$

with $\eta(t)$ a zero-mean additive noise of unit covariance. Similarly to a standard RnT process, the self-propulsion velocity $\nu(t) \in \{\nu_L, \nu_R\}$ switches between the two allowed values in the manner of a Markov jump process, sometimes referred to a dichotomous noise or telegraph process [291]. However, in this particular case, the transition rates are made position-dependent in order to capture the ability of the particle to measure its position relative to a target (here $x = 0$ without loss of generality) and adapt its

self-propulsion direction accordingly. In particular, we set the transition probabilities

$$\begin{aligned} P(\nu(t+\Delta t)=\nu_L|\nu(t)=\nu_R,x(t)=x') &= \Delta t\ \tau[(1-\epsilon)\theta(x')+\epsilon(1-\theta(x'))]+\mathcal{O}(\Delta t^2) \\ P(\nu(t+\Delta t)=\nu_R|\nu(t)=\nu_L,x(t)=x') &= \Delta t\ \tau[\epsilon\theta(x')+(1-\epsilon)(1-\theta(x'))]+\mathcal{O}(\Delta t^2) \end{aligned} \tag{8.2}$$

with $\theta(x)$ the Heaviside step function and $\epsilon \in [0, \frac{1}{2}]$ the error rate. In other words, the particle measures the sign of its position relative to the target position $x = 0$ and, with a Poisson rate τ, adjusts its self-propulsion direction based on the outcome of the measurement, so as to typically be self-propelling towards its target. In the limiting case $\epsilon = \frac{1}{2}$, the binary measurement conveys no information about the environment and the model reduces to the standard RnT process on the real line, as introduced in Chapter 1. Assuming $\nu_R = -\nu_L = \nu$ for the sake of simplicity, this model can be solved analytically starting from the set of coupled Fokker-Planck equations for the joint probability densities $P_L(x)$ and $P_R(x)$ of the particle being at position x while in the left or right self-propelling mode,

$$(\nu\partial_x + D\partial_x^2)P_L(x) = (\bar{\tau}-\tau(x))P_L(x) - (\bar{\tau}+\tau(x))P_R(x) \tag{8.3}$$

$$(-\nu\partial_x + D\partial_x^2)P_R(x) = (\bar{\tau}+\tau(x))P_R(x) - (\bar{\tau}-\tau(x))P_L(x) \tag{8.4}$$

with $\bar{\tau} = \tau/2$ and

$$\tau(x) = \tau\left(\frac{1}{2}-\epsilon\right)[\theta(x)-(1-\theta(x))] = \tau\left(\frac{1}{2}-\epsilon\right)[2\theta(x)-1]\ . \tag{8.5}$$

First, we perform a change of variable by introducing polarity and density fields as $\psi(x)$ and $\phi(x)$ respectively,

$$\psi(x) = \frac{1}{2}(P_L(x)-P_R(x)) \tag{8.6}$$

$$\phi(x) = \frac{1}{2}(P_L(x)+P_R(x))\ . \tag{8.7}$$

Adding Eq. (8.3) to (8.4) we thus obtain

$$\nu\psi(x) = -D\partial_x\phi(x)\ , \tag{8.8}$$

which can be read as a statement of probability current balance at steady state. Notice that, for $D = 0$, Eq. (8.8) imposes $\psi(x) = 0$, which in turn implies $P_R(x) = P_L(x)$. This may be counter-intuitive in this setup but it is a necessary consequence of currents only being induced by the drift component of the motion in this limit. Subtracting Eq. (8.3) from (8.4) and using (8.8) we then obtain a third order ODE for $\phi(x)$ only,

$$-\frac{D^2}{\nu}\partial_x^3\phi(x) + \left(\nu + \frac{D\tau}{\nu}\right)\partial_x\phi(x) + \tau(1-2\epsilon)\phi(x) = 0 \ . \tag{8.9}$$

For $D = 0$, Eq. (8.9) simplifies dramatically and find by inspection that the density has a simple exponential form,

$$\phi(x) = P_R(x) = P_L(x) = \frac{\tau(1-2\epsilon)}{8\nu}\exp\left(-\frac{\tau(1-2\epsilon)}{2\nu}|x|\right) \ . \tag{8.10}$$

For the more general case of $D > 0$ we make a double exponential ansatz for the steady-state density $\phi(x)$, eventually finding

$$\phi(x) = a_1 e^{-\alpha_1|x|} + a_2 e^{-\alpha_2|x|} \tag{8.11}$$

$$\psi(x) = \frac{\nu\ \mathrm{Sgn}(x)}{D}(a_1\alpha_1 e^{-\alpha_1|x|} + a_2\alpha_2 e^{-\alpha_2|x|}) \tag{8.12}$$

where $\mathrm{Sgn}(x)$ is the sign function and the constants of integration

$$a_1 = \frac{-\alpha_1\alpha_2^2}{4(\alpha_1^2 - \alpha_2^2)}, \qquad a_2 = \frac{\alpha_1^2\alpha_2}{4(\alpha_1^2 - \alpha_2^2)} \tag{8.13}$$

have been fixed by normalisation ($\int dx\ \phi(x) = 1/2$) and continuity of the total probability density at $x = 0$ ($\psi(0) = 0$). The coefficients $\alpha_{1,2}$ appearing in the above are the two positive roots of the characteristic depressed cubic equation

$$\frac{D^2}{\nu}\alpha^3 - \left(\nu + \frac{D\tau}{\nu}\right)\alpha + \tau(1-2\epsilon) = 0 \ . \tag{8.14}$$

See Fig. 8.1 for an example of the typical steady-state probabilities. With the analytical solution at hand we can compute a number of interesting observables but here we will focus on only two, namely the steady-state entropy production $\dot{S}_i$ and the variance σ_x^2

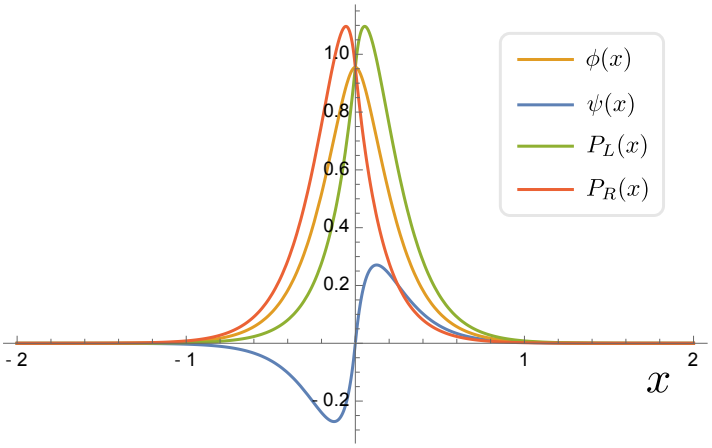

Figure 8.1: Steady-state probability density functions for the ARnT model with $D = 0.01$, $\nu = 0.1$, $\epsilon = 0$ and $\tau = 1$ as given in Eqs. (8.11) and (8.12).

of the resulting steady-state positional probability density function. These are given by

$$\sigma_x^2 = \int_{-\infty}^{\infty} dx\; x^2 (P_R(x) + P_L(x)) = \frac{\alpha_1^2 + \alpha_2^2}{\alpha_1^2 \alpha_2^2} = \frac{1}{\alpha_1^2} + \frac{1}{\alpha_2^2} \tag{8.15}$$

and, using the techniques of Chapter 1,

$$\dot{S}_i = \frac{\nu^2}{D} + \frac{\tau}{4} \left(\log \frac{1-\epsilon}{\epsilon} \right) \left((1 - 2\epsilon) + \frac{D}{\nu} \frac{\alpha_1 \alpha_2}{\alpha_1 + \alpha_2} \right) . \tag{8.16}$$

Interestingly, we find that the entropy production is made up of two non-negative contributions, the first of which is equal to the entropy production of a traditional RnT particle (see Chapter 1), while the second accounts for the thermodynamic cost of information processing. In particular, the second contribution vanishes at $\epsilon = 1/2$ and diverges logarithmically as $\epsilon \to 0$, as expected due to the irreversibility of the measurement process in this limit. The dependence of σ_x^2 and $\dot{S}_i$ on the parameters of the model is explored in more detail in Fig. 8.2.

8.3 Precision-dissipation tradeoff

Assuming D and ϵ are not under the control of the particle and are thus fixed, what choice for the pair (ν, τ) should the particle make in order to simultaneously minimise the typical distance from the target and the dissipation? Since the two cannot be

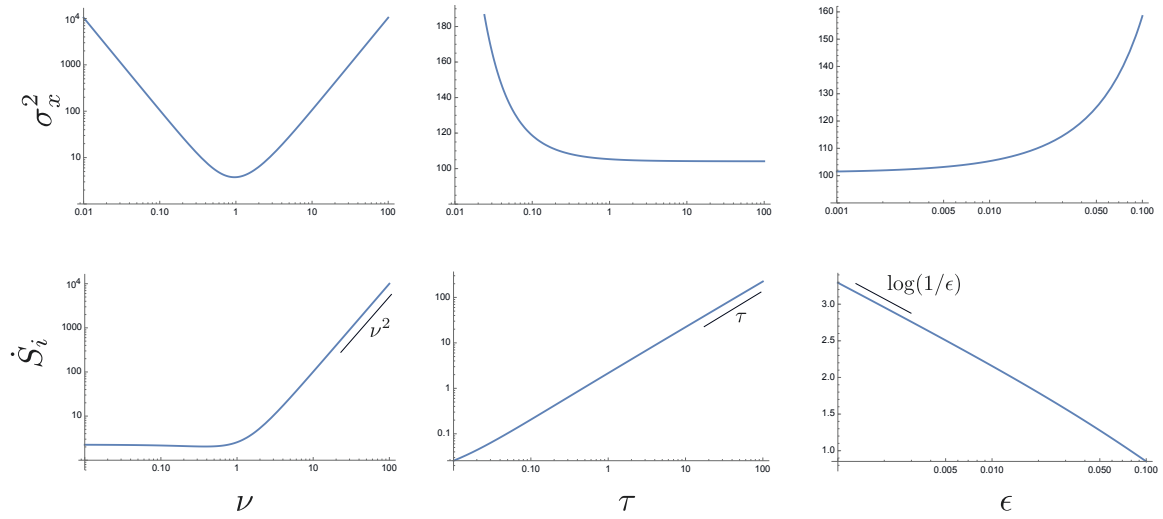

Figure 8.2: Parameter dependence of the variance (σ_x^2) and entropy production ($\dot{S}_i$) of the non-equilibrium steady state of the ARnT model, as given in Eq. (8.15) and (8.16). It is interesting to observe that σ_x^2 is a non-monotonic function of the self-propulsion velocity ν, suggesting a non-trivial connection between precision and the degree of activity. Similarly, increasing the measurement rate τ eventually leads to the asymptotic convergence of σ_x^2 to a finite value, while $\dot{S}_i$ diverges linearly, pointing to the fact that an increase in measurement frequency is not sufficient to achieve arbitrary precision. When not otherwise specified, $D = 0.01$, $\nu = 0.1$, $\epsilon = 0$, $\tau = 1$.

minimised independently, the solution is not unique. However, Pareto optimal solutions can be identified by scanning the accessible parameter space for those combinations for which the dissipation cannot be decreased without also increasing the variance, and vice versa. This family of solutions is known as the Pareto frontier [207] and is visualised for the ARnT model in Fig. 8.3.

8.4 Conclusion

The ARnT model is just one example of what we may refer to as adaptive active matter, a class of models that promises to push our understanding of non-equilibrium dynamics beyond the paradigm of unbiased self-propulsion. In fact, a number of well-known active matter models (RnT, Active Brownian Particles, Active Ornstein-Uhlenbeck Particles etc) whose self-propulsion velocity evolves stochastically but independently of the particle position, can be thought of as the limit of maximum measurement error rate of an associated adaptive model ($\epsilon = 1/2$ for binary self-propulsion states). While this

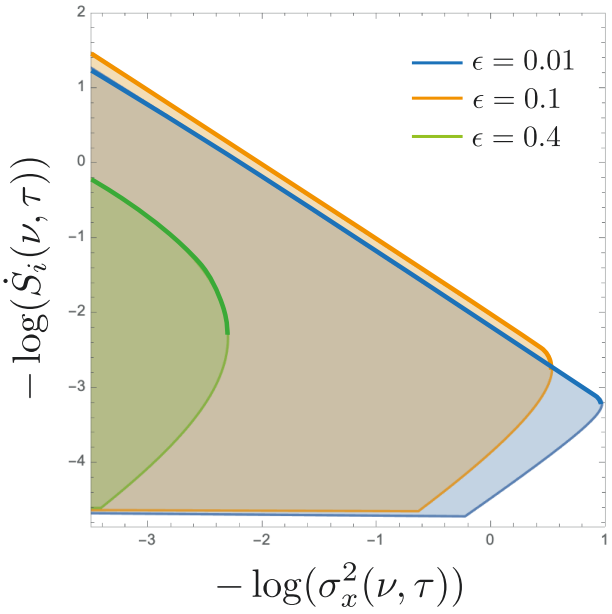

Figure 8.3: Numerically determined Pareto frontiers, thick lines, for the ARnT model at fixed diffusivity $D = 1$ and error rate $\epsilon \in \{0.01, 0.1, 0.4\}$. The shaded regions correspond to the accessible parameter space covered by physical choices of the self-propulsion speed $\nu > 0$ and measurement rate $\tau > 0$. Interestingly, it appears that the accessible values of $\dot{S}_i$ and σ_x^2 for the smallest error rate considered, $\epsilon = 0.01$, are not a superset of those of the intermediate error rate $\epsilon = 0.1$, suggesting that a higher error rate might be preferable when minimising dissipation is more important than minimising the spread of the distribution.

might often be a relevant limit in the case of synthetic self-propelled particles (see however [203]), adaptation and information processing are key features of real biological systems, from single cells to whole populations. The work presented in this chapter illustrates a promising route to further investigating the physical principles underlying their implementation.

ACKNOWLEDGMENTS

LC thanks Letian Chen for useful discussion.

Discussion and outlook

This thesis covers a fairly broad range of topics at the interface between mathematical physics and biology, one of the key conceptual threads being the development of theoretical tools for the quantification of the capabilities and limitations of active matter, as opposed to its passive counterpart. The assumption of thermodynamic equilibrium, which is crucially at the basis of much of our physical understanding of passive materials (think of the success of statistical mechanics in describing the properties of systems undergoing continuous phase transitions [135]) is broken by definition in living systems. This fact makes it necessary to develop new frameworks for their study, in what is a vast and interdisciplinary research program that continues to attract widespread interest. On the theoretical side, two complementary such frameworks are non-equilibrium statistical mechanics and stochastic thermodynamics, which are combined here to explore both the dynamics and energetics of microscopic systems subject to non-negligible noise. In particular, field theoretic approaches turn out to be particularly suited to this kind of analysis, thanks to their flexibility and applicability to both microscopic and effective models. Path integrals are also the natural framework for the study of thermodynamic quantities defined along single fluctuating trajectories [254]. While technically challenging, analytical approaches offer a more complete understanding of the model at hand, as they are generally not restricted to specific choices of parameters. On the experimental side, novel techniques are being developed to resolve the subcellular details of energy management and transduction in specific processes [306] and to explore the microscopic origins of seemingly generic metabolic principles, such as Kleiber's law [282].

In this thesis, after reviewing the basic tool kit of stochastic thermodynamics, we have compiled a catalogue of exact results for the entropy production of prototypical non-equilibrium processes characterised by both discrete and continuous state-spaces (Chapter 1). We have then applied the same methods to study the rate of heat dissipation for a Brownian particle trapped in a fluctuating potential, a model of direct relevance

in a number of contexts, from realistic implementations of stochastic resetting to the experimental manipulation of colloidal particles by means of optical tweezers (Chapter 2). In Chapters 3 and 4, we then turned our attention to two controversies arising from the thermodynamic characterisation of increasingly complex systems by means of effective mesoscopic theories, namely the effect of coarse graining on the inferred dissipation and the formalisation of 'single particle entity' in dynamical field theory. Having introduced the Coupon Collector and Cover Time problems, including a novel dynamically accelerated variant thereof, in Chapter 5, we proceed in Chapter 6 to demonstrate how path integral methods, specifically the Doi-Peliti formalism already introduced in the context of our study of single particle entity, offer a valid alternative to standard probabilistic approaches for the study of such non-equilibrium stochastic processes. Interestingly, the key features of these problems have to do with extreme events and are crucially related to the finiteness of the system size, in contrast to the more common focus of field-theoretic approaches on asymptotic behaviour in the infinite system-size limit. Chapter 7 offers an example of how mathematical modelling can shed light on a real-life non-equilibrium process of wide biological interest, namely morphogen transport *in vivo*. While the modelling is guided here by experiments in the specific context of the *Dpp* signalling network in the wing disc of *Drosophila Melanogaster*, the type of hindered diffusion that we study is believed to describe a number of other well known long-range morphogenetic signals (e.g. *Nodal-Lefty* in *Zebrafish* [162] and, potentially, the *Wnt* signalling network [197]). Finally, in Chapter 8, we discussed how the gap between analytically tractable and biologically relevant models could be bridged, at least in some regards, through the systematic study of information processing in "adaptive" active matter, focusing on a generalisation of the standard run-and-tumble process as a case study.

A question at the interface of bioenergetics and thermodynamics that has attracted growing attention in recent years is that of the extent to which energy can be efficiently harvested from microscopic active systems [77, 223, 281]. The qualifier 'microscopic' should be stressed here since, far from being a 21st century concept, the exploitation of non-human organisms' work (think horses and oxes) has been a staple of human technology and economy for millennia, at least up until the Industrial Revolution and the invention of the steam engine. Here, however, we are thinking of much smaller energy and length scales, such as those characterising collections of unicellular organ-

isms, which have only becomes accessible to direct physical manipulation over the last century. Technologies capable of harvesting energy from such microorganisms are of potential interest for at least two reasons: firstly, the nutrients required to sustain them might be easily available; secondly, such technologies could complement current ones in contexts where large scale energy production is infeasible, e.g. in microengineering designs for medical applications. Furthermore, rather than having to engineer efficient systems from scratch, "active matter engines" could allow us to leverage millions of years of evolution to efficiently convert chemical energy into a more directly usable form. Engines of this type, such as turbines driven by the persistent motion of bacteria in solution, already exist but are typically characterised by an extremely low efficiently due to the difficulty of rectifying the collective motion of swimmers with weak alignment interactions in the bulk [77]. One problem is thus how to improve the design of particular setups to achieve higher efficiency [314]. Other fundamental questions remain to be addressed, however, such as the intrinsic limits on energy extraction when inference of some hidden state is required [65]. Exploring these questions promises to cast light on stochastic thermodynamics more generally, for example by clarifying the extent to which entropy production represents an upper bound to the power extractable from an non-equilibrium process in cases where only coarse-grained observables are accessible.

In conclusion, the material presented in this thesis adds to the necessary groundwork for the refinement of our understanding of living matter at the microscopic scale and the establishment of the connection between fundamental physical concepts and observables of direct biological interest (e.g. time-reversal symmetry and energy expenditure). As it is often the case, the rapid development of new mathematical tools allows us to ask more detailed questions, which in turn highlight the limitations of our current mathematical tool-kit, in a virtuous cycle that makes the current state of this field extremely exciting.

Index

Bibliography

[1] J. B. G. Á. González and A. F. Pacheco. The occupation of a box as a toy model for the seismic cycle of a fault. *Am. J. Phys.* **73**:946, 2005. Cited on p. 219.

[2] D. Aldous. An introduction to covering problems for random walks on graphs. *J. Theor. Probab.* **2** (1):87, 1989. Cited on p. 219 and 225.

[3] D. Aldous. *Probability approximations via the Poisson clumping heuristic*. Springer-Verlag, New York, 1989. Cited on p. 219, 221, 225, and 236.

[4] D. Aldous and J. A. Fill. Reversible Markov Chains and Random Walks on Graphs. http://www.stat.berkeley.edu/users/aldous/RWG/book.html. In preparation. Cited on p. 225.

[5] D. J. Aldous. On the time taken by random walks on finite groups to visit every state. *Z. Wahrsch. Verw. Gebiete* **62** (3):361, 1983. Cited on p. 219 and 225.

[6] H. Alston, L. Cocconi, and T. Bertrand. Non-equilibrium thermodynamics of diffusion in fluctuating potentials. *Journal of Physics A: Mathematical and Theoretical* 2022. Cited on p. 32 and 87.

[7] H. Alston, A. O. Parry, R. Voituriez, and T. Bertrand. Intermittent attractive interactions lead to microphase separation in non-motile active matter. *arXiv:2201.04091* 2022. Cited on p. 90.

[8] C. P. Amann, T. Schmiedl, and U. Seifert. Communications: Can one identify nonequilibrium in a three-state system by analyzing two-state trajectories? *The Journal of Chemical Physics* **132** (4):041102, 2010. Cited on p. 127 and 128.

[9] D. Andrieux, P. Gaspard, S. Ciliberto, N. Garnier, S. Joubaud, and A. Petrosyan. Thermodynamic time asymmetry in non-equilibrium fluctuations. *J. Stat. Mech.: Theory Exp.* **2008** (01):01002, 2008. Cited on p. 73.

[10] T. Antal, M. Droz, G. Györgyi, and Z. Rácz. Roughness distributions for $1/f^{\alpha}$ signals. *Phys. Rev. E* **65**:046140, 2002. Cited on p. 220, 223, 224, 231, 236, and 237.

[11] Y. E. Antebi, J. M. Linton, H. Klumpe, B. Bintu, M. Gong, C. Su, R. McCardell, and M. B. Elowitz. Combinatorial signal perception in the bmp pathway. *Cell* **170** (6):1184, 2017. Cited on p. 297.

[12] N. V. Antonov, P. I. Kakin, and N. M. Lebedev. Static approach to renormalization group analysis of stochastic models with spatially quenched disorder. *Journal of Statistical Physics* **178** (2):392, 2020. ArXiv: 1905.04470. Cited on p. 136, 138, and 155.

[13] T. Ariga, K. Tateishi, M. Tomishige, and D. Mizuno. Noise-induced acceleration of single molecule kinesin-1. *Phys. Rev. Lett.* **127**:178101, 2021. Cited on p. 90.

[14] T. Ariga, M. Tomishige, and D. Mizuno. Nonequilibrium energetics of molecular motor kinesin. *Phys. Rev. Lett.* **121**:218101, 2018. Cited on p. 34 and 90.

[15] J. G. S. B. Ottino-Löffler and S. H. Strogatz. Takeover times for a simple model of network infection. *Phys. Rev. E* **96**:012313, 2017. Cited on p. 219.

[16] A. L. Barabasi and H. E. Stanley. *Fractal concepts in surface growth*. Cambridge University Press, 1995. Cited on p. 237.

[17] A. C. Barato, D. Hartich, and U. Seifert. Efficiency of cellular information processing. *New J. Phys.* **16** (10):103024, 2014. Cited on p. 33 and 41.

[18] A. C. Barato and U. Seifert. Thermodynamic uncertainty relation for biomolecular processes. *Physical review letters* **114** (15):158101, 2015. Cited on p. 34.

[19] A. C. Barato and U. Seifert. Cost and precision of brownian clocks. *Physical Review X* **6** (4):041053, 2016. Cited on p. 34.

[20] Y. Bashirzadeh and A. P. Liu. Encapsulation of the cytoskeleton: towards mimicking the mechanics of a cell. *Soft Matter* **15** (42):8425, 2019. Cited on p. 136.

[21] U. Basu, A. Kundu, and A. Pal. Symmetric exclusion process under stochastic resetting. *Phys. Rev. E* **100**:032136, 2019. Cited on p. 90.

[22] H. Bateman. *Higher transcendental functions [volumes i-iii]*, volume 1. McGraw-Hill Book Company, 1953. Cited on p. 162.

[23] C. Bechinger, R. Di Leonardo, H. Löwen, C. Reichhardt, G. Volpe, and G. Volpe. Active particles in complex and crowded environments. *Reviews of Modern Physics* **88** (4):045006, 2016. Publisher: American Physical Society. Cited on p. 34, 89, 119, and 136.

[24] D. Belius. Gumbel fluctuations for cover times in the discrete torus. *Probab. Theory Relat. Fields* **157** (3–4):635, 2013. Cited on p. 219, 225, 226, and 236.

[25] D. Belius and N. Kistler. The subleading order of two dimensional cover times. *Probab. Theory Relat. Fields* **167**:461, 2017. Cited on p. 225.

[26] E. A. Bender and S. G. Williamson. *Foundations of combinatorics with applications*. Courier Corporation, 2013. Cited on p. 248.

[27] O. Benichou, C. Loverdo, M. Moreau, and R. Voituriez. Intermittent search strategies. *Rev. Mod. Phys* **83**:81, 2011. Cited on p. 220.

[28] T. Bertrand, P. Illien, O. Bénichou, and R. Voituriez. Dynamics of run-and-tumble particles in dense single-file systems. *New Journal of Physics* **20** (11):113045, 2018. Cited on p. 119.

[29] T. Bertrand, Y. Zhao, O. Bénichou, J. Tailleur, and R. Voituriez. Optimized diffusion of run-and-tumble particles in crowded environments. *Phys. Rev. Lett.* **120**:198103, 2018. Cited on p. 119.

[30] P. Biane, J. Pitman, and M. Yor. Probability laws related to the jacobi theta and riemann zeta functions, and brownian excursions. *Bull. Amer. Math. Soc. (N.S.)* **38**:435, 2001. Cited on p. 223 and 227.

[31] J. J. Binney, N. J. Dowrick, A. J. Fisher, and M. E. J. Newman. *The Theory of Critical Phenomena*. Oxford University Press, Oxford, UK, 1998. Cited on p. 187 and 188.

[32] S. Bo and A. Celani. Entropy production in stochastic systems with fast and slow time-scales. *Journal of Statistical Physics* **154** (5):1325, 2014. Cited on p. 100 and 119.

[33] S. Bo and A. Celani. Multiple-scale stochastic processes: decimation, averaging and beyond. *Physics reports* **670**:1, 2017. Cited on p. 126 and 128.

[34] S. Bo, M. Del Giudice, and A. Celani. Thermodynamic limits to information harvesting by sensory systems. *Journal of Statistical Mechanics: Theory and Experiment* **2015** (1):P01014, 2015. Cited on p. 297.

[35] L. V. Bogachev. Random Walks in Random Environments. *Encyclopedia of Mathematical Physics* **4**:353–371, 2006. Cited on p. 130.

[36] T. Bollenbach, K. Kruse, P. Pantazis, M. González-Gaitán, and F. Jülicher. Morphogen transport in epithelia. *Physical Review E* **75** (1):011901, 2007. Cited on p. 286.

[37] D. Bonazzi, V. Lo Schiavo, S. Machata, I. Djafer-Cherif, P. Nivoit, V. Manriquez, H. Tanimoto, J. Husson, N. Henry, H. Chaté, R. Voituriez, and G. Duménil. Intermittent pili-mediated forces fluidize *neisseria meningitidis* aggregates promoting vascular colonization. *Cell* **174** (1):143, 2018. Cited on p. 90.

[38] L. L. Bonilla. Active ornstein-uhlenbeck particles. *Phys. Rev. E* **100**:022601, 2019. Cited on p. 119.

[39] I. Bordeu, S. Amarteifio, R. Garcia-Millan, B. Walter, N. Wei, and G. Pruessner. Volume explored by a branching random walk on general graphs. *Sci. Rep.* **9** (1):1, 2019. Cited on p. 85, 156, and 241.

[40] P. S. Bosch, R. Ziukaite, C. Alexandre, K. Basler, and J.-P. Vincent. Dpp controls growth and patterning in drosophila wing precursors through distinct modes of action. *Elife* **6**:e22546, 2017. Cited on p. 272.

[41] R. Botet and M. Płoszajczak. Exact Order-Parameter Distribution for Critical Mean-Field Percolation and Critical Aggregation. *Phys. Rev. Lett.* **95**:185702, 2005. Cited on p. 223.

[42] M. Bothe, L. Cocconi, Z. Zhen, and G. Pruessner. Particle entity in the doi-peliti and response field formalisms. *arXiv preprint arXiv:2205.10409* 2022. Cited on p. 32 and 167.

[43] M. Bothe and G. Pruessner. Doi-Peliti field theory of free active Ornstein-Uhlenbeck particles. *Physical Review E* **103** (6):062105, 2021. Cited on p. 90, 239, and 256.

[44] J.-P. Bouchaud and A. Georges. Anomalous diffusion in disordered media: Statistical mechanisms, models and physical applications. *Physics Reports* **195** (4-5):127, 1990. Cited on p. 130.

[45] A. C. Brańka and D. M. Heyes. Algorithms for brownian dynamics computer simulations: Multivariable case. *Phys. Rev. E* **60**:2381, 1999. Cited on p. 122.

[46] P. C. Bressloff. Modeling active cellular transport as a directed search process with stochastic resetting and delays. *Journal of Physics A: Mathematical and Theoretical* **53** (35):355001, 2020. Cited on p. 90.

[47] M. J. A. M. Brummelhuis and H. J. Hilhorst. Covering of a finite lattice by a random walk. *Physica A* **176**:387, 1991. Cited on p. 219.

[48] M. J. A. M. Brummelhuis and H. J. Hilhorst. How a random walk covers a finite lattice. *Physica A* **185**:35, 1992. Cited on p. 219 and 226.

[49] T. W. Burkhardt. Dynamics of absorption of a randomly accelerated particle. *Journal of Physics A: Mathematical and General* **33** (45):L429, 2000. Cited on p. 119.

[50] D. M. Busiello, D. Gupta, and A. Maritan. Entropy production in systems with unidirectional transitions. *Physical Review Research* **2** (2):023011, 2020. Cited on p. 90, 107, and 118.

[51] D. M. Busiello, J. Hidalgo, and A. Maritan. Entropy production for coarse-grained dynamics. *New Journal of Physics* **21** (7):073004, 2019. Cited on p. 169.

[52] C. J. Bustamante, Y. R. Chemla, S. Liu, and M. D. Wang. Optical tweezers in single-molecule biophysics. *Nature Reviews Methods Primers* **1**:1, 2021. Cited on p. 90 and 119.

[53] F. Caballero and M. E. Cates. Stealth entropy production in active field theories near ising critical points. *Physical Review Letters* **124** (24):240604, 2020. Cited on p. 35, 125, 127, and 128.

[54] Y. Cao, H. Wang, Q. Ouyang, and Y. Tu. The free-energy cost of accurate biochemical oscillations. *Nat. Phys.* **11** (9):772, 2015. Cited on p. 41.

[55] L. Caprini, U. M. B. Marconi, A. Puglisi, and A. Vulpiani. The entropy production of ornstein–uhlenbeck active particles: a path integral method for correlations. *Journal of Statistical Mechanics: Theory and Experiment* **2019** (5):053203, 2019. Cited on p. 119.

[56] J. Cardy. Reaction-diffusion processes. In *Non-equilibrium Statistical Mechanics and Turbulence* (edited by S. Nazarenko and O. V. Zaboronski), pp. 108–161. Cambridge University Press, Cambridge, UK, 2008. Cited on p. 169, 170, 171, 178, and 241.

[57] M. Castellana. Extreme-value distributions and the freezing transition of structural glasses. *Phys. Rev. Lett.* **112**:215701, 2014. Cited on p. 236.

[58] M. E. Cates and J. Tailleur. Motility-induced phase separation. *Annual Review of Condensed Matter Physics* **6** (1):219, 2015. https://doi.org/10.1146/annurev-conmatphys-031214-014710. Cited on p. 127.

[59] A. Celani, S. Bo, R. Eichhorn, and E. Aurell. Anomalous thermodynamics at the microscale. *Phys. Rev. Lett.* **109**:260603, 2012. Cited on p. 35, 88, 100, 119, and 127.

[60] Y. Chen, S. Guzik, J. P. Sumner, J. Moreland, and A. P. Koretsky. Magnetic manipulation of actin orientation, polymerization, and gliding on myosin using superparamagnetic iron oxide particles. *Nanotechnology* **22** (6):065101, 2011. Cited on p. 137.

[61] Z. Chen and Y. Zou. Anterior-posterior patterning of drosophila wing discs i: A baseline mathematical model. *Mathematical Biosciences* **314**:13, 2019. Cited on p. 261.

[62] O. Chepizhko and F. Peruani. Active particles in heterogeneous media display new physics. *The European Physical Journal Special Topics* **224** (7):1287, 2015. Cited on p. 127.

[63] M. Chupeau, O. Bénichou, and R. Voituriez. Cover times of random searches. *Nat. Phys.* **11**:844, 2015. Cited on p. 225 and 235.

[64] L. Cocconi, R. Garcia-Millan, Z. Zhen, B. Buturca, and G. Pruessner. Entropy Production in Exactly Solvable Systems. *Entropy* **22** (11):1252, 2020. Cited on p. 32, 39, 89, 95, 99, 118, 119, 127, 128, 169, and 214.

[65] L. Cocconi, J. Knight, and C. Roberts, 2022. In preparation. Cited on p. 307.

[66] L. Cocconi, G. Salbreux, and G. Pruessner. Scaling of entropy production under coarse graining in active disordered media. *Physical Review E* **105** (4):L042601, 2022. Cited on p. 32 and 125.

[67] A. Compte and J.-P. Bouchaud. Localisation in 1D random random walks. *Journal of Physics A: Mathematical and General* **31** (29):6113, 1998. Cited on p. 138.

[68] L. Comtet. *Advanced Combinatorics: The art of finite and infinite expansions*. Springer Science & Business Media, 2012. Cited on p. 190, 193, and 194.

[69] A.-S. Coquel, J.-P. Jacob, M. Primet, A. Demarez, M. Dimiccoli, T. Julou, L. Moisan, A. B. Lindner, and H. Berry. Localization of Protein Aggregation in Escherichia coli Is Governed by Diffusion and Nucleoid Macromolecular Crowding Effect. *PLOS Comput. Biol.* **9**:1, 2013. Cited on p. 220.

[70] D. Cox and V. Isham. *Point processes*. CRC Press, 1980. Cited on p. 222.

[71] F. Crick. Diffusion in embryogenesis. *Nature* **225** (5231):420, 1970. Cited on p. 260.

[72] L. F. Cugliandolo and V. Lecomte. Rules of calculus in the path integral representation of white noise langevin equations: the onsager–machlup approach. *Journal of Physics A: Mathematical and Theoretical* **50** (34):345001, 2017. Cited on p. 52 and 214.

[73] T. T. da Silva and M. D. Fragoso. Diffusion with stochastic resetting of interacting particles emerging from a model of population genetics. *Journal of Physics A: Mathematical and Theoretical* **55** (1):014003, 2021. Cited on p. 90.

[74] S. R. De Groot and P. Mazur. *Non-Equilibrium Thermodynamics*. Dover Publications, New York, 2003. Cited on p. 33, 39, and 137.

[75] D. S. Dean. Langevin equation for the density of a system of interacting langevin processes. *Journal of Physics A: Mathematical and General* **29** (24):L613, 1996. Cited on p. 169, 173, and 213.

[76] B. Derrida. Velocity and diffusion constant of a periodic one-dimensional hopping model. *Journal of Statistical Physics* **31** (3):433, 1983. Cited on p. 127, 130, 132, 137, and 149.

[77] R. Di Leonardo, L. Angelani, D. Dell'Arciprete, G. Ruocco, V. Iebba, S. Schippa, M. P. Conte, F. Mecarini, F. De Angelis, and E. Di Fabrizio. Bacterial ratchet motors. *Proceedings of the National Academy of Sciences* **107** (21):9541, 2010. Cited on p. 306 and 307.

[78] G. Diana and M. Esposito. Mutual entropy production in bipartite systems. *Journal of Statistical Mechanics: Theory and Experiment* **2014** (4):P04010, 2014. Cited on p. 44.

[79] J. Ding, J. R. Lee, and Y. Peres. Cover times, blanket times, and majorizing measures. *Ann. Math.* **175**:1409, 2012. Cited on p. 236.

[80] M. Doi. Second quantization representation for classical many-particle system. *J. Phys. A: Math. Gen.* **9** (9):1465, 1976. Cited on p. 85.

[81] C. D. Dominicis. Technics of field renormalization and dynamics of critical phenomena. In *J. Phys.(Paris), Colloq*, pp. C1–247. 1976. Cited on p. 169 and 198.

[82] S. Dorosz and M. Pleimling. Entropy production in the nonequilibrium steady states of interacting many-body systems. *Physical Review E* **83** (3):031107, 2011. Cited on p. 125, 127, and 128.

[83] A. Drewitz, B. Ráth, and A. Sapozhnikov. *An Introduction to Random Interlacements*. Springer Briefs in Mathematics, Springer, 2014. Cited on p. 219 and 226.

[84] A. A. Dubkov, P. N. Makhov, and B. Spagnolo. Nonequilibrium steady-state distributions in randomly switching potentials. *Physica A: Statistical Mechanics and its Applications* **325** (1):26, 2003. Cited on p. 98.

[85] J. O. Dubuis, G. Tkačik, E. F. Wieschaus, T. Gregor, and W. Bialek. Positional information, in bits. *Proceedings of the National Academy of Sciences* **110** (41):16301, 2013. Cited on p. 35 and 260.

[86] E. R. Dufresne, G. C. Spalding, M. T. Dearing, S. A. Sheets, and D. G. Grier. Computer-generated holographic optical tweezer arrays. *Review of Scientific Instruments* **72** (3):1810, 2001. Cited on p. 119.

[87] S. F. Edwards and D. R. Wilkinson. The surface statistics of a granular aggregate. *Philos. Trans. R. Soc. London, Ser. A* **381**:17, 1982. Cited on p. 223.

[88] D. A. Egolf. Equilibrium Regained: From Nonequilibrium Chaos to Statistical Mechanics. *Science* **287** (5450):101, 2000. Cited on p. 127.

[89] A. Einstein. On the movement of small particles suspended in a stationary liquid demanded by the molecular-kinetic theory of heat (english translation, 1956). *Investigations on the theory of the Brownian movement* 1905. Cited on p. 34 and 87.

[90] P. Erdős and A. Rényi. On a classical problem of probability theory. *Magyar. Tud Akad. Mat. Kutato Int. Közl* **6**:215, 1961. Cited on p. 219, 220, and 221.

[91] M. Esposito. Stochastic thermodynamics under coarse graining. *Physical Review E* **85** (4):041125, 2012. Cited on p. 35, 127, and 128.

[92] M. Esposito and C. Van den Broeck. Three faces of the second law. i. master equation formulation. *Phys. Rev. E* **82** (1):011143, 2010. Cited on p. 43, 53, and 59.

[93] M. R. Evans and S. N. Majumdar. Diffusion with optimal resetting. *Journal of Physics A: Mathematical and Theoretical* **44** (43):435001, 2011. Cited on p. 90.

[94] M. R. Evans and S. N. Majumdar. Diffusion with Stochastic Resetting. *Physical Review Letters* **106** (16):160601, 2011. Cited on p. 90.

[95] M. R. Evans and S. N. Majumdar. Effects of refractory period on stochastic resetting. *Journal of Physics A: Mathematical and Theoretical* **52** (1):01LT01, 2018. Cited on p. 107.

[96] M. R. Evans and S. N. Majumdar. Run and tumble particle under resetting: a renewal approach. *Journal of Physics A: Mathematical and Theoretical* **51** (47):475003, 2018. Cited on p. 90.

[97] M. R. Evans, S. N. Majumdar, and G. Schehr. Stochastic resetting and applications. *Journal of Physics A: Mathematical and Theoretical* **53** (19):193001, 2020. Cited on p. 90 and 118.

[98] É. Fodor, R. L. Jack, and M. E. Cates. Irreversibility and biased ensembles in active matter: Insights from stochastic thermodynamics. *arXiv preprint arXiv:2104.06634* 2021. Cited on p. 169 and 212.

[99] É. Fodor, C. Nardini, M. E. Cates, J. Tailleur, P. Visco, and F. van Wijland. How far from equilibrium is active matter? *Phys. Rev. Lett.* **117** (3):038103, 2016. Cited on p. 52.

[100] G. Foltin, K. Oerding, Z. Rácz, R. L. Workman, and R. K. P. Zia. Width distribution for random-walk interfaces. *Phys. Rev. E* **50**:R639, 1994. Cited on p. 223 and 227.

[101] F. Font-Clos and N. R. Moloney. Percolation on trees as a Brownian excursion: From Gaussian to Kolmogorov-Smirnov to exponential statistics. *Phys. Rev. E* **94**:030102(R), 2016. Cited on p. 223.

[102] D. Forster, D. R. Nelson, and M. J. Stephen. Large-distance and long-time properties of a randomly stirred fluid. *Physical Review A* **16** (2):732, 1977. Cited on p. 133 and 155.

[103] H. Freund and P. Grassberger. How uniformly a random walker covers a finite lattice. *Physica A* **192**:465, 1993. Cited on p. 219.

[104] P. C. Fridy, Y. Li, S. Keegan, M. K. Thompson, I. Nudelman, J. F. Scheid, M. Oeffinger, M. C. Nussenzweig, D. Fenyö, B. T. Chait, *et al.* A robust pipeline for rapid production of versatile nanobody repertoires. *Nature methods* **11** (12):1253, 2014. Cited on p. 273.

[105] J. Fuchs, S. Goldt, and U. Seifert. Stochastic thermodynamics of resetting. *EPL (Europhysics Letters)* **113** (6):60009, 2016. Cited on p. 90, 107, and 118.

[106] Y. V. Fyodorov and C. Nadal. Critical behavior of the number of minima of a random landscape at the glass transition point and the tracy-widom distribution. *Phys. Rev. Lett.* **109**:167203, 2012. Cited on p. 236.

[107] R. Garcia-Millan. The concealed voter model is in the voter model universality class. *J. Stat. Mech.* **2020** (5):053201, 2020. Cited on p. 85.

[108] R. Garcia-Millan, J. Pausch, B. Walter, and G. Pruessner. Field-theoretic approach to the universality of branching processes. *Phys. Rev. E* **98**:062107, 2018. Cited on p. 197, 248, and 250.

[109] R. Garcia-Millan and G. Pruessner. Run-and-tumble motion in a harmonic potential: field theory and entropy production. *Journal of Statistical Mechanics: Theory and Experiment* **2021** (6):063203, 2021. Cited on p. 85, 90, 99, 119, 169, 239, and 256.

[110] R. Garcia-Millan and G. Pruessner. Run-and-tumble motion in a harmonic potential: field theory and entropy production. *Journal of Statistical Mechanics: Theory and Experiment* **2021** (6):063203, 2021. Cited on p. 119.

[111] R. Garcia-Millan and G. Prussner, 2022. To be published. Cited on p. 35, 168, and 212.

[112] C. W. Gardiner. *Handbook of stochastic methods.* Springer, 1985. Cited on p. 89 and 93.

[113] P. Gaspard. Time-Reversed Dynamical Entropy and Irreversibility in Markovian Random Processes. *J. Stat. Phys.* **117** (3):599, 2004. Cited on p. 34, 40, 41, 42, 43, 44, 48, 53, 83, 89, 96, 107, 118, and 127.

[114] A. Gelimson and R. Golestanian. Collective dynamics of dividing chemotactic cells. *Phys. Rev. Lett.* **114**:028101, 2015. Cited on p. 169.

[115] A. Genthon, R. Garcia Garcia, and D. Lacoste. Branching processes with resetting as a model for cell division. *Journal of Physics A: Mathematical and Theoretical* 2022. Cited on p. 90.

[116] M. L. Glasser and I. J. Zucker. Extended watson integrals for the cubic lattices. *Proc. Natl. Acad. Sci. USA* **74**:1800, 1977. Cited on p. 226.

[117] B. Glise, D. L. Jones, and P. W. Ingham. Notch and wingless modulate the response of cells to hedgehog signalling in the drosophila wing. *Developmental biology* **248** (1):93, 2002. Cited on p. 280.

[118] M. Goldman. On the First Passage of the Integrated Wiener Process. *The Annals of Mathematical Statistics* **42** (6):2150 , 1971. Cited on p. 119.

[119] A. Gomez-Marin, J. M. R. Parrondo, and C. V. den Broeck. The "footprints" of irreversibility. *EPL (Europhysics Letters)* **82** (5):50002, 2008. Cited on p. 128.

[120] A. Gomez-Marin, J. M. R. Parrondo, and C. Van den Broeck. Lower bounds on dissipation upon coarse graining. *Physical Review E* **78** (1):011107, 2008. ArXiv: 0807.1027. Cited on p. 127.

[121] G. Gompper, R. G. Winkler, T. Speck, A. Solon, C. Nardini, F. Peruani, H. Löwen, R. Golestanian, U. B. Kaupp, L. Alvarez, *et al.* The 2020 motile active matter roadmap. *Journal of Physics: Condensed Matter* **32** (19):193001, 2020. Cited on p. 169.

[122] I. S. Gradshteyn and I. M. Ryzhik. *Table of integrals, series and products.* Academic Press, San Diego, CA, USA, 7th edition, 2007. Cited on p. 209.

[123] P. Grassberger. How fast does a random walk cover a torus? *Phys. Rev. E* **96**:012115, 2017. Cited on p. 225.

[124] B. R. Graveley, A. N. Brooks, J. W. Carlson, M. O. Duff, J. M. Landolin, L. Yang, C. G. Artieri, M. J. van Baren, N. Boley, B. W. Booth, *et al.* The developmental transcriptome of drosophila melanogaster. *Nature* **471** (7339):473, 2011. Cited on p. 295.

[125] D. G. Grier. Optical tweezers in colloid and interface science. *Current Opinion in Colloid & Interface Science* **2** (3):264, 1997. Cited on p. 88 and 119.

[126] D. Gupta. Stochastic resetting in underdamped brownian motion. *Journal of Statistical Mechanics: Theory and Experiment* **2019** (3):033212, 2019. Cited on p. 90.

[127] D. Gupta, C. A. Plata, A. Kundu, and A. Pal. Stochastic resetting with stochastic returns using external trap. *Journal of Physics A: Mathematical and Theoretical* **54** (2):025003, 2020. Cited on p. 90.

[128] D. Gupta, C. A. Plata, and A. Pal. Work Fluctuations and Jarzynski Equality in Stochastic Resetting. *Physical Review Letters* **124** (11):110608, 2020. Cited on p. 90.

[129] M. Hashemi Shabestari, A. Meijering, W. Roos, G. Wuite, and E. Peterman. Chapter four - recent advances in biological single-molecule applications of optical tweezers and fluorescence microscopy. In *Single-Molecule Enzymology: Nanomechanical Manipulation and Hybrid Methods* (edited by M. Spies and Y. R. Chemla), volume 582 of *Methods in Enzymology*, pp. 85–119. Academic Press, 2017. Cited on p. 90.

[130] R. Hatori, B. M. Wood, G. O. Barbosa, and T. B. Kornberg. Regulated delivery controls drosophila hedgehog, wingless, and decapentaplegic signaling. *Elife* **10**, 2021. Cited on p. 261.

[131] E. Helfand. Brownian dynamics study of transitions in a polymer chain of bistable oscillators. *The Journal of Chemical Physics* **69** (3):1010, 1978. Cited on p. 122.

[132] T. Herpich, T. Cossetto, G. Falasco, and M. Esposito. Stochastic thermodynamics of all-to-all interacting many-body systems. *New J. Phys.* **22** (6):063005, 2020. Cited on p. 61.

[133] J. A. Hertz, Y. Roudi, and P. Sollich. Path integral methods for the dynamics of stochastic and disordered systems. *Journal of Physics A: Mathematical and Theoretical* **50** (3):033001, 2016. Publisher: IOP Publishing. Cited on p. 127, 132, 138, 143, 144, 155, 169, and 173.

[134] M. Hidalgo-Soria and E. Barkai. Hitchhiker model for laplace diffusion processes. *Physical Review E* **102** (1):012109, 2020. Cited on p. 220.

[135] P. C. Hohenberg and B. I. Halperin. Theory of dynamic critical phenomena. *Rev. Mod. Phys.* **49**:435, 1977. Cited on p. 169 and 305.

[136] L. Holst. On Birthday, Collectors, Occupancy and Other Classical Urn Problems. *Int. Stat. Rev.* **54** (1):15, 1986. Cited on p. 217 and 219.

[137] L. Holst. Extreme Value Distributions for Coupon Collector and Birthday Problems . *Extremes* **4**:129, 2001. Cited on p. 219.

[138] R. L. Honeycutt. Stochastic runge-kutta algorithms. i. white noise. *Phys. Rev. A* **45**:600, 1992. Cited on p. 122.

[139] J. Honkonen. Ito and Stratonovich calculuses in stochastic field theory. *Invited talk presented at The 12th Small Triangle Meeting on Theoretical Physics* 2011. Cited on p. 155 and 174.

[140] J. E. Hooper. Smoothened translates hedgehog levels into distinct responses. *Development* 2003. Cited on p. 280.

[141] J. M. Horowitz and T. R. Gingrich. Thermodynamic uncertainty relations constrain non-equilibrium fluctuations. *Nat. Phys.* **16** (1):15, 2020. Cited on p. 41 and 89.

[142] W. Horsthemke and R. Lefever. *Noise-Induced Transitions - Theory and Applications in Physics, Chemistry, and Biology.* Springer-Verlag Berlin Heidelberg, 1984. Cited on p. 75.

[143] L. Hufnagel, J. Kreuger, S. M. Cohen, and B. I. Shraiman. On the role of glypicans in the process of morphogen gradient formation. *Developmental biology* **300** (2):512, 2006. Cited on p. 286.

[144] J. P. Imhof. On the range of Brownian motion and its inverse process. *Ann. Probab.* **13**:1011, 1985. Cited on p. 225.

[145] A. Iniesta and J. García de la Torre. A second-order algorithm for the simulation of the brownian dynamics of macromolecular models. *The Journal of Chemical Physics* **92** (3):2015, 1990. Cited on p. 122.

[146] H.-K. Janssen. On a lagrangean for classical field dynamics and renormalization group calculations of dynamical critical properties. *Zeitschrift für Physik B Condensed Matter* **23** (4):377, 1976. Cited on p. 169 and 198.

[147] C. Jarzynski. Equalities and Inequalities: Irreversibility and the Second Law of Thermodynamics at the Nanoscale. *Annual Review of Condensed Matter Physics* **2** (1):329, 2011. Cited on p. 89.

[148] M. J. Y. Jerez, M. A. Bonachita, and M. N. P. Confesor. Reversibility in nonequilibrium steady states as a measure of distance from equilibrium. *Physical Review E* **104** (4):044609, 2021. Cited on p. 90.

[149] D.-Q. Jiang, M. Qian, and M.-P. Qian. *Mathematical Theory of Nonequilibrium Steady States: On the Frontier of Probability and Dynamical Systems.* Lecture notes in Mathematics. Springer-Verlag, Berlin Heidelberg, 2004. Cited on p. 41.

[150] N. L. Johnson and S. Kotz. *Urn models and their application.* John Wiley & Sons, 1977. Cited on p. 219.

[151] L. P. Kadanoff. Scaling laws for ising models near T_c. *Physics Physique Fizika* **2**:263, 1966. Cited on p. 129.

[152] A. Kahana, G. Kenan, M. Feingold, M. Elbaum, and R. Granek. Active transport on disordered microtubule networks: The generalized random velocity model. *Physical Review E* **78** (5):051912, 2008. Cited on p. 127.

[153] S. Karthika and A. Nagar. Totally asymmetric simple exclusion process with resetting. *Journal of Physics A: Mathematical and Theoretical* **53** (11):115003, 2020. Cited on p. 90.

[154] A. Kicheva, P. Pantazis, T. Bollenbach, Y. Kalaidzidis, T. Bittig, F. Julicher, and M. González-Gaitán. Kinetics of morphogen gradient formation. *Science* **315** (5811):521, 2007. Cited on p. 276.

[155] J. Kim and S. Torquato. Effect of window shape on the detection of hyperuniformity via the local number variance. *Journal of Statistical Mechanics: Theory and Experiment* **2017** (1):013402, 2017. Cited on p. 163.

[156] S. Kim, M. Pochitaloff, G. A. Stooke-Vaughan, and O. Campàs. Embryonic tissues as active foams. *Nature Physics* **17** (7):859, 2021. Cited on p. 90.

[157] T. Kirsch, W. Sebald, and M. K. Dreyer. Crystal structure of the bmp-2–bria ectodomain complex. *Nature structural biology* **7** (6):492, 2000. Cited on p. 294.

[158] A. Kleidon. Life, hierarchy, and the thermodynamic machinery of planet earth. *Physics of life reviews* **7** (4):424, 2010. Cited on p. 33.

[159] A. N. Kolmogorov. Sulla determinazione empirica delle leggi di probabilita. *Giorn. Ist. Ital. Attuari* **4**:1, 1933. Cited on p. 223.

[160] A. Kopp and I. Duncan. Anteroposterior patterning in adult abdominal segments of drosophila. *Developmental biology* **242** (1):15, 2002. Cited on p. 280.

[161] M. H. Kubala, O. Kovtun, K. Alexandrov, and B. M. Collins. Structural and thermodynamic analysis of the gfp: Gfp-nanobody complex. *Protein Science* **19** (12):2389, 2010. Cited on p. 273 and 294.

[162] T. Kuhn, A. N. Landge, D. Moersdorf, J. Cossmann, J. Gerstenecker, P. Mueller, and J. C. M. Gebhardt. Single-molecule tracking of nodal and lefty in live zebrafish embryos supports hindered diffusion model. *bioRxiv* 2022. Cited on p. 262 and 306.

[163] S. Kullback and R. A. Leibler. On Information and Sufficiency. *The Annals of Mathematical Statistics* **22** (1):79, 1951. Cited on p. 44, 89, and 96.

[164] V. Kumar, O. Sadekar, and U. Basu. Active brownian motion in two dimensions under stochastic resetting. *Phys. Rev. E* **102**:052129, 2020. Cited on p. 90.

[165] L. Kusmierz, S. N. Majumdar, S. Sabhapandit, and G. Schehr. First order transition for the optimal search time of lévy flights with resetting. *Phys. Rev. Lett.* **113**:220602, 2014. Cited on p. 90.

[166] G. Lan, P. Sartori, S. Neumann, V. Sourjik, and Y. Tu. The energy–speed–accuracy trade-off in sensory adaptation. *Nature physics* **8** (5):422, 2012. Cited on p. 297.

[167] G. Lan and Y. Tu. Information processing in bacteria: memory, computation, and statistical physics: a key issues review. *Rep. Prog. Phys.* **79** (5):052601, 2016. Cited on p. 41.

[168] A. Lander, Q. Nie, B. Vargas, and F. Wan. Size-normalized robustness of dpp gradient in drosophila wing imaginal disc. *Journal of mechanics of materials and structures* **6** (1):321, 2011. Cited on p. 272 and 292.

[169] G. T. Landi, T. Tomé, and M. J. de Oliveira. Entropy production in linear Langevin systems. *J. Phys. A Math. Theor.* **46** (39):395001, 2013. Cited on p. 41.

[170] A. Lazarescu, T. Cossetto, G. Falasco, and M. Esposito. Large deviations and dynamical phase transitions in stochastic chemical networks. *The Journal of Chemical Physics* **151** (6):064117, 2019. Cited on p. 85.

[171] M. Le Bellac. *Quantum and Statistical Field Theory [Phenomenes critiques aux champs de jauge, English]*. Oxford University Press, New York, NY, USA, 1991. Translated by G. Barton. Cited on p. 169, 175, 187, 188, and 198.

[172] M. R. Leadbetter, G. Lindgren, and H. Rootzén. *Extremes and Related Properties of Random Sequences and Processes*. Springer-Verlag, New York, Heidelberg, Berlin, 1983. Cited on p. 222.

[173] J. L. Lebowitz and H. Spohn. A Gallavotti–Cohen-Type Symmetry in the Large Deviation Functional for Stochastic Dynamics. *Journal of Statistical Physics* **95** (1):333, 1999. Cited on p. 43, 49, 89, 95, and 96.

[174] J. J. Lee, D. P. von Kessler, S. Parks, and P. A. Beachy. Secretion and localized transcription suggest a role in positional signaling for products of the segmentation gene hedgehog. *Cell* **71** (1):33, 1992. Cited on p. 280.

[175] A. Lefèvre and G. Biroli. Dynamics of interacting particle systems: stochastic process and field theory. *Journal of Statistical Mechanics: Theory and Experiment* **2007** (07):P07024, 2007. Cited on p. 169, 177, and 241.

[176] H. Leff and A. F. Rex. *Maxwell's Demon 2 Entropy, Classical and Quantum Information, Computing*. CRC Press, 2002. Cited on p. 298.

[177] A. Lesne. Shannon entropy: a rigorous notion at the crossroads between probability, information theory, dynamical systems and statistical physics. *Math. Struct. Comput. Sci.* **24** (3), 2014. Cited on p. 53.

[178] J. Li, J. M. Horowitz, T. R. Gingrich, and N. Fakhri. Quantifying dissipation using fluctuating currents. *Nature communications* **10** (1):1, 2019. Cited on p. 127.

[179] F. Liu, A. H. Morrison, and T. Gregor. Dynamic interpretation of maternal inputs by the drosophila segmentation gene network. *Proceedings of the National Academy of Sciences* **110** (17):6724, 2013. Cited on p. 262.

[180] Z. Liu, O. Chen, J. Wall, M. Zheng, Y. Zhou, L. Wang, H. Ruth Vaseghi, L. Qian, and J. Liu. Systematic comparison of 2a peptides for cloning multi-genes in a polycistronic vector. *Scientific reports* **7** (1):1, 2017. Cited on p. 292.

[181] S. A. Loos and S. H. Klapp. Irreversibility, heat and information flows induced by non-reciprocal interactions. *New Journal of Physics* **22** (12):123051, 2020. Cited on p. 299.

[182] S. A. M. Loos and S. H. L. Klapp. Heat flow due to time-delayed feedback. *Sci. Rep.* **9** (1):2491, 2019. Cited on p. 41.

[183] J. E. Lovelock and L. Margulis. Atmospheric homeostasis by and for the biosphere: the gaia hypothesis. *Tellus* **26** (1-2):2, 1974. Cited on p. 33.

[184] Z. R. M. Plischke and R. K. P. Zia. Width distribution of curvature-driven interfaces: A study of universality. *Phys. Rev. E* **50**:3589, 1994. Cited on p. 223, 228, and 229.

[185] C. Maes. The Fluctuation Theorem as a Gibbs Property. *J. Stat. Phys.* **95** (1):367, 1999. Cited on p. 41.

[186] C. Maes, F. Redig, and A. V. Moffaert. On the definition of entropy production, via examples. *J. Math. Phys.* **41** (3):1528, 2000. Cited on p. 72.

[187] W. Magnus, F. Oberhettinger, and R. P. Soni. *Formulas and Theorems for the Special Functions of Mathematical Physics*. Springer-Verlag, Berlin, Germany, 1966. Cited on p. 67 and 69.

[188] B. F. Maier and D. Brockmann. Cover time for random walks on arbitrary complex networks. *Phys. Rev. E* **96**:042307, 2017. Cited on p. 225.

[189] S. N. Majumdar, F. Mori, H. Schawe, and G. Schehr. Mean perimeter and area of the convex hull of a planar brownian motion in the presence of resetting. *Phys. Rev. E* **103**:022135, 2021. Cited on p. 90.

[190] S. N. Majumdar, A. Rosso, and A. Zoia. Time at which the maximum of a random acceleration process is reached. *Journal of Physics A: Mathematical and Theoretical* **43** (11):115001, 2010. Cited on p. 119.

[191] B. B. Mandelbrot and J. W. V. Ness. Fractional brownian motions, fractional noises and applications. *SIAM Review* **10** (4):422, 1968. Cited on p. 138.

[192] M. C. Marchetti, J. F. Joanny, S. Ramaswamy, T. B. Liverpool, J. Prost, M. Rao, and R. A. Simha. Hydrodynamics of soft active matter. *Rev. Mod. Phys.* **85**:1143, 2013. Cited on p. 89.

[193] T. Markovich, E. Fodor, E. Tjhung, and M. E. Cates. Thermodynamics of active field theories: Energetic cost of coupling to reservoirs. *Phys. Rev. X* **11**:021057, 2021. Cited on p. 168 and 212.

[194] D. Martin, J. O'Byrne, M. E. Cates, E. Fodor, C. Nardini, J. Tailleur, and F. van Wijland. Statistical mechanics of active ornstein-uhlenbeck particles. *Phys. Rev. E* **103**:032607, 2021. Cited on p. 119.

[195] P. C. Martin, E. D. Siggia, and H. A. Rose. Statistical dynamics of classical systems. *Phys. Rev. A* **8**:423, 1973. Cited on p. 169 and 198.

[196] G. Maziya, L. Cocconi, G. Pruessner, and N. R. Moloney. Dynamically accelerated cover times. *Phys. Rev. Research* **2**:023421, 2020. Cited on p. 32, 217, and 252.

[197] I. J. McGough, L. Vecchia, B. Bishop, T. Malinauskas, K. Beckett, D. Joshi, N. O'Reilly, C. Siebold, E. Y. Jones, and J.-P. Vincent. Glypicans shield the wnt lipid moiety to enable signalling at a distance. *Nature* **585** (7823):85, 2020. Cited on p. 306.

[198] A. S. Monin and A. Yaglom. *Statistical Fluid Mechanics: Mechanics and Turbulence*, volume 2. MIT Press, Cambridge, MA, USA, 1975. Cited on p. 133 and 155.

[199] M. Montero and J. Villarroel. Monotonic continuous-time random walks with drift and stochastic reset events. *Phys. Rev. E* **87**:012116, 2013. Cited on p. 90.

[200] W. W. Mullins. Theory of Thermal Grooving. *J. Appl. Phys.* **28**:333, 1957. Cited on p. 223.

[201] T. Munakata and M. L. Rosinberg. Entropy production and fluctuation theorems for Langevin processes under continuous non-Markovian feedback control. *Phys. Rev. Lett.* **112** (18):180601, 2014. Cited on p. 41.

[202] C. Nardini, É. Fodor, E. Tjhung, F. van Wijland, J. Tailleur, and M. E. Cates. Entropy Production in Field Theories without Time-Reversal Symmetry: Quantifying the Non-Equilibrium Character of Active Matter. *Phys. Rev. X* **7** (2):021007, 2017. Cited on p. 35, 41, 52, 125, 127, 169, 212, 213, and 214.

[203] L. G. Nava, R. Grossmann, and F. Peruani. Markovian robots: Minimal navigation strategies for active particles. *Physical Review E* **97** (4):042604, 2018. Cited on p. 304.

[204] S. Nekovar and G. Pruessner. A field-theoretic approach to the wiener sausage. *Journal of Statistical Physics* **163**:604–641, 2016. Cited on p. 241.

[205] I. Neri, É. Roldán, S. Pigolotti, and F. Jülicher. Integral fluctuation relations for entropy production at stopping times. *J. Stat. Mech.: Theory Exp.* **2019** (10):104006, 2019. Cited on p. 74 and 75.

[206] K. Neuman and A. Nagy. Single-molecule force spectroscopy: optical tweezers, magnetic tweezers and atomic force microscopy. *Nature Methods* **5**:491, 2008. Cited on p. 90.

[207] P. Ngatchou, A. Zarei, and A. El-Sharkawi. Pareto multi objective optimization. In *Proceedings of the 13th international conference on, intelligent systems application to power systems*, pp. 84–91. IEEE, 2005. Cited on p. 303.

[208] G. Nicolis. Transformation properties of entropy production. *Phys. Rev. E* **83**:011112, 2011. Cited on p. 128.

[209] Y. Ogiso, K. Tsuneizumi, N. Masuda, M. Sato, and T. Tabata. Robustness of the dpp morphogen activity gradient depends on negative feedback regulation by the inhibitory smad, dad. *Development, growth & differentiation* **53** (5):668, 2011. Cited on p. 261.

[210] K. S. Olsen, L. Angheluta, and E. G. Flekkøy. Active brownian particles moving through disordered landscapes. *Soft Matter* **17** (8):2151, 2021. Cited on p. 127.

[211] L. Onsager and S. Machlup. Fluctuations and Irreversible Processes. *Phys. Rev.* **91** (6):1505, 1953. Cited on p. 51 and 213.

[212] D. Oriola, M. Marin-Riera, K. Anlas, N. Gritti, M. Matsumiya, G. Aalderink, M. Ebisuya, J. Sharpe, and V. Trivedi. Arrested coalescence of multicellular aggregates. *arXiv:2012.01455* 2021. Cited on p. 90.

[213] T. E. Ouldridge, R. A. Brittain, and P. R. t. Wolde. The power of being explicit: demystifying work, heat, and free energy in the physics of computation. In *The Energetics of Computing in Life and Machines* (edited by D. H. Wolpert). SFI Press, 2018. Cited on p. 41 and 298.

[214] A. Pal and S. Rahav. Integral fluctuation theorems for stochastic resetting systems. *Physical Review E* **96** (6):062135, 2017. Cited on p. 90.

[215] J. Pausch. *Topics in statistical mechanics*. Ph.D. thesis, Imperial College, 2019. Cited on p. 172, 189, and 241.

[216] J. Pausch and G. Pruessner. Is actin filament and microtubule growth reaction-or diffusion-limited? *J. Stat. Mech.: Theory Exp.* **2019** (5):053501, 2019. Cited on p. 85.

[217] G. Pavliotis and A. Stuart. *Multiscale methods: averaging and homogenization*. Springer, 2008. Cited on p. 99 and 115.

[218] G. A. Pavliotis. *Stochastic Processes and Applications - Diffusion Processes, the Fokker-Planck and Langevin Equations*. Springer-Verlag New York, 2014. Cited on p. 49 and 75.

[219] L. Peliti. Path integral approach to birth-death processes on a lattice. *J. Phys. (Paris)* **46**:1469, 1985. Cited on p. 85.

[220] L. Peliti and S. Pigolotti. *Stochastic Thermodynamics: An Introduction*. Princeton University Press, 2021. Cited on p. 34 and 89.

[221] F. Peruani and I. S. Aranson. Cold active motion: how time-independent disorder affects the motion of self-propelled agents. *Physical review letters* **120** (23):238101, 2018. Cited on p. 127.

[222] P. Pietzonka, A. C. Barato, and U. Seifert. Universal bound on the efficiency of molecular motors. *Journal of Statistical Mechanics: Theory and Experiment* **2016** (12):124004, 2016. Cited on p. 34.

[223] P. Pietzonka, É. Fodor, C. Lohrmann, M. E. Cates, and U. Seifert. Autonomous Engines Driven by Active Matter: Energetics and Design Principles. *Phys. Rev. X* **9** (4):041032, 2019. Cited on p. 41 and 306.

[224] P. Pietzonka and U. Seifert. Entropy production of active particles and for particles in active baths. *Journal of Physics A: Mathematical and Theoretical* **51** (1):01LT01, 2017. Cited on p. 51.

[225] S. Pigolotti, I. Neri, É. Roldán, and F. Jülicher. Generic properties of stochastic entropy production. *Phys. Rev. Lett.* **119** (14):140604, 2017. Cited on p. 74.

[226] E. Pinçe, S. K. Velu, A. Callegari, P. Elahi, S. Gigan, G. Volpe, and G. Volpe. Disorder-mediated crowd control in an active matter system. *Nature communications* **7** (1):1, 2016. Cited on p. 127.

[227] G. Pruessner. Lecture notes on non-equilibrium statistical mechanics, 2011. Cited on p. 169, 170, 171, 190, and 241.

[228] S. Rahav and C. Jarzynski. Fluctuation relations and coarse-graining. *Journal of Statistical Mechanics: Theory and Experiment* **2007** (09):P09012, 2007. Cited on p. 128.

[229] C. O. Reichhardt and C. Reichhardt. Ratchet effects in active matter systems. *Annual Review of Condensed Matter Physics* **8**:51, 2017. Cited on p. 136.

[230] P. Reimann, C. Van den Broeck, H. Linke, P. Hänggi, J. M. Rubi, and A. Pérez-Madrid. Giant Acceleration of Free Diffusion by Use of Tilted Periodic Potentials. *Phys. Rev. Lett.* **87** (1):010602, 2001. Cited on p. 74.

[231] S. I. Resnick. *A probability path.* Birkhäuser, Boston, 1999. Cited on p. 237.

[232] S. Reuveni. Optimal stochastic restart renders fluctuations in first passage times universal. *Phys. Rev. Lett.* **116**:170601, 2016. Cited on p. 90.

[233] S. Reuveni, M. Urbakh, and J. Klafter. Role of substrate unbinding in michaelis–menten enzymatic reactions. *Proceedings of the National Academy of Sciences* **111** (12):4391, 2014. Cited on p. 90.

[234] H. Risken and T. Frank. *The Fokker-Planck Equation - Methods of Solution and Applications.* Springer-Verlag Berlin Heidelberg, 1996. Cited on p. 71, 73, 75, 93, and 97.

[235] S. Ro, Y. Kafri, M. Kardar, and J. Tailleur. Disorder-induced long-ranged correlations in scalar active matter. *Phys. Rev. Lett.* **126**:048003, 2021. Cited on p. 127 and 136.

[236] C. Roberts and G. Pruessner. Exact solution of a boundary tumbling particle system in one dimension. *arXiv preprint arXiv:2206.06105* 2022. Cited on p. 239 and 256.

[237] J. Rodenfels, K. M. Neugebauer, and J. Howard. Heat Oscillations Driven by the Embryonic Cell Cycle Reveal the Energetic Costs of Signaling. *Dev. Cell* **48** (5):646, 2019. Cited on p. 41.

[238] E. Roldán, I. Neri, M. Dörpinghaus, H. Meyr, and F. Jülicher. Decision making in the arrow of time. *Phys. Rev. Lett.* **115**:250602, 2015. Cited on p. 45 and 89.

[239] P. Romanczuk, M. Bär, W. Ebeling, B. Lindner, and L. Schimansky-Geier. Active brownian particles. *The European Physical Journal Special Topics* **202** (1):1, 2012. Cited on p. 119.

[240] F. E. Rosas, P. A. Mediano, M. Gastpar, and H. J. Jensen. Quantifying high-order interdependencies via multivariate extensions of the mutual information. *Physical Review E* **100** (3):032305, 2019. Cited on p. 299.

[241] U. Rothbauer, K. Zolghadr, S. Tillib, D. Nowak, L. Schermelleh, A. Gahl, N. Backmann, K. Conrath, S. Muyldermans, M. C. Cardoso, *et al.* Targeting and tracing antigens in live cells with fluorescent nanobodies. *Nature methods* **3** (11):887, 2006. Cited on p. 273.

[242] H. Salman, A. Abu-Arish, S. Oliel, A. Loyter, J. Klafter, R. Granek, and M. Elbaum. Nuclear localization signal peptides induce molecular delivery along microtubules. *Biophysical journal* **89** (3):2134, 2005. Cited on p. 136.

[243] I. Santra, U. Basu, and S. Sabhapandit. Run-and-tumble particles in two dimensions under stochastic resetting conditions. *Journal of Statistical Mechanics: Theory and Experiment* **2020** (11):113206, 2020. Cited on p. 90.

[244] I. Santra, S. Das, and S. K. Nath. Brownian motion under intermittent harmonic potentials. *Journal of Physics A: Mathematical and Theoretical* **54** (33):334001, 2021. Cited on p. 90, 98, 99, 108, 120, and 121.

[245] P. Sartori and S. Pigolotti. Thermodynamics of error correction. *Physical Review X* **5** (4):041039, 2015. Cited on p. 34.

[246] T. Schmiedl and U. Seifert. Stochastic thermodynamics of chemical reaction networks. *J. Chem. Phys.* **126** (4):044101, 2007. Cited on p. 41.

[247] B. Schmittmann and R. K. P. Zia. Statistical mechanics of driven diffusive systems. In *Phase Transitions and Critical Phenomena* (edited by C. Domb and J. L. Lebowitz), volume 17, pp. 1–220. Academic Press, New York, NY, USA, 1995. Cited on p. 129.

[248] J. Schnakenberg. Network theory of microscopic and macroscopic behavior of master equation systems. *Rev. Mod. Phys.* **48** (4):571, 1976. Cited on p. 41, 43, 89, 95, 96, 130, 137, and 140.

[249] J. Schnakenberg. Network theory of microscopic and macroscopic behavior of master equation systems. *Reviews of Modern Physics* **48** (4):571, 1976. Cited on p. 96 and 130.

[250] M. J. Schnitzer. Theory of continuum random walks and application to chemotaxis. *Phys. Rev. E* **48** (4):2553, 1993. Cited on p. 77.

[251] E. Schrödinger *et al. What is life?: With mind and matter and autobiographical sketches*. Cambridge University Press, 1992. Cited on p. 31 and 33.

[252] G. Schwank, S. Restrepo, and K. Basler. Growth regulation by dpp: an essential role for brinker and a non-essential role for graded signaling levels. *Development* 2008. Cited on p. 261.

[253] A. Seif, M. Hafezi, and C. Jarzynski. Machine learning the thermodynamic arrow of time. *Nature Physics* **17** (1):105, 2021. Cited on p. 89.

[254] U. Seifert. Entropy production along a stochastic trajectory and an integral fluctuation theorem. *Phys. Rev. Let.* **95** (4):040602, 2005. Cited on p. 34, 41, 42, 49, 51, 89, 96, and 305.

[255] U. Seifert. Soft Matter: from Synthetic to Biological Materials, 2008. Lecture Notes. Cited on p. 51.

[256] U. Seifert. Stochastic thermodynamics, fluctuation theorems, and molecular machines. *Rep. Prog. Phys.* **75** (12):126001, 2012. Cited on p. 34, 41, 43, 49, 51, 89, 95, 127, and 215.

[257] U. Seifert. Stochastic thermodynamics: From principles to the cost of precision. *Physica A: Statistical Mechanics and its Applications* **504**:176, 2018. Cited on p. 41 and 89.

[258] U. Seifert. Stochastic thermodynamics: From principles to the cost of precision. *Physica A* **504**:176, 2018. Cited on p. 41.

[259] M. Semeraro, A. Suma, I. Petrelli, F. Cagnetta, and G. Gonnella. Work fluctuations in the active ornstein–uhlenbeck particle model. *Journal of Statistical Mechanics: Theory and Experiment* **2021** (12):123202, 2021. Cited on p. 119.

[260] E. M. Sevick, R. Prabhakar, S. R. Williams, and D. J. Searles. Fluctuation theorems. *Annu. Rev. Phys. Chem.* **59**:603, 2008. Cited on p. 89 and 96.

[261] C. E. Shannon. A Mathematical Theory of Communication. *Bell Syst. Tech. J* **27** (3):379, 1948. Cited on p. 42, 44, and 93.

[262] J. Shen, C. Dahmann, and G. O. Pflugfelder. Spatial discontinuity of optomotor-blind expression in the drosophila wing imaginal disc disrupts epithelial architecture and promotes cell sorting. *BMC developmental biology* **10** (1):1, 2010. Cited on p. 292.

[263] P.-S. Shim, H.-M. Chun, and J. D. Noh. Macroscopic time-reversal symmetry breaking at a nonequilibrium phase transition. *Physical Review E* **93** (1):012113, 2016. Cited on p. 127.

[264] V. P. Shkilev. Continuous-time random walk under time-dependent resetting. *Phys. Rev. E* **96**:012126, 2017. Cited on p. 90.

[265] P. Singh. Random acceleration process under stochastic resetting. *Journal of Physics A: Mathematical and Theoretical* **53** (40):405005, 2020. Cited on p. 90 and 119.

[266] A. Slowman, M. Evans, and R. Blythe. Jamming and attraction of interacting run-and-tumble random walkers. *Physical review letters* **116** (21):218101, 2016. Cited on p. 169.

[267] E. Smith and S. Krishnamurthy. Path-reversal, doi-peliti generating functionals, and dualities between dynamics and inference for stochastic processes. *arXiv:1806.02001* 2018. Cited on p. 85.

[268] L. Solnica-Krezel and D. S. Sepich. Gastrulation: making and shaping germ layers. *Annual review of cell and developmental biology* **28** (1):687, 2012. Cited on p. 259.

[269] A. P. Solon, M. E. Cates, and J. Tailleur. Active brownian particles and run-and-tumble particles: A comparative study. *The European Physical Journal Special Topics* **224** (7):1231, 2015. Cited on p. 119.

[270] Y. Song, J. O. Park, L. Tanner, Y. Nagano, J. D. Rabinowitz, and S. Y. Shvartsman. Energy budget of Drosophila embryogenesis. *Curr. Biol.* **29** (12):R566, 2019. Cited on p. 41.

[271] R. Soto and R. Golestanian. Self-assembly of active colloidal molecules with dynamic function. *Physical Review E* **91** (5):052304, 2015. Cited on p. 169.

[272] R. E. Spinney and I. J. Ford. Entropy production in full phase space for continuous stochastic dynamics. *Phys. Rev. E* **85** (5):051113, 2012. Cited on p. 72.

[273] K. S. Stapornwongkul, M. de Gennes, L. Cocconi, G. Salbreux, and J.-P. Vincent. Patterning and growth control in vivo by an engineered gfp gradient. *Science* **370** (6514):321, 2020. Cited on p. 22, 32, 36, 259, 262, 263, 265, 272, 273, and 290.

[274] K. S. Stapornwongkul and J.-P. Vincent. Generation of extracellular morphogen gradients: the case for diffusion. *Nature Reviews Genetics* **22** (6):393, 2021. Cited on p. 35 and 262.

[275] P. Strasberg and M. Esposito. Non-markovianity and negative entropy production rates. *Phys. Rev. E* **99**:012120, 2019. Cited on p. 128.

[276] A.-S. Sznitman. Random interlacements and the gaussian free field. *Ann. Probab.* **40**:2400, 2012. Cited on p. 219.

[277] T. Tabata, S. Eaton, and T. B. Kornberg. The drosophila hedgehog gene is expressed specifically in posterior compartment cells and is a target of engrailed regulation. *Genes & development* **6** (12b):2635, 1992. Cited on p. 280.

[278] K. A. Takeuchi. An appetizer to modern developments on the kardar–parisi–zhang universality class. *Physica A* **504**:77, 2018. Cited on p. 236.

[279] U. C. Täuber, M. Howard, and B. P. Vollmayr-Lee. Applications of field-theoretic renormalization group methods to reaction-diffusion problems. *J. Phys. A: Math. Gen.* **38** (17):R79, 2005. Cited on p. 85 and 170.

[280] G. Teza and A. L. Stella. Exact coarse graining preserves entropy production out of equilibrium. *Phys. Rev. Lett.* **125**:110601, 2020. Cited on p. 35 and 128.

[281] S. P. Thampi, A. Doostmohammadi, T. N. Shendruk, R. Golestanian, and J. M. Yeomans. Active micromachines: Microfluidics powered by mesoscale turbulence. *Science advances* **2** (7):e1501854, 2016. Cited on p. 306.

[282] A. Thommen, S. Werner, O. Frank, J. Philipp, O. Knittelfelder, Y. Quek, K. Fahmy, A. Shevchenko, B. M. Friedrich, F. Jülicher, *et al.* Body size-dependent energy storage causes kleiber's law scaling of the metabolic rate in planarians. *Elife* **8**:e38187, 2019. Cited on p. 305.

[283] J. Thurmond, J. L. Goodman, V. B. Strelets, H. Attrill, L. S. Gramates, S. J. Marygold, B. B. Matthews, G. Millburn, G. Antonazzo, V. Trovisco, *et al.* Flybase 2.0: the next generation. *Nucleic acids research* **47** (D1):D759, 2019. Cited on p. 295.

[284] M. Tikhonov, S. C. Little, and T. Gregor. Only accessible information is useful: insights from gradient-mediated patterning. *Royal Society Open Science* **2** (11):150486, 2015. Cited on p. 297.

[285] S. Torquato. Hyperuniformity and its Generalizations. *Physical Review E* **94** (2):022122, 2016. ArXiv: 1607.08814. Cited on p. 128, 133, 135, 159, and 163.

[286] B. K. Tripathi and K. D. Irvine. The wing imaginal disc. *Genetics* **220** (4):iyac020, 2022. Cited on p. 260.

[287] L. Turban. Random sequential adsorption of k-mers on the fully-connected lattice: probability distributions of the covering time and extreme value statistics. *J. Phys. A-Math. Gen.* **53**:035001, 2019. Cited on p. 219.

[288] A. M. Turing. The chemical basis of morphogenesis. *Bulletin of mathematical biology* **52** (1):153, 1990. Cited on p. 35 and 260.

[289] U. C. Täuber. *Critical Dynamics: A Field Theory Approach to Equilibrium and Non-Equilibrium Scaling Behavior*. Cambridge University Press, 2014. Cited on p. 51, 52, 169, 173, 176, 178, 198, and 241.

[290] C. Van den Broeck and M. Esposito. Three faces of the second law. ii. fokker-planck formulation. *Phys. Rev. E* **82** (1):011144, 2010. Cited on p. 71 and 72.

[291] N. G. van Kampen. *Stochastic Processes in Physics and Chemistry*. Elsevier Science B. V., Amsterdam, The Netherlands, 1992. Third impression 2001, enlarged and revised. Cited on p. 98, 187, and 299.

[292] A. Velenich, C. Chamon, L. F. Cugliandolo, and D. Kreimer. On the brownian gas: a field theory with a poissonian ground state. *Journal of Physics A: Mathematical and Theoretical* **41** (23):235002, 2008. Cited on p. 169, 174, and 198.

[293] B. Walter. *Field theories for stochastic processes*. Ph.D. thesis, Imperial College, 2020. Cited on p. 241.

[294] B. Walter, G. Pruessner, and G. Salbreux. Field theory of survival probabilities, extreme values, first passage times, and mean span of non-markovian stochastic processes. *arXiv preprint arXiv:2109.03649* 2021. Cited on p. 239 and 256.

[295] J. Wang. Landscape and flux theory of non-equilibrium dynamical systems with application to biology. *Advances in Physics* **64** (1):1, 2015. Cited on p. 33, 49, 129, and 130.

[296] O. Wartlick, P. Mumcu, A. Kicheva, T. Bittig, C. Seum, F. Jülicher, and M. Gonzalez-Gaitan. Dynamics of dpp signaling and proliferation control. *science* **331** (6021):1154, 2011. Cited on p. 262.

[297] G. S. Watson. Goodness-of-fit tests on a circle. *Biometrika* **48**:109, 1961. Cited on p. 223.

[298] M. B. Weissman. $1/f$ noise and other slow, nonexponential kinetics in condensed matter. *Phys. Rev. E* **60**:537, 1988. Cited on p. 223.

[299] H. S. Wilf. The editor's corner: the white screen problem. *Amer. Math. Mon.* **96** (8):704, 1989. Cited on p. 219 and 225.

[300] C. Wissel. Manifolds of equivalent path integral solutions of the Fokker-Planck equation. *Z. Phys. B: Condens. Matter* **35** (2):185, 1979. Cited on p. 47 and 75.

[301] D. H. Wolpert. The stochastic thermodynamics of computation. *Journal of Physics A: Mathematical and Theoretical* **52** (19):193001, 2019. Cited on p. 297 and 298.

[302] L. Wolpert. Positional information and the spatial pattern of cellular differentiation. *Journal of theoretical biology* **25** (1):1, 1969. Cited on p. 260.

[303] R. Yagi, F. Mayer, and K. Basler. Refined lexa transactivators and their use in combination with the drosophila gal4 system. *Proceedings of the National Academy of Sciences* **107** (37):16166, 2010. Cited on p. 272.

[304] N. Yamanaka, K. F. Rewitz, and M. B. O'Connor. Ecdysone control of developmental transitions: lessons from drosophila research. *Annual review of entomology* **58**:497, 2013. Cited on p. 260.

[305] S.-X. Yang and H. Ge. Decomposition of the entropy production rate and nonequilibrium thermodynamics of switching diffusion processes. *Phys. Rev. E* **98** (1):012418, 2018. Cited on p. 81.

[306] X. Yang, M. Heinemann, J. Howard, G. Huber, S. Iyer-Biswas, G. Le Treut, M. Lynch, K. L. Montooth, D. J. Needleman, S. Pigolotti, *et al.* Physical bioenergetics: Energy fluxes, budgets,

and constraints in cells. *Proceedings of the National Academy of Sciences* **118** (26):e2026786118, 2021. Cited on p. 33 and 305.

[307] K. T. Yiu. *Entropy Production and Time Reversal*. Master's thesis, Imperial College London, 2017. Cited on p. 85.

[308] Q. Yu, D. Zhang, and Y. Tu. Inverse power law scaling of energy dissipation rate in nonequilibrium reaction networks. *Phys. Rev. Lett.* **126**:080601, 2021. Cited on p. 127 and 129.

[309] S. Yu, C.-W. Qiu, Y. Chong, S. Torquato, and N. Park. Engineered disorder in photonics. *Nature Reviews Materials* **6** (3):226, 2021. Cited on p. 136.

[310] C. Yuan and X. Mao. Asymptotic stability in distribution of stochastic differential equations with markovian switching. *Stochastic processes and their applications* **103** (2):277, 2003. Cited on p. 98 and 102.

[311] F. Zhang, S. Wang, L. Yin, Y. Yang, Y. Guan, W. Wang, H. Xu, and N. Tao. Quantification of epidermal growth factor receptor expression level and binding kinetics on cell surfaces by surface plasmon resonance imaging. *Analytical chemistry* **87** (19):9960, 2015. Cited on p. 277.

[312] Z. Zhang and G. Pruessner. Field theory of free run and tumble particles in d dimensions. *Journal of Physics A: Mathematical and Theoretical* **55** (4):045204, 2022. Cited on p. 239 and 256.

[313] Z. Zhang and W. Wang. The stationary distribution of Ornstein–Uhlenbeck process with a two-state Markov switching. *Communications in Statistics - Simulation and Computation* **46** (6):4783, 2017. Cited on p. 98, 99, 108, and 120.

[314] Z. Zhen and G. Pruessner. Optimal ratchet potentials for run-and-tumble particles. *arXiv preprint arXiv:2204.04070* 2022. Cited on p. 307.

[315] K. Zhou, M. Hennes, B. Maier, G. Gompper, and B. Sabass. Non-equilibrium dynamics of bacterial colonies – growth, active fluctuations, segregation, adhesion, and invasion. *arXiv:2106.06729* 2021. Cited on p. 90.

[316] S. Zhou, W.-C. Lo, J. L. Suhalim, M. A. Digman, E. Gratton, Q. Nie, and A. D. Lander. Free extracellular diffusion creates the dpp morphogen gradient of the drosophila wing disc. *Current Biology* **22** (8):668, 2012. Cited on p. 273.

[317] T. Zhou, P. Xu, and W. Deng. Continuous-time random walks and lévy walks with stochastic resetting. *Phys. Rev. Research* **2**:013103, 2020. Cited on p. 90.

[318] J. Zinn-Justin. *Quantum field theory and critical phenomena*, volume 171. Oxford university press, 2021. Cited on p. 127, 132, 138, 143, 152, and 161.

[319] N. Zlatanov and L. Kocarev. Random walks on networks: Cumulative distribution of cover time. *Phys. Rev. E* **80**:041102, 2009. Cited on p. 225.

[320] N. Zoroa, E. Lesigne, M. J. Fernández-Sáez, P. Zoroa, and J. Casas. The coupon collector urn model with unequal probabilities in ecology and evolution. *J. R. Soc Interface* **14**:20160643, 2017. Cited on p. 219.

A

Right to reproduce

Most of the work presented in this thesis has been previously published in peer-reviewed journals. This appendix contains references to the different publishers' Authors Rights Policy statements (in particular regarding reproduction of third-party copyrighted work) and the approval of all co-authors.

A.1 Copyright permission

Entropy published by MDPI

Chapter 1 was originally published in *Entropy*. As stated on their website, "*for all articles published in MDPI journals, copyright is retained by the authors. Articles are licensed under an open access Creative Commons CC BY 4.0 license, meaning that anyone may download and read the paper for free. In addition, the article may be reused and quoted provided that the original published version is cited.*" More information at https://www.mdpi.com/authors/rights.

Journal of Physics A: Mathematical and Theoretical PUBLISHED BY IOP

Chapter 2 was originally published in *JPA*. As stated on their website, "*When you transfer the copyright in your article to IOP, we grant back to you certain rights, including the right to include all or part of the Final Published Version of the article within any thesis or dissertation*". More information at https://publishingsupport.iopscience.iop.org/permissionsfaq/.

Physical Review E and Physical Review Research PUBLISHED BY APS

Chapter 3 and Chapter 5 was originally published in *PRE* and *PRR*, respectively. The APS Authors Rights Policy states, regarding inclusion of published papers in an author's thesis or dissertation, that "*the author has the right to use the article or a portion of the article in a thesis or dissertation without requesting permission from APS, provided the bibliographic citation and the APS copyright credit line are given on the appropriate pages.*" More information at https://journals.aps.org/authors/transfer-of-copyright-agreement.

Science PUBLISHED BY THE AAAS

Chapter 7 was originally published in *Science*. Following the instructions on their website, I requested permission by email. This was the answer from the editorial office.

> **From:** Editorial Office <permissions@aaas.org>
> **Sent:** 2 Aug 2022, at 16:56
> **To:** Luca Cocconi <luca.cocconi@crick.ac.uk>
> **Subject:** PERMISSION QUERY - AUTHOR USE - License to publish - inclusion of SM in thesis
>
> Dear Luca:
>
> Thank you for getting in touch. I am writing to confirm that the use of your paper's Supplementary Material (with attribution) in your thesis (both print

and electronic) is permitted under the terms and conditions of the Science License to Publish and no further permission from AAAS is needed. If you have any questions, please just let me know.

Kind regards,

Elizabeth Sandler (Ms.)
Rights & Permissions, Science family of journals
American Association for the Advancement of Science (AAAS)

A.2 Approval of co-authors

This section contains the proof of approval of all co-authors to reproduce published or submitted work, organised by publication.

Entropy 22 (11), 1252 (2020)

From: Luca Cocconi <luca.cocconi@crick.ac.uk>
Sent: 2 Aug 2022, at 17:04
Subject: Approval for citation in thesis - Entropy 22 (11), 1252 (2020)

Dear Rosalba, Zigan, Bianca, Gunnar,

I am completing my PhD thesis at Imperial College London entitled "Statistical mechanics of non equilibrium matter: from minimal models to morphogen gradients". I would like to use our jointly published paper “Entropy production in exactly solvable systems” (2020) as a part of my PhD thesis and cite it as a whole and verbatim. I would like to ask you as my co-authors for your approval. Your responses to this email will be included in the thesis as evidence.

Best wishes,
Luca

From: Zhen, Zigan <z.zhen19@imperial.ac.uk>
Sent: 2 Aug 2022, at 22:10
Subject: RE: Approval for citation in thesis - Entropy 22 (11), 1252 (2020)

Dear Luca,

I approve this request.

Best wishes,
Zigan

From: Bianca Buturca <Bianca.Buturca@physik.uni-muenchen.de>
Sent: 3 Aug 2022, at 15:52
Subject: RE: Approval for citation in thesis - Entropy 22 (11), 1252 (2020)

Dear Luca,

It is great hearing from you!
Many congratulations on completing your PhD thesis and I wish you the best of luck in your future work!
Thus I also give my approval for using our paper in your thesis, and I would really like to have a read of it when it is finished!

Best wishes,
Bianca

From: Rosalba Garcia-Millan <rg646@cam.ac.uk>
Sent: 11 Aug 2022, at 13:09
Subject: RE: Approval for citation in thesis - Entropy 22 (11), 1252 (2020)

Dear Luca

Of course, I am happy for you to cite the paper and reproduce it verbatim in your thesis.

All the best,
Rosalba

From: Pruessner, Gunnar <g.pruessner@imperial.ac.uk>
Sent: 11 Aug 2022, at 12:28
Subject: Citation approval

Dear Luca,

I would like to give you my blanket approval to use and/or reproduce in your PhD thesis any of the manuscripts that we have published together or are planning to publish.

All the best,
Gunnar

J. Phys. A Math. Theor. 55 (27) (2022)

From: Luca Cocconi <luca.cocconi@crick.ac.uk>
Sent: 2 Aug 2022, at 17:04
Subject: Approval for citation in thesis - J. Phys. A Math. Theor. 55 (27) (2022)

Dear Henry, Thibault,

I am completing my PhD thesis at Imperial College London entitled "Statistical mechanics of non equilibrium matter: from minimal models to morphogen gradients". I would like to use our jointly published paper “Non-equilibrium thermodynamics of diffusion in fluctuating potentials” (2022) as a part of my PhD thesis and cite it as a whole and verbatim. I would like to ask you as my co-authors for your approval. Your responses to this email will be included in the thesis as evidence.

Best wishes,
Luca

From: Bertrand, Thibault <t.bertrand@imperial.ac.uk>
Sent: 2 Aug 2022, at 17:10
Subject: RE: Approval for citation in thesis - J. Phys. A Math. Theor. 55 (27) (2022)

Dear Luca,

I give my approval.

Best,
-Thibault

From: Alston, Henry <henry.alston16@imperial.ac.uk>
Sent: 2 Aug 2022, at 17:17
Subject: RE: Approval for citation in thesis - J. Phys. A Math. Theor. 55 (27) (2022)

Hi Luca,

I also give my approval to include the work in your thesis.

Best,
Henry

Phys. Rev. E 105 (2022)

From: Luca Cocconi <luca.cocconi@crick.ac.uk>
Sent: 2 Aug 2022, at 17:17
Subject: Approval for citation in thesis - Phys. Rev. E 105 (2022)

Dear Guillaume, Gunnar,

I am completing my PhD thesis at Imperial College London entitled "Statistical mechanics of non equilibrium matter: from minimal models to morphogen gradients". I would like to use our jointly published paper “Scaling of entropy production under coarse graining in disordered active media" (2022) as a part of my PhD thesis and cite it as a whole and with minor modifications. I would like to ask you as my co-authors for your approval. Your responses to this email will be included in the thesis as evidence.

Best wishes,
Luca

From: Guillaume Salbreux <Guillaume.Salbreux@unige.ch>
Sent: 3 Aug 2022, at 21:11
Subject: RE: Approval for citation in thesis - Phys. Rev. E 105 (2022)

Dear Luca,

I am happy to approve the inclusion of our joint paper in your PhD thesis.

Best wishes,
Guillaume

Preprint arXiv:2205.10409 (2022)

From: Luca Cocconi <luca.cocconi@crick.ac.uk>
Sent: 2 Aug 2022, at 17:04
Subject: Approval for citation in thesis - arXiv:2205.10409 (2022)

Dear Marius, Zigan, Gunnar,

I am completing my PhD thesis at Imperial College London entitled "Statistical mechanics of non equilibrium matter: from minimal models to morphogen gradients". I would like to use our preprint “Particle entity in the

Doi-Peliti and response-field formalisms" (2022) as a part of my PhD thesis and cite it as a whole and with minor edits. I would like to ask you as my co-authors for your approval. Your responses to this email will be included in the thesis as evidence.

Best wishes,
Luca

From: Marius Bothe <m.bothe19@imperial.ac.uk>
Sent: 2 Aug 2022, at 17:37
Subject: RE: Approval for citation in thesis - arXiv:2205.10409 (2022)

Hey Luca,

of course that is fine by me.

Best regards,
Marius

From: Zhen, Zigan <z.zhen19@imperial.ac.uk>
Sent: 2 Aug 2022, at 22:10
Subject: RE: Approval for citation in thesis - arXiv:2205.10409 (2022)

Dear Luca,

I approve this request.

Best wishes,
Zigan

Phys. Rev. Res. 2 (2), 023421 (2020)

From: Luca Cocconi <luca.cocconi@crick.ac.uk>
Sent: 2 Aug 2022, at 17:04

Subject: Approval for citation in thesis - Phys. Rev. Res. 2 (2), 023421 (2020)

Dear Gcina, Gunnar, Nicholas,

I am completing my PhD thesis at Imperial College London entitled "Statistical mechanics of non equilibrium matter: from minimal models to morphogen gradients". I would like to use our jointly published paper “Dynamically accelerated cover times” (2020) as a part of my PhD thesis and cite it as a whole and verbatim. I would like to ask you as my co-authors for your approval. Your responses to this email will be included in the thesis as evidence.

Best wishes,
Luca

From: Gcina Maziya <gcina@aims.ac.za>
Sent: 2 Aug 2022, at 17:29
Subject: RE: Approval for citation in thesis - Phys. Rev. Res. 2 (2), 023421 (2020)

Hi Luca,

Thanks for your email and letting me know that you want to use the article in your thesis. That’s perfectly fine with me, so you can go ahead and use the article in your thesis the way you’ve mentioned.
All the best with your thesis!

Best wishes,
Gcina.

From: Nicholas Moloney <n.moloney.lml@gmail.com>
Sent: 2 Aug 2022, at 17:49
Subject: RE: Approval for citation in thesis - Phys. Rev. Res. 2 (2),

023421 (2020)

Dear Luca,

I approve.

Best,
Nicholas

Science 370 (6514), 321-327 (2020)

From: Luca Cocconi <luca.cocconi@crick.ac.uk>
Sent: 2 Aug 2022, at 17:04
Subject: Approval for citation in thesis - Science 370 (6514), 321-327 (2020)

Dear Kristina, Marc, Guillaume, Jean-Paul,

I am completing my PhD thesis at Imperial College London entitled "Statistical mechanics of non equilibrium matter: from minimal models to morphogen gradients". I would like to use our jointly published paper "Patterning and growth control in vivo by an engineered GFP gradient" (2020) as a part of my PhD thesis and cite its Supplementary Material with minor edits. I have inquired AAAS about copyright separately, but would like to ask you as my co-authors for your approval. Your responses to this email will be included in the thesis as evidence.

Best wishes,
Luca

From: Jean-Paul Vincent <JP.Vincent@crick.ac.uk>
Sent: 2 Aug 2022, at 17:05
Subject: RE: Approval for citation in thesis - Science 370 (6514), 321-327 (2020)

Dear Luca

I agree to your using of material from our paper in your thesis.

JP

From: Kristina Stapornwongkul <kristina.stapornwongkul@embl.es>
Sent: 2 Aug 2022, at 22:11
Subject: RE: Approval for citation in thesis - Science 370 (6514), 321-327 (2020)

Dear Luca,

I agree as well. Please use whatever material from our paper you need for your thesis.
Good luck for the submission!

All the best,
Kristina

From: Guillaume Salbreux <Guillaume.Salbreux@unige.ch>
Sent: 3 Aug 2022, at 21:12
Subject: RE: Approval for citation in thesis - Science 370 (6514), 321-327 (2020)

Dear Luca,

I am also happy for you to use our joint manuscript in your PhD thesis.

Best wishes,
Guillaume

From: marc de gennes <marcdegennes@gmail.com>
Sent: 13 Aug 2022, at 19:35

Subject: RE: Approval for citation in thesis - Science 370 (6514), 321-327 (2020)

Dear Luca,

I also agree with you using the material from our paper in your PhD thesis.

All the best,
Marc